UNIVERSIDAD COMPLUTENSE DE MADRID

FACULTAD DE CIENCIAS QUÍMICAS

Departamento de Ingeniería Química

TESIS DOCTORAL

Procesos de oxidación avanzada para el tratamiento de aguas residuales industriales contaminadas con 1,4 dioxano

Advanced oxidation processes for the treatment of industrial wastewaters containing 1,4-dioxane

MEMORIA PARA OPTAR AL GRADO DE DOCTOR

PRESENTADA POR

Helen Barndok

Directores

Ángeles Blanco Suárez
Daphne Hermosilla Redondo

Madrid, 2017

COMPLUTENSE UNIVERSITY OF MADRID
FACULTY OF CHEMICAL SCIENCES
DEPARTMENT OF CHEMICAL ENGINEERING

Procesos de oxidación avanzada para el tratamiento de aguas residuales industriales contaminadas con 1,4-dioxano / Advanced oxidation processes for the treatment of industrial wastewaters containing 1,4-dioxane

DOCTORAL DISSERTATION

Submitted to the Complutense University of Madrid for the degree of Doctor in Chemical Engineering by

Helen Barndõk

2015

ÁNGELES BLANCO SUÁREZ Y MARÍA DAPHNE HERMOSILLA REDONDO, PROFESORA TITULAR DEL DEPARTAMENTO DE INGENIERÍA QUÍMICA DE LA UNIVERSIDAD COMPLUTENSE DE MADRID Y PROFESORA CONTRATADO DOCTOR DEL DEPARTAMENTO DE INGENIERÍA AGRÍCOLA Y FORESTAL DE LA UNIVERSIDAD DE VALLADOLID

INFORMAN

Que el trabajo de investigación titulado "PROCESOS DE OXIDACIÓN AVANZADA PARA EL TRATAMIENTO DE AGUAS RESIDUALES INDUSTRIALES CONTAMINADAS CON 1,4-DIOXANO / ADVANCED OXIDATION PROCESSES FOR THE TREATMENT OF INDUSTRIAL WASTEWATERS CONTAINING 1,4-DIOXANE" ha sido realizado bajo su dirección en el Departamento de Ingeniería Química, dentro del Grupo de Investigación de Celulosa y Papel de la Universidad Complutense de Madrid, y constituye la memoria que presenta Dña. Helen Barndõk para optar al Grado de Doctor.

Y para que conste a los efectos oportunos, firman la presente, en Madrid a 8 de octubre de 2015.

ACKNOWLEDGEMENTS

I owe my greatest gratitude to Prof. Ángeles Blanco and Prof. Daphne Hermosilla for their careful supervision and expert assistance that were invaluable in delivering this dissertation. I would also like to thank Prof. Carlos Negro for his help and encouraging words whenever needed. I recognise that their guidance and support made possible my research and my stay in this beautiful country in the city of Madrid that I adore. I also acknowledge the Estonian Ministry of Education and Research and the Archimedes Foundation for the financial support provided through the Kristjan Jaak scholarship.

I would like to thank Prof. Dion Dionysiou and his research group in the University of Cincinnati for their input to my research and the opportunity to work in their facilities under their patient assistance. My special thanks go to Miguel Pelaez for his supervision as well as for his friendship and warm Mexican-style welcome to the United States.

I wish to express my great appreciation to my lab companions Laura and Noemi for their assistance in part of my experimental work and articles. I would also like to thank Prof. Estrella Cadahía for my successful research visit in the laboratory of CIFOR-INIA (*Centro de Investigación Forestal, Instituto Nacional de Investigación y Tecnología Agraria y Alimentaria*). I appreciate Paz Andrés for her help with the chromatographic measurements in E.T.S.I. Montes (*Escuela Técnica Superior de Ingenieros de Montes*), and I fully acknowledge the collaboration of the Gas Chromatography Service of the Spanish National Research Council (CIB-CSIC) and the Laboratory of Geochemical and Environmental Analyses of the Complutense University of Madrid.

I appreciate Holmen Paper Madrid enterprise for the fruitful collaboration and the time spent in their water lab, especially thanks to the help and company of Miguel, Victor and Dani.

I also want to acknowledge the advice and support of the rest of the members of the Cellulose and Paper Research Group: Prof. Julio Tijero, Prof. Mª Concepción Monte, Prof. Antonio Tijero, Prof. Helena de la Fuente, Ruben Miranda, Ana Balea, Cristina Campano and Sara Gilarranz, with a special mention to my dear friends and workmates Patricio, Rocio, Monica and Esperanza, as without them my time in this university would not have been the same. Above all, I wish to thank my true friend, flatmate and lab companion Isabel for being unconditionally protective and understanding, and also, for the carefully selected musical background I shall greatly miss.

I am indebted with my partner Luis for his love, patience and companionship throughout all these years that he has made so enjoyable to me with his reassuring and easy-going nature. I wish to thank all my friends for the 24/7 on-line support, the cybernetic girls&wine events and all the backpacker-invasions of my living room. Lastly, and most importantly, my overwhelming thanks go to my supportive family for their encouragement and understanding, despite of my absence during these busy years of my study abroad.

I would like to dedicate this thesis to my beloved friend Manuel Cortijo, not only for his help and support, but for his everlasting belief in me that always managed to keep my moral up. Somehow, I know he would have been very proud of me reading it.

ORIGINAL PUBLICATIONS LIST

I. H. Barndõk, L. Cortijo, D. Hermosilla, C. Negro, A. Blanco, Removal of 1,4-dioxane from industrial wastewaters: Routes of decomposition under different operational conditions to determine the ozone oxidation capacity, *Journal of Hazardous Materials* 280 (2014) 340-347.

II. H. Barndõk, D. Hermosilla, L. Cortijo, E. Torres, A. Blanco, Electrooxidation of industrial wastewater containing 1,4-dioxane in the presence of different salts, *Environmental Science and Pollution Research* 21 (2014) 5701-5712.

III. H. Barndõk, L. Blanco, D. Hermosilla, A. Blanco, Heterogeneous photo-Fenton processes using zero valent iron microspheres for the treatment of wastewaters contaminated with 1,4-dioxane; *Chemical Engineering Journal* 284 (2016) 112-121.

IV. H. Barndõk, M. Pelaez, C. Han, W.E. Platten, III, P. Campo, D. Hermosilla, A. Blanco, D.D. Dionysiou, Photocatalytic degradation of contaminants of concern with composite NF-TiO_2 films under visible and solar light, *Environmental Science and Pollution Research* 20 (2013) 3582-3591.

V. H. Barndõk, D. Hermosilla, C. Han, D.D. Dionysiou, C. Negro, A. Blanco, Degradation of 1,4-dioxane from industrial wastewater by solar photocatalysis using immobilized NF-TiO_2 composite with monodisperse TiO_2 nanoparticles, *Applied Catalysis B: Environmental* 180 (2016) 44-52.

VI. H. Barndõk, N, Merayo, L. Blanco, D. Hermosilla, A. Blanco, Application of on-line FTIR methodology to study the mechanisms of heterogeneous advanced oxidation processes. Sent to: *Applied Catalysis B: Environmental*.

VII. H. Barndõk, D. Hermosilla, A. Blanco, Comparison and predesign cost assessment of ozonation, electro-oxidation and heterogeneous photo-Fenton processes for the treatment of wastewaters from chemical industry. In progress.

AUXILIAR PUBLICATION (PRELIMINARY RESEARCH):

A. H. Barndõk, D. Hermosilla, L. Cortijo, C. Negro, A. Blanco, Assessing the Effect of Inorganic Anions on TiO_2-Photocatalysis and Ozone Oxidation Treatment Efficiencies, *Journal of Advanced Oxidation Technologies* 15 (2012) 125-132.

INDEX

SUMMARY

Water quality is becoming one of the biggest emerging problems of the industrial world. As the public awareness of environmental protection and water pollution increases, the legislation on wastewater discharge is also becoming stricter and new monitoring, risk management and control policies are adopted every year. Therefore, improved wastewater reclamation technologies are required to meet the stringent discharge limits for toxic and hazardous substances.

Among the common industrial wastewater contaminants are organic solvents, used as cleaning agents, dissolvents, dispersion medium, viscosity and surface tension adjusters, plasticisers, preservatives, etc. A great number of the industrial solvents and their stabilizing chemicals are biorefractory and even toxic to the bacterial communities in conventional wastewater treatment plants (WWTPs). In fact, the solvent stabilizers used to avoid solvent break down (antioxidants, acid acceptors, corrosion inhibitors, etc.) are meant to be especially persistent as they are chosen specifically for their ability to remain stable throughout the industrial processes.

One of the persistent and problematic solvents, corrosion inhibitors and swelling agents is 1,4-dioxane. Despite the stricter discharge limits, it is continuously discovered in secondary effluents of conventional WWTPs as well as in natural water supplies. This synthetic cyclic ether comes into our water resources primarily from direct use in, for instance, pharmaceutical industry and polymer (plastics, rubber and fibre) production, but it is also generated as an industrial by-product of, for example, ethoxylated surfactants production or polyester and resin manufacture. 1,4-Dioxane may pose a multitude of harmful health effects, such as kidney failure and liver damage; furthermore, it is also classified as a probable human carcinogen. Unfortunately, the traditional methods of treating wastewaters with organic solvents (including distillation, air stripping, carbon adsorption, membrane processes and conventional biological treatment) tend to fail in completely removing the 1,4-dioxane due to its high solubility, low vapour pressure and biorefractory nature. Thus, more efficient wastewater treatment methods are needed to prevent the pile-up of this persistent and bio-accumulative chemical in the environment.

The objective of this PhD thesis was driven by an actual industrial case of water contamination by 1,4-dioxane that was not degraded by the conventional wastewater treatment in the biological unit of the plant and, thus, remained in the final effluent at high concentrations. Through extensive research during the last two decades, advanced oxidation processes (AOPs) have shown a great capacity to decontaminate industrial effluents containing diverse biorefractory substances. Therefore, this alternative was chosen for the treatment of this effluent during the development of this doctoral thesis.

In terms of actual on-site and pre-industrial implementation of AOPs for the treatment of different industrial wastewaters, Fenton (including photo-Fenton) and ozone (O_3) based processes are the most common ones, whereas fewer reports are available on photocatalysis with titanium dioxide (TiO_2). Although highly efficient, the classical Fenton processes have various disadvantages, including the need for acidification and subsequent neutralization, and the production of iron sludge. Photocatalysis with suspended TiO_2 requires the laborious step of catalyst separation by filtration, and, in addition, all the UV-catalysed processes imply the cost of radiation. It is of great interest to search for more cost-effective and less residues-producing alternatives, e.g. by employing solar light; using solid iron

sources and milder pH conditions to avoid iron leaching; developing new photocatalysts with improved properties; and immobilizing the titanium-based materials to enhance process engineering and catalyst separation.

The conductive diamond electrochemical oxidation (CDEO) seems to be gaining more attention lately, as it has demonstrated very high productions of hydroxyl radicals with a tendency to produce no secondary pollution. However, its efficiency seems to be limited by the mass transport to the electrode surface comprised of an expensive material with little know-how in full scale applications. Ozonation treatment, on the contrary, is a widely implemented method in which no residues are produced either; but the molecular O_3 is highly selective, exhibiting very low reactivity towards 1,4-dioxane, and the promotion of radical pathway through O_3 decomposition has so far been overlooked.

1,4-Dioxane removal from synthetic solutions with ultrapure water has been achieved with various common AOPs, like Fenton, UV/TiO_2, etc. However, very little research has been done on the treatment of industrial wastewater with substantial concentrations of different salts and carbonaceous alkalinity that could abate the effectiveness of AOPs. Furthermore, if the initial salts and alkalinity could actually provide the necessary conductivity for electrolysis or the correct pH buffer for non-selective ozonation treatment, the possible beneficial influence of the water matrix is also an important factor to study. Moreover, optimized conditions must be determined in order to reduce the amount of oxidants involved and the decomposition pathways must be studied, as the routes of degradation in different AOPs in different operational conditions could significantly affect the process efficiency. Finally, new on-line methodologies need to be developed to improve the control of the oxidation reactions and to monitor the target pollutants.

Therefore, the objective of this PhD thesis is to generate new knowledge on the applicability of AOPs for the treatment of industrial wastewaters containing recalcitrant contaminants like 1,4-dioxane, using green and environmentally friendly methods under optimized conditions, minimizing both the production of residues and the volume of oxidants.

In the first part of this thesis, during the initial optimization study on synthetic 1,4-dioxane solution, O_3 was proven efficient as a sole oxidant to degrade 1,4-dioxane in controlled basic conditions (removals of chemical oxygen demand (COD) >90%), pH≥9.0 being the key factor for the process viability. Non-selective anodic oxidation on boron doped diamond (BDD) electrodes resulted in COD removals close to 100%, whereas sulphates and bicarbonates both served as efficient electrolyte salts without presenting any scavenging of the reactive radical species. Employing zero valent iron (Fe^0) microspheres as an iron source for photo-Fenton treatment gave excellent results at neutral pH and even in slightly basic conditions (≈100% of COD), at which the morphology of microspheres remained intact and no iron leaching was detected. Therefore, the sludge production could be greatly reduced, as total recovery of the catalyst is expected when used in heterogeneous conditions. Meanwhile, immobilized nitrogen and fluorine doped TiO_2 catalysts (NF-TiO_2) were synthesized, using different nanoparticle additives and incorporation methods. Minor formation of aggregates, improved distribution and significantly superior photocatalytic performance was obtained by adding monodisperse TiO_2 layer-by-layer on top of NF-TiO_2 instead of the direct incorporation of the particles into the sol of NF-TiO_2. Thus, composite NF-TiO_2 with monodisperse TiO_2 (NF-TiO_2-monodisp.TiO_2) from layer-by-layer method was used for the subsequent degradation of 1,4-dioxane in different wastewater matrices under solar light. The photocatalytic removal of the compound in ultra pure water (k=0.34±0.02 h^{-1}) decreased in the presence of inorganic constituents (k=0.26±0.01 h^{-1}).

Secondly, industrial wastewaters from chemical manufacturing were treated successfully by the above-mentioned AOPs under optimized conditions. The original carbonaceous alkalinity of the industrial effluents resulted to be an advantage in both Fe^0-based photo-Fenton and O_3 treatment, since it served as pH buffer that promoted the radical pathway of non-selective ozonation in basic conditions and avoided the solubilisation of the Fe^0 microspheres without producing any significant radical scavenging effect. Furthermore, carbonates initially present in the water were also beneficial in CDEO by providing the necessary electrical conductivity. Basic ozonation, CDEO on BDD and Fe^0-based photo-Fenton were all fit for the treatment of concentrated effluents (COD=450-2400 $mg \cdot L^{-1}$), whereas the higher the initial COD, the higher the oxidant-efficiency of the AOP in terms of the COD removed per oxidant consumed. In the treatment of the typical sample (COD=475±25 $mg \cdot L^{-1}$), the fastest COD removal was achieved by heterogeneous UV photo-Fenton (98% in 40 min), followed by CDEO on BDD electrodes (84% in 3 h) and basic ozonation (69% in 3 h), whereas the solar photo-Fenton treatment that appeared to be rather comparable to CDEO in shorter treatment times (36-38% in 1 h) slowed down in time (60% in 3 h). Meanwhile, solar photocatalysis on immobilized NF-TiO_2-monodisp.TiO_2 was found suitable for the polishing of low-concentration wastewater streams (COD≤260 $mg \cdot L^{-1}$), achieving almost complete degradation of 1,4-dioxane along with 65% of COD removal after 10 h of treatment. The catalyst immobilization would greatly enhance the process engineering and, thus, increase the cost-effectiveness of the treatment. For the industrial implementation, these treatment times would directly depend on the reactor design (available catalyst/electrode surface, etc.).

Thirdly, the decomposition pathways of 1,4-dioxane were established and compared based on extensive chromatography analysis, whereas Fourier transform infrared spectroscopy served as a powerful tool for on-line reaction monitoring. According to the major decomposition route, the initial radical intermediate, 1,4-dioxan-α-oxyl radical, is degraded into ethylene glycol di- and monoformates (EGDF and EGMF) through ΔC-C splitting. The major difference between the studied AOPs is due to their pH profile, because, in basic conditions, EGDF and EGMF are hydrolysed to ethylene glycol. Alternatively, methoxyacetic and acetic acids can be produced in the decomposition of the α-oxyl radical through an intramolecular reaction followed by fragmentation. This pathway has greater importance in CDEO and photo-Fenton treatments, whereas relatively low concentrations of methoxyacetic and acetic acids were detected in ozonation and photocatalytic trials. Regardless of the AOP, the decomposition of the primary intermediates continued over the generation of short chain carboxylic acids, formic acid being the most prevalent intermediate by-product.

Finally, to compare the AOPs, the possible industrial implementation of O_3, CDEO, and Fe^0-based photo-Fenton processes was evaluated in a pre-design cost assessment, considering the treatment of 43800 $m^3 \cdot y^{-1}$ of industrial wastewater from chemical manufacturing (COD_0=475±25 $mg \cdot L^{-1}$). At the design point of 40% COD removal at which sufficient biodegradability (≈60%) was reached, UV photo-Fenton was found as the cheapest option (4.1 $€ \cdot m^{-3}$), followed very closely by ozonation treatment (4.3 $€ \cdot m^{-3}$), whereas CDEO and solar/Fe^0/H_2O_2 treatments resulted more costly (5.2 and 6.2 $€ \cdot m^{-3}$, respectively). Given that the use of oxidants is generally more efficient in fully optimized industrial units, the costs referred to are expected to be lower at industrial scale. At the current design point, the sunlight-driven photo-Fenton is unfeasible due to the cost and size of the required plant space, but it could become an important alternative for lower COD reductions (<20%). On the other hand, to reach COD removals above 50%, O_3 appears to be more economic process, whereas the price of the BDD unit still limits its industrial application, despite the high oxidant-efficiency.

RESUMEN EXTENDIDO

La mayor concienciación medio ambiental, una legislación cada vez más rigurosa, la optimización de los circuitos de agua, la reutilización de los efluentes industriales, así como los nuevos métodos de monitorización y control, obligan al desarrollo de nuevas tecnologías, cada vez más avanzadas, que permitan una mejor depuración de las aguas residuales industriales.

Entre los contaminantes comunes en las aguas residuales industriales están los disolventes orgánicos, usados como productos de limpieza, disolventes, medio de dispersión, agentes de control de viscosidad y tensión superficial, plastificadores, conservantes, etc. A pesar de los beneficios, muchos de los disolventes y sus estabilizadores son biorecalcitrantes o incluso tóxicos para el tratamiento biológico de una depuradora convencional. De hecho, los estabilizadores (antioxidantes, inhibidores de corrosión, etc.) son especialmente resistentes, ya que están diseñados para mantenerse estables durante todo el proceso industrial para evitar la descomposición del disolvente.

El 1,4-dioxano es un éter cíclico sintético que llega a los recursos acuáticos mayoritariamente a través de su uso directo en la producción industrial como disolvente, en la fabricación de, por ejemplo, fármacos y polímeros (plásticos, gomas y fibras), pero también se genera como un subproducto de la fabricación de surfactantes, poliésteres, resinas, etc. Además de estar clasificado como probable carcinógeno para el ser humano, el 1,4-dioxano presenta múltiples efectos dañinos para la salud, como fallo renal y daño hepático. Desafortunadamente, los métodos tradicionales de tratamiento de aguas residuales contaminadas con disolventes (como destilación, *air stripping*, adsorción con carbono, procesos de membrana y tratamiento biológico convencional) tienden a fallar en la eliminación completa de 1,4-dioxano debido a su gran solubilidad en agua, baja presión de vapor y naturaleza biorefractaria. Por ello, se requieren tratamientos específicos de aguas para prevenir la entrada y acumulación de este compuesto persistente en el medio acuático.

En las últimas dos décadas se ha demostrado que los procesos de oxidación avanzada (POAs) son capaces de descontaminar efluentes industriales contaminados con diversas sustancias biorefractarias. Por lo tanto, en esta Tesis Doctoral se estudian como alternativa para el tratamiento de 1,4-dioxano en efluentes industriales.

En términos de implementación a escala industrial o pre-industrial, los tratamientos Fenton (incluido foto-Fenton) y oxidación con ozono (O_3) son los más comunes, mientras que hay menos referencias sobre la fotocatálisis con dióxido de titanio (TiO_2). Aunque son altamente eficaces, los procesos Fenton clásicos tienen varias desventajas, ya que requieren acidificación y neutralización, produciendo lodos de hierro. Por otro lado, la fotocatálisis con TiO_2 en suspensión implica la separación del catalizador por filtración y, además, todos los procesos catalizados por luz UV conllevan el coste de radiación. Por lo tanto, es de gran interés buscar alternativas más económicas y de menor producción de residuos, empleando luz solar; utilizando catalizadores de hierro sólidos en condiciones de pH neutro para evitar su solubilización; desarrollando fotocatalizadores nuevos con propiedades mejoradas; e inmovilizando los materiales de TiO_2 para facilitar la separación del catalizador.

La oxidación electroquímica con diamante conductivo (OEDC) está ganando atención últimamente por la producción alta de radicales hidroxilo sin ninguna contaminación secundaria. Sin embargo, su eficacia parece estar limitada por el transporte de masa a la superficie del electrodo, de cuyo material, de alto coste, aún se tienen pocos conocimientos en las aplicaciones a escala industrial. La ozonización, en cambio, es un método ampliamente implementado industrialmente con el que

tampoco se producen residuos. No obstante, el O_3 molecular es altamente selectivo, teniendo poca reactividad con el 1,4-dioxano, y la promoción de la oxidación con radicales por la descomposición del O_3 a pH básico no ha sido considerada por ahora.

La degradación de 1,4-dioxano en soluciones sintéticas con agua ultra pura ha sido llevada a cabo mediante varios POAs comunes como Fenton, UV/TiO_2, etc. Sin embargo, hay escasos estudios sobre el tratamiento de aguas residuales industriales con elevadas concentraciones de sales y alcalinidad, que pueden disminuir la eficacia de los POAs. Es más, si las sales y la alcalinidad inicial ofrecen la conductividad necesaria para la OEDC o el tapón de pH adecuado para la ozonización no-selectiva, el posible efecto positivo de la matriz del agua es también un factor importante a estudiar. Además, las condiciones óptimas han de ser determinadas para reducir la cantidad de oxidantes, y se deben estudiar las rutas de degradación, ya que los mecanismos de descomposición por distintos POAs en distintas condiciones de operación pueden afectar significativamente a la eficacia del proceso. Finalmente, se necesitan nuevas metodologías *on-line* para mejorar el control de las reacciones de oxidación y monitorizar los contaminantes clave.

El objetivo general de esta tesis doctoral es aportar nuevos conocimientos que permitan la aplicación de los POAs en el tratamiento de aguas residuales industriales contaminadas con productos químicos recalcitrantes como el 1,4-dioxano, utilizando métodos sostenibles e innovadores para minimizar tanto la producción de residuos como el volumen de oxidante requerido.

Los resultados mostraron que el O_3 era eficaz para degradar el 1,4-dioxano en soluciones sintéticas y condiciones básicas controladas (reducciones de demanda química de oxígeno (DQO) >90%), siendo el pH≥9.0 el factor clave para la viabilidad del proceso. La oxidación anódica no-selectiva con electrodos de diamante dopado con boro (DDB) también resultó en una casi completa reducción de DQO, mientras los sulfatos y bicarbonatos sirvieron como electrolitos eficientes sin presentar el efecto *scavenging* de los radicales reactivos. El uso de microesferas de hierro zero valente (Fe^0) para el tratamiento foto-Fenton dio resultados excelentes a pH neutro, e incluso ligeramente básico (≈100% de DQO), con el que la morfología de las microesferas se mantuvo intacta y no se produjo solubilización del hierro. Paralelamente, se sintetizaron catalizadores inmovilizados de TiO_2 dopados con nitrógeno y flúor (NF-TiO_2) con varios aditivos de nanopartículas de TiO_2 monodisperso, usando distintos métodos de adición. Se obtuvo una formación menor de agregados con una mejor distribución y, además, un rendimiento fotocatalítico superior al agregar TiO_2 monodisperso capa-por-capa sobre el NF-TiO_2 en lugar de la incorporación directa al sol-gel. Por lo tanto, el catalizador compuesto de NF-TiO_2 con TiO_2 monodisperso (NF-TiO_2-monodisp.TiO_2) del método capa-por-capa se utilizó para la degradación de 1,4-dioxano con luz solar. La degradación del compuesto en agua ultra pura (k=0,34±0,02 h^{-1}) se ralentizó en la presencia de aniones inorgánicos (k=0,26±0,01 h^{-1}).

Una vez optimizadas las condiciones de operación de los distintos tratamientos, se trataron las aguas residuales procedentes de una planta química. La alcalinidad inicial de los efluentes industriales resultó ser una ventaja tanto en el proceso foto-Fenton con Fe^0 como en la oxidación con O_3, ya que los carbonatos sirvieron como tapón de pH para evitar la solubilización del hierro y para promover la ozonización por la ruta de radicales no-selectiva en condiciones básicas sin producir ningún efecto *scavenging* significativo. Además, los carbonatos presentes en el efluente fueron también beneficiosos en la OEDC, ofreciendo la conductividad necesaria para la electrolisis. La ozonización en condiciones básicas, la OEDC con DDB y los procesos foto-Fenton con Fe^0 fueron adecuados para el tratamiento de aguas residuales de alta carga orgánica (DQO=450-2400 mg·L^{-1}), siendo la eficacia oxidativa de los

POAs más alta cuanto más DQO inicial tenía el agua, en términos de DQO eliminado por oxidante consumido. En el tratamiento de una muestra típica (DQO≈475 $mg \cdot L^{-1}$), la eliminación de DQO más rápida se obtuvo con el proceso UV foto-Fenton heterogéneo (98% en 40 min), seguida por la OEDC con el DDB (84% en 3 h) y el O_3 (69% en 3 h). Sin embargo, el proceso foto-Fenton solar, que dio resultados comparables a OEDC a tiempos cortos (36-38% en 1 h), se ralentizó al final del experimento (60% en 3 h). Por otro lado, la fotocatálisis solar con NF-TiO_2-monodisp.TiO_2 inmovilizado fue adecuada para descontaminar aguas residuales poco cargadas (DQO≤260 $mg \cdot L^{-1}$), obteniendo casi una completa degradación del 1,4-dioxano junto a un 65% de reducción de la DQO, en 10 h de tratamiento. La inmovilización del catalizador mejora significativamente la ingeniería del proceso, haciendo más económica la separación del mismo. En una aplicación industrial a gran escala, estos tiempos de tratamiento dependerían directamente del diseño de reactor (superficie disponible del catalizador/electrodo, etc).

Asimismo, se establecieron y compararon las rutas de descomposición del 1,4-dioxano por análisis cromatográfico. Paralelamente, se utilizó con éxito una sonda de FTIR (*Fourier transform infrared*) para el control en línea de las reacciones de oxidación. Según la ruta principal, el 1,4-dioxano se degrada inicialmente a etilenglicol diformato y monoformato (EGDF y EGMF). La principal diferencia entre los POAs estudiados se debe a sus condiciones de pH, porque en condiciones básicas los EGDF y EGMF se hidrolizan a etilenglicol. Alternativamente, se pueden producir ácidos metoxiacéticos y acéticos en la descomposición inicial de 1,4-dioxano, siendo esta ruta más significativa en la OEDC y en los procesos foto-Fenton que en ozonización y fotocatálisis donde se detectaron relativamente bajas concentraciones de estos subproductos. Independientemente del POA, la descomposición de los intermediarios principales continuó por la generación de distintos ácidos carboxílicos de cadena corta, siendo el ácido fórmico el producto predominante.

Por último, para comparar los POAs, la posible aplicación industrial del O_3, la OEDC y los procesos foto-Fenton con Fe^0 se evaluó en una pre-estimación de costes considerando el tratamiento de 43800 m^3 de agua industrial al año, con unos 475 $mg \cdot L^{-1}$ de DQO inicial. El objetivo del tratamiento fue reducir un 40% la DQO inicial para alcanzar una biodegradabilidad satisfactoria (≈60%). El proceso UV foto-Fenton resultó la opción más barata para lograr este objetivo, siendo los costes totales anuales de los distintos POAs: 4,1 $€ \cdot m^{-3}$ (UV foto-Fenton) < 4,3 $€ \cdot m^{-3}$ (O_3) < 5,2 $€ \cdot m^{-3}$ (OEDC) < 6,2 $€ \cdot m^{-3}$ (foto-Fenton solar). Debido a la mayor eficacia de oxidación en instalaciones industriales, estos costes de tratamiento serían menores a escala industrial. En este punto de diseño, el proceso foto-Fenton solar sería inviable por el elevado coste de la instalación y el espacio requerido para la unidad del tratamiento, sin embargo, se podría convertir en una alternativa importante para reducciones menores de la DQO (<20%). Por otro lado, para obtener reducciones de DQO mayores del 50%, el O_3 aparece como el proceso más económico, mientras que el coste de la instalación con los electrodos de DDB aún limita su aplicación industrial, a pesar de su alto rendimiento oxidativo.

1. INTRODUCTION

1.1. ORGANIC CONTAMINANTS IN INDUSTRIAL WASTEWATER

Sustainable management of water resources is essential to ensure a circular and green economy, and, therefore, an optimum water-energy-food-health nexus. As the world's population expands by about 80 million people a year, the global water demand is estimated to increase a 55% by 2050 (WWAP, 2009, 2012), whereas the water demand for the manufacturing industry is expected to increase by 400%, leading all other sectors (UNWWAP, 2015). Therefore, water quality is becoming one of the biggest emerging problems of the industrial world, as the aquatic ecosystem is also exposed to a constantly growing number of contaminants (EC, 2006, 2013; OSPAR, 2010). In Europe, the industrial sector accounts for about 40% of total water abstraction of which around 30 km^3 is consumed every year in production (EC, 2010a; Eurostat, 2014). The contaminants released with industrial wastewater may pose a multitude of harmful effects, ranging from specific toxicity for selected organisms, reproductive and mutagenic effects, to carcinogenicity and endocrine disruption (CNRS, 2014; Köhler, 2006). Thus, the treatment of industrial wastewater is crucial to prevent the pile-up of persistent and bio-accumulative chemicals in the environment.

Depending on the characteristics of industrial wastewater, its treatment must be specifically designed (Rosenwinkel *et al.*, 2005; Wang *et al.*, 2004). Industrial effluent flows vary with the size and type of the industry, the degree of water use and the on-site reclamation methods implemented, while the type of contaminants depends on raw materials and additives used in the process (Metcalf&Eddy, 1981; Woodard, 2001). Organic substances constitute one of the main pollutant sources in most industrial plants because of the vast use of cleaning agents, biocides, lubricants, dyes, solvents, stabilizers, etc. (Rosenwinkel *et al.*, 2005). The major producers of organic industrial wastewaters are the following plants and industries (Shi, 2009; Wang *et al.*, 2004):

- Factories manufacturing pharmaceuticals, cosmetics, organic dye-stuffs, glue and adhesives, soaps, synthetic detergents, pesticides and herbicides;
- Tanneries and leather factories;
- Textile and timber industries;
- Polymer plants (plastics, synthetic rubber and man-made fibres);
- Pulp and paper mills;
- Oil refineries and metal processing industry;
- Breweries and fermentation plants;
- Food industry (dairy, meat, seafood, bakery, soft drinks, etc.).

Traditionally, biological treatments are preferred as the most economical option adopted in most of the wastewater treatment plants (WWTPs) (Metcalf&Eddy, 1981; Rosenwinkel *et al.*, 2005). However, a great number of the industrial organic contaminants are biorefractory and even toxic to the bacterial communities in conventional bioreactors (Inanc *et al.*, 2002; Oz *et al.*, 2004). The need for improved wastewater reclamation technologies increases along with the stricter control of toxic and hazardous substances. In the European Union (EU) and in the United States (US), for example, all dischargers are required to treat effluents to a certain degree, as a minimum, while new monitoring, risk management and control policies are adopted every year (EC, 2008, 2014; USEPA, 2014; Woodard, 2001). The Water

Framework Directive (EC, 2000) of the EU is one of the most ambitious and challenging pieces of water legislation in the world, thus, providing a unique regulatory drive for innovation.

1.1.1. Solvents and stabilizers

In the past decades, solvents have become an invaluable material in the manufacture of industrial products as diverse as pharmaceuticals, chemicals, cosmetics, food products, rubber, plastics, adhesives, paints, coatings, etc. (CEFIC, 1997; Deußing, 2014; EC, 2010b). The global demand for industrial solvents shows an average annual growth rate of 3.2% and it is estimated to reach 21.5 million of tons by 2018 (TMP, 2014). Solvents can be used as cleaning products, viscosity adjusters, dispersion medium, surface tension adjusters, plasticisers and/or preservatives (EC, 2010b). Apart from their advantages, these solvents also pose environmental difficulties given that they usually become part of the wastewaters after aqueous finishing works. The mixed aqueous/organic wastes are difficult and costly to separate in terms of both energy requirements and capital equipment (Constable *et al.*, 2007).

Wastewater containing organic solvents is typical for pharmaceutical and fine chemical industries where organic solvents are mostly used for product washing and equipment cleaning, but also as reaction media for separation and purification processes (Grodowska and Parczewski, 2010; Koczka and Mizsey, 2010). In fact, solvents account for 80-90% of mass utilized in a typical pharmaceutical chemical operation, determining the toxicity of the process (Constable *et al.*, 2007). Another growing source of wastewater with solvents is the polymer industry (Deußing, 2014), as the global plastic and rubber production has been growing since 1950s, reaching 288 million tonnes in 2012 and increasing continuously by about 2.7% per year (PEMRG, 2013). Wastewater from plastics production is mainly contaminated by the chemical additives and solvents used in material finishing (e.g. welding, cleaning and coating) and routine maintenance (DeMatteo, 2011).

Table 1.1 lists the commonly used industrial solvents arranged by their functional groups (Grodowska and Parczewski, 2010; Henderson *et al.*, 2011).

Table 1.1: Organic solvents commonly used in industry

Alcohols	***Aliphatics***	***Chlorocarbons***	***Dipolar aprotics***	***Ethers***	***Ketones***
2-Ethyl-hexanol	Cyclohexane	Carbon tetrachloride	Acetonitrile	**1,4-Dioxane**	Acetone
Butanol	Heptane	Chloroform	Dimethylacetamide	1,2-Dimethoxy-ethane	Methyl ethyl ketone
Ethanol	Hexane	Dichloromethane	Dimethylformamide	2-Methyl-tetrahydrofuran	Methyl isobutyl ketone
Isobutanol	Isooctane	Ethylene chloride	Dimethylsulfoxide	Diisopropyl ether	Methyl isopropyl Ketone
Isopropanol	***Aromatics***	Tetrachloro-ethylene	***Esters***	Diethyl ether	
Methanol	Toluene	Trichloroethylene	Butylacetate	tert-Butyl methyl ether	
Propanol	Xylene		Dimethyl carbonate	Tetrahydrofuran	
Propylene glycol	Benzene		Ethylacetate		
			Isopropylacetate		

Several of these solvents are considered undesired either due to their low flash point (e.g. diethyl ether), high volume use (e.g. dichloromethane), ozone depleting properties (e.g. carbon tetrachloride) or, even worse, due to their acute toxicity (e.g. hexane, benzene, dimethylformamide, dimethylacetamide, dimethoxyethane and carbon tetrachloride) and/or carcinogenicity (e.g. benzene, dimethoxyethane, 1,4-dioxane and most of the chlorinated solvents) (CNRS, 2014; Henderson *et al.*, 2011). Although the use of toxic and/or carcinogenic solvents is strongly regulated by international

directives (EC, 2010b) and company-specific guidelines (Henderson *et al.*, 2011), their substitution by other ("greener") solvents is not always possible due to both technical and economic reasons.

Alongside with the use of parent solvents, the addition of stabilizing chemicals (additional solvents or other stabilizer compounds) is inevitable to prevent solvent break down with time and during industrial applications. **Table 1.2** lists the commonly known solvent stabilizers according to their function in preventing solvent breakdown (Mohr, 2010).

Table 1.2: Typical solvent stabilizer compounds

	Antioxidants	***Acid acceptors***	***Corrosion inhibitors***
Function	Prevent reactions that form acids (oxidation by air, light or temperature)	Prevent hydrolysis reactions, neutralizing acids if present	Prevent condensation reactions with alkali metals and their salts
Main organic groups	Phenols, amines, aminophenols	Epoxides, amines	Lewis bases
Typical examples	2-Methyl-2-butene Cresol Methylpyrrole Phenol p-t-Amyl phenol Pyrrole Resorcinol Thymol	Amylene Butoxymethyl oxirane Diisobutylene Epichlorohydrin Methylmorpholine Methylpyrrole Pyridine Triethylamine	1,3-Dioxolane **1,4-Dioxane** Benzotriazoles Ethanolamines Isopropyl nitrate Methyl ethyl ketone Nitromethane tert-Amyl alcohol

These chemicals are meant to be much more persistent than the host solvents, as they are supposed to remain stable throughout the industrial processes without being subjected to oxidation, hydrolysis, pyrolysis, UV light or reactions with alkali metals (Mohr, 2010). Therefore, they are also more persistent to decay in wastewater treatment. For example, 1,4-dioxane, ethanolamines, benzotriazoles and similar stabilizer chemicals are commonly found in municipal WWTP effluents in Germany (Reemtsma *et al.*, 2010; Weiss *et al.*, 2006), Italy (Libralato *et al.*, 2008) and Switzerland (Hollender *et al.*, 2009) as well as in China (Lian *et al.*, 2009; Ruan *et al.*, 2012; Song *et al.*, 2014) and the US (Soliman *et al.*, 2007).

1.1.2. 1,4-Dioxane

One of the persistent and problematic solvents that, despite the stricter discharge limits, is continuously discovered in natural water supplies, is 1,4-dioxane. In Southern California, for instance, the findings of 1,4-dioxane have led to several cases of quarantine of aquifers and closure of valuable wells (Audenaert, 2012; Mohr, 2010; TrojanUV, 2010). This bioaccumulative compound comes into our water resources primarily from industrial use (Mohr, 2010; Razavi, 2013). **Table 1.3** sums up the main physico-chemical properties of this compound (BASF, 2013; Mohr, 2010; USEPA, 2009).

1,4-Dioxane is an aprotic, relatively inert solvent miscible with water in all proportions and capable of solubilizing a large range of organic and even some inorganic compounds (BASF, 2013; Ferro, 2014). It is used in many industrial sectors intentionally (as a solvent, solvent stabilizer, swelling agent, cleaning agent, etc.), but it can also be produced as an industrial by-product (**Table 1.4**; Mohr, 2004, 2010). According to the major producers (BASF, 2013; Ferro, 2014), 1,4-dioxane is an excellent solvent for electrolyte solutions, pharmaceutical and fine chemical synthesis, teflon and fluoropolymer etching with alkali metal dispersions, organometallic reactions, and as polycarbonate swelling agent and activator for metal borohydrates.

Table 1.3: Properties of 1,4-dioxane

1,4-DIOXANE	
Synonyms: *dioxane, glycol ethylene ether, diethylene dioxide, diethylene ether*	
Flammable liquid with a fain, pleasant odor	
Molecular weight, $g \cdot mol^{-1}$	**88.11**
Density, $g \cdot mL^{-1}$ (20°C)	**1.03**
Viscosity, mPa·s (25°C)	**1.19**
Boiling point, °C	**101.1**
Melting point, °C	**11.8**
Flash point, °C	**11**
Specific heat, $J \cdot g^{-1} \cdot K^{-1}$	**1.74**
Vapor pressure, mmHg (20°C)	**37.88**
Octanol-water partition coefficient ($logK_{ow}$)	**-0.27**
Octanol-carbon partition coefficient ($logK_{oc}$)	**1.23**
Polarity	**16.4**
Solubility	**Miscible**
Acid dissociation constant (pKa)	**-2.92**

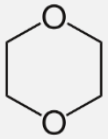

$C_4H_8O_2$

CASNR: 123-91-1
EINICS nr: 204-661-8

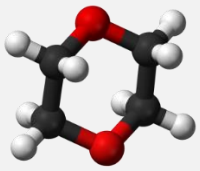

This synthetic cyclic ether is also a hazardous waste for humans and for the environment, classified as a probable human carcinogen both by the EU Directive 2008/105/EC (category 2 carcinogen; CNRS, 2014; EC, 2008) and by the US Environmental Protection Agency (class B2 carcinogen; USEPA, 2010). While it has been published in the 2nd priority list of the European Chemicals Bureau (ECB, 2002) and classified as an emerging contaminant by the USEPA (2009), it is also declared a priority existing chemical in Australia (NICNAS, 1998) and it is regulated as a hazardous substance in Japan (USFJ, 2012), as well as in many other countries.

Table 1.4: 1,4-Dioxane in industry

Direct industrial uses	***By-product of manufacturing***
• Pharmaceutical industry • Polymer (plastics, rubber, fibre) production • Solvent based cleaning • Textile finishing • Printing inks and paints production; printing operations; painting, coating and paint stripping • Cellulose acetate membrane production • Flame retardant production • Aircraft deicing fluid and antifreeze production • Adhesives production	• Production of ethoxylated surfactants, such as: ○ personal care products ○ lubricants ○ contraceptive sponges ○ polyethylene glycol ○ glyphosphate herbicides ○ pesticides • Polyester and resin manufacture

1,4-Dioxane is found in soil and groundwater at solvent recycling and vapour degreasing sites, in landfill gas and landfill leachates, and in industrial wastewater (Mohr, 2004, 2010). Regarding the 1,4-dioxane emissions, what is punctually detected in trace concentrations in the natural waters, measured in rivers/wells/etc., is only the tip of the iceberg. Much more concentrated flows of 1,4-dioxane exit many industrial facilities with their final treated effluent; however, so far this data is usually confidential or still not even reported nor registered in many countries.

1.2. REMOVAL OF 1,4-DIOXANE BY CONVENTIONAL TREATMENTS

Conventional wastewater treatment facilities usually comprise of various combinations of physicochemical and biological treatment steps. The general process of wastewater treatment by industrial companies can be roughly divided into production-integrated techniques and post-positioned wastewater purification (Rosenwinkel *et al.*, 2005). In case of wastewater containing solvents, distillation is a typical production-integrated method for solvent recovery. Several other physicochemical methods (e.g., carbon adsorption) can be used for solvents removal, mostly in 'end-of-pipe' units. When possible, biological treatment is traditionally the favoured option for removing organic contaminants and reducing chemical oxygen demand (COD) from industrial wastewater.

1.2.1. Physico-chemical methods

Solvent recovery by distillation

Distillation is one of the most widely used technologies to remove the volatile organic compounds (VOCs) from wastewater containing organic solvents like ethanol, ethyl-acetate, toluene, halogenated solvents, etc. Industrial case studies show that distillation is a feasible method of solvent recovery with a reasonable investment cost, allowing a simultaneous extraction of the impurities, reuse of the distilled materials and disposal of the pollutants in concentrated form (Koczka and Mizsey, 2010; Toth *et al.*, 2011). The disadvantage of distillation is that the separation of several solvents with similar boiling points is usually a very difficult task and the separation of azeotropic mixtures with simple distillation is not possible at all (Toth *et al.*, 2011). When it comes to the wastewater treatment, the distillation of 1,4-dioxane has been attempted; however, due to its boiling point (101 °C; **Table 1.3**) similar to the one of water, it is considered an excessively expensive method (Adams *et al.*, 1994). On the other hand, when a host solvent with a lower boiling point (e.g. dichloromethane, 39.75°C) is boiled and recycled in an industrial application, the stabilizers that tend to have lower vapour pressure and/or higher boiling point, like 1,4-dioxane, would more likely end up concentrated in the still bottoms, ultimately posing an environmental hazard (Mohr, 2010).

Air stripping

Air stripping is also a common method for removing VOCs from water, as the relationship between solubility and volatility is optimal in this contaminant group. Air stripping is a non-destructive transfer of contaminants from the liquid phase to the vapour phase, which often requires a subsequent treatment by, for example, carbon adsorption and thermal destruction before discharging the air to the atmosphere (Koczka and Mizsey, 2010; Mohr, 2010). Nevertheless, although 1,4-dioxane is highly volatile in its pure form, its infinite water solubility prevents its efficient removal from water by air stripping. For instance, in an optimizing test carried out at the US Air Force Plant 44 in Arizona, the maximum removal rate of 1,4-dioxane reached was only about 10% even with air:water ratios as high as 291:1 (EarthTech, 2004; Mohr, 2010).

Carbon adsorption

Carbon adsorption is also a recognized technology for the removal of organic contaminants. Granular activated carbon (AC) can be used as a replacement for anthracite media in conventional filters, providing both adsorption and filtration (Deegan *et al.*, 2011). However, carbon adsorption is not considered an efficient method for the removal of 1,4-dioxane. This organic chemical had the lowest overall adsorption rates compared to the other solvents, when the sorption effectiveness of various

types of AC were tested for several organic contaminants, including 1,4-dioxane, acetone, acetonitrile, benzene, methanol and toluene (Johns *et al.*, 1998; Mohr, 2010). Furthermore, the regeneration and disposal of carbon may present also important environmental considerations (Deegan *et al.*, 2011).

Membrane processes

Several membrane applications have been assessed for the removal of organic contaminants from water (Kegel *et al.*, 2010; Kim *et al.*, 2007; Snyder *et al.*, 2007; Yangali-Quintanilla *et al.*, 2010). Microfiltration and ultrafiltration are generally not fully effective in removing micropollutants that may be 100-1000 times smaller than the membranes (Deegan *et al.*, 2011; Snyder *et al.*, 2007). Nevertheless, the pressure-driven membrane processes, nanofiltration and reverse osmosis, have shown efficient removal of several personal care products, pharmaceuticals and pesticides, including various endocrine disrupting chemicals (Kegel *et al.*, 2010; Kim *et al.*, 2007; Snyder *et al.*, 2007; Yangali-Quintanilla *et al.*, 2010).

There are no reports on membrane processes for the removal of elevated concentrations of 1,4-dioxane from highly loaded industrial wastewater; however, the studies on trace pollutant removal suggest that it would not be a viable option. While reverse osmosis followed by AC filtration was studied for a drinking water treatment, achieving very high removal efficiencies for nearly all of the 47 studied micropollutants, only a partial removal of 1,4-dioxane was obtained (Kegel *et al.*, 2010). Alike, when tight nanofiltration membranes were proven an effective barrier for a variety of organic contaminants, microconcentrations of 1,4-dioxane already gave difficulties and only partial removal was achieved (Yangali-Quintanilla *et al.*, 2010).

1.2.2. Biological wastewater treatment

Biological processes are considered the most traditional and less expensive wastewater treatment methods (Metcalf&Eddy, 1981; Rosenwinkel *et al.*, 2005). Biodegradation of various organic contaminants such as chlorinated solvents and petroleum hydrocarbons has been demonstrated using both aerobic and anaerobic processes. Typical aerobic treatments are activated sludge; membrane batch reactors and sequence batch reactors (Chen *et al.*, 2008; Libralato *et al.*, 2008; Raj and Anjaneyulu, 2005), whereas the anaerobic options include anaerobic sludge reactors, anaerobic film reactors and anaerobic filters (Enright *et al.*, 2005; Gangagni Rao *et al.*, 2005; Inanc *et al.*, 2002; Oktem *et al.*, 2008).

However, highly loaded solvent effluents incur an excessive COD loading and concurrent nutrient deficiency that can be problematic (Freedman *et al.*, 2005). For example, the conventional activated sludge process is considered unsuitable for the treatment of wastewater with COD levels higher than 4000 $mg \cdot L^{-1}$ (Raj and Anjaneyulu, 2005). Moreover, if solvents, stabilizers and other chemical additives occur in high concentrations, an inhibiting or even toxic impact on the conventional biological treatment methods is expected (Inanc *et al.*, 2002; Oz *et al.*, 2004).

1,4-Dioxane as a cyclic ether is a relatively stable molecule with strong internal bonding, hence it is not readily biodegradable as a sole source of carbon and energy (Mohr, 2010), especially when high strength industrial waters are under consideration. Although works on successful bioremediation of 1,4-dioxane at low concentrations, in the presence of extra carbon source and using modified reactor configurations have been published (Han *et al.*, 2012a; Shin *et al.*, 2010; Zenker *et al.*, 2000, 2004), and a substantial amount of research has been done on specific organisms that ultimately degrade this compound (Shen *et al.*, 2008; Shin *et al.*, 2010), the reports on the conventional full scale WWTP performances in different countries demonstrate that 1,4-dioxane usually passes the traditional biological reactors unchanged and remains in the final effluent (Mohr, 2010; Skadsen *et al.*, 2004; Zenker *et al.*, 2003).

1.2.3. Advanced oxidation processes – an alternative

Through an extensive research during the last two decades, advanced oxidation processes (AOPs) have shown great capacity to decontaminate effluent streams containing biorefractory substances (Andreozzi *et al.*, 1999; Comninellis *et al.*, 2008). 1,4-Dioxane removal from synthetic solutions with ultrapure water has been achieved with various common AOPs (Chitra *et al.*, 2012; Maurino *et al.*, 1997; Merayo *et al.*, 2014). Therefore, this alternative has been chosen for the development of this doctoral thesis for the treatment of industrial wastewaters containing 1,4-dioxane.

Following chapters cover the principles, advantages, major limitations and the level of implementation of the most commonly known AOPs, as well as the level of application of these AOPs for the treatment of waters contaminated with 1,4-dioxane.

1.3. PRINCIPLES OF ADVANCED OXIDATION PROCESSES

The AOPs are defined as oxidation processes based on the generation of hydroxyl radicals (OH•) in sufficient quantity for water treatment (Glaze *et al.*, 1987). The OH• is a highly reactive and non-selective chemical species with the second largest redox potential (2.80 V at 25°C; Ullmann's, 1991) after fluorine.

In general, AOP is a wide term used for multiple systems and their combinations that could include various oxidants, catalysts, irradiation, electrical charge, etc. The most typical AOPs are ozone (O_3) based systems, Fenton processes and photochemical processes, like titanium dioxide (TiO_2)-based photocatalysis, photo-Fenton processes, etc. On the other hand, electrochemical methods, like anodic electro-oxidation and electro-Fenton are also well-known, and the processes based on conductive diamond technology have gained a lot of attention is the last 10 years.

1.3.1. Ozonation processes

In O_3 based processes (**Fig. 1.1**), the destruction of organics can occur either *via* direct oxidation by molecular O_3 or through indirect reactions with radical species (OH•, HO_2•) formed when O_3 decomposes in water (Glaze, 1986; Glaze *et al.*, 1987; Hoigne and Bader, 1976; Staehelin and Hoigne, 1982). The radical mechanism is favoured in basic conditions in the presence of hydroxide anions (OH^-), but it is also very commonly initiated and/or accentuated in the presence of hydrogen peroxide (H_2O_2) through the adduct (HO_5^-) formation (Fischbacher *et al.*, 2013; Sein *et al.*, 2007).

While molecular O_3 is highly selective, mostly limited to unsaturated aliphatics and aromatics (Hoigne and Bader, 1976), the radical reactions are non-selective and several orders of magnitude faster than the direct oxidation (Hoigne and Bader, 1983; Ross, 1977), being, thus, often the desired pathway (El-Din *et al.*, 2006; Suh and Mohseni, 2004). However, due to the high reactivity, the radicals could also be spent to undesirable reactions with matrix compounds (Adams *et al.*, 1994; Chiang *et al.*, 2006; Hoigne and Bader, 1976), and, depending on the wastewater and its major contaminants, the selective pathway could be preferred (Merayo, 2014).

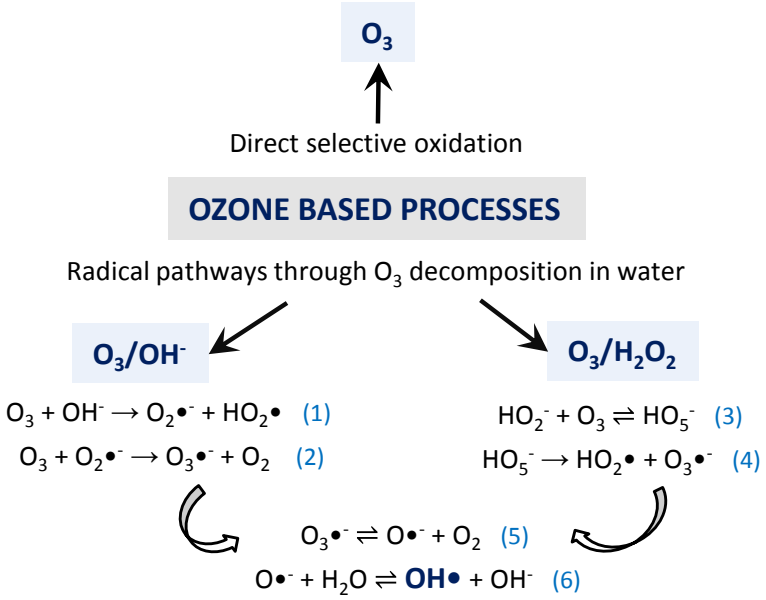

Fig. 1.1: Major ozonation mechanisms

1.3.2. Fenton processes

The classical Fenton process is based on the electron transfer reaction between H_2O_2 and ferrous iron (Fe^{2+}) (**Eq. 7**; Harber and Weiss, 1934). The main factors affecting the Fenton process are the concentration of reagents, the type of iron source and the pH, the optimum value being in the range of 2.5-3.0 (Hermosilla *et al.*, 2009a; Pontes *et al.*, 2010).

$$Fe^{2+} + H_2O_2 \rightarrow Fe^{3+} + OH^- + OH\bullet \qquad (7)$$

The application of UV radiation enhances the conventional Fenton process by reducing the sludge production by a photo-recovery of the catalytic Fe^{2+}, and increasing the mineralization rates by the photo-decarboxylation of the refractory ferric (Fe^{3+}) carboxylate complexes (**Eqs. 8** and **9**; Hermosilla *et al.*, 2009a; Kavitha and Palanivelu, 2004; Prousek *et al.*, 2007).

$$Fe(III)OH^{2+} + h\nu \rightarrow Fe^{2+} + OH\bullet \qquad (8)$$

$$Fe(III)(RCO_2)^{2+} + h\nu \rightarrow Fe^{2+} + CO_2 + R\bullet \qquad (9)$$

Alternatively, zero valent iron (Fe^0) from solid sources may be used to produce Fe^{2+} (**Eq. 10**) for the Fenton reaction (**Eq. 7**). UV radiation significantly contributes to the activation of Fe^0 and generation of Fe^{2+} (**Eq. 11**; Cooper *et al.*, 2009; Prousek *et al.*, 2007). The use of Fe^0 has been reported to reduce the sludge production, as Fe^{3+} is recycled in a so-called pseudo-catalytic Fe^0/Fe^{2+} system (**Eq. 12**; Bremner *et al.*, 2006; Kallel *et al.*, 2009a; Prousek *et al.*, 2007).

$$Fe^0 + H_2O_2 \rightarrow Fe^{2+} + 2OH^- \qquad (10)$$

$$Fe^0 + h\nu \rightarrow Fe^{2+} + 2e^- \qquad (11)$$

$$2Fe^{3+} + Fe^0 \rightarrow 3Fe^{2+} \qquad (12)$$

1.3.3. Photocatalysis

The TiO_2-photocatalysis is based on the photon-assisted generation of catalytically active species, when TiO_2 interacts with light of energy greater than the band gap of the semiconductor, generating electron-hole pairs when an electron is excited from the valence band (VB) to the conduction band (CB) (**Eq. 13**, **Fig. 1.2**; Fujishima *et al.*, 2000; Linsebigler *et al.*, 1995).

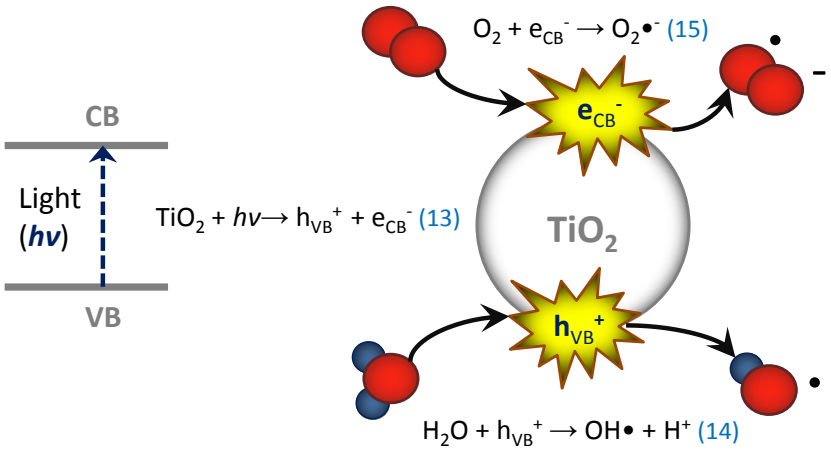

Fig. 1.2: Photon-assisted generation of catalytically active species

The band gap energy of anatase TiO_2 is 3.2 eV, therefore, UV light (λ<387nm) is required; however, modified TiO_2-based materials could possess enhanced catalytic properties that enable using a broader

light spectrum (Pelaez *et al.*, 2009). There are several techniques to enhance the photocatalytic properties of TiO_2, including doping, dye-sensitization, noble metal deposition, and coupled semiconductors (Pelaez *et al.*, 2012a).

The traditional TiO_2-photocatalysis in suspension requires a subsequent filtration, increasing the treatment cost. The immobilization of the photocatalyst would greatly enhance the process engineering by straight-forward separation and recovery of the catalyst from process stream (Pelaez *et al.*, 2010), but it could also restrict the reactant mass transfer (Vescovi *et al.*, 2010), which is the main obstacle in the ongoing research in immobilized photocatalysis.

1.3.4. Conductive-diamond electrochemical oxidation

The conductive-diamond electrochemical oxidation (CDEO) differs from the conventional electrolytic method, as instead of the anodic generation of oxidants like chlorine and hypochlorite that selectively react with the organics in the solution bulk, the oxidation is mainly expected to occur directly on the electrode surface by means of physically adsorbed OH• generated from water (**Eq. 16**), leading to the complete oxidation of organic compounds (Montilla *et al.*, 2002; Panizza *et al.*, 2001).

$$BDD + H_2O \rightarrow BDD(OH\bullet) + H^+ + e^- \qquad (16)$$

Boron doped diamond (BDD) is considered the most efficient electrode material for anodic oxidation due to its high over potential for water electrolysis, high stability, good conductivity, inert character and weak adsorption properties. Such anodic oxidation does not need a large amount of additional chemicals or O_2 feed to cathodes, with no tendency to produce secondary pollution. The efficiency of the technology only seems to be limited by the transport of the pollutants to the anodic surface (Comninellis *et al.*, 2008; Rodrigo *et al.*, 2010).

Comparison of the most commonly used AOPs is presented in **Table 1.5**:

TABLE 1.5: Comparison of the common AOPs

	Advantages	***Disadvantages***
$Fe^{2+}/H_2O_2/UV$	low material cost, very high oxidation power	high energy demand*, very corrosive treatment, need for acidification and posterior neutralization, production of iron sludge
Fe^{2+}/H_2O_2	low material cost, low energy demand, high oxidation power	production of refractory ferric-complexes, very corrosive treatment, need for acidification and posterior neutralization, production of iron sludge
O_3	no residues, in-situ generated, oxidant, average oxidation power	medium to high energy demand
TiO_2/UV	low production of residues, cheap material, mild pH conditions, average oxidation power	very high energy demand*, need for catalyst separation by filtration
CDEO	no residues, no need for additional oxidants, mild pH conditions, high oxidation power	high capital cost, medium to high energy demand

**energy demand in UV-enhanced processes can be drastically reduced by employing solar light*

1.4. LEVEL OF IMPLEMENTATION OF AOPs

In terms of actual on-site and pre-industrial implementation considering the latest scientific publications on the application of AOPs used for industrial wastewater treatment in pilot and full scale (**Table 1.6**), Fenton (including photo-Fenton) and O_3-based processes are the most common ones, whereas fewer reports are available on TiO_2-photocatalysis. CDEO seems to be gaining more attention lately, although only pilot scale studies have been published so far. Total mineralization by AOPs is normally not the aim, as it would be too expensive, and AOPs for highly contaminated waters are nearly always used in combination with traditional biological methods, either as a pre-treatment for biodegradability enhancement or as a polishing step after the conventional treatment system.

TABLE 1.6: Latest examples of common AOPs for industrial wastewater treatment in pilot and full scale

Wastewater	*AOP*	*AOP scale*	*Process stage and results*
[a]**Tank truck cleaning wastewater** COD=880 mg·L^{-1}	**O_3** **O_3/H_2O_2**	pilot scale 35-L batch reactor	Post-treatment to an industrial WWTP (reverse osmosis concentrate). O_3 was more effective in COD removal than O_3/H_2O_2.
[b]**Pharmaceutical wastewater** COD=35-40 g·L^{-1}	**Fe^{2+}/H_2O_2**	Industrial scale (2-3 $m^3 \cdot d^{-1}$) 2-m^3 reaction tank	45-50% COD removal. Pre-treatment to an aerobic process in sequencing batch reactors
[c,d]**Mixed industrial wastewater** (textile, paint, ceramic, pharmaceutical, metallurgical, food and chemical)	**Fe^{2+}/H_2O_2** - industrial WWTP + **O_3** pilot (+ NF, UF) - different combinations	industrial and pre-industrial scale WWTP with a full capacity of about 200,000 $m^3 \cdot y^{-1}$	Industrial: Fe^{2+}/H_2O_2 as pre-treatment for hazardous waste streams before biological process. Pre-industrial: a) O_3 as post-treatment to biological process to recycle the effluent into physicochemical stage; b) O_3 as final step after NF proceeding sand-filtration to discharge the effluent.
[e]**Landfill leachate** COD=1750 mg·L-1	**Fe^{2+}/H_2O_2** followed by **CDEO**	pilot plant (50 L·h^{-1}) 1.05-m^2 BDD in stacks	Post-treatment to a full-scale on-site activated sludge process. Almost complete removal of COD and N-NH_4.
[f]**Polyester manufacturing wastewater** **[dioxane]=600 mg·L^{-1}**	**$UV/Fe^{2+}/H_2O_2$**	pilot scale 10 UV-C lamps 10-m^3 reactor	90% 1,4-dioxane removal. Pre-treatment to an activated sludge process.
[g]**Rinse water with pesticide residues** DOC=500 mg·L^{-1}	**$Solar/Fe^{2+}/H_2O_2$**	industrial plant CPC of 150 m^2 1060-L reactor	35% DOC removal. Pre-treatment to a biological treatment (IBR). Total efficiency was 84%.
[h]**Winery wastewater** COD=2958 mg·L^{-1}	**$Solar/TiO_2/H_2O_2$** **$Solar/Fe^{2+}/H_2O_2$**	pilot scale CPC of 2.08 m^2 40 L recirc. volume	COD lower than 150 mg· L^{-1} was reached in agreement with the discharge limits into receiving waters.

[a]De Schepper *et al.*, 2012; [b]Tekin *et al.*, 2006; [c]Ferella *et al.*, 2013; [d]Macolino *et al.*, 2009; [e]Urtiaga *et al.*, 2009; [f]So *et al.*, 2009; [g]Zapata *et al.*, 2010; [h]Souza *et al.*, 2013.

When it comes to the heavily loaded industrial wastewaters contaminated with strongly regulated substances, the literature on AOPs in full scale applications is scarce and the access to case studies is complicated because they belong to industrial protected know-how. Nevertheless, there are multiple lab-scale reports on the treatment of industrial wastewaters containing solvents, stabilizers and other biorefractory additive compounds by commonly known AOPs (**Table 1.7**). According to the general tendency, very high COD removals (up to 90%) are obtained in prolonged experiments, whereas most of the authors report possible bioaugmentation at shorter treatment times.

TABLE 1.7: Latest examples of common AOPs for solvent and stabilizer removal from industrial wastewaters in lab scale studies

AOP	*Wastewater*	*Major contaminants*	*Treatment results*
[a]O_3	Metalworking fluid wastewater	alkalonamine corrosion inhibitors	70% COD removal, pre-treatment to a biological process
[b]Fe^{2+}/H_2O_2	Acrylic fibre manufacturing wastewater	solvents, plasticizers, polymerization precursors and inhibitors, etc.	47% COD removal, BOD/COD ratio increased to 0.7
[c]**High-temp. Fenton**	Powerplant wastewater from pipeline cleaning	corrosion inhibitors, foaming agents, etc.	>90% COD removal, biodegradability was increased
[d]H_2O_2/UV	Bulk drug (cresol) plant wastewater	cresol and sulfites	bioaugmentation was achieved
[e]TiO_2/UV	Refinery wastewater	refining solvents and petroleum hydrocarbons	up to 90% COD removal
[f]**CDEO (BDD)**	Acrylic fibre manufacturing wastewater	solvents, stabilizers, oils, PAN low polymers	60% COD removal was sufficient for pre-treatment

[a]Jagadevan *et al.*, 2013; [b]Wei *et al.*, 2013; [c]Pliego *et al.*, 2013; [d]Pandya, 2007; [e]Saien and Nejati, 2007; [f]Zhang *et al.*, 2010.

Very few scientific reports exist on the treatment of highly loaded industrial wastewaters containing 1,4-dioxane (So *et al.*, 2009; **Table 1.6**). However, there are numerous studies on oxidizing synthetic 1,4-dioxane solutions in ultrapure water (**Table 1.8**).

TABLE 1.8: State of the art in 1,4-dioxane degradation in synthetic water solutions by common AOPs in lab scale studies

AOP	$C_{0\_1,4\text{-dioxane}}$ $mg \cdot L^{-1}$	*Studied pH values*	*Removal at optimal conditions*	*Metabolites study*
[a]Fe^{2+}/H_2O_2/UV	8810	3	<90% 1,4-dioxane in 30 min (100% in 1,75 h)	-
[b]Fe^{2+}/H_2O_2/UV	50	3	~100% 1,4-dioxane in 30 min	yes
[c]Fe^{2+}/H_2O_2	200…500	3	98% 1,4-dioxane in 30 min	-
[d]Fe^{2+}/H_2O_2	248	2.8	65% COD in the end of the reaction	yes
[a]Fe^{2+}/H_2O_2	8810	3	100% 1,4-dioxane in 8 h	-
[b]Fe^{2+}/H_2O_2	50	3	<30% 1,4-dioxane in 30 min	-
[e]CDEO	260...780	1.7, 7, 12.4	>95% COD in 5 h	-
[f]O_3/H_2O_2/UV	20…100	4, 7, 10	94% COD in 90 min	-
[g]TiO_2/UV	36	3, 7, 11	100% 1,4-dioxane in 3 min	-
[h]TiO_2/UV	14	5.5, 11	~90% TOC in 60 min	yes
[i]H_2O_2/UV	88	5	~100% 1,4-dioxane in 10 min	yes
[j]O_3/H_2O_2	3…180	5.8, 9, 11	>90% 1,4-dioxane in 30 min	-
[f]O_3/UV	20…100	as is*	52% COD in 90 min	-
[f]O_3	20…100	as is*	35% COD in 90 min	-

[a]Chitra *et al.*, 2012; [b]Kim *et al.*, 2008; [c]Ghosh *et al.*, 2010; [d]Merayo *et al.*, 2014; [e]Choi *et al.*, 2010; [f]Kwon *et al.*, 2012; [g]Vescovi *et al.*, 2010; [h]Maurino *et al.*, 1997; [i]Stefan and Bolton, 1998; [j]Suh and Mohseni, 2004.
*Initial pH of 1,4-dioxane solution in ultrapure water (pH=5.5…5.8).

The fastest initial decomposition of 1,4-dioxane in synthetic solution was observed in photo-Fenton treatment (Chitra *et al.*, 2012; Kim *et al.*, 2008), whereas the mechanism of both classical Fenton and photo-Fenton processes has been studied by various authors (Chitra *et al.*, 2012; Ghosh *et al.*, 2010; Kim *et*

al., 2008; Merayo *et al.*, 2014). The degradation of 1,4-dioxane was also achieved by anodic oxidation on BDD electrodes (Choi *et al.*, 2010), O_3-based processes combined with H_2O_2 (Suh and Mohseni, 2004) and/or UV light (Kwon *et al.*, 2012), H_2O_2/UV oxidation (Stefan and Bolton, 1998) and heterogeneous photocatalysis with TiO_2 suspension (Maurino *et al.*, 1997; Vescovi *et al.*, 2010).

Ozonation has been rendered unfeasible to oxidize 1,4-dioxane due to very low reaction rates by molecular O_3 (Adams *et al.*, 1994; Kwon *et al.*, 2012; Suh and Mohseni, 2004); however, the promotion of radical pathway at basic conditions (*Section 1.3.1.*) was never studied. As O_3 is an easily implemented technique for treating large water flows at full scale (Bertanza *et al.*, 2013; Oller *et al.*, 2011), it is of great interest to re-assess its application for 1,4-dioxane removal by maintaining an adequate pH range.

On the other hand, the substantial concentrations of salts and bicarbonate alkalinity often present in wastewaters can influence the effectiveness of AOPs (Adams *et al.*, 1994; Beckett and Hua, 2000; Burns *et al.*, 1999; Maurino *et al.*, 1997). Nevertheless, their effect on the removal of 1,4-dioxane from heavily loaded industrial effluents by AOPs has not been assessed yet. For example, electrolysis requires the presence of electrical conductivity, whereas the use of bicarbonate as a supporting electrolyte has generally been overlooked, although its presence in industrial wastewater is often inevitable.

Regarding Fenton processes, the production of Fe^{3+} sludge and the optimum acid pH required for the process are still important drawbacks that restrict its implementation for environmental applications (Pignatello *et al.*, 2006; Son *et al.*, 2009). Although employing irradiation enables reducing the sludge production (Hermosilla *et al.*, 2009a; Kavitha and Palanivelu, 2004; Prousek *et al.*, 2007), considerable amounts of residues are still produced. Nevertheless, none of the papers on the 1,4-dioxane treatment by photo-Fenton processes, considers the application of Fe^0. It would be important to study the feasibility of heterogeneous photo-Fenton in milder pH conditions to avoid iron leaching.

Considering photocatalysis, the traditional method with P25-TiO_2 in slurry suspension requires a subsequent filtration step to remove the catalyst from water. The immobilization of the catalyst would greatly enhance the process engineering (Pelaez *et al.*, 2010), but it could also restrict the reactant mass transfer (Vescovi *et al.*, 2010), which is the main obstacle to the industrial viability of supported photocatalysis. Several methods are used to enhance the properties of TiO_2, including doping, dye-sensitization, noble metal deposition, and coupled semiconductors (Pelaez *et al.*, 2012a). With regard to degradation of 1,4-dioxane, however, very few studies deal with the modified immobilized TiO_2. Nakajima *et al.* (2009) reported only 30% removal after 4 h of UV radiation using TiO_2–$Cs_{2.5}H_{0.5}PW_{12}O_{40}$ hybrid films. There are no studies on the removal of 1,4-dioxane from concentrated industrial effluents with salts and alkalinity, although the influence of the water matrix is an important factor to study.

Moreover, no research has been published on the decomposition routes of 1,4-dioxane by O_3, immobilized photocatalysis, CDEO nor heterogeneous photo-Fenton on Fe^0, although the understanding of the degradation mechanism could play a great role in process optimization. Stefan and Bolton (1998) proposed a degradation mechanism for 1,4-dioxane in UV/H_2O_2 oxidation, and Kim *et al.* (2008) suggested a reaction pathway for homogeneous photo-Fenton reaction, both by exhaustive series of chromatographic methods. As an alternative to the expensive and time-consuming chromatographic analysis, on-line Fourier transform infrared (FTIR) spectroscopy has been successfully applied for the *in situ* control of the intermediate species during the classical Fenton process (Merayo *et al.*, 2014). Since the different AOPs involve multiple possible transformations of catalyst and reactive radical species, different degradation routes could be expected, depending on the treatment. Moreover, running information of the whole reaction during the experiment would not only provide a straightforward understanding of the reaction mechanism, but also an accurate optimization of the reagent doses and reaction time, thus reducing the treatment cost.

2. OBJECTIVES OF THE RESEARCH

As the public awareness of environmental protection and water pollution increases year by year alongside with the global water consumption by manufacturing industry, the legislation on wastewater discharge is also becoming stricter and new monitoring, risk management and control policies are adopted every year (EC, 2008, 2014; USEPA, 2014; Woodard, 2001). Therefore, improved wastewater reclamation technologies are needed to meet the stringent discharge limits of the toxic and hazardous substances.

The elaboration of this PhD thesis was driven by an actual industrial case of water contamination by 1,4-dioxane that was not degraded by the conventional wastewater treatment in a biological unit and remained, thus, in the final effluent at high concentrations. As explained above, the traditional methods of treating wastewaters with organic solvents fail to remove 1,4-dioxane due to its high solubility, low vapour pressure and biorefractory nature (*Chapter 1.2*). Nevertheless, AOPs have shown great capacity of removing this compound from synthetic solutions with ultrapure water in lab scale experiments (*Chapter 1.4*).

Although the substantial concentrations of salts and bicarbonate alkalinity often present in wastewaters can abate the effectiveness of AOPs (Adams *et al.*, 1994; Beckett and Hua, 2000; Burns *et al.*, 1999; Maurino *et al.*, 1997), their effect on the removal of 1,4-dioxane from heavily loaded industrial effluents by AOPs has not been assessed yet (*Chapter 1.4*). Furthermore, if the initial salts and alkalinity could actually provide the necessary conductivity for electrolysis or the correct pH buffer for non-selective ozonation treatment by radical production mechanism, the possible beneficial influence of water matrix is also an important factor to study. The classical Fenton processes and photocatalysis with suspended TiO_2, on the other hand, have various disadvantages, like the cost of UV radiation, the production of iron sludge and the need for catalyst separation by filtration (*Chapter 1.3*). It is of great interest to search for more cost-effective and less residues-producing alternatives, e.g. by employing solar light, using solid iron sources and milder pH conditions to avoid iron leaching; developing new photocatalysts with an improved properties; and immobilizing the titanium-based materials to enhance process engineering and catalyst separation. Moreover, optimized conditions must be determined, in order to reduce the amount of oxidants involved, and decomposition pathways must be studied, as the routes of degradation in different AOPs in different operational conditions could significantly affect the process efficiency. Finally, new on-line methodologies need to be developed to improve the control of the oxidation reactions and to monitor the target pollutants.

Therefore, the objective of this PhD thesis is to generate new knowledge on the applicability of AOPs for the treatment of industrial wastewaters containing recalcitrant contaminants like 1,4-dioxane, using greener and more environmentally friendly methods and minimizing both the production of residues and the volume of oxidants.

To achieve the main goal of this thesis, the following specific objectives were defined:

1. To re-assess the use of ozonation as an easily implemented process at industrial scale by promoting the radical pathway for a better (non-selective) oxidation by OH•, studying the influence of pH and carbonaceous alkalinity (***Publication I***).
2. To study the anodic oxidation of 1,4-dioxane on BDD, the most successful anode material for non-selective mineralization of organics, by assessing the use of different electrolyte salts and the effect of initial alkalinity of the industrial wastewaters (***Publication II***).

3. To study the use of Fe^0 for heterogeneous photo-Fenton processes under different light sources, assessing the influence of pH, reagent dose and carbonaceous alkalinity in order to work under milder pH conditions and to avoid iron leaching (***Publication III***).
4. To develop novel catalytic materials for immobilized solar photocatalysis for an improved decontamination of wastewaters with different organic contaminants and to assess the photocatalytic degradation of 1,4-dioxane by a previously selected supported catalyst, assessing the effect of different water matrices (***Publications IV and V***).
5. To study the routes of 1,4-dioxane decomposition in different AOPs, applying an on-line FTIR technology and chromatography analysis to monitor the reaction intermediates (***Publications I, III and V-VII***).
6. To perform a comparative study for the evaluation of the different AOPs under concern in energetic/economic terms (***Publication VII***).

Fig. 2.1 shows the schematic summary of the performed investigation to achieve the global objective of this thesis.

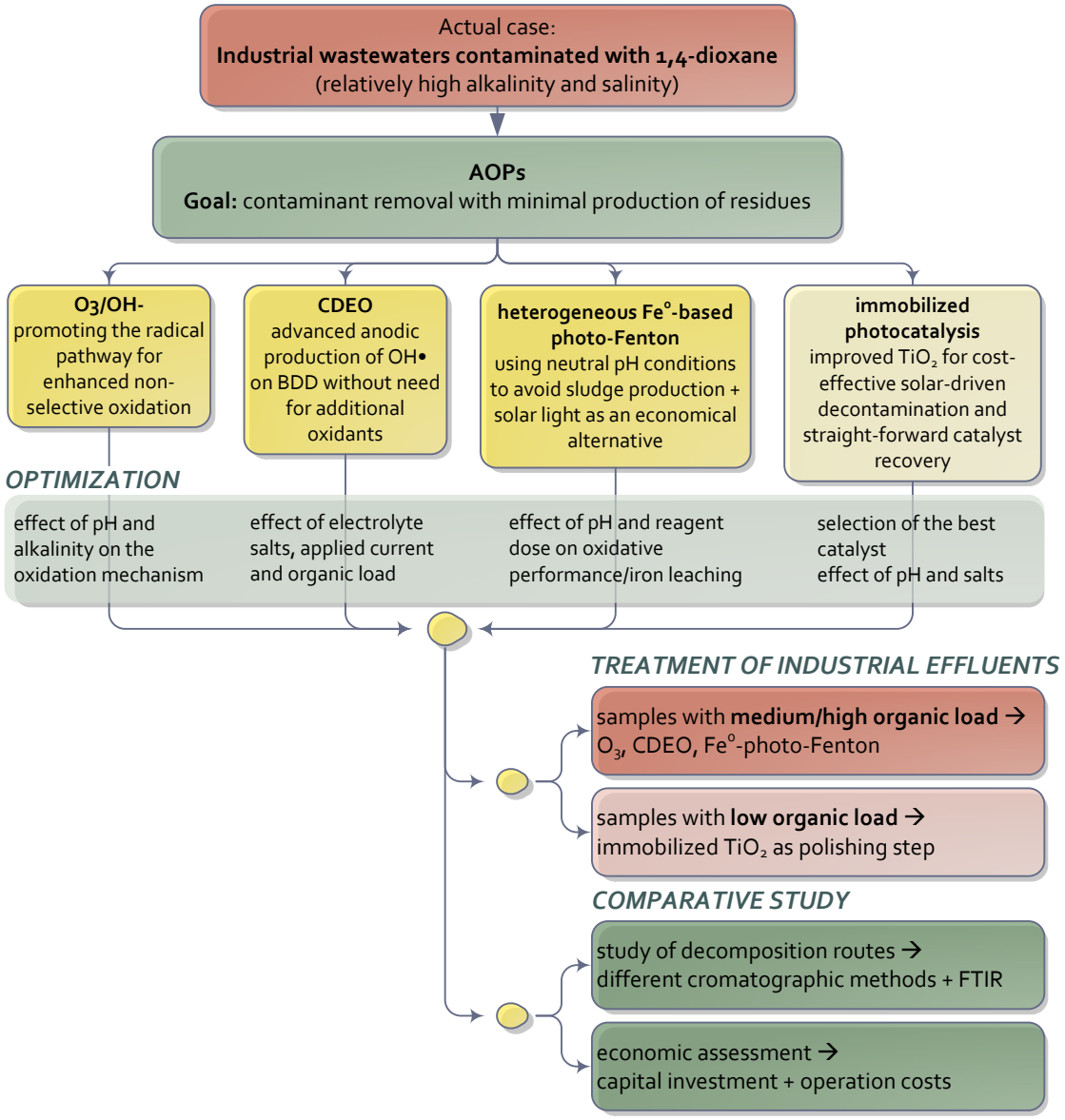

Fig. 2.1: Schematic summary of the performed research to achieve the global objective of this thesis.

3. METHODOLOGY

Two types of experiments were carried out: the initial optimization experiments on synthetic water solutions and the experiments under optimized conditions conducted with industrial wastewaters.

3.1. WASTEWATER SAMPLES

The optimization experiments were carried out on a synthetic solution of 1,4-dioxane, prepared with ultra-pure deionized water after pH adjustment to a desired value. When desired, the conductivity and ionic strength of the solution were increased by adding different inorganic salts of sodium, specified throughout the text. All the used reagents were of analytical grade.

Optimal conditions found in the experiments with synthetic waters were applied to treat actual industrial wastewaters of relatively high alkalinity and conductivity (samples 1-4, **Table 3.1**). These industrial effluents of a particular chemical factory manufacturing plastics were still contaminated with 1,4-dioxane after a biological treatment step. In some cases (samples 2 and 3), its industrial by-product 2-methyl-1,3-dioxolane (MDO) was also present.

TABLE 3.1: Characterization of industrial wastewaters from a chemical industry

	sample 1	***sample 2***	***sample 3***	***sample 4***
COD, mg·L^{-1}	475±25	1,360±40	2,300±100	250±10
1,4-dioxane, mg·L^{-1}	265±15	290±10	315±15	135±5
MDO, mg·L^{-1}	-	415±15	625±15	-
Total alkalinity, mgCaCO$_3$·L^{-1}	950±50	950±50	1,050±50	275±5
pH	8.8±0.1	7.9±0.1	6.8±0.1	6.9±0.1
Conductivity, mS·cm^{-1}	2.0±0.1	2.0±0.1	2.2±0.1	2.4±0.1

The samples sent from the fabric varied in time and the selection of the samples to treat with different AOPs depended directly on the actual manufacturing process of the industrial plant at the time of experimentation.

3.2. ANALYSIS

The preservation of the samples and all the analyses described below were made according to the standard methods for the examination of water and wastewaters (APHA et al., 2005). When required, temperature was kept constant using a thermostatic bath (Model FL300, JULABO, Seelbach, Germany). Probes for pH, conductivity, redox potential and dissolved oxygen (ProODO, YSI Inc., OH, US) were used for the on-line control. All the pH adjustments during the experimentation and sample analysis were done with NaOH and H_2SO_4 (2N).

3.2.1. Organic matter

Organic matter was measured by COD and TOC data. COD was measured by the colorimetric method at 600 nm using an Aquamate-spectrophotometer (Thermo Scientific AQA 091801, Waltham, US); and, when needed, the values were corrected with the residual concentration of H_2O_2, according to Hermosilla *et al.* (2009b). Total organic carbon (TOC) was measured by the combustion-infrared

method using a TOC/TN analyser multi N/C® 3100 (Analytik Jena AG, Jena, Germany) with catalytic oxidation on cerium oxide at 850ºC.

3.2.2. H_2O_2 and iron species

H_2O_2 concentration was measured using the titanium sulphate spectrophotometric method (Pobiner, 1961). Fe^{2+} concentration was measured with the 1,10-phenanthroline colorimetric method (Tamura *et al.*, 1974), using ammonium fluoride as masking agent for Fe^{3+} to avoid its potential interference. Total soluble iron concentration was measured under acidic conditions reducing Fe^{3+} to Fe^{2+} iron adding hydroxylamine.

3.2.3. Biodegradability: Pseudomonas putida

Biodegradability was evaluated in tests with *Pseudomonas putida* (*P. putida*) CECT 324 (Spanish Type Culture Collection, Valencia, Spain). Cultures were grown at pH=7 in 1 $g \cdot L^{-1}$ of beef extract, 1 $g \cdot L^{-1}$ of yeast extract, 5 $g \cdot L^{-1}$ of peptone, and 5 $g \cdot L^{-1}$ of NaCl; and kept at -80 ºC in a cryogenic solution (glycerol 87%). To remove the baseline COD for the biodegradability assays, the bacterial stock was cleaned twice with saline solution (0.9% NaCl) by centrifuging at 10,000 rpm for 5 min. The sample pH was adjusted to 7.0 adding HCl and a culture medium was made up of 40 mL of sample and 10 mL of a previously prepared mineral solution, made of 0.5 $g \cdot L^{-1}$ of NH_4Cl, 0.5 $g \cdot L^{-1}$ of K_2HPO_4, 0.5 $g \cdot L^{-1}$ of KH_2PO_4, 0.5 $g \cdot L^{-1}$ of $MgSO_4 \cdot 7H_2O$, and 10 $ml \cdot L^{-1}$ of trace minerals solution providing a final concentration of 0.6 $mg \cdot L^{-1}$ of $FeSO_4 \cdot 7H_2O$, 0.2 $mg \cdot L^{-1}$ of $CoCl_2$, 0.2 $mg \cdot L^{-1}$ of $MnSO_4 \cdot H_2O$, and 0.2 $mg \cdot L^{-1}$ of $CuSO_4 \cdot 5H_2O$. The culture medium was inoculated with 200 µL of cleaned bacterial stock and incubated at 30 ºC for 100 h inside a 250-mL Erlenmeyer flask placed on a rotary platform. Assays were passed through 0.20-µm syringe filters (Minisart SRP 15, Sartorius Stedim Biotech, Germany) and analysed for COD content, taking into account the dilution ratio resulting from the addition of the mineral solution.

3.2.4. Biodegradability: respirometric trials with activated sludge

Biodegradability was also studied with respirometry trials in an ECHO R6 respirometer (Echo Instruments, Slovenske Konjice, Slovenia) equipped with 6 parallel measuring channels and gas analyser. The trials were conducted at 20°C in the presence of constant air supply, using activated sludge from a local paper mill (1.5 $g \cdot L^{-1}$ in final solution; OECD, 2010) mixed either with the wastewater sample, with a blank sample of deionized water or with a reference sample of a biodegradable substrate containing the same COD as the wastewater. The COD of the biodegradable organic matter was provided 25% by yeast, 25% by peptone, 20% by Na-Acetate, 20% by glucose and 10% by urea. Nutrients were added to all tests in a form of NH_4Cl, KH_2PO_4, $MgSO_4$, $FeCl_3$ and $CaCl_2$. The pH of all the waters was adjusted to about 7.0-7.5 before the addition of sludge. All samples were aerated for 30 min before adding the sludge. The respirometric measurement was based on analysing the CO_2 content in the incoming and outgoing air and the output data was the accumulated production of CO_2 during 60 min. The results were corrected by subtracting the results of endogenous activity with the blank sample.

3.2.5. Fourier transform infrared spectroscopy

FTIR spectrometer ReactIR iC10 (Mettler-Toledo, Columbia, US) was used for the *in situ* monitoring of the oxidation reactions when desired. This on-line spectrometer is able to follow all the organic chemical species that are present in the solution as the reaction is performed over time. The

equipment had a mercury-cadmium telluride detector cooled by liquid nitrogen. Measurements were taken optically using a diamond tipped probe with a fibre optic conduit (1 m). An instrument grade air was used to purge the system, which prevents the accumulation of water vapour inside the optics. Data acquisition was performed from 1800 to 800 cm^{-1} with an 8 cm^{-1} nominal resolution. 256 scans were co-added for each spectrum. Background of water was carried out before recording the spectra. Real-time component analyses were run using ConcIRT software (Mettler-Toledo, Columbia, US), which calculates the associated component spectra, and relative concentration profiles.

3.2.6. Gas-chromatography with a quadruple mass spectrometry

1,4-dioxane and its metabolites ethylene glycol diformate (EGDF) and ethylene glycol monoformate (EGMF) were identified and quantified by an Agilent 6890N gas-chromatograph (GC) (Palo Alto, CA, US) equipped with a quadrupole mass spectrometer (MS) Agilent 5975B. Internal standard (5 $mg \cdot L^{-1}$ of octanol) and 1,4 g of ammonium sulphate were added to 10 mL of sample, and the solution was extracted threefold with dichloromethane (40:10:10 mL). The organic fraction was dried on anhydrous sodium sulphate, concentrated to 1 mL and analysed by GC-MS. Samples (3 µl) were injected in split mode (30:1), and volatiles were separated using a fused silica capillary column (HP-INNOWAX; Agilent, Madrid, Spain). The pressure of the GC-grade He carrier gas was 7.7 psi with a linear velocity of 1.0 $mL \cdot min^{-1}$; the initial oven temperature was 45°C, first increased at 3 $°C \cdot min^{-1}$ to 100°C, held for 1 min, and then heated at 15 $°C \cdot min^{-1}$ to 270°C, and held at this temperature for an additional 5 min. The injection temperature was 230°C. Detection was carried out by EI mode (70 eV), interphase detection temperature was 290°C (MS source at 230°C and MS quad at 150°C) and scanning mass was ranged between 35 and 400 amu. Quantitative determinations were carried out by the internal standard method, using peak areas obtained from selected ion monitoring (88, 1,4-dioxane; 60, EGDF/EGMF; 45, octanol) and calibrations made with pure reference compounds analysed under the same conditions.

3.2.7. Gas–liquid chromatography with a flame ionization detector

1,4-dioxane was also identified and quantified along with its industrial by-product MDO and possible decomposition product ethylene glycol using a gas–liquid chromatography on a 7980A instrument (Agilent, Palo Alto, CA, US) equipped with a flame ionization detector. Injector and detector were respectively set up at 310 and 280°C. Samples (2 µL) were injected using the pulsed-split mode (split ratio 5:1) and analysed in a TRB-FFAP fused silica column (Teknokroma, Sant Cugat del Vallès, Spain) with He (43 psi) as carrier gas and a temperature programme (80°C to 240°C, 9 min initial hold, 15°C min^{-1} ramp rate). Peaks were identified on the basis of sample coincidence with relative retention times of commercial standards. Quantification was performed according to peak area, corrected with the response factors calculated for each compound using 1-butanol (250 ppm) as the internal standard and the software GC-ChemStation Rev.B.04.02 (96) from Agilent.

3.2.8. Liquid chromatography-electrospray ionization-tandem mass spectrometry

Model compounds studied in the preliminary experiments of photocatalyst selection, namely atrazine (ATR), caffeine (FAF) and carbamazepine (CMP) were analysed by liquid chromatography-electrospray ionization-tandem mass spectrometry (LC-ESI-MS/MS) with a 1200 Series rapid resolution LC and 6410A triple quadrupole MS equipped with a G1948B ESI source (Agilent, Palo Alto, CA, US) operated in positive mode. The analytes were separated with a Zorbax Eclipse XDB-C18 column (Agilent, Palo Alto, CA, US). The flow was 0.5 $mL \cdot min^{-1}$. The mobile phase was comprised of water (A)

and methanol (B), both containing ammonium formate (5 mM). At time 0, the eluent composition was 90% (A) and 10% (B), being 36% (A) and 64% (B) after 12 minutes. The analytes were detected in the following selected reactions: ATR *m/z* 216 → *m/z* 174, CAF *m/z* 195 → *m/z* 138, and CMP *m/z* 237 → *m/z* 194.

3.2.9. Ion chromatography with a conductivity detector

Some possible by-products of 1,4-dioxane, namely formic, oxalic, acetic, glycolic, glyoxylic and methoxyacetic acids were identified and quantified by ion chromatography using a Dionex DX-500 instrument (Thermo Scientific, Sunnyvale, CA, US) equipped with a conductivity detector. A gradient of NaOH from 40 mM to 60 mM was used as eluent for the measurements with an eluent flow of 1.5 $L \cdot min^{-1}$. The injection loop was 75 µL. They were analysed in an AS11HC Ion Pac ionic resin column with a previous Anion Trap Column ATC3 and guard column AG11-HC.

3.2.10. High pressure liquid chromatography with diode array detector

In the industrial waters, with high salinity interfering the analysis by ion chromatography, carboxylic acids were complementary measured by high pressure liquid chromatography (Model L920, Varian, CA, US) with diode array detection. Acetonitrile - water (50%:50%) was used as eluent. Sample injections of 20 µL were separated on a C-18 column (Vydac) at 30ºC. The target compounds, acetic acid and oxalic acid, were measured at 200 nm.

3.2.11. Morphological, structural and crystallographic properties of catalytic materials

For the characterization of the composite NF-TiO_2 films, a Tristar 3000 (Micromeritics) porosimetry analyser was employed for the determination of the Brunauer–Emmett–Teller (BET) surface area, pore volume, porosity and the pore size distribution. The films were scraped and the samples were collected as powder and purged with N_2 for 2 h at 150°C using Flow prep 060 (Micromeritics). The film morphology was characterized with an environmental scanning electron microscope (ESEM, Philips XL 30 ESEM-FEG) at an accelerating voltage of 30 kV. The crystallographic structure of the synthesized TiO_2 films was determined with a X'Pert PRO (Philips) XRD diffractometer with Cu Kα (λ = 1.5406 Å) radiation. Optoelectronic properties of the composite NF-TiO_2 films were derived from diffuse reflectance spectra obtained on a UV-Vis spectrophotometer (Shimadzu 2501 PC) equipped with an integrated sphere attachment (ISR 1200) with $BaSO_4$ reference standard.

The structure of Fe^0 microspheres was analysed by scanning electron microscopy (SEM) - energy dispersive X-ray (EDX) spectroscopy. The analysis of the images was carried out by SEM (JEOL JSM-6400) coupled with an EDX analyser (EDS system).

3.3. EXPERIMENTAL SET-UP

3.3.1. Ozonation system

Ozonation was conducted at 25 ºC in a jacketed cylindrical bubble reactor (height=1 m, diameter=5 cm) with a continuous feed of O_3-riched gas (4.0 $L \cdot min^{-1}$; **Fig. 3.1**). The system consisted of an O_3 generator (Model 6020, Rilize, Gijon, Spain), a flow controller Bronkhorst® (Model F-201AV, Ruurlo, The Netherlands), and two on-line O_3 analysers (Model 964C, BMT Messtechnik GMBH, Berlin, Germany). The O_3-gas was introduced continuously into the reactor through a sparger from the bottom of the column. Meanwhile, the water sample was recirculated in the reactor column, passing

through an external vessel for on-line monitoring when required. O_3/H_2O_2 experiments were carried out adding H_2O_2 at the stoichiometric ratio proposed by Kim *et al.* (1997; 2.125 $g \cdot L^{-1}$ of H_2O_2 per 1 $g \cdot L^{-1}$ of COD).

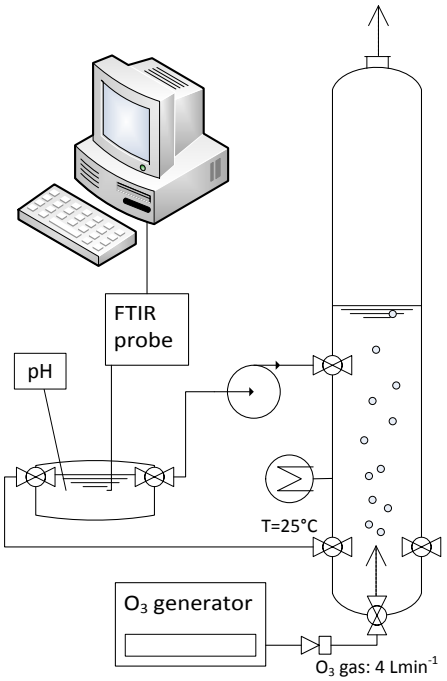

Figure 3.1: Schematic set-up of the ozonation system

3.3.2. Photocatalytic set-up

Photocatalytic experiments were carried out both with suspended P25-TiO_2 powder and with lab-made immobilized TiO_2. Commercial photocatalyst AEROXIDE® TiO_2-P25 (Degussa, Essen, Germany; BET surface area = 50 $m^2 \cdot g^{-1}$; pore volume = 0.25 $m^3 \cdot g^{-1}$, and mean particle size of ca. 21 nm) was used in the conventional slurry experiments with continuous mixing on magnetic device. For analysis, the samples were centrifuged for 15 min at 335 g and the supernatant was filtrated through 0.45 μm. For supported photocatalysis, TiO_2 was immobilized as films and placed in the bottom of the reactor perpendicular to the irradiation. During the experimentation at different laboratories, several light sources were used, as follows.

3.3.2.1. 450-W high-pressure mercury immersion lamp

UV-light enhanced experiments were performed using a high-pressure mercury immersion lamp of 450 W from ACE-glass (Model 7825-30, Vineland, US) placed in a quartz glass cooling jacket and located in a vertical manner in the centre of the reactor (**Fig. 3.2A**). The total photon flux of $1.1 \cdot 10^{20}$ photon$\cdot s^{-1}$ was calculated to flow inside the photochemical reactor as described by Liang *et al.* (2011). Light intensity on the illuminated liquid surface (1.5 cm from the light source) was 186 $mW \cdot cm^{-2}$ at the mid-height of the UV-lamp, recorded using UV-VIS Radiometer RM-21 (UV-Elektronik, Ettlingen, Germany).

3.3.2.2. 500-W solar simulator

Preliminary experiments of immobilized catalyst selection (*Section 4.4.2*) were carried out with a 500-W solar simulator (Newport Corporation, Irvine, US) equipped with AM 1.5 and infrared filters

(**Fig. 3.2B**). The light intensity on the illuminated liquid surface was 70 mW·cm^{-2} measured with a radiant power meter (Newport Corporation, Irvine, US).

3.3.2.3. 300-W solar simulator

The rest of the solar-light enhanced experiments were carried out with a 300-W solar simulator (Newport Corporation, Irvine, US) equipped with a Xe lamp using a correction filter ASTM E490-73a (**Fig. 3.2B**). The total photon flux was 6.8·10^{19} photon·s^{-1}. Depending on the distance between the sample and the light source, the light intensity on the illuminated liquid surface was in the range of 44 to 99 mW·cm^{-2}.

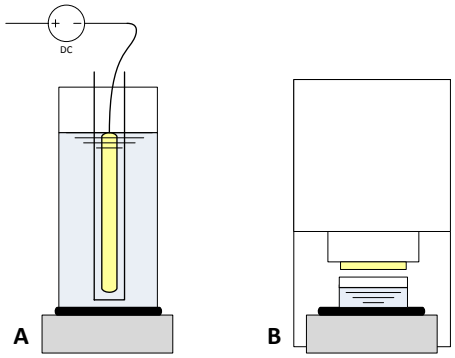

Figure 3.2: Schematic set-up of different irradiation sources: (A) UV lamp; (B) solar simulator

3.3.3. Fenton and photo-Fenton treatments

Experiments were performed in a glass reactor placed on a magnetic mixing device. After initial pH adjustment, iron was added to the wastewater either as ferrous sulphate ($FeSO_4$) or as Fe^0. The latter was employed in the form of ZVI Microspheres 800 (BASF, Ludwigshafen, Germany) with 1 µm of particle size and 800 m^2·kg^{-1} of surface area (>98.3% Fe, <1% C, <1% N, <0.7% O). The reaction was started by H_2O_2 addition up to desired concentration and, for analysis, aliquots were withdraw, the reaction was quenched by increasing the pH to 9.0, and the samples were filtered through 0.45 µm. The UV or solar light assisted Fenton experiments were performed following the same procedure, while using either the 450-W high-pressure mercury immersion lamp (*Section 3.3.2.1.*) or the 300-W solar simulator (*Section 3.3.2.3.*) described above, respectively.

3.3.4. Electrochemical flow-cell

Electrochemical treatment was performed at ambient temperature (25 ºC) in an undivided rectangular electrolytic flow-cell (methacrylate, 10x7x15 cm^3) in a batch recirculation mode, passing the wastewater sample (1.5 L) through a vessel with on-line probes (**Fig. 3.3**).

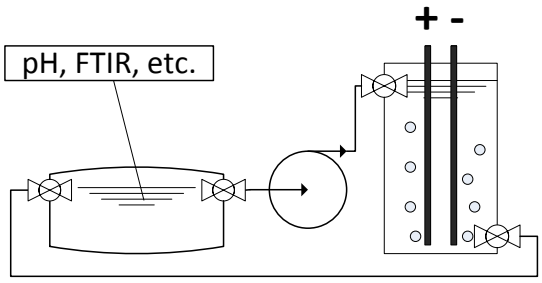

FIGURE 3.3: Schematic set-up of the electrolytic flow-cell

Commercial BDD electrodes of 100 cm^2 (Metakem GmbH, Usingen, Germany) were used as both, anode and cathode, arranged parallel to each other at a distance of 2.4 cm. Electrodes were fed with ordinary grade air (4.5 $L \cdot min^{-1}$) rate to facilitate mass transfer in the reactor. Experiments were carried out under galvanostatic conditions using AMEL potentiostat/galvanostat 7050 (AMEL Instruments, Milano, Italy). The pH of the solution was not controlled, and it increased from 8.0-8.5 up to 9.0-9.5 during the process.

The photos of the above-mentioned equipment are shown in **Fig 3.4**:

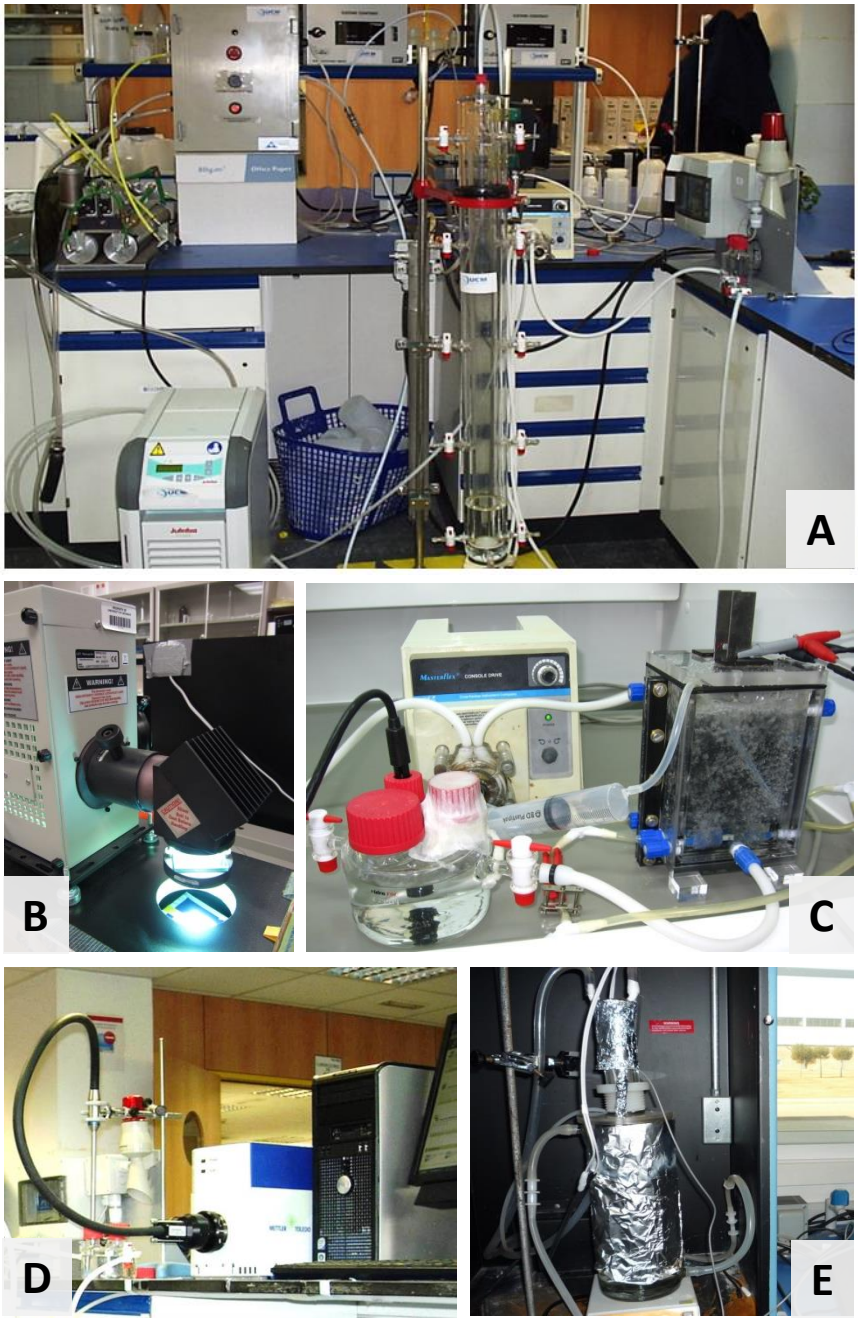

FIGURE 3.4: Photos of (A) ozonation system; (B) solar simulator; (C) electrolytic flow-cell; (D) FTIR instrument; (E) UV-lamp

4. RESULTS AND DISCUSSION

4.1. OZONATION: PROMOTING THE RADICAL PATHWAY

Although ozonation is one of the most common AOPs used in industry as an easily implemented process for treating large water flows at full scale (Bertanza *et al.*, 2013; Oller *et al.*, 2011), the degradation of 1,4-dioxane by O_3 as a sole oxidant has been ruled out by different authors due to previously reported low efficiencies (Adams *et al.*, 1994; Kwon *et al.*, 2012; Suh and Mohseni, 2004). Nevertheless, none of these scientists considered the use of O_3 oxidation in basic conditions to promote the production of OH• through O_3/OH^- oxidation (*Section 1.3.1*). Therefore, the main objective of this section of the doctoral research was to re-assess the use of ozonation for oxidation of 1,4-dioxane by promoting the radical pathway instead the oxidation by molecular O_3. The aim was to demonstrate the viability of ozonation for 1,4-dioxane degradation, to assess the influence of bicarbonate alkalinity and to treat real industrial wastewaters containing 1,4-dioxane and relatively high carbonaceous alkalinity (***Publication I***).

4.1.1. Optimization study: effect of pH and carbonaceous alkalinity

Initial optimization experiments were carried out on synthetic 1,4-dioxane solution under different constant pH conditions. Solution pH was controlled throughout the experiment by adding NaOH when needed to keep it at the set value, except for the experiments with the single addition of $NaHCO_3$ buffer (11.9 mM) that caused the pH to increase from 9.0 to 10.0 during the experiment.

The ozonation experiments at different pH (**Fig. 4.1**) showed that an important turning point exists at pH≈9 for the treatment of wastewaters with 1,4-dioxane. While rather similar results were obtained at pH 9.0 and pH 10.0 (around 80% removal of COD at a consumption of 1.3 and 1.0 $g \cdot L^{-1}$ of O_3 respectively), the COD removal decreased considerably at pH<9. Namely, 60% of COD was degraded at pH of 8.5 by a similar O_3 dose (1.3 $g \cdot L^{-1}$), and only 20% was removed at pH=7.0.

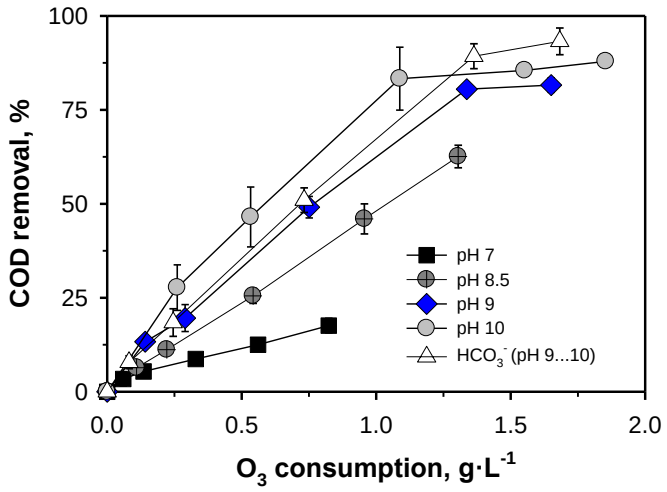

FIG. 4.1: COD removal in ozonation of synthetic 1,4-dioxane solution (C_0 = 247.8 mg·L^{-1}) under different pH conditions.

Due to the fact that the industrial wastewaters under concern contained (bi)carbonates and since carbonate and bicarbonate ions are often considered OH• scavengers (Hoigne *et al.*, 1985; Ma and Graham, 2000), an additional ozonation experiment was carried out in the presence of HCO_3^- (9.0≤pH≤10.0), to test the possible negative effect on the process (**Fig. 4.1**). However, instead of producing an inhibition, the presence of carbonates enhanced the removal of COD (>90%), compared to the experiments at neutral conditions, due to the carbonate buffer which kept the pH in the optimal range. This is in concordance with an auxiliary study performed on phenol (***Publication A***), showing that the buffering effect of carbonaceous alkalinity could outbalance the negative OH• scavenging effect during ozonation.

The disappearance of 1,4-dioxane was apparently found to fit first order kinetics (El-Din *et al.*, 2006; Suarez *et al.*, 2007; Suh and Mohseni, 2004). According to the found pseudo first order rate constants (**Table 4.1**), increasing the solution pH from 7.0 to 10.0 had a significant promoting effect on 1,4-dioxane degradation rate both in O_3 and O_3/H_2O_2 processes. Namely, the half-life ($t_{1/2}$) of 1,4-dioxane was reduced about 20 times when increasing operating pH of the O_3 process to values above 9. This indicates that the oxidation of 1,4-dioxane is mainly initiated by the OH• produced in ozonation at high pH (Glaze, 1986; Glaze *et al.*, 1987; Hoigne and Bader, 1976; Staehelin and Hoigne, 1982), and that the reaction by molecular O_3 at lower pH conditions has a very low efficiency in the treatment of this particular compound.

Although the addition of H_2O_2 to the ozonation system fastened the 1,4-degradation in time, both processes (O_3 and O_3/H_2O_2) at basic conditions achieved very similar overall removals in terms of O_3 consumption (100% of 1,4-dioxane and around 85% of COD with the consumption of about 1.7 gO_3/L). These results demonstrate that working at the optimum pH, both high 1,4-dioxane and COD removals can be achieved with a sole O_3 treatment, while the addition of H_2O_2 enhances the reaction rates for the 1,4-dioxane degradation, but also increases the oxidant consumption, thus, the treatment cost.

TABLE 4.1: First order kinetics of 1,4-dioxane (C_0 = 247.8 $mg \cdot L^{-1}$) degradation in O_3 and O_3/H_2O_2 processes

	O_3			O_3/H_2O_2		
pH	$t_{1/2}$ *min*	k min^{-1}	R^2	$t_{1/2}$ *min*	k min^{-1}	R^2
7.0	578	1.2	0.99	29	24	0.92
9.0	29	24	0.91	19	36	0.99
10.0	23	30	0.94	14	48	1.00

4.1.2. Treatment of industrial wastewaters

Three industrial samples were treated by O_3 at pH>9 (**Fig. 4.2**), whereas the initial carbonaceous alkalinity resulted beneficial to maintain the basic conditions. The percentage of COD removal as well as the quantity of COD removed depended highly on the initial organic load. The effluent containing only 1,4-dioxane at a concentration similar to the synthetic water (sample 1) showed an analogous behaviour to the previous trials: 85% of COD was degraded by ozonation (0.23 g of COD per 1 g of O_3). On the other hand, samples 2 and 3 with a higher COD, containing both 1,4-dioxane and MDO (**Table 3.1**), reached a smaller COD removal percentage (63% and 53%, respectively), but a higher total amount of COD removed per oxidant consumed (0.44 and 0.93 $gCOD \cdot gO_3^{-1}$, respectively).

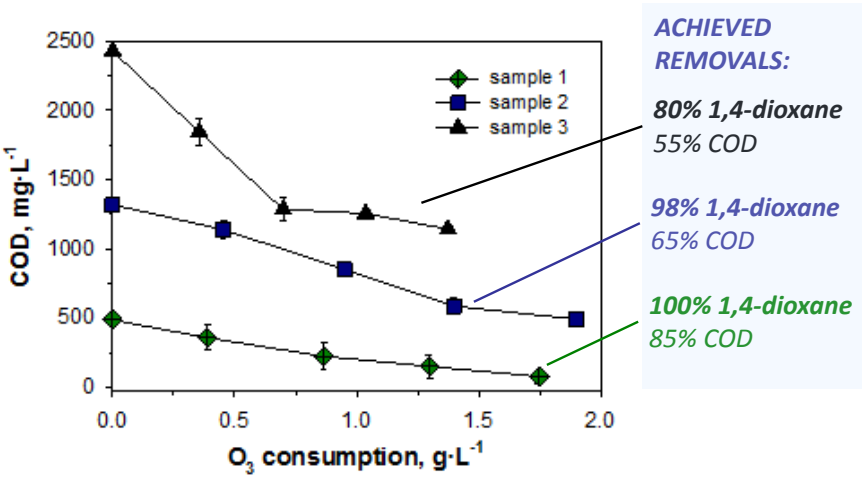

FIG. 4.2: Ozonation of industrial wastewaters under basic conditions (pH>9). Sample 1: COD_0=574±25 mg·L^{-1}; sample 2: COD_0=1360±40 mg·L^{-1}; sample 3: COD_0=2300±100 mg·L^{-1} (Table 3.1).

According to the chromatography data (**Table 4.2**), a high degradation of 1,4-dioxane from the samples 2 and 3 was achieved with approximately 1 g·L^{-1} of O_3. The degradation intermediates were mainly ethylene glycol and volatile fatty acids (VFA), which are more biodegradable, meaning they could be removed in a traditional biological process. However, the MDO was almost completely degraded, even being in much higher quantities, which proves that it is oxidized more readily than 1,4-dioxane, and thus, it competes with 1,4-dioxane for the available oxidants (Adams *et al.*, 1994).

TABLE 4.2: Concentration of major contaminants remaining in industrial wastewater samples after 1 g·L^{-1} of O_3 consumption

	1,4-dioxane *mg·L^{-1}*	***MDO*** *mg·L^{-1}*	***ethylene glycol*** *mg·L^{-1}*	***VFA*** *mg·L^{-1}*
Sample 1	0	-	0	36
Sample 2	<5	<15	22	204
Sample 3	65	<5	267	237

4.2. CONDUCTIVE DIAMOND FOR NON-SELECTIVE ANODIC OXIDATION

As CDEO is gaining more and more attention in wastewater treatment applications, the objective of this section of the PhD research was to study the anodic oxidation of 1,4-dioxane on BDD. BDD is considered the most efficient electrode material for non-selective mineralization of organics due to its high over potential for water electrolysis, high stability, good conductivity, inert character and weak adsorption properties (Comninellis *et al.*, 2008; Rodrigo *et al.*, 2010). Thus, the aim of this work was to carry out an experimental design for the optimization of CDEO for the treatment of wastewater containing 1,4-dioxane by studying the effect of different electrolyte salts, initial organic load and applied current density (*j*). Subsequently, treatment of real industrial wastewaters was carried out, taking advantage of the initial bicarbonate alkalinity of the water samples (***Publication II***).

4.2.1. Effect of electrolyte salts, applied current and organic load

Central composite design and response surface methodology were applied to optimize the treatment of 1,4-dioxane in synthetic solution. The levels of the independent variables of the experimental design are presented in **Table 4.3**.

TABLE 4.3: Levels of independent variables of the experimental design

	-2	*-1*	*0*	*+1*	*+2*
X_1: [SO_4^{2-}], *mEq·L^{-1}*	0	10.4	20.8	31.2	41.6
X_2: [HCO_3^-], *mEq·L^{-1}*	0	8.2	16.4	24.6	32.8
X_3: COD_0, *mg·L^{-1}*	150	300	450	600	750
X_4: j, *mA·cm^{-2}*	2	6	10	14	18
X_5: time, *h*	1	2	3	4	5

The studied responses were COD removal (%), amount of COD removed (ΔCOD, $kgCOD_{removed}·m^{-3}$), total current efficiency (TCE), and energy consumption (EC, $kWh·kgCOD_{removed}^{-1}$). Particularly, TCE and EC were calculated by **Eqs. 17** and **18** (Montilla *et al.*, 2002; Panizza *et al.*, 2001), where COD_0 and COD_t (mol $O_2·m^{-3}$) are the values of the initial COD and the COD at treatment time t, respectively. I (A) is the applied current, F ($C·mol^{-1}$) is the Faraday constant, V (m^3) is the sample volume; and U (V) is the average cell voltage.

$$TCE = 4FV \cdot \left(\frac{COD_0 - COD_t}{I \cdot t} \right) \qquad (17)$$

$$EC = \frac{(t \cdot I \cdot U/V) \cdot 10^{-3}}{(COD_0 - COD_t) \cdot 10^{-6}} \qquad (18)$$

Reaction time was the most important factor increasing COD removal (**Fig. 4.3A**). Up to 100% of COD removal could be achieved in 5 h of electro-oxidation (≈130 $kWh·kgCOD_{removed}^{-1}$); whereas about 85% of the COD was already removed in 3 h (≈85 $kWh·kgCOD_{removed}^{-1}$). Applied *j* also had an important positive influence on COD removal, stabilizing at ≈12 $mA·cm^{-2}$.

Although the percentage of COD removal was greater with a lower initial COD, the actual amount of COD removed in terms of kg per sample volume resulted greater when working with a higher initial COD and, therefore, the EC was lower at higher COD_0 as well (**Fig. 4.3B**). In 3 h of electro-oxidation at 12 $mA·cm^{-2}$, ≈190 kWh was consumed per 1 kg of COD removed when COD_0 was 150 $mg·L^{-1}$; whereas much less EC (≈50 $kWh·kgCOD_{removed}^{-1}$) was consumed when 750 $mg·L^{-1}$ of COD_0 were used.

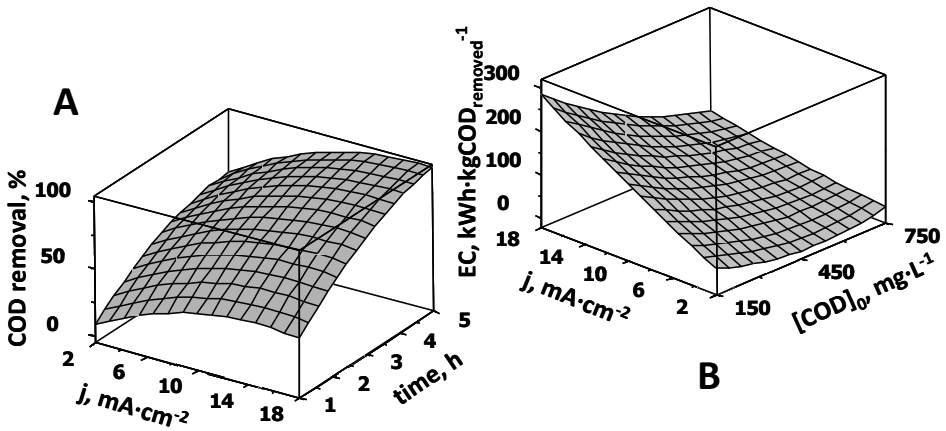

FIGURE 4.3: 3D response surfaces of (A) COD removal in time at varying j (COD_0=450 mg·L^{-1}); and (B) EC as a function of applied j and initial COD (t=3h).

In terms of current efficiency, the TCE was the highest at the lowest applied *j* and at the shortest reaction time because, as COD decreased in time, more excess current was gradually provided for its oxidation. This current did not contribute to the degradation of such a low COD because the process was limited by mass transportation (Montilla *et al.*, 2002; Panizza *et al.*, 2001). For instance, TCE dropped from about 0.75 after 1 h to approximately 0.4 after 5 h when using *j*=12 mA·cm^{-2}.

According to the Minitab software (**Fig. 4.4**), the optimal compromise was reached in the presence of the maximum concentrations of both electrolytes (41.6 mEq·L^{-1} of SO_4^{2-} and 32.8 mEq·L^{-1} of HCO_3) when the maximum initial COD of 750 mg·L^{-1} was used and a *j*=11.9 mA·cm^{-2} was applied for 3.8 hours.

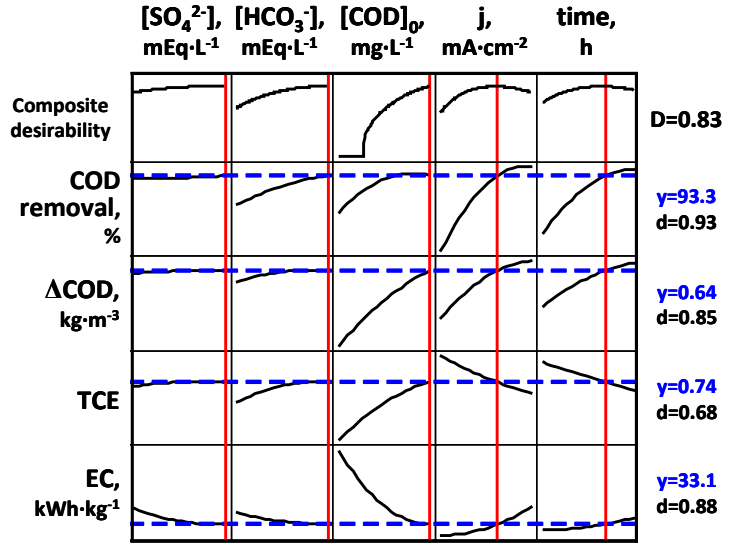

FIGURE 4.4: Optimal compromise for maximum COD removal (% and ΔCDO) at a maximum TCE and a minimum EC (y = process response; d = desirability of the process response; D = composite desirability).

Regarding the supporting electrolytes, no radical scavenging effect was found with either SO_4^{2-} or HCO_3^-. On the contrary, the presence of both salts increased the COD removal, although the effect was rather small. Both salts were important factors to be considered for decreasing the consumption of electricity, meaning that their principal effect simply laid on providing the necessary conductivity for electrolysis. Neither the scavenging effect of bicarbonate nor the additional oxidative effect of

sulphate played an important role, indicating that the natural bicarbonate alkalinity of certain wastewater may serve as electrolyte for performing CDEO just as well as SO_4^{2-} salts.

4.2.2. Treatment of industrial wastewaters

Considering the results of the experimental design, the treatment of industrial wastewater samples 1 and 2 (**Table 3.1**) was carried out applying a current density of 12 mA·cm^{-2}, in the presence of the initial bicarbonate alkalinity of the effluent (16.4 mEq·L^{-1}), and using 20.8 mEq·L^{-1} of SO_4^{2-} as a supporting electrolyte, which is a concentration that still meets discharge limitation in force. As shown in **Fig. 4.5**, up to 98% of COD removal was achieved for sample 1 after 5 h using 114 kWh·kgCOD$_{removed}^{-1}$; and about 91% of the COD was removed from sample 2 using 49 kWh·kgCOD$_{removed}^{-1}$ (≈60 kWh·m^{-3} were used in both cases). The results for the electrochemical oxidation of the effluent just containing 1,4-dioxane were in a good correlation with the model prediction for a synthetic solution of 1,4-dioxane ($R^2_{COD\%}$=99.01%; $R^2_{\Delta COD}$=99.21%; R^2_{TCE}=99.27%; and R^2_{EC}=98.95%).

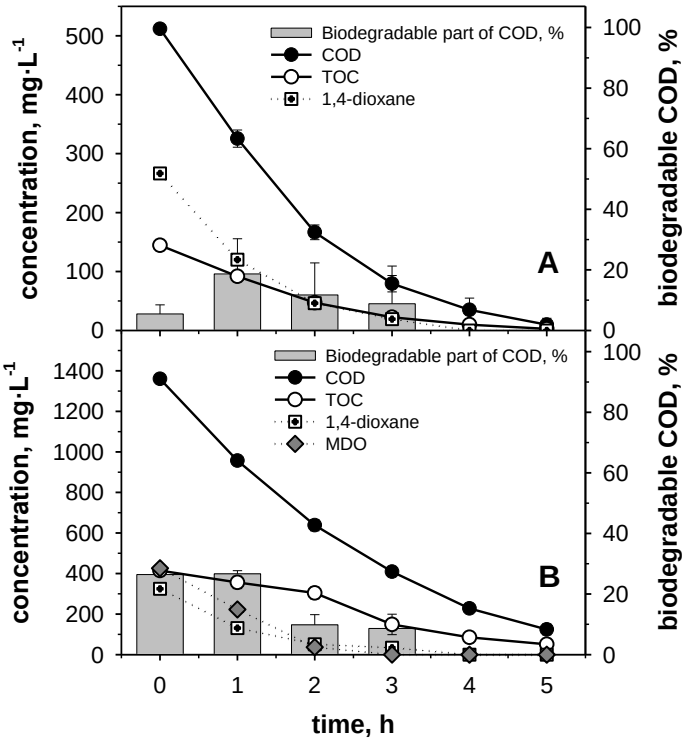

FIGURE 4.5: Profiles of COD, TOC, 1,4-dioxane, and MDO along with the effluent biodegradability by P. putida (100-h bioassays) during the anodic oxidation of industrial wastewaters: (A) sample 1, COD_0=475±25 mg·L^{-1}; (B) sample 2, COD_0=1360±40 mg·L^{-1} (Table 3.1). Applied j=12 mA·cm^{-2}; [HCO_3^-]=16.4 mEq·L^{-1}; [SO_4^{2-}]=20.8 mEq·L^{-1}.

1,4-dioxane removal was independent of the presence of MDO, following a similar trend in both effluents. The initial biodegradability by *P. putida* of sample 1 was significantly increased after 1 h of electro-oxidation treatment (from 5% to 20% of the initial COD), whereas the biodegradability of sample 2 with MDO was initially higher and remained the same (≈26-27%), which means that MDO is more susceptible to biodegradation (more than a 50% of the initial MDO content was removed by *P. putida*, whilst a negligible amount of 1,4-dioxane was degraded). After 1 h of electro-oxidation (27%), as an overall result, almost 50% of the COD along with 85% of the MDO content and 75% of 1,4-dioxane were removed by the combined process (CDEO + *P. putida*).

4.3. Fe^0 FOR HETEROGENEOUS PHOTO-FENTON PROCESSES

Regarding actual on-site and pre-industrial applications, Fenton processes are among the most common AOPs, offering decades of know-how for relatively cheap and easy implementation. As one of the most aggressive treatments well suitable for industrial wastewaters, classical Fenton oxidation is also the most corrosive method due to its reaction conditions. The production of Fe^{3+} sludge and the optimum acid pH required for the process are still important drawbacks that restrict its implementation (Pignatello *et al.*, 2006; Son *et al.*, 2009). Therefore, the objective of this part of the PhD thesis was to study the use of Fe^0 for heterogeneous photo-Fenton processes in order to work under milder pH conditions and avoid iron leaching. Different light sources were tested and the influence of pH, reagent dose and carbonaceous alkalinity were assessed (***Publication III***).

4.3.1. UV photo-Fenton

The UV photo-Fenton experiments were carried out on 2 L of synthetic 1,4-dioxane solution. The influence of H_2O_2 dose was studied at following ratios to the initial COD: 4, 2.625, 2.125 and 1.625 (H_2O_2/COD_0=2.125 was selected based on the stoichiometrical relation with the COD; Kim *et al.*, 1997). H_2O_2/Fe^0 ratio of 60 was selected as the optimal found in a preliminary study. Different pH conditions were investigated: acidic (pH=2.8), neutral (pH=7.0, adjusted with NaOH), and slightly basic (pH=8.2, in the presence of 1000 $mg \cdot L^{-1}$ of $NaHCO_3$ buffer). Finally, treatment of a real industrial wastewater (sample 1, **Table 3.1**) was carried out.

4.3.1.1. Effects of pH and reagent dose

1,4-dioxane was eliminated in 5 min of UV photo-Fenton treatment using Fe^0 microspheres under different pH conditions. The removals of COD and TOC were somewhat faster under acidic conditions (**Fig. 4.6**, **Table 4.4**), as expected for a Fenton reaction (Pignatello *et al.*, 2006). Nevertheless, the differences were rather small, as working both with an initial neutral pH and in the presence of $NaHCO_3$, an almost complete COD removal (98-99%) was obtained after 30 min, similarly to the acidic conditions.

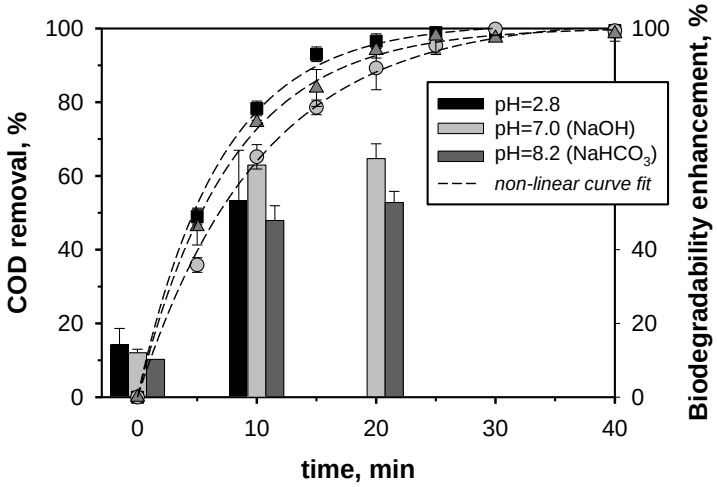

FIG. 4.6: Removal of COD and the enhancement of biodegradability by P. putida during the treatment of 1,4-dioxane solution by UV photo-Fenton process using Fe^0 microspheres at different pH conditions (H_2O_2/COD=4).

Meanwhile, the initial biodegradability of the solution (10-15%, by *P. putida*) was considerably increased. Namely, after 10 min of photo-Fenton, biodegradabilities of 63%, 53% and 48% were obtained at pH_0=7.0, pH=2.8 and pH_0=8.2, respectively. Therefore, the combination of photo Fenton processes and biological treatment is a promising solution for the treatment of effluents containing 1,4-dioxane.

At both pH_0=7 and in the presence of bicarbonates, the removals of organic matter in term of TOC degradation rate at different H_2O_2/COD_0 ratios were in the following order: 2.625 > 2.125 > 4 > 1.625 (**Table 4.4**).

TABLE 4.4: Pseudo-first order rate constants for TOC removal during the treatment of 1,4-dioxane solution by UV photo-Fenton processes using Fe^0 microspheres.

	pH=2.8		***pH_0=7***		***$NaHCO_3$***	
H_2O_2/COD	*k x 10^2 (min^{-1})*	*R^2*	*k x 10^2 (min^{-1})*	*R^2*	*k x 10^2 (min^{-1})*	*R^2*
4	8.5	0.916	7.11	0.956	7.18	0.960
2.625	-	-	8.56	0.973	8.58	0.980
2.125	-	-	7.81	0.947	7.81	0.975
1.625	-	-	6.55	0.877	6.98	0.968

This most likely occurs because the small excess of reagent (H_2O_2/COD_0=2.625) promotes the Fenton-type reaction on Fe^0 as well as the direct production of OH• from H_2O_2 and the UV radiation. However, the further increase to H_2O_2/COD_0=4 resulted in a diminished degradation, as the production of OH• was scavenged by the high amount of reagent itself (Hermosilla *et al.*, 2009a). Similarly, when using the lowest H_2O_2/COD_0 ratio, the scarcity of H_2O_2 also decreased the desirable reactions.

4.3.1.2. Oxidation mechanism and iron leaching

As relevant iron leaching to the solution ($[Fe^{2+}]$=3 $mg \cdot L^{-1}$) was detected at pH=2.8 and comparable 1,4-dioxane degradations were achieved with neutral and slightly basic pH, the acidic treatment was excluded from further study because, for environmental applications, the concentration of Fe^{2+} in the final effluent should be reduced by posterior precipitation, which newly leads to the classical problem of Fenton operations: the production of iron sludge.

When working at initially neutral conditions, the pH_0=7.0 actually decreased to about 4 in the course of experiment due to the formation of short chain organic acids (Kallel *et al.*, 2009a,b), and some Fe^{2+} was still detected in all waters. The iron corrosion was greater and appeared earlier when the amount of H_2O_2 was reduced (**Fig. 4.7A**), most likely, because after the depletion of H_2O_2 at longer treatment times, the Fe^{2+} was still continuously generated on the microsphere surface by UV radiation (**Eq. 11**), but not used for the Fenton process anymore. Apparently, as organic matter was not being oxidized anymore, the iron started to be transfered into the dissolved state.

On the other hand, when working in the presence of carbonates, $[Fe^{2+}]$<1 $mg \cdot L^{-1}$ was only measured using the lowest H_2O_2/COD_0 ratio (**Fig. 4.7B**). Thus, when working with Fe^0 microspheres, the presence of carbonaceous alkalinity can actually be desired, as it avoids the pH dropping below 6.5 at which the Fe^{2+} is not expected to be in soluble state (Liu and Liptak, 1997).

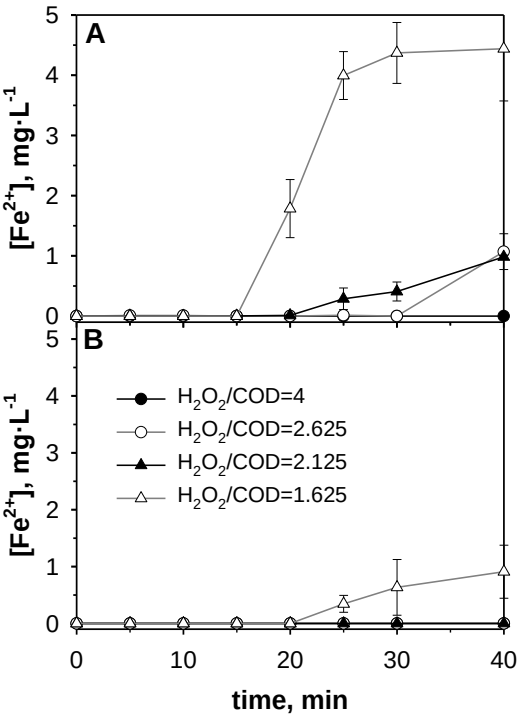

FIG. 4.7: Iron leaching during the treatment of 1,4-dioxane solution by UV photo-Fenton process using Fe^0 microspheres at different H_2O_2 doses.

To have a clearer insight of the fate and stability of Fe^0 microspheres in different pH conditions, a SEM-EDX study was carried out on Fe^0 samples already used for photo-Fenton experiments (**Fig. 4.8**). It was observed that the morphology of microspheres remained intact after photo-Fenton treatment in neutral conditions, whereas the spherical structure of Fe^0 was lost after photo-Fenton process under acidic conditions, indicating the modification and solubilisation of the material.

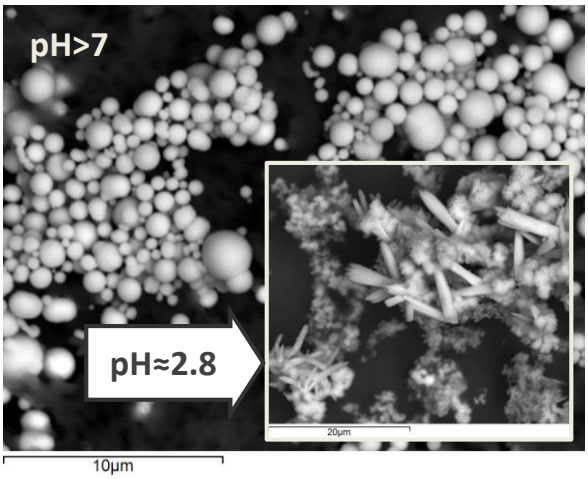

FIG. 4.8: SEM-EDX images of the unmodified Fe^0 microspheres after UV photo-Fenton treatment at neutral pH and the loss of spherical structure through iron leaching UV photo-Fenton process under acidic conditions.

In view of the similar degradation efficiencies and H_2O_2 consumption, it was concluded that the iron corrosion and Fe^{2+} solubilisation are not essential for the Fenton reaction on Fe^0 microspheres. In

fact, it has led us to conclude that, in heterogeneous conditions, the Fe^{2+} created from metallic iron, either by reacting with H_2O_2 (**Eq. 10**) or induced by UV radiation (**Eq. 11**; Bergendahl and Thies, 2004; Pignatello *et al.*, 2006; Prousek *et al.*, 2007; Son *et al.*, 2009), initially remains anchored on the surface of Fe^0 microspheres while taking part of the classical Fenton reaction (**Eq. 7**; Pignatello, 1992) without passing to the solution, whereas the produced Fe^{3+} is recycled in a so-called pseudo-catalytic Fe^0/Fe^{2+} system (**Eq. 12**; Bremner *et al.*, 2006; Kallel *et al.*, 2009a,b), while the UV radiation additionally contributes to the regeneration of Fe^{2+} (Prousek *et al.*, 2007; Son *et al.*, 2009). Thus, in principle, the Fe^0 microspheres should be totally recoverable, maintaining an unmodified morphology when used under steady neutral pH.

4.3.2. Solar photo-Fenton

Solar photo-Fenton experiments were carried out on 0.1 L of synthetic 1,4-dioxane solution. Different H_2O_2/Fe^0 ratios (60, 30, 15 and 1) were assessed while maintaining the ratio H_2O_2/COD_0=2.125. 1000 $mg \cdot L^{-1}$ of $NaHCO_3$ buffer was added to the water in order to assure the heterogeneous photo-Fenton process in all the solutions. Finally, treatment of industrial wastewater (sample 1) was carried out under optimized conditions.

Both the H_2O_2 consumption and the organics degradation were slower under solar radiation than with UV, mainly due to the lower OH• production, as the solar simulator emits a weaker radiation. Nevertheless, up to 91% removal of 1,4-dioxane removal was achieved after 3 h of solar photo-Fenton process using heterogeneous Fe^0 in the presence of bicarbonate alkalinity (**Fig. 4.9**), whereas up to 45% of COD and more than 20% of TOC were removed as well.

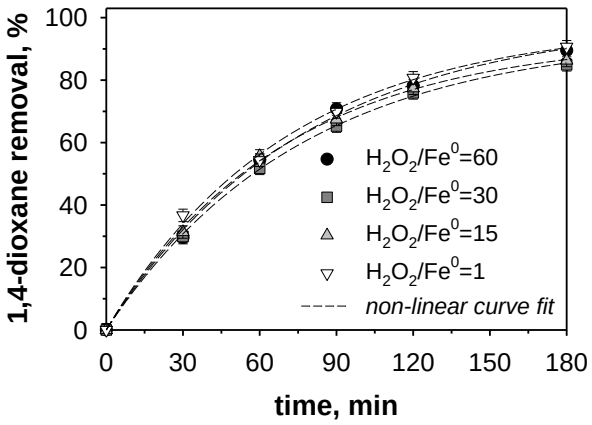

FIG. 4.9: 1,4-dioxane removal by solar photo-Fenton process using Fe^0 microspheres at different Fe^0 dose.

No significantly big differences were found between the different H_2O_2/Fe^0 ratios. Namely, the TOC degradation rates (pseudo first order kinetics) were 1.46, 1.50, 1.51 and 1.62 $\times 10^{-3}$ min^{-1} for H_2O_2/Fe^0 ratios of 60, 30, 15 and 1, respectively. In all cases, pH was buffered at about 8 and no Fe^{2+} was detected in the medium. With all H_2O_2/Fe^0 ratios, the consumption of H_2O_2 was linear in time (R^2=96-98%), and after the 3 h-treatment, about 70% was used up. Therefore, the smallest amount of Fe^0 (H_2O_2/Fe^0=60) could be selected as optimum for these processes.

4.3.3. Treatment of industrial wastewater

Industrial wastewater containing 1,4-dioxane (sample 1, COD_0=475±25 mg·L^{-1}) was treated by both UV and solar photo-Fenton process, taking advantage of its own relatively high alkalinity (950±50 mg$CaCO_3$·L^{-1}) to maintain the Fe^0 microspheres in heterogeneous conditions (pH≈8).

About 98% of COD and 90% of TOC were removed from the effluent by UV photo-Fenton oxidation (**Fig. 4.10**), whereas solar photo-Fenton process was able to reach approximately 60 and 35% of COD and TOC removals (**Fig. 4.11**).

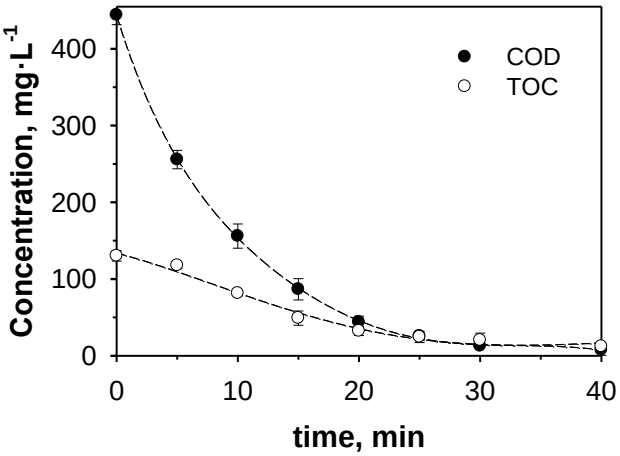

FIG. 4.10: COD and TOC removal in the treatment of industrial wastewater (sample 1) by UV photo-Fenton process using Fe^0 microspheres. H_2O_2/COD=2.125; H_2O_2/Fe^0=60.

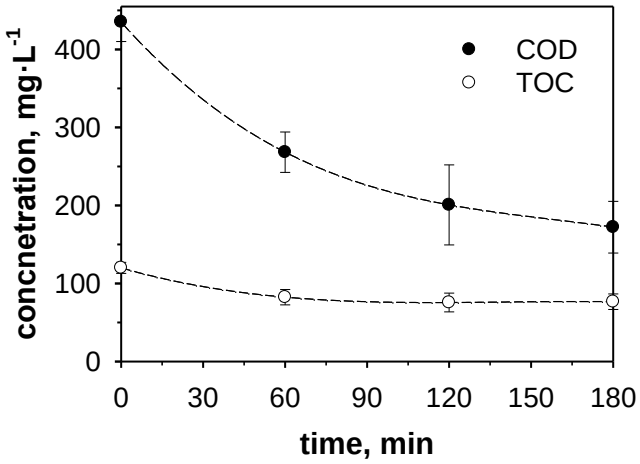

FIG. 4.11: COD and TOC removal in the treatment of industrial wastewater (sample 1) by solar photo-Fenton process using Fe^0 microspheres. H_2O_2/COD=2.125; H_2O_2/Fe^0=60.

Considering these results, sunlight driven photo-Fenton is an important economical alternative to the UV catalysed process if biodegradability enhancement by partial removal of organic load is the aim of the treatment.

4.4. IMMOBILIZED TiO_2 FOR SOLAR PHOTOCATALYSIS

TiO_2-based nanotechnology has gained recognition as a promising AOP for water remediation due to the green characteristics of TiO_2, e.g., low toxicity, inert nature, and relatively low cost (Choi *et al.*, 2007; Fujishima *et al.*, 2000). TiO_2-photocatalysis offers several advantages such as mild reaction conditions, flexible in operation variables, and no waste/sludge production (Perathoner, 2013). As the expense of electricity constitutes one of the major drawbacks for the implementation of UV catalysed water treatments, more and more research is focusing on sunlight-driven photo-reactors (Braham and Harris, 2009; Malato *et al.*, 2009; Singh *et al.*, 2013; Soares *et al.*, 2014). It is of great interest to search for more cost-effective and less residues-producing alternatives, e.g. by employing solar light, developing new photocatalysts with an improved properties and immobilizing the titanium-based materials to enhance process engineering and catalyst separation.

Among the various approaches, non-metal doping is an advantageous technique to improve the photoactivation of TiO_2 at a broader range of solar spectrum compared to metal-doped TiO_2, since the possible toxicity emission associated to metal leaching diminishes its potential for environmental applications. Successful water remediation was obtained by nitrogen and fluorine doped titania (NF-TiO_2; Pelaez *et al.*, 2009), and the immobilization of this catalyst resulted in active and mechanically stable photocatalytic films (Pelaez *et al.*, 2010). Additionally, the incorporation of Evonik® P25-TiO2 nanoparticles into the sol–gel improved the physicochemical and optical properties of the TiO_2 film (Chen and Dionysiou, 2008; Pelaez *et al.*, 2012b). Therefore, studying the effect of different nanoparticles added into the NF-TiO2 sol–gel to improve its photocatalytic efficiency is of great interest.

In this part of the doctoral thesis, different modifications of NF-TiO_2 were studied in preliminary photocatalytic experiments with model organics. Subsequently, the NF-TiO_2 composite with the best performance was chosen for the final experiments conducted on industrial waters contaminated with 1,4-dioxane (***Publications IV and V***).

4.4.1. Catalyst preparation and characterization

The supported photocatalysts were prepared from different sol-gel modifications by a dip-coating method (Pelaez *et al.*, 2012b). For that, the sols were deposited on borosilicate glass substrate with an immersion/withdrawal velocity of 12.5±0.3 $cm \cdot min^{-1}$ and immobilized by calcination in a 30-min treatment at 400°C in air atmosphere and cooled down naturally.

The basic NF-TiO_2 sol-gel was prepared as reported by Pelaez *et al.* (2010). Flurosurfacant Zonyl FS300, which served as a pore template and fluorine dopant, was dissolved in isopropyl alcohol. After the addition of glacial acetic acid, ethylenediamine was added as a nitrogen precursor. Then, titanium tetraisopropoxide (TTIP) was added dropwise to the sol, followed by additional acetic acid for peptidization. Monodisperse anatase titania was synthesized by a sol-gel method described by Han *et al.* (2012b). For that, $CaCl_2$ solutions of varying concentrations (to provide different ionic strength for the particle size control) were added to methanol. After mixing, TTIP was added dropwise as the titanium precursor.

To modify the basic NF-TiO_2, different types of nanoparticles were incorporated to the catalyst (**Fig. 4.12**).

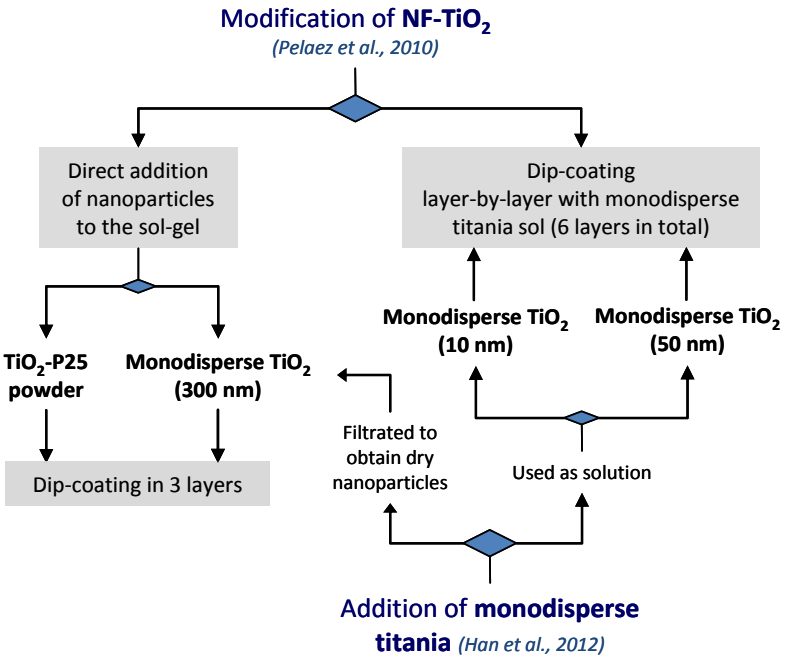

Figure 4.12: Different modifications of NF-TiO_2 sol-gel

Two different ways of adding nanoparticles to produce composite NF-TiO_2 films were implemented. In the first method, either commercial TiO_2-P25 particles or lab-made monodisperse titania nanoparticles (300 nm) were incorporated directly into the NF-TiO_2 sol-gel at 5 $g \cdot L^{-1}$. This sol was immobilized in three consequent dip-coating layers, as described previously. The second approach consisted in a layer-by-layer technique employing alternatively the basic NF-TiO_2 and a separate solution of monodisperse titania with a particle size of 10 or 50 nm. The first coating was NF-TiO_2 followed by the monodisperse titania one. This process of merging NF-TiO2 with monodisperse titania on top of it was repeated 3 times layer-by-layer (6 layers in total).

4.4.2. Catalyst selection

According to the ESEM images, rough and porous surface was observed in all of the studied composite films, whereat the difference among films was mainly due to the surface coverage. The dispersion of the monodisperse particles was higher when employing the layer-by-layer method than when added directly into the NF-TiO_2 sol in a powdered, since with the layer-by-layer technique, fewer aggregates and improved distribution of monodisperse titania was obtained (**Fig. 4.13**).

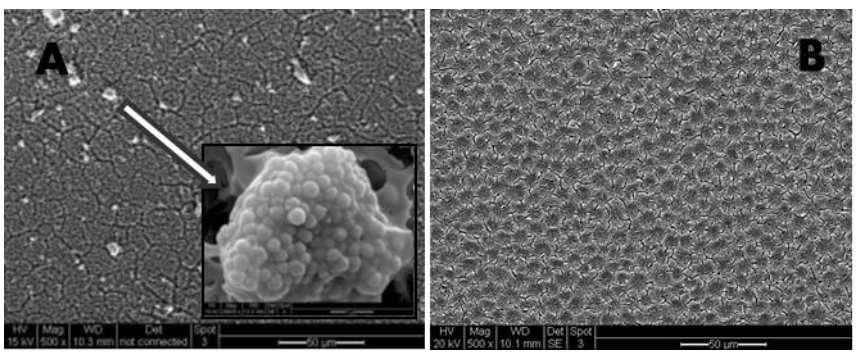

FIG. 4.13: ESEM images of (A) NF-TiO_2 + monodisperse TiO_2 particles (300 nm) added directly to the sol; (B) NF-TiO_2-monodisperse TiO_2 (50 nm) from layer-by-layer method.

The BET surface areas of the films with monodisperse titania added by the layer-by-layer method (99.4 and 110.6 $m^2 \cdot g^{-1}$ with monodisperse TiO_2 of 10 and 50 nm, respectively) were similar to the NF-TiO_2-P25 (111.5 $m^2 \cdot g^{-1}$), whereas the larger aggregates with monodisperse TiO_2 of 300 nm resulted in higher S_{BET}=147.7 $m^2 \cdot g^{-1}$. Compared to the reference of P25 that showed no absorption towards visible light, the composite NF-TiO_2 exhibited absorption spectra extended to the visible range of 400-500 nm to a small degree, owing to the N and F doping (Pelaez *et al.*, 2012b).

The four catalysts were compared in photocatalytic degradation of model organics (ATR, CAF and CMP) spiked together at 4 $\mu mol \cdot L^{-1}$. Experiments were run in a borosilicate glass vessel reactor (i.d. 4.7 cm) containing 10-mL of spiked solution (0.58 cm of aqueous irradiated layer) and 1 composite film (12.5 cm^2). All three compounds were effectively degraded in solar photocatalysis, whereas the best results were obtained using NF-TiO_2 layer-by-layer with monodisperse TiO_2 of 50 nm (**Fig. 4.14**). Namely, for ATR that was the most complicated compound to remove, the first order degradation rates were 10.9×10^{-3} min^{-1} with NF-TiO_2-monodisp.TiO_2(50nm), 9.9×10^{-3} min^{-1} with NF-TiO_2-monodisp.TiO_2(10nm), 8.8×10^{-3} min^{-1} with NF-TiO_2-P25 and 2.5×10^{-3} min^{-1} with NF-TiO_2-monodisp.TiO_2(300nm).

As witnessed in the characterization of the composite films, the difference between the catalyst materials was mainly due to the surface area coverage. Although the composite film containing monodisperse nanoparticles of 300 nm presented a higher surface area than others, its highly aggregated monodisperse particles brought along poor surface area coverage. Meanwhile, the catalysts from layer-by-layer method presented a much more uniform dispersion of the nanoparticle additives and, thus, superior photocatalytic efficiency.

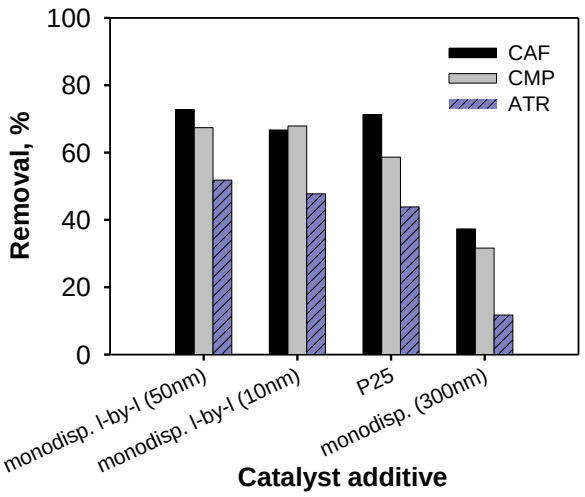

FIG. 4.14: Removal of organics in 2h of solar photocatalytic treatment using NF-TiO_2 composite films with different nanoparticle additives.

4.4.3. Degradation kinetics: effects of pH and salt content

In compliance with the best photocatalytic performance observed in the preliminary experiments (*Chapter 4.4.2*), the photocatalytic removal of 1,4-dioxane was carried out using a composite NF-TiO_2-monodisp.TiO_2(50nm) photocatalyst synthesized by the modified layer-by-layer method, as described in *Chapter 4.4.1*. The degradation of 1,4-dioxane by immobilized photocatalysis was studied in different water matrices. The experiments were carried out in a borosilicate glass vessel reactor (i.d.

11.5 cm) containing 50 mL of sample (approx. 0.50 cm of aqueous irradiated layer) and 5 catalytic films with a total surface of 75 cm^2.

The photocatalytic oxidation of 1,4-dioxane resulted in a linear removal of TOC with time, whereas 1,4-dioxane removal followed first order reaction kinetics (**Table 4.5**). When inorganic ions were present, either initially in the industrial effluent or in a form of added salts (250 $mgSO_4^{2-}\cdot L^{-1}$; 575 $mgCl^-\cdot L^{-1}$; 275 $mgCaCO_3\cdot L^{-1}$), the photocatalytic degradation decreased. Namely, the half-lives of 1,4-dioxane in different conditions were in the following order: pH=5.7 ($t_{1/2}$ = 124 min) > pH 6.9 ($t_{1/2}$ = 134 min) > pH 6.9, industrial effluent ($t_{1/2}$ = 156 min) > pH 6.9, simulated salt content ($t_{1/2}$ = 161 min).

TABLE 4.5: 1st order kinetics of 1,4-dioxane degradation and linear removal rates of TOC in the solar photocatalysis using NF-TiO_2-monodisp.TiO_2 films

Wastewater matrix	$k_{dioxane}$ (1st order) h^{-1}	k_{TOC} (linear) $mg\cdot L^{-1}\cdot h^{-1}$
pH=5.7 (as it is)	0.34 ± 0.02	5.65 ± 0.10
pH=6.9 (+NaOH)	0.31 ± 0.01	5.62 ± 0.34
simulated salt content	0.26 ± 0.02	4.70 ± 0.36
industrial effluent	0.27 ± 0.01	4.16 ± 0.34

Nevertheless, the overall 1,4-dioxane removal was only slightly affected by the increase of pH from 5.7 to 6.9 (90% and 88 %, respectively), and the degradation of TOC per catalyst surface was about 3.4 $\mu gC\cdot cm^{-2}\cdot h^{-1}$ in synthetic wastewaters at both pH=5.7 and pH=6.9 (**Fig. 4.15**). This implies that the reduced photocatalytic degradation in industrial water was mainly caused by the presence of inorganic constituents (~2.8 $\mu gC\cdot cm^{-2}\cdot h^{-1}$ in both the industrial effluent and the synthetic water with simulated salt content).

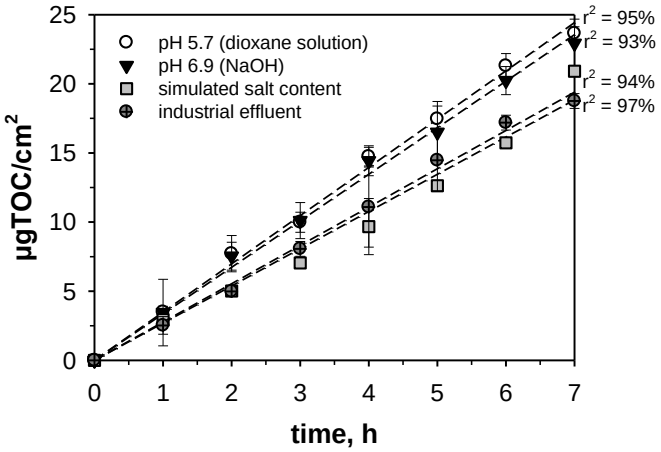

FIG. 4.15: Decomposition of TOC per unit of film area in the solar photocatalytic degradation of 1,4-dioxane on immobilized NF-TiO_2-monodisp.TiO_2.

The negative effect of inorganic anions on the efficiency of photocatalytic oxidation has been attributed to various mechanisms, such as OH• and "hole" scavenging (Burns *et al.*, 1999), and competitive adsorption (Chen *et al.*, 1997). Moreover, there is always a concentration gradient through a molecular transfer towards the catalyst surface because the photocatalytic degradation is expected to occur at the liquid-solid interface (Augugliaro *et al.*, 1995; Linsebigler *et al.*, 1995). Therefore, the concentration and adsorption of inorganic anions on the surface of TiO_2 could result in a loss of active sites for the oxidation of organic molecules.

4.4.4. Treatment of industrial wastewater

In the photocatalytic treatment of an industrial effluent (sample 4, COD_0=250±10 mg·L^{-1}; **Table 3.1**), almost the complete degradation of 1,4-dioxane (≤100%) was achieved along with the 65% and 50% removal of COD and TOC, respectively (**Fig. 4.16**).

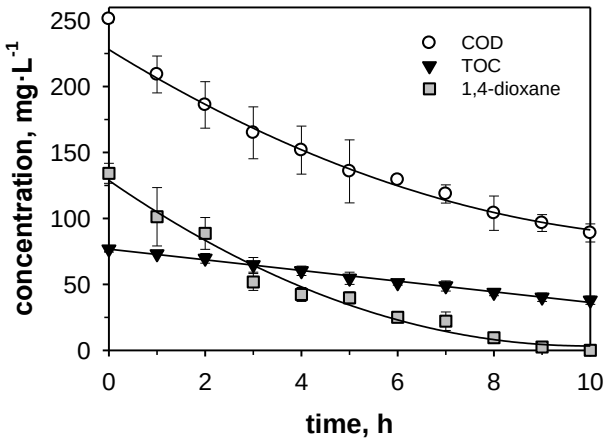

FIG. 4.16: The evolution of 1,4-dioxane, COD and TOC in the treatment of industrial effluent (sample 4) by solar photocatalysis using NF-TiO_2-monodisp.TiO_2 films.

While the concentration of TOC decreased in a linear manner, the degradation of COD followed a trend similar to that of 1,4-dioxane removal (the first order rate constant was k_{COD} = 0.11 h^{-1}, r^2 = 97%), which implies the accumulation and slower degradation of reaction intermediates. The slow but persistent removal of carbon in the experiments with the supported catalyst reflects that a complete mineralization of contamination from the real industrial effluent could be feasible using immobilized NF-TiO_2-monodisp.TiO_2. Total mineralization could be reached either by elongating the reaction time or, preferably, by increasing the catalyst surface. Using an immobilized catalyst would permit working without the need of an additional costly filtration step, which would greatly enhance the engineering of the process.

4.5. PATHWAYS OF 1,4-DIOXANE DECOMPOSITION

Since the different AOPs involve multiple possible transformations of catalyst and reactive radical species, different degradation routes could be expected, depending on the treatment. Therefore, the understanding of the degradation mechanism could play a great role in process optimization. Thus, the main objective of this section of the doctoral investigation was studying and comparing the mechanisms of 1,4-dioxane decomposition by the AOPs under concern (***Publications I, III, V-VII***). Apart from the chromatographic analysis, on-line FTIR spectroscopy was used as an innovative tool for the *in situ* monitoring of the intermediate chemical species generated during the oxidation reaction.

4.5.1. On-line Fourier transform infrared monitoring

For a better observation of the reaction products, the experiments with FTIR monitoring were carried out in a concentrated synthetic solution of 1,4-dioxane (≈7 $g \cdot L^{-1}$; Merayo *et al.*, 2014). As immobilized photocatalytic experiments would not be feasible in so highly concentrated 1,4-dioxane solution, additional trials were conducted with suspended TiO_2–P25. For comparison purposes, classic (Fe^{2+}-based) photo-Fenton experiments in acidic conditions (pH_0=2.8) were conducted as well. The heterogeneous photo-Fenton with Fe^0 and the CDEO were carried out in slightly basic conditions (pH_0≈8.5), whereas the ozonation trials were conducted both at basic pH above 9 and at initial pH_0=5.7, while the photocatalysis was performed at initial pH_0=5.7. Without any control, the initial pH dropped to 3.1 during the oxidation.

4.5.1.1. Oxidation with molecular O_3 vs. radical pathway vía O_3/OH^-

Basic conditions clearly favoured faster kinetics of 1,4-dioxane degradation, as 93% of 1,4-dioxane (66% of the COD) was removed at pH>9, whereas only 63% removal of 1,4-dioxane (40% of the COD) was achieved at pH<5.7 (**Fig. 4.17**).

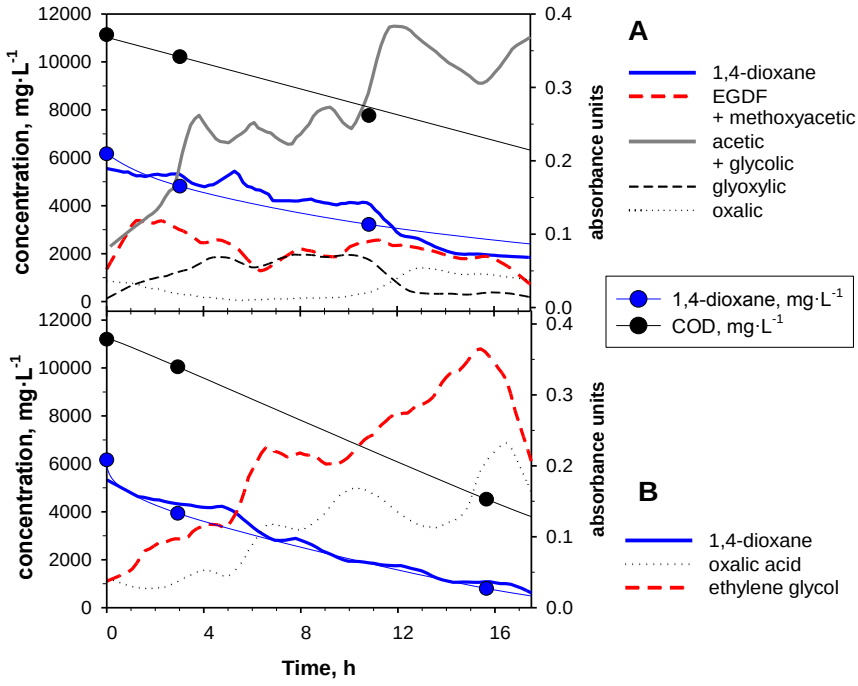

FIG. 4.17: (A) Oxidation by molecular O_3 (pH<5.7; route of EGDF) vs. (B) O_3/OH^- oxidation through ethylene glycol (pH>9; radical pathway of O_3 decomposition to OH•).

According to the ConcIRT software that associates the important organic bonds to the different organic molecules, the oxidation by molecular O_3 (pH<5.7; **Fig. 4.17A**) occurs through intermediates like EGDF, and acetic, glycolic and glyoxylic acids; whereas less oxalic acid was produced (this tendency is also supported by the chromatographic analyses of carboxylic acids). At pH>9 (**Fig. 4.17B**), the major intermediate identified by ConcIRT software were ethylene glycol and oxalic acid. When most of the 1,4-dioxane was consumed, the concentrations of ethylene glycol and, subsequently, oxalic acid started to decrease as well.

As oxalic acid is one of the last intermediates expected (Cooper *et al.*, 2009; Stefan and Bolton, 1998), its disappearance indicates that the reaction has reached a stage where total mineralization of the organics occurs. This is not the case at pH<5.7 where the increment of oxalic acid was still very low at the end of the reaction.

4.5.1.2. Heterogeneous AOPs: CDEO, Fe^0-based photo-Fenton and TiO_2-photocatalysis

The fastest disappearance of 1,4-dioxane was observed with CDEO (≥99% in 80 min), although the degradation with UV photo-Fenton was only slightly slower (95%; **Fig. 4.18**). Considerable amounts of EGDF, EGMF and ethylene glycol (up to 360 $mg \cdot L^{-1}$) were measured in CDEO, whereas only traces of EGDF and EGMF were detected in Fe^0-based photo-Fenton experiments, but much higher accumulation of ethylene glycol was observed (up to 2100 $mg \cdot L^{-}$; **Fig 4.19**).

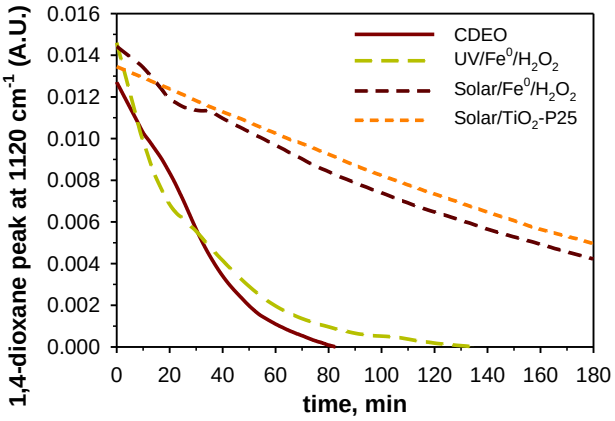

FIG. 4.18: Comparison of AOPs: decrease of 1,4-dioxane peak in relative absorbance units (A.U.) monitored by FTIR spectrometry.

In both processes (CDEO and photo-Fenton), formic acid was the most abundant reaction intermediate (peaks of 4000-5000 $mg \cdot L^{-1}$), generated since the beginning of the reaction. In both cases, formic acid was followed by smaller concentrations of several other carboxylic acids, like methoxyacetic and glycolic acids, whereas acetic and oxalic acids appeared later. Apparently, the mineralization of these short chain carboxylic acids was faster with CDEO, as observed by their disappearance in **Fig. 4.19**.

The radiation source did not influence the 1,4-dioxane decomposition products during photo-Fenton, as similar intermediates were detected with Fe^0/H_2O_2/UV and Fe^0/H_2O_2/solar. The more intensive UV lamp simply favoured the earlier appearance and faster degradation of these by-products.

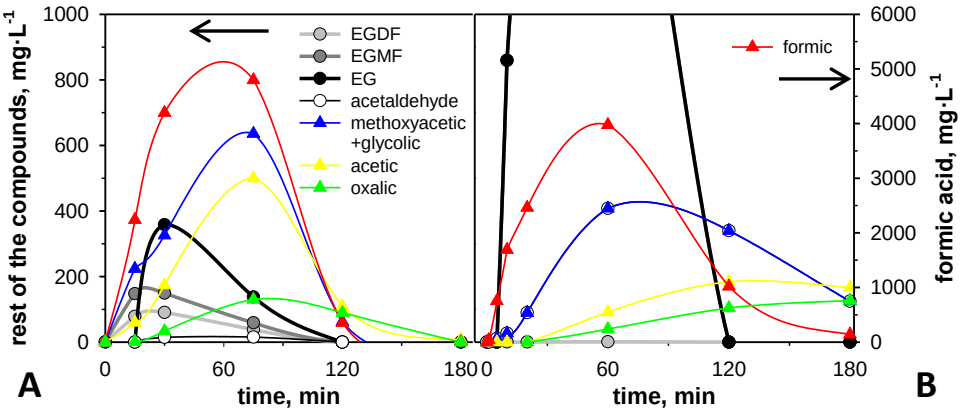

FIG. 4.19: Profiles of 1,4-dioxane decomposition products during (A) CDEO; and (B) UV/Fe^0/H_2O_2

Only slightly slower removal of 1,4-dioxane was achieved with solar photocatalysis (60%) than with solar photo-Fenton (65%), but unlike in photo-Fenton experiments, no ethylene glycol was detected in the system with either UV or solar photocatalysis. The degradation by-products were the same for suspended photocatalysis with TiO_2-P25 as for immobilized NF-TiO_2-monodisp.TiO_2, as described in the following chapter.

4.5.2. Degradation *via* immobilized photocatalysis

The study of degradation routes by immobilized photocatalysis was carried out in a solution with 135 mg·L^{-1} of 1,4-dioxane. EGDF, EGMF and formic acid were identified as major reaction intermediates in the experiments (**Fig. 4.20**). In lesser extent (≤4.0±0.1 mg L^{-1}), some acetic acid was produced along the process, while traces of methoxyacetic and glycolic acids were detected as mixture at concentrations below 1.16±0.06 mg L^{-1}.

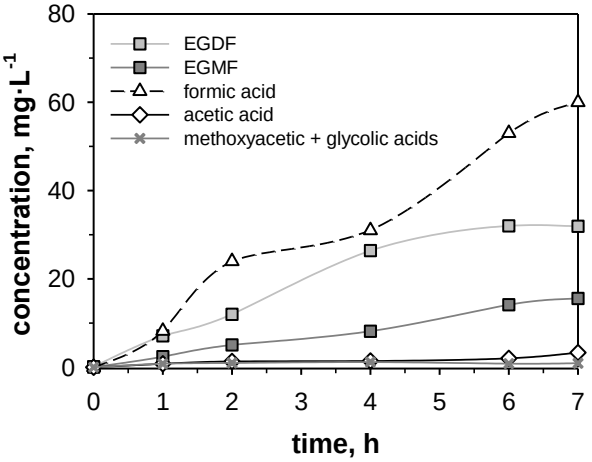

FIG. 4.20: Major reaction intermediates in the photocatalytic degradation of 1,4-dioxane under solar light using immobilized NF-TiO_2-monodisp.TiO_2

4.5.3. Comparison of the degradation routes

The major routes proposed for 1,4-dioxane degradation with the studied treatments are presented in **Fig. 4.21**. Most of the intermediate degradation steps omitted in this simplified scheme occur through radical intermediates following the mechanism of tetroxide formation over peroxyl radical, as

proposed by several authors (Cooper *et al.*, 2009; vonSonntag and Schuchmann, 1997). 1,4-Dioxan-α-oxyl radical has been suggested to be the precursor of the major primary decomposition products of 1,4-dioxane (Merayo *et al.*, 2014; Stefan and Bolton, 1998). In agreement with Stefan and Bolton (1998), this α-oxyl radical can be degraded either through ΔC-C splitting at the α-C position (**route A**, red line) or through an intramolecular reaction (H abstraction from the α´-C position) followed by fragmentation (**route B**, blue line).

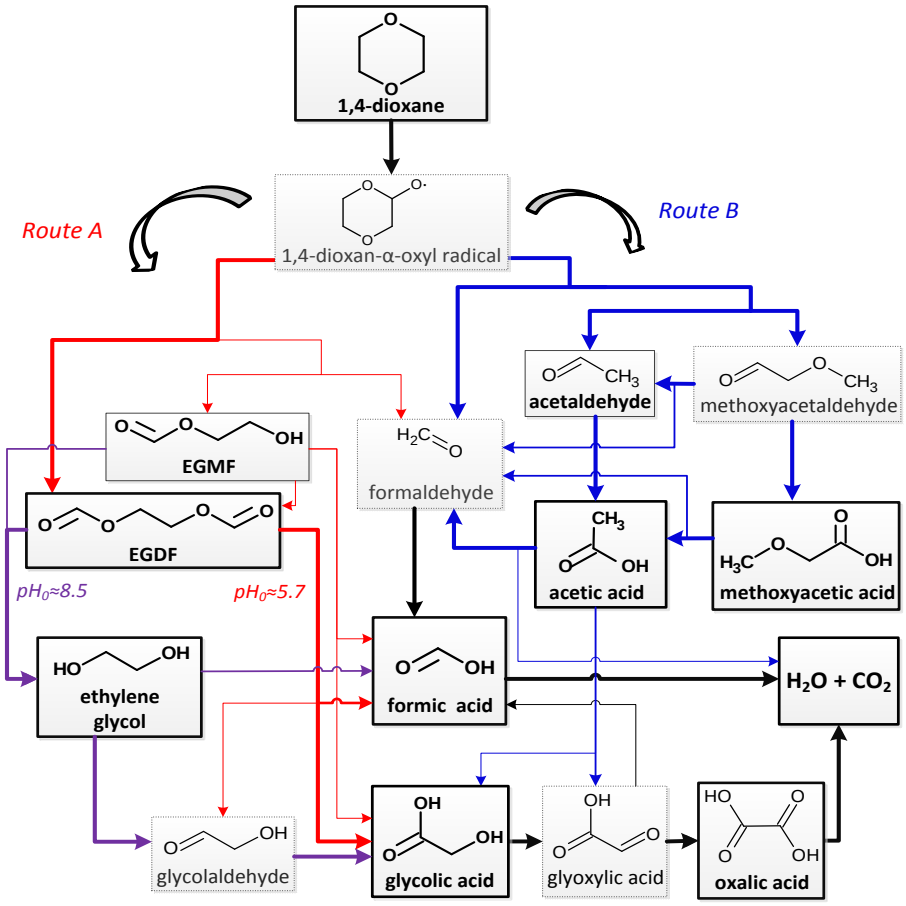

FIG. 4.21: Proposed simplified schematic of 1,4-dioxane decomposition routes. ***The bold-faced arrows denominate the prevalent pathways suggested for each route; the boxes with continuous line = detected compounds / discontinuous line = suggested intermediates.***

Considering the chromatography analysis, the primary degradation pathway for all the studied AOPs was route A, in which either EGDF or EGMF and formaldehyde are produced (Merayo *et al.*, 2014; Stefan and Bolton, 1998). The major difference between the studied AOPs seems to be due to the variation in their pH profiles (**Fig. 4.22**). Namely, in acidic conditions in classic (Fe^{2+}-based) Fenton processes EGDF (and EGMF) are hydrolysed to ethylene glycol (Merayo *et al.*, 2014). Similar tendency, but *via* basic hydrolysis, was observed in basic conditions ($pH_0 \geq 8.5$) in O_3/OH^-, CDEO and heterogeneous photo-Fenton processes (denominated by the purple line in **Fig. 4.21**), whereas the operating pH of photocatalysis ($pH_0 \approx 5.7$) was neither acidic nor basic enough for the hydrolysis to occur. The CDEO seems to be a good example of a transition process where both pathways are represented (**Fig. 4.19A**).

Regardless, the subsequent decomposition of EGDF/EGMF as well as ethylene glycol is rather similar. Namely, the degradation of EGDF and EGMF is started with H-abstraction by OH• or HO_2• attack, resulting in formic and glycolic acids as final products (Beckett and Hua, 2000; Stefan and Bolton,

1998), while ethylene glycol is also subsequently degraded to glycolic acid through the formation of glycolaldehyde (Dow, 2014; Merayo *et al.*, 2014), whereas possible generation of some formic acid has been reported as well (Dow, 2014; Rossiter *et al.*, 1983). In further oxidation, formic acid is directly mineralized to CO_2 (Cooper *et al.*, 2009; Stefan and Bolton, 1998) at a high reaction rate with OH• (3.2 x 10^9 $M^{-1}{\cdot}s^{-1}$; Buxton *et al.*, 1988). Glycolic acid decomposes to glyoxylic acid which is next rapidly oxidized to oxalic acid (Cooper *et al.*, 2009; Karpel Vel Leitner and Dore, 1997; Merayo *et al.*, 2014). Oxalic acid appears as one of the most common last detected intermediates before the mineralization of organics (Cooper *et al.*, 2009; Stefan and Bolton, 1998). To a lesser extent, some glyoxylic acid could also decompose to formic acid, which is easily degraded to water and CO_2 (Cooper *et al.*, 2009; Karpel Vel Leitner and Dore, 1997).

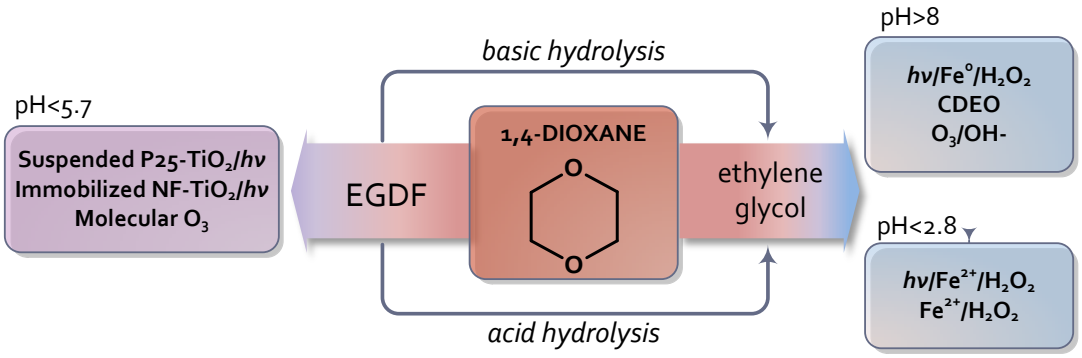

FIG. 4.22: Schematic division of AOPs by the major primary intermediate

Another major difference between the AOPs is apparently the greater importance of an alternative degradation route B in CDEO and photo-Fenton treatments. In route B, according to Stefan and Bolton (1998), 1,4-dioxan-α-oxyl radical is degraded through an intramolecular reaction producing formaldehyde (and, thus, formic acid) along with methoxyacetaldehyde and acetaldehyde (**Fig. 4.21**). Methoxyacetaldehyde is subsequently oxidized to methoxyacetic and acetic acids, while acetaldehyde yields acetic acid (Kim *et al.*, 2008; Merayo *et al.*, 2014; Stefan and Bolton, 1998). The subsequent degradation of acetic acid gives formaldehyde and glycolic and glyoxylic acids as major by-products in free-radical-induced degradation, whereas CO_2 is produced as well, indicating that some mineralization also occurs in that stage of decomposition (Cooper *et al.*, 2009; Karpel Vel Leitner and Dore, 1997; Tan *et al.*, 2012). Comparing the profiles of methoxyacetic and acetic acids, relatively low concentrations (50-100 $mg{\cdot}L^{-1}$) were detected in ozonation trials compared to photo-Fenton and CDEO (up to 500 $mg{\cdot}L^{-1}$ of acetic acid). In CDEO, some acetaldehyde could also be measured, as a further proof of this degradation pathway. Meanwhile, the alternative route B was hardly significant in TiO_2–photocatalytic process.

4.6. ECONOMIC ASSESSMENT

To evaluate the industrial implementation of the studied AOPs, a preliminary economic assessment was made for the treatment of the industrial wastewater sample with a COD of 475±25 $mg \cdot L^{-1}$ (**Table 3.1**), considering a capacity of 43800 $m^3 \cdot y^{-1}$ which is the flow rate of the plant producing this effluent (***Publication VII***). Ozonation, electro-oxidation on BDD and Fe^0-based photo-Fenton processes were chosen to reach the established objective, whereas the immobilized photocatalytic treatment was considered a rather emerging technology, more suitable for polishing wastewaters with lower organic load and smaller flow rate. For the pre-design of the chosen AOPs, several assumptions were made, described as follows.

4.6.1. Design conditions

The respirometric trials of biodegradability assessment with activated sludge showed that all three AOPs increased the initial biodegradability of the industrial wastewater (≈6%), whereas the bio-augmentation seemed to be in correlation with the previous COD removal by AOP, indifferent to the pre-treatment (**Fig. 4.23**). Therefore, as a simplification, COD removal was taken as the basis of design point selection, according to which, sufficient biodegradability (≈60%) was reached when advanced oxidation pre-treatment was conducted up to 40% removal of COD. In this case, the resulting effluent would be returned to the biological treatment unit of the plant.

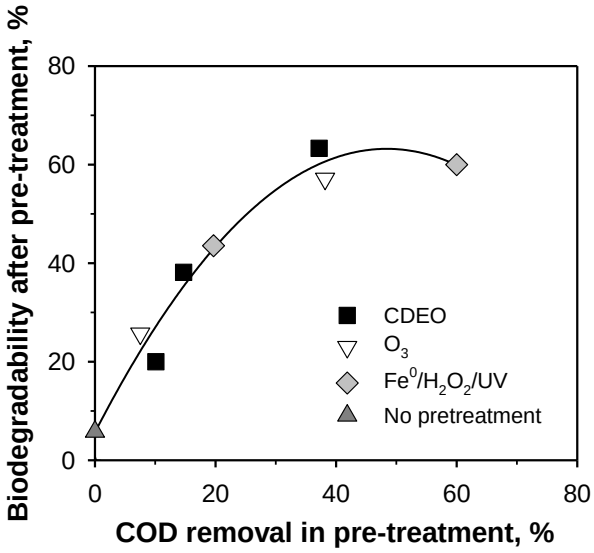

FIG. 4.23: Evolution of the biodegradability of industrial wastewater (Sample 1) as a function of the COD removal in its pre-treatment by different AOPs.

4.6.2. Capital cost

The size and cost of AOP units were calculated taking into account both the experimentally found oxidant requirements and the existing literature on such treatments. All prices were updated, considering the change in chemical engineering plant cost index (CEPCI, 2015). When necessary, the prices were rescaled for different treatment capacities, using the logarithmic relationship known as the six-tenths-factor rule (Chatzisymeon *et al.*, 2010; Peters *et al.*, 2003).

Considering the necessary total O_3 production (4.2 $kgO_3 \cdot h^{-1}$), the cost of the ozonation unit (including generator, dosification system and refrigeration) was facilitated by two commercial

manufacturers of industrial ozonation systems (Xylem and Primozone). The price of the CDEO unit was found based on the literature (Cañizares *et al.*, 2009; Chatzisymeon *et al.*, 2010) and the average unit price of BDD provided by NeoCoat SA (14,000 €·m^{-2}). The price of the UV photo-Fenton unit was found by the study of Muñoz *et al.* (2008), whereas the cost of solar photo-Fenton was calculated by the necessary compound parabolic collector (CPC) area (Muñoz, 2006), considering the unit price of CPC to be 349 €·m^{-2} (De Torres-Socias *et al.*, 2015).

Based on the price of each AOP unit, the fixed capital investment was found incorporating the estimated cost of piping, valves, and electrical work (30%), site work (10%), engineering (15%), contractor (15%) and contingency (20%; Kommineni *et al.*; Mahamuni and Adewuyi, 2010). The working capital investment required for the start-up was considered 15% of the fixed capital investment (Chatzisymeon *et al.*, 2010).

4.6.3. Operation cost

The operating parameters used for the assessment were the cost of energy, chemicals, maintenance, analytic monitoring and labour-hours. The energy consumption for CDEO and UV photo-Fenton was obtained from the experimental data, taking into account the price of industrial electricity in Spain (0.1 €·kWh^{-1}; Eurostat, 2015). Additional consumption in pumping, cooling and reagent injection operations was added according to the literature (10-40% depending on the AOP; Chang *et al.*, 2008; Karat, 2013; Kommineni *et al.*; Mahamuni and Adewuyi, 2010). The total energy consumed by an industrial O_3 generator was considered to be 18 kWh·kgO_3^{-1}, already including both O_3 generation and the additional consumption for refrigeration, in accordance with the commercial providers (Xylem, Inc.) and the literature (Karat, 2013). In solar applications, pumping was considered the main source of electricity withdrawal, in correlation with the area of the compound parabolic collector, as described in detail by Muñoz (2006).

The chemicals cost was calculated, considering the latest industrial prices, wherefore all the prices were updated by the annual cost indexes for chemical products (INE, 2015). The price of the off–fence O_2 gas for O_3 production at was 85 €·t^{-1} (Karat, 2013) and the optimized industrial consumption rate was considered 10 kgO_2·kgO_3^{-1} (Muñoz, 2006). The costs of the rest of reagents were 0.45 €·kg^{-1} for H_2O_2 (50%), 0.3 €·kg^{-1} for NaOH, 0.09 €·kg^{1} for Na_2SO_4 and 5 €·kg^{-1} for Fe^0 powder (Alibaba, 2015). The calculations were done assuming 90% of catalyst recovery on daily basis, whereas the waste catalyst landfilling was considered to cost 0.07 €·kg^{-1} (Muñoz, 2006).

The annual cost of maintenance and parts replacement was considered to be 3% of the fixed capital investment for CDEO and solar-enhanced systems and 1.5% for ozonation (Chatzisymeon *et al.*, 2010; Mahamuni and Adewuyi, 2010; Muñoz, 2006). The maintenance (mainly lamps replacement) of UV photo-Fenton was calculated as 45% of annual electricity consumption (Mahamuni and Adewuyi, 2010). The cost of the required labour and the laboratory work for analytic monitoring was found by consulting with a local a firm that offer wastewater treatment solutions, considering the required work as an additional task for the existing personnel.

4.6.4. Total cost

The total annual cost of the treatments consisting of annual capital investment and annual operation cost was found, defining the useful life of AOP plant at 15 years (Muñoz *et al.*, 2008) and using an interest rate of 5%, leading to a capital recovery factor of 9.6% (Chatzisymeon *et al.*, 2010). The main

components of the total investment required for the industrial implementation of the AOPs under study are presented in **Table 4.6**.

Table 4.6: Estimation of the total costs of different AOPs for the treatment of 43800 $m^3 \cdot y^{-1}$ of industrial wastewater (Sample 1, Table 3.1) until 40% of COD removal.

	O_3	CDEO (BDD)	UV/Fe^0/H_2O_2	Solar/Fe^0/H_2O_2
CAPITAL INVESTMENT				
Fixed capital investment, €	366,823	881,361	237,904	1,494,574
Working capital investment, €	55,023	132,204	35,686	224,186
Total capital investment, €	**421,847**	**1,013,566**	**273,590**	**1,718,760**
Annual capital cost, $€ \cdot y^{-1}$	**40,642**	**97,649**	**26,358**	**165,589**
Capital cost per m^3, $€ \cdot m^{-3}$	*0.9*	*2.2*	*0.6*	*3.8*
OPERATION AND MAINTENANCE (O&M) COST				
Energy	65,752	59,218	58,632	3,620
Chemicals	37,830	5,830	29,912	18,677
Repairs and maintenance	5,502	26,441	26,392	44,845
Labour	25,000	25,000	25,000	25,000
Analysis	12,000	12,000	12,000	12,000
Annual O&M cost, $€ \cdot y^{-1}$	**146,085**	**128,489**	**151,936**	**104,142**
O&M cost per m^3, $€ \cdot m^{-3}$	*3.3*	*2.9*	*3.5*	*2.4*
TOTAL COST				
Total annual cost, $€ \cdot y^{-1}$	**186,726**	**226,138**	**178,294**	**269,731**
Annual cost per m^3, $€ \cdot m^{-3}$	*4.3*	*5.2*	*4.1*	*6.2*

According to this preliminary economic assessment, UV photo-Fenton is the cheapest option at the chosen design point (4.1 $€ \cdot m^{-3}$ for 40-% COD removal at a plant capacity of 43800 $m^3 \cdot y^{-1}$), followed very closely by ozonation treatment (4.3 $€ \cdot m^{-3}$). Meanwhile, CDEO and solar/Fe^0/H_2O_2 treatments were found to be more costly (5.2 and 6.2 $€ \cdot m^{-3}$, respectively). Although much less energy is consumed in solar photo-Fenton process (≈4,000 $€ \cdot y^{-1}$) than in UV photo-Fenton treatment (≈59,000 $€ \cdot y^{-1}$), the sunlight-driven process is unfeasible in this scale due to the cost of CPC installation (≈1,495,000 €) and the required plant space (2254 m^2). Nevertheless, due to the different reaction kinetics of the studied processes, their economic comparison is quite different when changing the objective of organics degradation (**Fig. 4.24**).

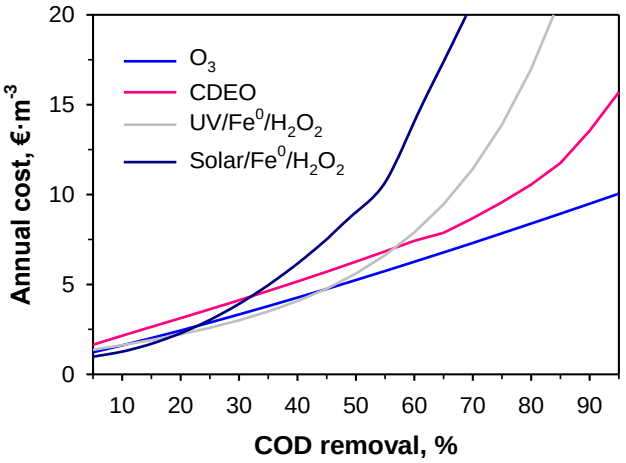

FIG. 4.24: Prevised annual cost of different AOPs for varying COD removals at the plant capacity of 43800 $m^3 \cdot y^{-1}$.

According to the graph of annual costs as a function of COD removal (**Fig. 4.24**), UV enhanced photo-Fenton is the most economical solution at COD removals in the range of 20-45%, whereas ozonation appears to be more suitable application when the AOP is designed for COD removals higher than 50% at which UV photo-Fenton becomes unviable due to the excessive electricity expenses. Although faster and, thus, more energy-efficient reduction is achieved with CDEO than with O_3, the cost of the electro-oxidation unit with BDD electrodes still limits its industrial application. While ozonation technology exhibits much greater know-how of full scale implementation, CDEO is still a process not yet fully explored in the field of industrial wastewater treatment. However, the advances in the field of conductive diamond technology could change that situation, converting CDEO an important competitor to both O_3 and Fenton-based processes in the future.

In addition, it is important to note that solar photo-Fenton appears to become profitable at COD removals below 20%, as shown in **Fig. 4.24**, provided that the enterprise has the space required for the CPC unit. As the cost and viability of the solar/Fe^0/H_2O_2 application is directly related to the CPC area, the required area was plotted as a function of both COD removal and plant capacity (**Fig. 4.25A**). According to this 3D-plot, if 20% of COD removal was sufficient, the CPC area required to treat 43800 $m^3 \cdot y^{-1}$ would decrease to approximately 500 m^2, whereas the area to treat 10000 $m^3 \cdot y^{-1}$ would be around 130 m^2. These are space requirements that still become an obstacle for many industrial plants, but could already be considered by many others (according to the proposal of Muñoz (2006), one of the solution would be installing the CPC unit on the rooftops of the existing facilities). On the other hand, when considering the treatment for even smaller wastewater flows, it is important to note that the predicted annual costs of all the studied AOPs (in terms of $€ \cdot m^{-3}$) shoot up for capacities lower than 10000 $m^3 \cdot y^{-1}$, as shown for solar photo-Fenton in **Fig. 4.25B**.

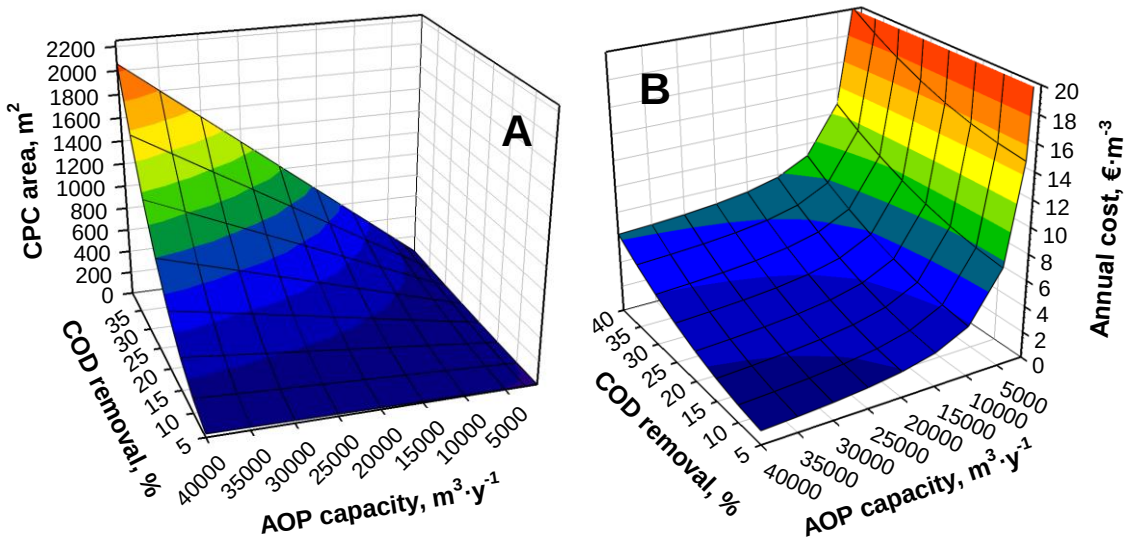

FIG. 4.25: 3D plots of (A) CPC area and (B) annual cost required for the solar photo-Fenton treatment as functions of COD removal (5-40%) and plant capacity (1000-40000 $m^3 \cdot y^{-1}$).

The predictions presented in Table 4.7 principally allow the comparison of the installation and the operation costs of the different technologies. Nonetheless, care must be taken when interpreting the exact figures based on laboratory scale experimentation, since much more efficient use of the oxidant is expected in fully optimized industrial units. There are different factors affecting different AOPs, such as the position and the number of UV lamps in the photo-Fenton reactor, the bubble size and the O_3

injection method used in ozonation process (bubble diffusers, venturi eductors, membrane contactors, etc.), the flow pattern and the configuration of electrodes in the electrolytic cell, and the thickness of the illuminated wastewater layer and the configuration of the solar collector in solar photo-Fenton. Moreover, an AOP unit can be comprised of one reactor or multiple consecutive units, depending on the optimal combination, whereas the size of the reactor(s) can greatly affect the process efficiency as well. For instance, the mass transfer and, thus, the oxidation rate in an electrolytic flowcell is greater when the layer of water between the electrodes is thinner, and the industrial BDD units normally consist of small modules of electrodes in multiple stacks. On the other hand, the contact time and, thus, the oxidation rate with O_3 is greater in large full scale reactors, especially when pressure driven O_3 injection is used that allows greater dissolution of O_3 than the bubble diffusers. Furthermore, for any of these AOPs, before an actual industrial implementation, a preliminary pilot scale study coupled with the real biological treatment unit of the plant would be obligatory in order to correctly determine the optimal design point of biodegradability enhancement. Nevertheless, since similar hypothesis were used to calculate the cost of each treatment, this preliminary cost assessment permits comparing these four processes, offering a good insight of the components constituting the final price of the treatments.

5. CONCLUSION

In this PhD thesis, the treatment of wastewaters containing 1,4-dioxane was studied by means of AOPs, with the focus on the development and optimization of efficient and environmentally sustainable technologies. Ozonation, CDEO, Fe^0 photo-Fenton and immobilized photocatalytic processes were studied in detail and routes of 1,4-dioxane degradation in the different oxidation processes were established. Furthermore, novel on-line analytical methodologies were employed for reaction monitoring and process optimization. Therefore, this research presents new knowledge on the treatment of industrial effluents with such bio-recalcitrant contaminants, addressing technological, mechanistic and economic aspects of the three studied treatment methods.

The viability and the mechanisms of ozonation, CDEO and Fe^0-based photo-Fenton processes were assessed with a synthetic 1,4-dioxane solution. In addition, synthesis and characterization of different modifications of immobilized NF-TiO_2 were performed, and the degradation of 1,4-dioxane using the best catalyst was studied in different water matrices.

- O_3 was proven efficient as a sole oxidant to degrade 1,4-dioxane from wastewaters in controlled basic conditions. pH≥9.0 was the key factor to make the ozonation a viable process, since 1,4-dioxane and its by-products are degraded preferentially by OH• generated from O_3 in the presence of OH^-. Namely, the $t_{1/2}$ of 1,4-dioxane was reduced about 20-fold when increasing the operating pH from 7 ($t_{1/2}$=578 min) to 9 ($t_{1/2}$=29 min). Working at pH 10.0, close to 90% of the COD was removed and almost a complete degradation of 1,4-dioxane was reached with the consumption of 1.8 $gO_3 \cdot L^{-1}$, whereas about 80% of the COD was already degraded by 1 $gO_3 \cdot L^{-1}$. The presence of carbonaceous alkalinity also enhanced the O_3 process due to its buffer effect that kept the pH≈9.
- Non-selective anodic oxidation on BDD electrodes resulted in COD removals close to 100% in 5 h (≈130 $kWh \cdot kgCOD_{removed}^{-1}$); whereas about 85% of the COD was already removed in 3 h (≈85 $kWh \cdot kgCOD_{removed}^{-1}$). Regarding the supporting electrolytes, no radical scavenging effect was found with either SO_4^{2-} or HCO_3^-, whereas their principal effect simply laid on providing the necessary conductivity for electrolysis. The optimal compromise for achieving a maximum COD removal at a maximum current efficiency and producing the minimum energy consumption was reached using the highest concentrations of SO_4^{2-} (41.6 $mEq \cdot L^{-1}$) , HCO_3^- (32.8 $mEq \cdot L^{-1}$) and initial COD (750 $mg \cdot L^{-1}$), and applying a current density of 11.9 $mA \cdot cm^{-2}$ for 3.8 hours.
- Employing Fe^0 microspheres as an iron source for photo-Fenton treatment resulted in excellent results at neutral and even slightly basic pH without any iron leaching. The presence of bicarbonate buffer (pH_0≈8.5) resulted beneficial to maintain the heterogeneous conditions. The destruction of organics in UV photo-Fenton process with different H_2O_2/COD_0 ratios was in the following decreasing order: 2.625 > 2.125 > 4 > 1.625. Complete removal of 1,4-dioxane was reached in 5 min and almost total COD removal was obtained after 30 min of treatment (≥98%). Meanwhile, H_2O_2/Fe^0 ratio of 60 was found an optimum value for the sunlight driven photo-Fenton, whereby more than 90% of 1,4-dioxane was degraded after 180 min, presenting an important economic alternative when biodegradability enhancement was the aim of the treatment. According to the SEM-EDX study, the morphology of microspheres remained intact after photo-Fenton treatment in neutral conditions. Therefore, it is proposed that the Fe^{2+} generated in the presence of H_2O_2, remains anchored on the iron surface, taking part of the Fenton reaction directly on the Fe^0 microsphere, and a total recovery of the catalyst is expected when used in heterogeneous conditions.

- Various nanoparticle sizes and different incorporation methods were tested for the addition of monodisperse TiO_2 to the NF-TiO_2 catalyst. The incorporation method of the monodisperse titania to NF-TiO_2 played a significant role in the final physicochemical and photocatalytic properties of the composite film. Minor aggregation and improved distribution of monodisperse TiO_2 particles as well as significantly superior photocatalytic performance was obtained with the layer-by-layer technique than with the monodisperse TiO_2 directly incorporated into the sol. Considering these results, the layer-by-layer method was used to synthesize NF-TiO_2-monodisp.TiO_2 for the subsequent degradation of 1,4-dioxane under solar light to study the effect of different wastewater matrices. Removal of the compound decreased for different wastewater conditions in the following order: pH=5.7 (k=0.34±0.02 h^{-1}) > pH 6.9 (k=0.31±0.01 h^{-1}) > industrial effluent (k=0.27±0.01 h^{-1}) > simulated salt content (k=0.26±0.01 h^{-1}). This indicates that the degradation of 1,4-dioxane decreased in the industrial effluent mainly due to its inorganic constituents, whereas the change in the effluent pH only produced a slight decrease in the degradation efficiency.

The studied AOPs were used for the treatment of real industrial wastewaters from a chemical factory. Ozonation, CDEO and Fe^0-based photo-Fenton processes were chosen to treat industrial samples with high organic load (≥450 mg·L^{-1} of COD), whereas immobilized solar photocatalysis was employed to polish the wastewaters with low organics content (≤260 mg·L^{-1} of COD).

- By ozonation, 85% of COD was removed in 4 h from the industrial effluent containing only 1,4-dioxane (COD_0≈475 mg·L^{-1}), degrading 0.23 g of COD per 1 g of O_3, whereas nearly 70% was already removed in 3 h. The original carbonaceous alkalinity of the wastewater was beneficial for maintaining the optimal conditions (pH>9). The treatment of wastewaters with higher COD (1360 and 2300 mg·L^{-1}), containing both 1,4-dioxane and MDO, reached a smaller COD removal percentage (63% and 53% in 4 h, respectively), but a higher total amount of COD removed per oxidant consumed (0.44 and 0.93 gCOD·gO_3^{-1}, respectively).
- By CDEO treatment, up to 98% of the COD was removed in 5 h and nearly 85% already in 3 h of electro–oxidation of the effluent just containing 1,4-dioxane (COD_0≈475 mg·L^{-1}), consuming 114 kWh·$kgCOD_{removed}^{-1}$. Meanwhile, up to 91% COD removal was achieved in 5-h treatment of the effluent containing both 1,4-dioxane and MDO (COD_0≈1360 mg·L^{-1}), resulting in the consumption of 49 kWh·$kgCOD_{removed}^{-1}$. By both CDEO and O_3, MDO was degraded more easily than 1,4-dioxane and, therefore, its presence offered competition for the OH• radicals and reduced the efficiency of the 1,4-dioxane degradation.
- By heterogeneous photo-Fenton treatment, about 98% of COD and 90% of TOC were removed from the industrial effluent after 40 min of UV/Fe^0/H_2O_2 oxidation, whereas solar driven process was able to reach approximately 60 and 35% of COD and TOC removals in 3 h of treatment, respectively. The relatively high alkalinity of the effluent resulted to be an advantage, as heterogeneous conditions without any iron leaching were maintained throughout the experiments. The opportunity to avoid sludge production and pH adjustments makes the Fe^0 microspheres an efficient catalyst for the treatment of wastewaters containing 1,4-dioxane by photo-Fenton processes
- By immobilized solar photocatalysis on NF-TiO_2-monodisp.TiO_2, despite the salt content in the industrial wastewater, almost complete degradation of 1,4-dioxane was achieved along with 65% and 50% removal of COD and TOC, respectively, after 10 h of treatment. In industrial implementation, the treatment time would directly depend on the available catalytic surface. The slow but persistent removal of organic carbon throughout the experiment reflects that a complete mineralization of contamination from actual industrial effluents could be feasible using this supported catalyst. Immobilization, in turn, would greatly enhance the process engineering and, thus, increase the cost-effectiveness of the treatment.

The decomposition pathways of 1,4-dioxane were established and compared based on extensive chromatography analysis, whereas FTIR monitoring served as a powerful tool for on-line reaction monitoring.

- Most of the interim steps of 1,4-dioxane degradation follow the mechanism of tetroxide formation from radical intermediates over corresponding peroxyl radical. According to the major decomposition route, the initial radical intermediate, 1,4-dioxan-α-oxyl radical, is degraded through ΔC-C splitting, producing EGDF and/or EGMF. Alternatively, methoxyacetic and acetic acids can be produced in the decomposition of the α-oxyl radical through an intramolecular reaction followed by fragmentation.
- The major difference between the studied AOPs is due to their pH profiles. Namely, in basic conditions ($pH_0 \geq 8.5$) EGDF and EGMF are hydrolysed to ethylene glycol *via* basic hydrolysis. Therefore, the oxidation by molecular O_3 (pH<5.7) occurs through the production of EGDF as major intermediate, whereas in controlled basic ozonation at pH>9 the major intermediate identified was ethylene glycol. While CDEO seems to be a good example of a transition process where both pathways are represented. In heterogeneous photo-Fenton processes ethylene glycol was primarily detected. Meanwhile, no hydrolysis of EGDF occurs at the operating pH of photocatalysis ($pH_0 \approx 5.7$).
- The alternative pathway of methoxyacetic acid has greater importance in CDEO and photo-Fenton treatments. Meanwhile, relatively low concentration profiles of methoxyacetic and acetic acids were detected in ozonation and photocatalytic trials.
- Regardless of the AOP, the decomposition of the primary intermediates continued over the generation of short chain carboxylic acids, being formic acid the most prevalent intermediate by-product. The decomposition of EGDF/EGMF as well as ethylene glycol is rather similar, resulting in formic and glycolic acids as final products. In further oxidation, formic acid is directly mineralized to CO_2, while glycolic acid decomposes to glyoxylic acid which is next rapidly oxidized to oxalic acid, one of the most common last detected intermediates before the mineralization of organics. The degradation of acetic acid gives formaldehyde and glycolic and glyoxylic acids as major by-products in free-radical-induced degradation, whereas some mineralization also occurs in that stage.

The possible industrial implementation of O_3, CDEO, and Fe^0-based photo-Fenton processes was pre-evaluated, comparing the costs for treating 43800 $m^3 \cdot y^{-1}$ of the industrial wastewater from chemical manufacturing ($COD_0 \approx 475$ mg$\cdot L^{-1}$).

- According to the respirometric assays, all chosen AOPs were fit to increase the biodegradability of the wastewater. Sufficient biodegradability (≈60%) was reached when the pre-treatment was conducted until 40% of COD removal, at which point most of the 1,4-dioxane was degraded to ethylene glycol and short chain carboxylic acids.
- According to this preliminary cost assessment, UV photo-Fenton is the cheapest option (4.1 €$\cdot m^{-3}$), followed very closely by ozonation (4.3 €$\cdot m^{-3}$), whereas CDEO and solar/Fe^0/H_2O_2 treatments resulted more costly (5.2 and 6.2 €$\cdot m^{-3}$, respectively). Given that the use of oxidants is generally more efficient in fully optimized industrial units, these costs would be lower at industrial scale.
- At the current design point, the sunlight-driven photo-Fenton is unfeasible due to the cost and size of the required plant space, but it could become an important alternative for lower COD reductions (<20%).
- On the other hand, to reach COD removals above 50%, O_3 appears to be more economic, whereas the price of the BDD unit still limits its industrial application, despite of its high oxidant-efficiency.

6. REFERENCES

Adams, C.D., Scanlan, P.A. and Secrist, N.D., 1994. Oxidation and biodegradability enhancement of 1,4-dioxane using hydrogen-peroxide and ozone. Environmental Science & Technology, 28(11): 1812-1818.

Alibaba, 2015. Alibaba Chemicals Market, www.alibaba.com, Accessed: June 5, 2015.

Andreozzi, R., Caprio, V., Insola, A. and Marotta, R., 1999. Advanced oxidation processes (AOP) for water purification and recovery. Catalysis Today, 53(1): 51-59.

Audenaert, W.T.M., 2012. Ozonation and UV/hydrogen peroxide treatment of natural water and secondary wastewater effluent: experimental study and mathematical modelling. PhD thesis, Ghent University, Belgium.

Augugliaro, V., Loddo, V., Marci, G., Palmisano, L. and Schiavello, M., 1995. Performance of a continuous flat reactor for phenol degradation in heterogeneous photocatalytic system. Chemical and Biochemical Engineering Quarterly, 9(3): 133-139.

BASF, 2013. High-performance solvents: Glymes, 1,3-Dioxolane and 1,4-Dioxane. BASF - The Chemical Company, www.basf.com/performance-materials. Accessed: September 19, 2014.

Beckett, M.A. and Hua, I., 2000. Elucidation of the 1,4-dioxane decomposition pathway at discrete ultrasonic frequencies. Environmental Science & Technology, 34(18): 3944-3953.

Bergendahl, J.A. and Thies, T.P., 2004. Fenton's oxidation of MTBE with zero-valent iron. Water Research, 38(2): 327-334.

Bertanza, G., Papa, M., Pedrazzani, R., Repice, C. and Dal Grande, M., 2013. Tertiary ozonation of industrial wastewater for the removal of estrogenic compounds (NP and BPA): a full-scale case study. Water Science and Technology, 68(3): 567-574.

Braham, R.J. and Harris, A.T., 2009. Review of Major Design and Scale-up Considerations for Solar Photocatalytic Reactors. Industrial & Engineering Chemistry Research, 48(19): 8890-8905.

Bremner, D.H., Burgess, A.E., Houllemare, D. and Namkung, K.C., 2006. Phenol degradation using hydroxyl radicals generated from zero-valent iron and hydrogen peroxide. Applied Catalysis B: Environmental, 63(1-2): 15-19.

Burns, R.A., Crittenden, J.C., Hand, D.W., Selzer, V.H., Sutter, L.L. and Salman, S.R., 1999. Effect of inorganic ions in heterogeneous photocatalysis of TCE. Journal of Environmental Engineering-Asce, 125(1): 77-85.

Buxton, G.V., Greenstock, C.L., Helman, W.P. and Ross, A.B., 1988. Critical review of rate constants for reactions of hydrated electrons, hydrogen atoms and hydroxyl radicals ($\bullet OH/\bullet O^-$) in aqueous solution. Journal of Physical and Chemical Reference Data, 17(2): 513-886.

Cañizares, P., Paz, R., Saez, C. and Rodrigo, M.A., 2009. Costs of the electrochemical oxidation of wastewaters: A comparison with ozonation and Fenton oxidation processes. Journal of Environmental Management, 90(1): 410-420.

CEFIC, 1997. Use of solvents by sector. The European Chemical Industry Council, European Solvents Industry Group, Solutions, 1: 4.

CEPCI, 2015. Economic indicators: Chemical Engineering Plant Cost Index, Chemical Engineering, http://www.chemengonline.com/pci-home, Accessed: June 12, 2015.

CNRS, 2014. European harmonised classification and labelling of carcinogenic, mutagenic and toxic for reproduction (CMR) substances according to the criteria of the CLP Regulation, Chemical Risk Prevention Unit, www.prc.cnrs-gif.fr. Accessed: September 18, 2014.

Comninellis, C., Kapalka, A., Malato, S., Parsons, S.A., Poulios, L. and Mantzavinos, D., 2008. Advanced oxidation processes for water treatment: advances and trends for R&D. Journal of Chemical Technology and Biotechnology, 83(6): 769-776.

Constable, D.J.C., Jimenez-Gonzalez, C. and Henderson, R.K., 2007. Perspective on solvent use in the pharmaceutical industry. Organic Process Research & Development, 11(1): 133-137.

Cooper, W.J., Cramer, C.J., Martin, N.H., Mezyk, S.P., O'Shea, K.E. and von Sonntag, C., 2009. Free Radical Mechanisms for the Treatment of Methyl tert-Butyl Ether (MTBE) via Advanced Oxidation/Reductive Processes in Aqueous Solutions. Chemical Reviews, 109(3): 1302-1345.

Couper, J.R., 2004. Process Engineering Economics. Marcel Dekker, New York.

Chang, Y., Reardon, D.J., Kwan, P., Boyd, G., Brant, J., Rakness, K.L. and Furukawa, D., 2008. Evaluation of Dynamic Energy Consumption of Advanced Water and Wastewater Treatment Technologies. Awwa Research Foundation, Denver.

Chatzisymeon, E., Diamadopoulos, E. and Mantzavinos, D., 2010. Comparison and predesign cost estimation of advanced oxidation processes for olive mill wastewater treatment, Proceedings of the 2nd International Conference on Hazardous and Industrial Waste Management, October 5-8, 2010, Chania.

Chen, H.Y., Zahraa, O. and Bouchy, M., 1997. Inhibition of the adsorption and photocatalytic degradation of an organic contaminant in an aqueous suspension of TiO_2 by inorganic ions. Journal of Photochemistry and Photobiology A: Chemistry, 108(1): 37-44.

Chen, Y. and Dionysiou, D.D., 2008. Bimodal mesoporous TiO_2-P25 composite thick films with high photocatalytic activity and improved structural integrity. Applied Catalysis B: Environmental, 80(1-2): 147-155.

Chen, Z., Ren, N., Wang, A., Zhang, Z.-P. and Shi, Y., 2008. A novel application of TPAD-MBR system to the pilot treatment of chemical synthesis-based pharmaceutical wastewater. Water Research, 42(13): 3385-3392.

Chiang, Y.-P., Liang, Y.-Y., Chang, C.-N. and Chao, A.C., 2006. Differentiating ozone direct and indirect reactions on decomposition of humic substances. Chemosphere, 65(11): 2395-2400.

Chitra, S., Paramasivan, K., Cheralathan, M. and Sinha, P.K., 2012. Degradation of 1,4-dioxane using advanced oxidation processes. Environmental Science and Pollution Research, 19(3): 871-878.

Choi, H., Antoniou, M.G., Pelaez, M., De la Cruz, A.A., Shoemaker, J.A. and Dionysiou, D.D., 2007. Mesoporous nitrogen-doped TiO2 for the photocatalytic destruction of the cyanobacterial toxin Microcystin-LR under visible light irradiation. Environmental Science & Technology, 41(21): 7530-7535.

Choi, J.Y., Lee, Y.J., Shin, J. and Yang, J.W., 2010. Anodic oxidation of 1,4-dioxane on boron-doped diamond electrodes for wastewater treatment. Journal of Hazardous Materials, 179(1-3): 762-768.

De Schepper, W., Vanparys, C., Dries, J., Geuens, L. and Blust, R., 2012. Evaluation of the Partial Ozonation and Partial Hydrogen Peroxide Oxidation Process for the Removal of COD and Estrogenic Activity from a Tank Truck Cleaning Generated Concentrate. Ozone-Science & Engineering, 34(1): 32-41.

De Torres-Socias, E., Prieto-Rodriguez, L., Zapata, A., Fernandez-Calderero, I., Oller, I. and Malato, S., 2015. Detailed treatment line for a specific landfill leachate remediation. Brief economic assessment. Chemical Engineering Journal, 261: 60-66.

Deegan, A.M., Shaik, B., Nolan, K., Urell, K., Oelgemoeller, M., Tobin, J. and Morrissey, A., 2011. Treatment options for wastewater effluents from pharmaceutical companies. International Journal of Environmental Science and Technology, 8(3): 649-666.

DeMatteo, R., 2011. Chemical exposure and plastics production: Issues for women's healt - Review of Literature. The National Network on Environments and Women's Health, http://www.nnewh.org/overview.php?section=4. Accessed: September 19, 2014.

Deußing, G., 2014. Focus on solvents in polymer production. K Trade Fair, http://www.k-online.de/cipp/md_k/custom/pub/content,oid,49813/lang,2/ticket,g_u_e_s_t/local_lang,2. Accessed: September 19, 2014.

Dow, 2014. LTTF - DOWCAL, DOWTHERM SR-1, DOWTHERM 4000, DOWFROST - Thermal Degradation. The Dow Chemical Company, http://dowac.custhelp.com/app/answers/detail/a_id/11979, Accessed: March 13, 2015.

EC, 2000. European Commission: Directive 2000/60/EC of the European Parliament and of the Council of 23 October 2000 establishing a framework for Community action in the field of water policy. Official Journal of the European Union, 327: 1-92.

EC, 2006. European Commission: Directive 2006/11/EC of the European Parliament and of the Council of 15 February 2006 on pollution caused by certain dangerous substances discharged into the aquatic environment of the Community. Official Journal of the European Union, L 64: 52-59.

EC, 2008. European Commission: Directive 2008/105/EC of the European Parliament and of the Council of 16 December 2008 on environmental quality standards in the field of water policy, amending and subsequently repealing Council Directives 82/176/EEC, 83/513/EEC, 84/156/EEC, 84/491/EEC, 86/280/EEC and amending Directive 2000/60/EC of the European Parliament and of the Council. Official Journal of the European Union, L 348: 84-97.

EC, 2010a. European Commission: Second Follow-up Report to the Communication on water scarcity and droughts in the European Union (COM (2007) 414 final). Report from the Commision to the Council and the European Parliament, Brussels.

EC, 2010b. European Commission: Directive 2010/75/EU of the European Parliament and of the Council of 24 November 2010 on industrial emissions (integrated prevention and control). Official Journal of the European Union, L 334: 17-119.

EC, 2013. European Commission: Directive 2013/39/EU of the European Parliament and of the Council of 12 August 2013 amending Directives 2000/60/EC and 2008/105/EC as regards priority substances in the field of water policy. Official Journal of the European Union, L 226: 1-17.

EC, 2014. European Commission: Strategies against chemical pollution of surface waters, http://ec.europa.eu/environment/water/water-dangersub/index.htm#disc. Accessed: September 18, 2014.

ECB, 2002. European Chemicals Bureau: European Union Risk Assessment Report. 1,4-dioxane (CAS No: 123-91-1; EINECS No: 204-661-8). 2nd Priority List, 21: 1-129.

El-Din, M.G., Smith, D.W., Al Momani, F. and Wang, W.X., 2006. Oxidation of resin and fatty acids by ozone: Kinetics and toxicity study. Water Research, 40(2): 392-400.

Enright, A.M., McHugh, S., Collins, G. and O'Flaherty, V., 2005. Low-temperature anaerobic biological treatment of solvent-containing pharmaceutical wastewater. Water Research, 39(19): 4587-4596.

Eurostat, 2014. Water Statistics, http://ec.europa.eu/eurostat/statistics-explained/index.php/Water_statistics. Accessed: June 8, 2015.

Eurostat, 2015. Electricity prices components for industrial consumers - annual data, http://appsso.eurostat.ec.europa.eu/nui/show.do?dataset=nrg_pc_205_c&lang=en. Accessed: June 4, 2015.

Ferella, F., De Michelis, I., Zerbini, C. and Veglio, F., 2013. Advanced treatment of industrial wastewater by membrane filtration and ozonization. Desalination, 313: 1-11.

Ferro, 2014. Ferro Product Data Sheet: 1,4-Dioxane (CAS: 123-91-1), Ferro Corporation, http://www.ferro.com/. Accessed: September 19, 2014.

Fischbacher, A., von Sonntag, J., von Sonntag, C. and Schmidt, T.C., 2013. The (•)OH Radical Yield in the $H_2O_2 + O_3$ (Peroxone) Reaction. Environmental Science & Technology, 47(17): 9959-9964.

Freedman, D.L., Payauys, A.M. and Karanfil, T., 2005. The effect of nutrient deficiency on removal of organic solvents from textile manufacturing wastewater during activated sludge treatment. Environmental Technology, 26(2): 179-188.

Fujishima, A., Rao, T.N. and Tryk, D.A., 2000. Titanium dioxide photocatalysis. Journal of Photochemistry and Photobiology C: Photochemistry Reviews, 1: 1–21.

Gangagni Rao, A., Venkata Naidu, G., Krishna Prasad, K., Chandrasekhar Rao, N., Venkata Mohan, S., Jetty, A. and Sarma, P.N., 2005. Anaerobic treatment of wastewater with high suspended solids from a bulk drug industry using fixed film reactor (AFFR). Bioresource technology, 96(1): 87-93.

Ghosh, P., Samanta, A.N. and Ray, S., 2010. Oxidation kinetics of degradation of 1,4-dioxane in aqueous solution by H_2O_2/Fe(II) system. Journal of Environmental Science and Health-Part A: Toxic/Hazardous Substances & Environmental Engineering, 45(4): 395-399.

Glaze, W.H., 1986. Reactions products of ozone – A review. Environmental Health Perspectives, 69: 151-157.

Glaze, W.H., Kang, J.W. and Chapin, D.H., 1987. The Chemistry of water treatment processes involving ozone, hydrogen peroxide and ultraviolet radiation. Ozone-Science & Engineering, 9(4): 335-352.

Grodowska, K. and Parczewski, A., 2010. Organic solvents in the pharmaceutical industry. Acta Poloniae Pharmaceutica, 67(1): 3-12.

Han, T.-H., Han, J.-S., So, M.-H., Seo, J.-W., Ahn, C.-M., Min, D.H., Yoo, Y.S., Cha, D.K. and Kim, C.G., 2012a. The removal of 1,4-dioxane from polyester manufacturing process wastewater using an up-flow Biological Aerated Filter (UBAF) packed with tire chips. Journal of Environmental Science and Health-Part A: Toxic/Hazardous Substances and Environmental Engineering, 47(1): 117-129.

Han, C., Luque, R. and Dionysiou, D.D., 2012b. Facile preparation of controllable size monodisperse anatase titania nanoparticles. Chemical Communications, 48(13): 1860-1862.

Harber, F. and Weiss, J.J., 1934. The catalytic decomposition of Hydrogen Peroxide by iron salts. Journal of American Chemical Society, 45: 338-351.

Henderson, R.K., Jimenez-Gonzalez, C., Constable, D.J.C., Alston, S.R., Inglis, G.G.A., Fisher, G., Sherwood, J., Binks, S.P. and Curzons, A.D., 2011. Expanding GSK's solvent selection guide - embedding sustainability into solvent selection starting at medicinal chemistry. Green Chemistry, 13(4): 854-862.

Hermosilla, D., Cortijo, M. and Huang, C.P., 2009a. Optimizing the treatment of landfill leachate by conventional Fenton and photo-Fenton processes. Science of the Total Environment, 407: 3473-3481.

Hermosilla, D., Cortijo, M. and Huang, C.P., 2009b. The role of iron on the degradation and mineralization of organic compounds using conventional Fenton and photo-Fenton processes. Chemical Engineering Journal, 155(3): 637-646.

Hoigne, J. and Bader, H., 1976. The role of hydroxyl radical reactions in ozonation processes in aqueous solutions. Water Research 10: 377-386.

Hoigne, J. and Bader, H., 1983. Rate constants of reactions of ozone with organic and inorganic compounds in water-II: Dissociating organic compounds. Water Research, 17(2): 11.

Hoigne, J., Bader, H., Haag, W.R. and Staehelin, J., 1985. Rate constants of reactions of ozone with organic and inorganic compounds in water-III: Inorganic compounds and radicals. Water Research, 19(8): 993-1004.

Hollender, J., Zimmermann, S.G., Koepke, S., Krauss, M., McArdell, C.S., Ort, C., Singer, H., von Gunten, U. and Siegrist, H., 2009. Elimination of Organic Micropollutants in a Municipal Wastewater Treatment Plant Upgraded with a Full-Scale Post-Ozonation Followed by Sand Filtration. Environmental Science & Technology, 43(20): 7862-7869.

Inanc, B., Calli, B., Alp, K., Ciner, F., Mertoglu, B. and Ozturk, I., 2002. Toxicity assessment on combined biological treatment of pharmaceutical industry effluents. Water Science and Technology, 45(12): 135-142.

INE, 2015. Instituto Nacional de Estadística, www.ine.es. Accessed: June 5, 2015.

Jagadevan, S., Graham, N.J. and Thompson, I.P., 2013. Treatment of waste metalworking fluid by a hybrid ozone-biological process. Journal of Hazardous Materials, 244: 394-402.

Johns, M.M., Marshall, W.E. and Toles, C.A., 1998. Agricultural by-products as granular activated carbons for adsorbing dissolved metals and organics. Journal of Chemical Technology and Biotechnology, 71(2): 131-140.

Kallel, M., Belaid, C., Boussahel, R., Ksibi, M., Montiel, A. and Elleuch, B., 2009a. Olive mill wastewater degradation by Fenton oxidation with zero-valent iron and hydrogen peroxide. Journal of Hazardous Materials, 163(2-3): 550-554.

Kallel, M., Belaid, C., Mechichi, T., Ksibi, M. and Elleuch, B., 2009b. Removal of organic load and phenolic compounds from olive mill wastewater by Fenton oxidation with zero-valent iron. Chemical Engineering Journal, 150(2-3): 391-395.

Karat, I., 2013. Advanced Oxidation Processes for Removal of COD from Pulp and Paper Mill Effluents. A Technical, Economical and Environmental Evaluation. MSc Thesis, Royal Institute of Technology, Sweden.

Karpel Vel Leitner, N. and Dore, M., 1997. Mechanism of the reaction between hydroxyl radicals and glycolic, glyoxylic, acetic and oxalic acids in aqueous solution: Consequence on hydrogen peroxide consumption in the H_2O_2/UV and O_3/H_2O_2 systems. Water Research, 31(6): 1383-1397.

Kavitha, V. and Palanivelu, K., 2004. The role of ferrous ion in Fenton and photo-Fenton processes for the degradation of phenol. Chemosphere, 55(9): 1235-1243.

Kegel, F.S., Rietman, B.M. and Verliefde, A.R.D., 2010. Reverse osmosis followed by activated carbon filtration for efficient removal of organic micropollutants from river bank filtrate. Water Science and Technology, 61(10): 2603-2610.

Kim, H.-S., Kwon, B.-H., Yoa, S.-J. and Kim, I.-K., 2008. Degradation of 1,4-Dioxane by Photo-Fenton Processes. Journal of Chemical Engineering of Japan, 41(8): 829-835.

Kim, S.D., Cho, J., Kim, I.S., Vanderford, B.J. and Snyder, S.A., 2007. Occurrence and removal of pharmaceuticals and endocrine disruptors in South Korean surface, drinking, and waste waters. Water Research, 41(5): 1013-1021.

Kim, S.M., Geissen, S.U. and Vogelpohl, A., 1997. Landfill leachate treatment by a photoassisted Fenton reaction. Water Science and Technology, 35(4): 239-248.

Koczka, K. and Mizsey, P., 2010. New area for distillation: wastewater treatment. Periodica Polytechnica-Chemical Engineering, 54(1): 41-45.

Köhler, A., 2006. Environmental Assessment of Industrial Wastewater Treatment Processes and Waterborne Organic Contaminant Emissions. PhD thesis, Swiss Federal Institute of Technology, Switzerland.

Kommineni, S., Zoeckler, J., Stocking, A., Liang, S., Flores, A., Kavanaugh, M., Rodriguez, R., Browne, T., Roberts, R., Brown, A. and Stocking, A., 2015. Advanced Oxidation Processes. National Water Research Institute, http://www.nwri-usa.org/pdfs/TTChapter3AOPs.pdf. Accessed: June 12, 2015.

Kwon, S.C., Kim, J.Y., Yoon, S.M., Bae, W., Kang, K.S. and Rhee, Y.W., 2012. Treatment characteristic of 1,4-dioxane by ozone-based advanced oxidation processes. Journal of Industrial and Engineering Chemistry, 18: 1951-1955.

Lian, J., Liu, J.X. and Wei, Y.S., 2009. Fate of nonylphenol polyethoxylates and their metabolites in four Beijing wastewater treatment plants. Science of the Total Environment, 407(14): 4261-4268.

Liang, X., Zhu, X. and Butler, E.C., 2011. Comparison of four advanced oxidation processes for the removal of naphthenic acids from model oil sands process water. Journal of Hazardous Materials, 190: 168-176.

Libralato, G., Ghirardini, A.V. and Avezzu, F., 2008. Evaporation and air-stripping to assess and reduce ethanolamine s toxicity in oily wastewater. Journal of Hazardous Materials, 153(3): 928-936.

Linsebigler, A.L., Lu, G.Q. and Yates, J.T., 1995. Photocatalysis on TiO_2 surfaces – principles, mechanisms, and selected results. Chemical Reviews, 95(3): 735-758.

Liu, D.H.F. and Liptak, B.G., 1997. Environmental Engineers' Handbook, 2nd ed. CRC Press LLC, Boca Raton.

Ma, J. and Graham, N.J.D., 2000. Degradation of atrazine by manganese-catalysed ozonation - Influence of radical scavengers. Water Research, 34(15): 3822-3828.

Macolino, P., Bianco, B. and Veglio, F., 2009. Drying Process of a biological industrial sludge: experimental and process analysis. In: S. Pierucci (Editor), Icheap-9: 9th International Conference on Chemical and Process Engineering, Pts 1-3. Chemical Engineering Transactions, pp. 699-704.

Mahamuni, N.N. and Adewuyi, Y.G., 2010. Advanced oxidation processes (AOPs) involving ultrasound for waste water treatment: A review with emphasis on cost estimation. Ultrasonics Sonochemistry, 17(6): 990-1003.

Malato, S., Fernandez-Ibanez, P., Maldonado, M.I., Blanco, J. and Gernjak, W., 2009. Decontamination and disinfection of water by solar photocatalysis: Recent overview and trends. Catalysis Today, 147(1): 1-59.

Maurino, V., Calza, P., Minero, C., Pelizzetti, E. and Vincenti, M., 1997. Light-assisted 1,4-dioxane degradation. Chemosphere, 35(11): 2675-2688.

Merayo, N., 2014. Development and assessment of advanced oxidation propcesses for the treatment of pulp and paper mill effluents. PhD thesis, Complutense University of Madrid, Spain.

Merayo, N., Hermosilla, D., Cortijo, L. and Blanco, Á., 2014. Optimization of the Fenton treatment of 1,4-dioxane and on-line FTIR monitoring of the reaction. Journal of Hazardous Materials 268(15): 102–109.

Metcalf&Eddy, 1981. Wastewater engineering: collection and pumping of wastewater. McGraw-Hill, New York.

Mills, A. and LeHunte, S., 1997. An overview of semiconductor photocatalysis. Journal of Photochemistry and Photobiology A: Chemistry, 108(1): 1-35.

Mohr, T.K.G., 2004. 1,4-dioxane (and other Solvent Stabilizer Compounds) - ROD Re-Opener?. USEPA Technical Support Project Meeting, October 18-21, 2004, Sacramento, California.

Mohr, T.K.G., 2010. Environmental Investigation and remediation: 1,4-dioxane and other solvent stabilizers. CRC Press, Boca Raton.

Montilla, F., Michaud, P.A., Morallon, E., Vazquez, J.L. and Comninellis, C., 2002. Electrochemical oxidation of benzoic acid at boron-doped diamond electrodes. Electrochimica Acta, 47(21): 3509-3513.

Muñoz, I., 2006. Life Cycle Assessment as a Tool for Green Chemistry: Application to Different Advanced Oxidation Processes for Wastewater Treatment. PhD thesis, Autonomous University of Barcelona, Spain.

Muñoz, I., Malato, S., Rodriguez, A. and Domenech, X., 2008. Integration of environmental and economic performance of processes. Case study on advanced oxidation processes for wastewater treatment. Journal of Advanced Oxidation Technologies, 11(2): 270-275.

Nakajima, A., Matsui, S., Yanagida, S., Kameshima, Y. and Okada, K., 2009. Preparation and properties of titania-$Cs_{2.5}H_{0.5}PW_{12}O_{40}$ hybrid films. Surface & Coatings Technology, 203(9): 1133-1137.

NICNAS, 1998. National Industrial Chemical Notification and Assessment Scheme: 1,4-Dioxane, Priority Existing Chemical No. 7, Full Public Report. Australian Government Publishing Service, Canberra.

OECD, 2010. Activated Sludge, Respiration Inhibition Test (Carbon and Ammonium Oxidation). OECD guidelines for the testing of chemicals, 209 (Adopted: 22 July 2010).

Oktem, Y.A., Ince, O., Sallis, P., Donnelly, T. and Ince, B.K., 2008. Anaerobic treatment of a chemical synthesis-based pharmaceutical wastewater in a hybrid upflow anaerobic sludge blanket reactor. Bioresource technology, 99(5): 1089-1096.

Oller, I., Malato, S. and Sanchez-Perez, J.A., 2011. Combination of Advanced Oxidation Processes and biological treatments for wastewater decontamination - A review. Science of the Total Environment, 409(20): 4141-4166.

OSPAR, 2010. OSPAR Convention for the protection of the marine environment of the North-east Atlantic. Quality Status Report, 2010.

Oz, N.A., Ince, O. and Ince, B.K., 2004. Effect of wastewater composition on methanogenic activity in an anaerobic reactor. Journal of Environmental Science and Health-Part A: Toxic/Hazardous Substances & Environmental Engineering, 39(11-12): 2941-2953.

Pandya, M.T., 2007. Treatment of industrial wastewater using photooxidation and bioaugmentation technology. Water Science and Technology, 56(7): 117-124.

Panizza, M., Michaud, P.A., Cerisola, G. and Comninellis, C., 2001. Anodic oxidation of 2-naphthol at boron-doped diamond electrodes. Journal of Electroanalytical Chemistry, 507(1-2): 206-214.

Pelaez, M., de la Cruz, A.A., Stathatos, E., Falaras, P. and Dionysiou, D.D., 2009. Visible light-activated N-F-codoped TiO(2) nanoparticles for the photocatalytic degradation of microcystin-LR in water. Catalysis Today, 144(1-2): 19-25.

Pelaez, M., Falaras, P., Likodimos, V., Kontos, A.G., de la Cruz, A.A., O'Shea, K. and Dionysiou, D.D., 2010. Synthesis, structural characterization and evaluation of sol-gel-based NF-TiO(2) films with visible light-photoactivation for the removal of microcystin-LR. Applied Catalysis B: Environmental, 99(3-4): 378-387.

Pelaez, M., Nolan, N.T., Pillai, S.C., Seery, M.K., Falaras, P., Kontos, A.G., Dunlop, P.S.M., Hamilton, J.W.J., Byrne, J.A., O'shea, K., Entezari, M.H. and Dionysiou, D.D., 2012a. A review on the visible light active titanium dioxide photocatalysts for environmental applications. Applied Catalysis B: Environmental, 125: 331-349.

Pelaez, M., Falaras, P., Kontos, A.G., de la Cruz, A.A., O'Shea, K., Dunlop, P.S.M., Byrne, J.A. and Dionysiou, D.D., 2012b. A comparative study on the removal of cylindrospermopsin and microcystins from water with NF-TiO2-P25 composite films with visible and UV-vis light photocatalytic activity. Applied Catalysis B: Environmental, 121: 30-39.

PEMRG, 2013. Plastics - the Facts 2013. An analysis of European latest plastics production, demand and waste data. PlasticsEurope Market Research Group, http://www.plasticseurope.org/Document/plastics-the-facts-2013.aspx?FolID=2. Accessed: September 19, 2014.

Perathoner, S., 2013. The future prospects of catalysts in water treatment. ChemH_2O2013 Leading-Edge Conference on Sustainable Water Management, October 1-2, 2013, Madrid.

Peters, M.S., Timmerhaus, K.D. and West, R.E., 2003. Plant Design and Economics for Chemical Engineers, 5th Ed. McGraw-Hill, New York.

Pignatello, J.J., 1992. Dark and photoassisted Fe^{3+}-catalyzed degradation of chlorophenoxy herbicides by hydrogen peroxide. Environmental Science & Technology, 26(5): 944-951.

Pignatello, J.J., Oliveros, E. and MacKay, A., 2006. Advanced oxidation processes for organic contaminant destruction based on the Fenton reaction and related chemistry. Critical Reviews in Environmental Science and Technology, 36(1): 1-84.

Pliego, G., Zazo, J.A., Casas, J.A. and Rodriguez, J.J., 2013. Case study of the application of Fenton process to highly polluted wastewater from power plant. Journal of Hazardous Materials, 252: 180-185.

Pobiner, H., 1961. Determination of hydroperoxides in hydrocarbon by conversion to hydrogen peroxide and measurement by titanium complexing. Analytical Chemistry, 33: 1423-1428.

Pontes, R.F.F., Moraes, J.E.F., Machulek, A., Jr. and Pinto, J.M., 2010. A mechanistic kinetic model for phenol degradation by the Fenton process. Journal of Hazardous Materials, 176(1-3): 402-413.

Prousek, J., Palackova, E., Priesolova, S.A., Markova, L. and Alevova, A., 2007. Fenton- and fenton-like AOPs for wastewater treatment: From Laboratory-to-plant-scale application. Separation Science and Technology, 42(7): 1505-1520.

Raj, D.S.S. and Anjaneyulu, Y., 2005. Evaluation of biokinetic parameters for pharmaceutical wastewaters using aerobic oxidation integrated with chemical treatment. Process Biochemistry, 40(1): 165-175.

Razavi, A., 2013. Treating 1,4-Dioxane in an era of water scarcity, Water Technology, http://www.watertechonline.com/articles/print/165872-treating-14-dioxane-in-an-era-of-water-scarcity. Accessed: September 19, 2014.

Reemtsma, T., Miehe, U., Duennbier, U. and Jekel, M., 2010. Polar pollutants in municipal wastewater and the water cycle: Occurrence and removal of benzotriazoles. Water Research, 44(2): 596-604.

Rodrigo, M.A., Cañizares, P., Sanchez-Carretero, A. and Saez, C., 2010. Use of conductive-diamond electrochemical oxidation for wastewater treatment. Catalysis Today, 151(1-2): 173-177.

Rosenwinkel, K.-H., Austermann-Haun, U. and Meyer, H., 2005. Industrial Wastewater Sources and Treatment Strategies. In: H.J. Jördening and J. Winter (Editors), Environmental Biotechnology. Concepts and Applications. Wiley-VCH Verlag GmbH & Co. KGaA, Weinheim.

Ross, A.B., 1977. Selected Specific Rates of Reactions of Transients from Water in Aqueous Solution: III. Hydroxyl Radical and Perhydroxyl Radical and Their Radical Ions. U.S. Department of Commerce, National Bureau of Standards, Washington, 113 pp.

Rossiter, W.J., Brown, P.W. and Godette, M., 1983. The determination of acidic degradation products in aqueous ethylene glycol and propylene glycol solutions using ion chromatography. Solar Energy Materials, 9(3): 267-279.

Ruan, T., Liu, R., Fu, Q., Thanh, W., Wang, Y., Song, S., Wang, P., Teng, M. and Jiang, G., 2012. Concentrations and Composition Profiles of Benzotriazole UV Stabilizers in Municipal Sewage Sludge in China. Environmental Science & Technology, 46(4): 2071-2079.

Saien, J. and Nejati, H., 2007. Enhanced photocatalytic degradation of pollutants in petroleum refinery wastewater under mild conditions. Journal of Hazardous Materials, 148(1-2): 491-495.

Sein, M.M., Golloch, A., Schmidt, T.C. and von Sonntag, C., 2007. No marked kinetic isotope effect in the peroxone ($H_2O_2/D_2O_2+O_3$) reaction: Mechanistic consequences. Chemphyschem, 8(14): 2065-2067.

Shen, W., Chen, H. and Pan, S., 2008. Anaerobic biodegradation of 1,4-dioxane by sludge enriched with iron-reducing microorganisms. Bioresource Technology, 99: 2483-2487.

Shi, H., 2009. Industrial Wastewater - Types, Amounts and Effects. In: Q. Yi (Editor), Point Sources of Pollution. Local Effects and Their Control, in Encyclopedia of Life Support Systems (EOLSS). Eolss Publishers (UNESCO), Paris.

Shin, D., Sung, D.Y., Moon, H.S. and Nam, K., 2010. Microbial succession in response to 1,4-dioxane exposure in activated sludge reactors: Effect of inoculum source and extra carbon addition. Journal of Environmental Science and Health-Part A: Toxic/Hazardous Substances & Environmental Engineering, 45(6): 674-681.

Singh, C., Chaudhary, R. and Gandhi, K., 2013. Solar photocatalytic oxidation and disinfection of municipal wastewater using advanced oxidation processes based on pH, catalyst dose, and oxidant. Journal of Renewable and Sustainable Energy, 5(2).

Skadsen, J.M., Rice, B.L. and Meyering, D.J., 2004. The occurence and fate of pharmaceuticals, personal care products, and endocrine disrupting compounds in a municipal water use cycle: A

case study in the City of Ann Arbor. Water Utilities, City of Anna Arbor, and Fleis & VendenBrink Engineering, Inc.

Snyder, S.A., Adham, S., Redding, A.M., Cannon, F.S., DeCarolis, J., Oppenheimer, J., Wert, E.C. and Yoon, Y., 2007. Role of membranes and activated carbon in the removal of endocrine disruptors and pharmaceuticals. Desalination, 202(1-3): 156-181.

So, M.H., Han, J.S., Han, T.H., Seo, J.W. and Kim, C.G., 2009. Decomposition of 1,4-dioxane by photo-Fenton oxidation coupled with activated sludge in a polyester manufacturing process. Water Science and Technology, 59(5): 1003-1009.

Soares, P.A., Silva, T.F.C.V., Manenti, D.R., Souza, S.M.A.G.U., Boaventura, R.A.R. and Vilar, V.J.P., 2014. Insights into real cotton-textile dyeing wastewater treatment using solar advanced oxidation processes. Environmental Science and Pollution Research, 21(2): 932-945.

Soliman, M.A., Pedersen, J.A., Park, H., Castaneda-Jimenez, A., Stenstrom, M.K. and Suffet, I.H., 2007. Human pharmaceuticals, antioxidants, and plasticizers in wastewater treatment plant and water reclamation plant effluents. Water Environment Research, 79(2): 156-167.

Son, H.-S., Im, J.-K. and Zoh, K.-D., 2009. A Fenton-like degradation mechanism for 1,4-dioxane using zero-valent iron (Fe^0) and UV light. Water Research, 43(5): 1457-1463.

Song, S., Ruan, T., Wang, T., Liu, R. and Jiang, G., 2014. Occurrence and removal of benzotriazole ultraviolet stabilizers in a wastewater treatment plant in China. Environmental science. Processes & impacts, 16(5): 1076-1082.

Souza, B.S., Moreira, F.C., Dezotti, M.W.C., Vilar, V.J.P. and Boaventura, R.A.R., 2013. Application of biological oxidation and solar driven advanced oxidation processes to remediation of winery wastewater. Catalysis Today, 209: 201-208.

Staehelin, J. and Hoigne, J., 1982. Decomposition of ozone in water – Rate of initiation by hydroxide ions and hydrogen peroxide. Environmental Science & Technology, 16(10): 676-681.

Stefan, M.I. and Bolton, J.R., 1998. Mechanism of the degradation of 1,4-dioxane in dilute aqueous solution using the UV hydrogen peroxide process. Environmental Science & Technology, 32(11): 1588-1595.

Suarez, S., Dodd, M.C., Omil, F. and von Gunten, U., 2007. Kinetics of triclosan oxidation by aqueous ozone and consequent loss of antibacterial activity: Relevance to municipal wastewater ozonation. Water Research, 41(12): 2481-2490.

Suh, J.H. and Mohseni, M., 2004. A study on the relationship between biodegradability enhancement and oxidation of 1,4-dioxane using ozone and hydrogen peroxide. Water Research, 38(10): 2596-2604.

Tamura, H., Goto, K., TYotsuyanagi, T. and Nagayama, M., 1974. Spectrophotometric determination of iron(II) with 1,10-phenanthroline in the presence of large amounts of iron(III). Talanta, 21: 314-318.

Tan, Y., Lim, Y.B., Altieri, K.E., Seitzinger, S.P. and Turpin, B.J., 2012. Mechanisms leading to oligomers and SOA through aqueous photooxidation: insights from OH radical oxidation of acetic acid and methylglyoxal. Atmospheric Chemistry and Physics, 12(2): 801-813.

Tekin, H., Bilkay, O., Ataberk, S.S., Balta, T.H., Ceribasi, I.H., Sanin, F.D., Dilek, F.B. and Yetis, U., 2006. Use of Fenton oxidation to improve the biodegradability of a pharmaceutical wastewater. Journal of Hazardous Materials, 136(2): 258-265.

TMP, 2014. Solvents Market (Alcohols, Hydrocarbons, Ketones, Esters, Chlorinated and Others) for Paints and Coatings, Printing Inks, Pharmaceuticals, Adhesives and Cosmetics and Other Applications - Global Industry Analysis, Size, Share, Growth, Trends and Forecast 2012 – 2018, http://www.transparencymarketresearch.com/pressrelease/solvents-market.htm. Accessed: May 7, 2015.

Toth, A.J., Gergely, F. and Mizsey, P., 2011. Physicochemical treatment of pharmaceutical process wastewater: distillation and membrane processes. Periodica Polytechnica-Chemical Engineering, 55(2): 59-67.

TrojanUV, 2010. Site Example: Treatment of NDMA and 1,4-Dioxane. Drinking Water Projects, San Gabriel Valley, California. TrojanUV case studies, http://trojanuv.com/resources/trojanuv/casestudies/Trojan_ECT_Case_Study___San_Gabriel_Projects.pdf. Accessed: September 19, 2014.

Ullmann's, 1991. Encyclopedia of industrial chemistry. VCH Verladsgesellschaft, Weinheim.

Urtiaga, A., Rueda, A., Anglada, A. and Ortiz, I., 2009. Integrated treatment of landfill leachates including electrooxidation at pilot plant scale. Journal of Hazardous Materials, 166(2-3): 1530-1534.

USEPA, 2009. Emerging Contaminant - 1,4-Dioxane. Fact Sheet, EPA 505-F-09-006, U.S. Environmental Protection Agency, Office of Solid Waste and Emergency Response, Washington, DC.

USEPA, 2010. Toxicological review of 1,4-dioxane (CAS No. 123-91-1), EPA/635/R-09/005-F, U.S. Environmental Protection Agency, Washington, DC.

USEPA, 2014. Effluent Limitation Guidelines. U.S. Environmental Protection Agency, http://water.epa.gov/scitech/wastetech/guide/. Accessed: September 18, 2014.

USFJ, 2012. Japan Environmental Governing Standards. U.S. Forces Japan, http://www.usfj.mil/Documents/References/JEGS/2012%20Japan%20Environmental%20Governing%20Final.pdf. Accessed: September 19, 2014.

Vescovi, T., Coleman, H.M. and Amal, R., 2010. The effect of pH on UV-based advanced oxidation technologies - 1,4-Dioxane degradation. Journal of Hazardous Materials, 182(1-3): 75-79.

vonSonntag, C. and Schuchmann, H.-P., 1997. Peroxyl radicals in aqueous solutions. In: Z. Alfassi (Editor), Peroxyl radicals. John Wiley, New York, pp. 173-234.

Wang, L.K., Hung, Y.-T., Lo, H.H. and Yapijakis, C., 2004. Handbook of Industrial and Hazardous Wastes Treatment, 2nd ed., revised and expanded. CRC Press, Boca Raton.

Wei, J., Song, Y., Tu, X., Zhao, L. and Zhi, E., 2013. Pretreatment of dry-spun acrylic fiber manufacturing wastewater by Fenton process: Optimization, kinetics and mechanisms. Chemical Engineering Journal, 218: 319-326.

Weiss, S., Jakobs, J. and Reemtsma, T., 2006. Discharge of three benzotriazole corrosion inhibitors with municipal wastewater and improvements by membrane bioreactor treatment and ozonation. Environmental Science & Technology, 40(23): 7193-7199.

WWAP, 2009. Water in a changing world. The united Nations World Water Development Report 3, World Water Assesment Program, UNESCO, Paris.

WWAP, 2012. Managing water under uncertainty and risk. The united Nations World Water Development Report 4, World Water Assesment Program, UNESCO, Paris.

WWAP, 2015. Water for a Sustainable World. The United Nations World Water Development Report 2015, World Water Assesment Program, UNESCO, Paris.

Woodard, F., 2001. Industrial Waste Treatment Handbook. Butterworth-Heinemann, Woburn.

Yangali-Quintanilla, V., Maeng, S.K., Fujioka, T., Kennedy, M. and Amy, G., 2010. Proposing nanofiltration as acceptable barrier for organic contaminants in water reuse. Journal of Membrane Science, 362(1-2): 334-345.

Zapata, A., Malato, S., Sanchez-Perez, J.A., Oller, I. and Maldonado, M.I., 2010. Scale-up strategy for a combined solar photo-Fenton/biological system for remediation of pesticide-contaminated water. Catalysis Today, 151(1-2): 100-106.

Zenker, M.J., Borden, R.C. and Barlaz, M.A., 2000. Mineralization of 1,4-dioxane in the presence of a structural analog. Biodegradation, 11(4): 239-246.

Zenker, M.J., Borden, R.C. and Barlaz, M.A., 2003. Occurrence and treatment of 1,4-dioxane in aqueous environments. Environmental Engineering Science, 20(5): 423-432.

Zenker, M.J., Borden, R.C. and Barlaz, M.A., 2004. Biodegradation of 1,4-dioxane using trickling filter. Journal of Environmental Engineering-Asce, 130(9): 926-931.

Zhang, C., Wang, J., Zhou, H., Fu, D. and Gu, Z., 2010. Anodic treatment of acrylic fiber manufacturing wastewater with boron-doped diamond electrode: A statistical approach. Chemical Engineering Journal, 161(1-2): 93-98.

ORIGINAL PUBLICATIONS

PUBLICATION I

H. Barndõk, L. Cortijo, D. Hermosilla, C. Negro, A. Blanco

Removal of 1,4-dioxane from industrial wastewaters: Routes of decomposition under different operational conditions to determine the ozone oxidation capacity

Journal of Hazardous Materials 280 (2014) 340-347

Journal of Hazardous Materials 280 (2014) 340–347

Contents lists available at ScienceDirect

Journal of Hazardous Materials

journal homepage: www.elsevier.com/locate/jhazmat

Removal of 1,4-dioxane from industrial wastewaters: Routes of decomposition under different operational conditions to determine the ozone oxidation capacity

Helen Barndõk, Luis Cortijo, Daphne Hermosilla*, Carlos Negro, Ángeles Blanco

Department of Chemical Engineering, Universidad Complutense de Madrid, Avda. Complutense, s/n, 28040 Madrid, Spain

HIGHLIGHTS

- Wastewaters containing 1,4-dioxane were successfully degraded by ozone.
- Ozonation alone has been formerly considered insufficient for such effluents.
- The key for the 1,4-dioxane removal by ozone was to maintain the pH above 9.
- FTIR spectroscopy was applied as a powerful tool to monitor the intermediate species.
- Decomposition of 1,4-dioxane was shown to follow different routes at different pH.

GRAPHICAL ABSTRACT

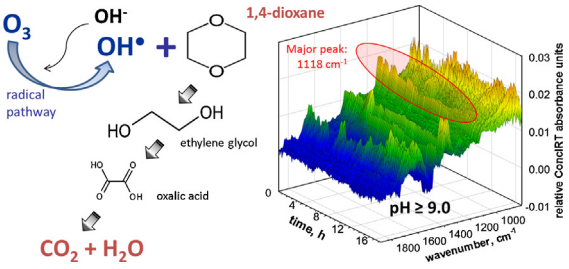

ARTICLE INFO

Article history:
Received 27 March 2014
Received in revised form 19 July 2014
Accepted 28 July 2014
Available online 14 August 2014

Keywords:
Ozone
1,4-Dioxane
Chemical industry
Wastewater treatment
FTIR spectroscopy

ABSTRACT

This paper denotes the importance of operational parameters for the feasibility of ozone (O_3) oxidation for the treatment of wastewaters containing 1,4-dioxane. Results show that O_3 process, which has formerly been considered insufficient as a sole treatment for such wastewaters, could be a viable treatment for the degradation of 1,4-dioxane at the adequate operation conditions. The treatment of both synthetic solution of 1,4-dioxane and industrial wastewaters, containing 1,4-dioxane and 2-methyl-1,3-dioxolane (MDO), showed that about 90% of chemical oxygen demand can be removed and almost a total removal of 1,4-dioxane and MDO is reached by O_3 at optimal process conditions. Data from on-line Fourier transform infrared spectroscopy provides a good insight to its different decomposition routes that eventually determine the viability of degrading this toxic and hazardous compound from industrial waters. The degradation at pH > 9 occurs faster through the formation of ethylene glycol as a primary intermediate; whereas the decomposition in acidic conditions (pH < 5.7) consists in the formation and slower degradation of ethylene glycol diformate.

1. Introduction

1,4-Dioxane is widely used in industry as a solvent in the production processes of various pharmaceuticals, pesticides, magnetic tapes, paper, cotton, textile, adhesives, cosmetics, dyes, oils, waxes, resins, cellulosic esters and ethers. It is also a common by-product of chemical processes, like those involving ethylene glycol (EG).

* Corresponding author. Tel.: +34 91 394 4645; fax: +34 91 394 4243.
E-mail addresses: hbarndok@quim.ucm.es (H. Barndõk), lcortijo@quim.ucm.es (L. Cortijo), dhermosilla@quim.ucm.es, dahermosilla@yahoo.es (D. Hermosilla), cnegro@quim.ucm.es (C. Negro), ablanco@quim.ucm.es (Á. Blanco).

http://dx.doi.org/10.1016/j.jhazmat.2014.07.077
0304-3894/

Nowadays, the environmental interest of 1,4-dioxane is growing since it is listed as a priority pollutant, and a hazardous waste for humans and environment, classified as a probable human (B2) carcinogen [1–3].

1,4-Dioxane was considered non-biodegradable by microorganisms [3–5], although some recent investigations have shown its biodegradation under certain conditions; Han et al. [6] obtained appreciable eliminations of 1,4-dioxane at low initial concentrations, using an up-flow biological aerated filter; Shin et al. [7] reported that the biodegradation of 1,4-dioxane by different bacteria depends strongly on the community structure and the presence of an extra carbon source. Adsorption on activated carbon and air-stripping cannot remove 1,4-dioxane from water due to its high solubility and low vapor pressure. Distillation can be employed, but it is expensive due to its boiling point of 101 °C. Traditional oxidation methods are not effective eliminating this contaminant from water, as the oxidation of 1,4-dioxane using chlorine produces other compounds more toxic than 1,4-dioxane [3,4,8].

Many researchers have studied the application of advanced oxidation processes (AOPs) in the treatment of refractory organic pollutants in water [9–12]. AOPs involve the generation of hydroxyl radicals ($OH^{\bullet}$) with very high oxidation capacity, capable of mineralizing different organic pollutants into carbon dioxide [13,14]. Among the different AOPs, ozone (O_3) is particularly promising for treating recalcitrant materials at industrial scale, firstly, due to its capability to produce high levels of $OH^{\bullet}$ without producing residues and, secondly, because of the possibility of treating large water flows at full scale [15–19]. O_3 process presents important pollutant removal efficiencies when applied to several toxic non-biodegradable compounds [20–23].

Ozonation may be produced directly by O_3 or indirectly by $OH^{\bullet}$, produced through the O_3 decomposition [24,25], whereas $OH^{\bullet}$ is a much stronger and less selective oxidant than O_3 [26,27]. Furthermore, the O_3 does not react strongly with the 1,4-dioxane molecule and the removal is mainly produced by $OH^{\bullet}$ radicals [19]. Thus, it is possible to increase its degradation, working with a higher pH at which $OH^{\bullet}$ radicals are more effectively formed [14,24,28]. Combination of O_3 with hydrogen peroxide (H_2O_2) is also known to accelerate the process [19]; however, the required H_2O_2 can be costly for high organic loads, and in industrial scale facilities the use of O_3 alone is usually preferred [15].

Few studies deal with the degradation of 1,4-dioxane by O_3, while most of the reports focus on the H_2O_2 assisted ozonation [8,19,25,29]; and there is even less literature on the treatment of industrial effluents, as most studies report the removal of low-concentration of 1,4-dioxane from synthetic solutions. The use of O_3 as a sole oxidant to remove the 1,4-dioxane has been discarded by several authors due to the low elimination reached at chosen process conditions [8,19,30]. However, ozonation of organics is strongly affected by process pH, depending on the compounds dissociation as well as on the dominant oxidation mechanism ($OH^{\bullet}$ vs. O_3 production) [14,24,28]. As high initial pH was reported beneficial in the O_3/H_2O_2 oxidation of 1,4-dioxane [25], it is of great interest to study the possible improvement of the O_3 process when adequate pH conditions are maintained throughout the experiment. No reports have been published on the decomposition pathways of 1,4-dioxane by classical ozonation process, although the understanding of the degradation mechanism could play a great role in the process optimization. So far, the intermediates and by-products of 1,4-dioxane degradation have been studied based on chromatography analyses for UV-based AOPs [31,32].

Fourier transform infrared (FTIR) spectroscopy is an alternative method to analyze different molecule groups and structures [33,34]. Recently, Merayo et al. [35] demonstrated the advantages of on-line FTIR spectroscopy to monitor the evolution of reaction intermediates during the Fenton oxidation of aqueous 1,4-dioxane, showing that a good calibration could provide valuable information *in situ*, avoiding expensive and time-consuming sample preparation and analyses. For ozonation process, this on-line method presents an appealing opportunity to track the different reaction pathways under varying process conditions, as different degradation by-products of 1,4-dioxane could be expected to dominate depending on the reaction pH [31].

Therefore, the objective of this paper was to study the feasibility of O_3 oxidation of 1,4-dioxane and, consequently, to treat real industrial wastewaters at optimal conditions. FTIR spectroscopy was applied as a powerful tool to monitor the intermediate species generated during the decomposition of 1,4-dioxane for the better understanding of the degradation mechanisms under different operational conditions.

2. Materials and methods

2.1. Reagents

1,4-Dioxane (99.99%) was supplied by Sigma–Aldrich Chemie® GmbH, Steinheim, Germany). H_2O_2 (30%, v/v), NaOH (98.0%) and $NaHCO_3$ (99%) were purchased from PANREAC S.A. (Barcelona, Spain).

2.2. Experimental procedure

Ozonation was conducted at 25 °C in a jacketed cylindrical bubble reactor (height = 1 m, diameter = 5 cm) with a continuous feed of O_3-riched gas (4.0 L min^{-1}). The system consisted of an O_3 generator (Model 6020, Rilize, Gijon, Spain), a flow controller Bronkhorst® (Model F-201AV, Ruurlo, The Netherlands), and two on-line O_3 analyzers (Model 964C, BMT Messtechnik GMBH, Berlin, Germany). During the operation, 1000 mL of sample was recirculated in the reactor column, whereas O_3-gas was introduced continuously into the solution through a sparger from the bottom of the column (Fig. 1).

The optimization experiments were carried out on a synthetic solution of 1,4-dioxane (247.8 mg L^{-1}; 450 mg L^{-1} COD_0), prepared by diluting with ultra-pure deionized water after pH adjustment

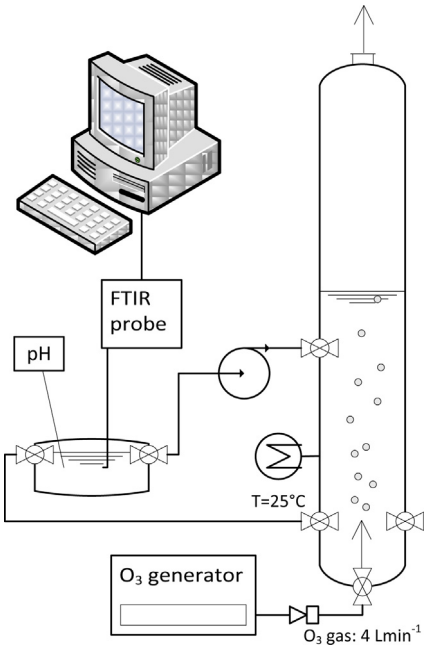

Fig. 1. Schematic of experimental setup.

Table 1
Characterization of industrial wastewaters.

	Units	Sample 1	Sample 2	Sample 3
1,4-Dioxane	$mg\,L^{-1}$	250	280	300
MDO	$mg\,L^{-1}$	0	669	606
pH		8.7–9.0	7.8–8.1	6.7–6.9
Conductivity	μScm^{-1}	2000	2000	1800
Redox	MV	8	12	5
Hardness	$mg\,L^{-1}$ $Ca^{2+} + Mg^{2+}$	50	25	60
Alkalinity	$mg\,CaCO_3\,L^{-1}$	1045	865	983
COD_t	$mg\,O_2\,L^{-1}$	463	1319	2230
N_{total}	$mg\,L^{-1}$	0	0	0
P_{total}	$mg\,L^{-1}$	2.48	3.57	1.49
Fe_{total}	$mg\,L^{-1}$	0.030	0.000	0.067

to a desired value [31,36]. The pH was controlled throughout the experiment by adding NaOH when needed to keep it at the set value, except the experiments with the single addition of $NaHCO_3$ buffer (11.9 mM) that caused the pH to increase from 9.0 ± 0.1 to 10.0 ± 0.1 during the experimental run. Additional experiments were carried out adding H_2O_2 at the stoichiometric ratio proposed by Kim et al. [37] ($1\,g\,L^{-1}$ chemical oxygen demand (COD) = $2.125\,g\,L^{-1}$ H_2O_2). Optimal conditions were applied to treat three actual industrial wastewaters (Samples 1–3, Table 1) that were still contaminated with 1,4-dioxane and 2-methyl-1,3-dioxolane (MDO) after a biological treatment step of a particular factory. All experiments were carried out in triplicates.

In the experiments with FTIR monitoring, synthetic solution with a substantially higher initial 1,4-dioxane concentration of $6168\,mg\,L^{-1}$ was used, according to Merayo et al. [35]. Instead of using NaOH, the basic conditions with the pH above 9 were maintained by a one-time addition of 23.8 mM of $NaHCO_3$ as a buffer to ensure a constant background for the FTIR measurements. In the experiment where the pH was not controlled it dropped from the initial value of 5.7 ± 0.1 to 3.1 ± 0.1.

2.3. Analytical methods

pH was measured on-line with a pH electrode (720 A+, Thermos Scientific, Waltham, USA). Conductivity was measured with a non ionic-selective conductivity probe (Crison, GLP 31/32, Barcelona, Spain). COD was measured, according to the Standard Methods for the Examination of Water and Wastewater [38], by the colorimetric method at 600 nm. H_2O_2 content was analyzed using the titanium sulfate spectrophotometric method [39]. Colorimetric measurements were made on an Aquamate-spectrophotometer (Thermos Scientific AQA 091801, Waltham, USA).

1,4-Dioxane, MDO and EG were identified and quantified by gas–liquid chromatography (GLC) on a 7980A instrument (Agilent Technologies Inc., Palo Alto (CA), USA) equipped with a flame ionization detector. Injector and detector were respectively set up at 310 and 280 °C. Samples (2 μL) were injected using the *pulsed-split* mode (*split* ratio 5:1) and analyzed in a TRB-FFAP (Teknokroma, Sant Cugat del Vallès (Barcelona), Spain) fused silica column (30 m × 0.25 mm internal diameter × 0.25 μm film thickness), with He (43 psi) as carrier gas and a temperature programme (80–240 °C, 9 min initial hold, 15 °C min^{-1} ramp rate). Peaks were identified on the basis of sample coincidence with relative retention times of commercial standards. Quantification was performed according to peak area, corrected with the response factors calculated for each compound using 1-butanol (250 ppm) as the internal standard and the software *GC-ChemStation Rev.B.04.02 (96)* from Agilent.

Oxalic, acetic, glycolic, glyoxylic and methoxyacetic acids were identified and quantified by ion chromatography (IC) using a Dionex DX-500 instrument (Thermo Scientific, Sunnyvale, CA) equipped with a conductivity detector. A gradient of NaOH from 40 mM to 60 mM was used as eluent for the measurements keeping an eluent flow of $1.5\,L\,min^{-1}$. The injection loop was 75 μL. They were analyzed in an AS11HC Ion Pac ionic resin column with a previous Anion Trap Column ATC3 and guard column AG11-HC.

In the waters with high bicarbonate content interfering the analysis by ion chromatography, carboxylic acids were complementary measured by High Pressure Liquid Chromatography (Model L920, Varian, CA, USA) with diode array (PDA) detection. Acetonitrile–water (50%:50%) was used as eluent. Sample injections of 20 μL were separated on a C-18 column (Vidac 250 mm × 4.6 mm ID × 5 μm) at 30 °C. The target compounds, acetic acid and oxalic acid, were measured at 200 nm.

2.4. On-line FTIR analysis

FTIR spectrometer ReactIR iC10 (Mettler-Toledo, Columbia, USA) was used to monitor the ozonation reaction *in situ*. Detailed description of the equipment and the data adquisition is published elsewhere [35]. Real-time component analyses were run using ConcIRT software (Mettler-Toledo, Columbia, USA), which calculates the associated component spectra, and relative concentration profiles.

2.5. Oxygen-equivalent chemical-oxidation capacity

The oxygen-equivalent chemical-oxidant capacity (OCC) parameter, proposed by Cañizares et al. [40] to quantify in arbitrary units the oxidants consumed was used to compare the performance of different AOPs. This parameter is related to the O_3 and H_2O_2 consumption, according to Eqs. (1) and (2).

$$1\left(\frac{\text{kg O}_2}{\text{m}^3}\right) = [O_3]\left(\frac{\text{kg O}_3}{\text{m}^3}\right)\cdot\frac{1\ \text{kmol O}_3}{48\ \text{kg O}_3}\cdot\frac{6\ \text{kmol}^-}{1\ \text{kmol O}_3}\cdot\frac{1\ \text{kmol O}_2}{4\ \text{kmol}^-}\cdot\frac{32\ \text{kg O}_2}{1\ \text{kmol O}_2} = 1.000\cdot[O_3]\left(\frac{\text{kg O}_3}{\text{m}^3}\right), \quad (1)$$

$$1\left(\frac{\text{kg O}_2}{\text{m}^3}\right) = [H_2O_2]\left(\frac{\text{kg H}_2\text{O}_2}{\text{m}^3}\right)\cdot\frac{1\ \text{kmol H}_2\text{O}_2}{34\ \text{kg H}_2\text{O}_2}\cdot\frac{2\ \text{kmol}^-}{1\ \text{kmol H}_2\text{O}_2}\cdot\frac{1\ \text{kmol O}_2}{4\ \text{kmol}^-}\cdot\frac{32\ \text{kg O}_2}{1\ \text{kmol O}_2} = 0.471\cdot[H_2O_2]\left(\frac{\text{kg H}_2\text{O}_2}{\text{m}^3}\right), \quad (2)$$

2.6. Statistical analysis

One-way ANOVA was run (SigmaPlot 11, SPSS Inc.) to determine the significant level of differences among experimental runs. *Post hoc* all pairwise comparisons were performed using Tukey's test ($P < 0.05$).

3. Results and discussion

3.1. Ozonation treatment

3.1.1. Influence of pH

The optimization experiments carried out on synthetic 1,4-dioxane solution showed that an important turning point for the ozonation treatment of such wastewaters (COD removal >80%) exists at pH ≈ 9 (Fig. 2A). At pH 10.0 ± 0.1, a COD removal close

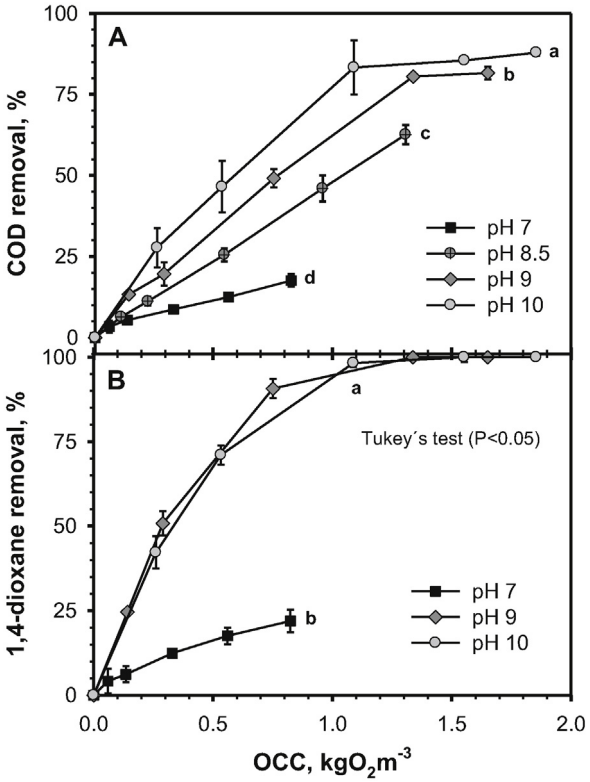

Fig. 2. Ozonation at different pH: removal of COD (A) and 1,4-dioxane (B) with respect to OCC. $[1,4\text{-dioxane}]_0 = 247.8\ mg\ L^{-1}$. Letters (a, b, c, d) identify different statistically significant groups (Tukey's test, $P < 0.05$).

to 90% ($P < 0.050$) was reached, while at pH below 9, the COD removal decreased considerably: 60% of COD was degraded at pH of 8.5 ± 0.1, and only a 20% removal was achieved at pH 7.0 ± 0.1. This phenomenon shows that the OH• produced in ozonation at high pH [14,28,41–44] is a dominant oxidant for 1,4-dioxane and its decomposition intermediates, and that the reaction by molecular O_3 at lower pH conditions has a very low efficiency in the treatment of this particular compound.

In terms of OCC (1 OCC is equivalent to $1\ g\ L^{-1}$ of O_3, in this case), the most efficient COD removal was achieved at pH 10.0 ± 0.1, in this case a significant 82% ($P < 0.050$) of COD removal was obtained at 1 OCC consumed, while the further COD removal was negligible, only 6% more of the total COD was removed consuming an extra $1\ g\ L^{-1}$ of O_3 (OCC = 2). Working at pH 9.0 ± 0.1, the COD removal achieved was close to 80%, but the reaction was slower, 1.5 OCC was necessary to reach the same degradation as at pH 10.0 ± 0.1 (Fig. 2A).

The chromatographic analyses showed that 1,4-dioxane was completely removed from the water at pH ≥ 9.0 (Fig. 2B). The removal of the compound was similar ($P < 0.050$) when working at pH 9.0 ± 0.1 and 10.0 ± 0.1; most of 1,4-dioxane was degraded with 1.25 OCC. On the contrary, in the experiments ran at pH 7.0 ± 0.1, the 1,4-dioxane reduction was very low (<15%), in accordance with the COD removal rates. This explains why the use of O_3 as the only oxidant was ruled out for the treatment of 1,4-dioxane when the experiments were conducted in a solution of distilled water at unmodified pH below 7 [8,19,30]. The lower pH does not favor the decomposition of O_3 to OH• [14,24,28] that has a much greater reactivity with 1,4-dioxane than O_3 [19]. Without the presence of H_2O_2, this chain mechanism of OH• production is initiated by hydroxide anions at higher pH values (Eqs. (3) and (4)) [14,45,46], whereat the

Table 2
Kinetics of 1,4-dioxane degradation in O_3 and O_3/H_2O_2 processes.

Treatment	O_3			O_3/H_2O_2		
pH	$t_{1/2}$ (min)	k (min^{-1})	R^2	$t_{1/2}$ (min)	k (min^{-1})	R^2
7.0	578	1.2	0.99	29	24	0.92
9.0	29	24	0.91	19	36	0.99
10.0	23	30	0.94	14	48	1.00

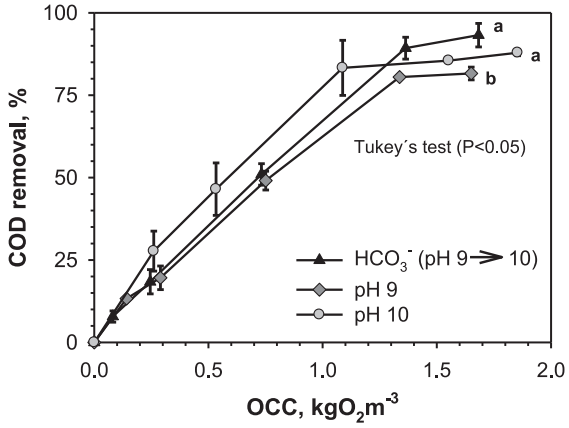

Fig. 3. Ozonation in different alkaline wastewater matrices: removal of COD with respect to OCC. Basic conditions maintained either by on-line control with NaOH or punctual addition of $NaHCO_3$ (11.9 mM). $[1,4\text{-dioxane}]_0 = 247.8\ mg\ L^{-1}$. Letters (a, b) identify different statistically significant groups (Tukey's test, $P < 0.05$).

reactions proceeds over the conversion of $O_3\bullet^-$ into OH• (Eqs. (5) and (6)) [47,48].

$$O_3 + OH^- \rightarrow O_2\bullet^- + HO_2\bullet \quad (3)$$

$$O_3 + O_2\bullet^- \rightarrow O_3\bullet^- + O_2 \quad (4)$$

$$O_3\bullet^- \rightleftharpoons O\bullet^- + O_2 \quad (5)$$

$$O\bullet^- + H_2O \rightleftharpoons OH\bullet + OH^- \quad (6)$$

For a better comparison of the drastic difference in 1,4-dioxane removal by ozonation at different pH values, the reaction kinetics are presented in Table 2. Since surplus O_3 was continuously fed into the reactor, simplified approach was taken and the oxidant species were considered to be in excess [49]. Thus, the degradation of 1,4-dioxane was considered to follow the pseudo first-order kinetics that depend on the decreasing concentration of the solute [19,26,49–51]. The 1,4-dioxane degradation reaction was significantly faster when the process was conducted at pH ≥ 9.0, compared to the reaction rate at pH of 7.0 ± 0.1. Namely, 1,4-dioxane half-life ($t_{1/2}$) was reduced about 20 times when increasing the process pH from 7.0 ± 0.1 to the optimal pH conditions, pH ≥ 9.0.

3.1.2. Effect of bicarbonates

Due to the fact that the industrial wastewaters under concern contained (bi)carbonates and since the carbonate and bicarbonate ions are often considered OH• scavengers [52–54], an additional ozonation experiment was carried out in the presence of carbonates ($9.0 \le pH \le 10.0$), to test the possible negative effect on the process. However, instead of producing an inhibition in the ozonation process, the presence of carbonates also enhanced the removal of COD (>90%), compared to the experiments at neutral conditions (Fig. 3), due to the carbonate buffer which kept the pH in the optimal range. The COD removal obtained in the presence of HCO_3^- ($pH \le 10.0$) was similar, in terms of statistical significance, to the experiments where the pH was kept at 10.0 ± 0.1 by a constant NaOH addition; whereas somewhat slower ($P < 0.05$) degradation was presented at pH 9.0 ± 0.1. This is in concordance with the study done by Barndõk

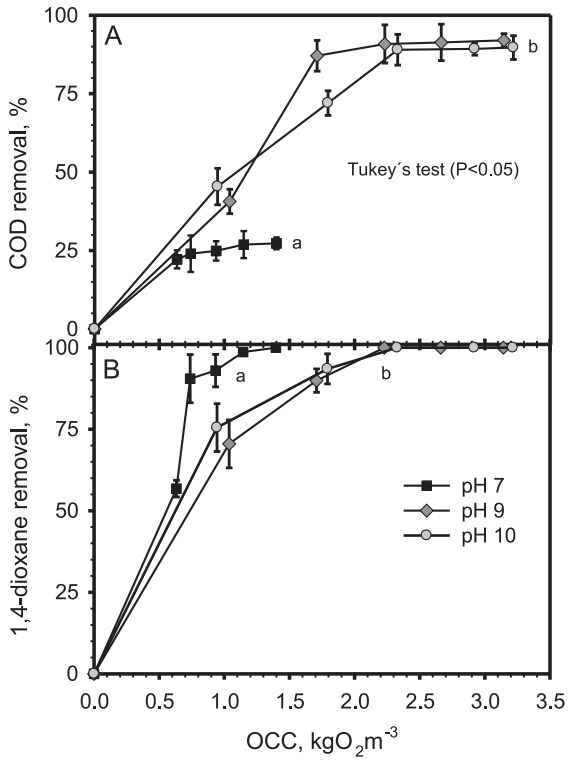

Fig. 4. O_3/H_2O_2 at different pH: removal of COD (A) and 1,4-dioxane (B) with respect to OCC. $[1,4\text{-dioxane}]_0 = 247.8\ mg\ L^{-1}$; $[H_2O_2]_0 = 2.125 \times COD\ (mg\ L^{-1})$. Letters (a, b) identify different statistically significant groups (Tukey's test, $P < 0.05$).

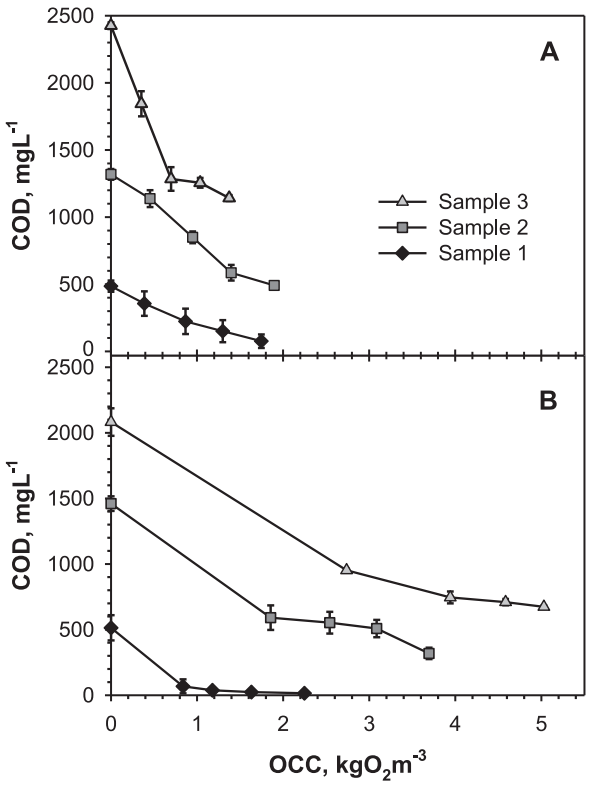

Fig. 5. COD removal from industrial samples by O_3 (A) and O_3/H_2O_2 (B). $[H_2O_2]_0 = 2.125 \times COD\ (mg\ L^{-1})$. Sample 1 consumed 4.27 (O_3) and 4.77 (O_3/H_2O_2) OCC/gL^{-1}COD; sample 2, 2.29 (O_3) and 3.24 (O_3/H_2O_2) OCC/gL^{-1}COD, and sample 3, 1.07 and 3.57 (O_3/H_2O_2) OCC/gL^{-1} COD.

et al. [55], showing that the buffering effect of (bi)carbonate alkalinity could outbalance the negative $OH^\bullet$ scavenging effect during ozonation. This enhancing effect of the bicarbonate alkalinity by maintaining the desired pH is demonstrated in greater detail in Section 4.

3.2. O_3/H_2O_2 treatment

The influence of higher pH on COD and 1,4-dioxane removal by O_3/H_2O_2 process is presented in Fig. 4. When compared with O_3, the oxidation of 1,4-dioxane solution with O_3/H_2O_2 at pH ≥ 9.0 achieved final COD and 1,4-dioxane removals very similar to the sole ozonation (Fig. 2). Although the oxidation with H_2O_2 was faster (Table 2), also more oxidants were consumed in terms of OCC. For example, 1 OCC by O_3 degraded more than 75% of total COD (Fig. 2A) while in the O_3/H_2O_2 process only 40% of COD was removed at 1 OCC (Fig. 4A). In terms of 1,4-dioxane removal, in both cases (Figs. 2B and 4B), at pH ≥ 9.0 approximately 1 OCC was needed to remove most of the compound present in the water. At pH 7.0 ± 0.1, the elimination of 1,4-dioxane was enhanced by the addition of H_2O_2: almost all the 1,4-dioxane was removed employing 1.4 OCC (Fig. 4B). There was no significant difference ($P < 0.05$) in COD and 1,4-dioxane removal between experiments carried out at pH 9.0 ± 0.1 or 10.0 ± 0.1.

The decrease of 1,4-dioxane concentration was apparently found to fit first order kinetics, considering the oxidant species to be in excess, and the pseudo first order rate constants were found [19,26,49–51]. The presence of H_2O_2 significantly enhanced the oxidation process at pH 7.0 ± 0.1 (Table 2), as the H_2O_2 contributes to the generation of $OH^\bullet$ through adduct formation (Eqs. (7) and (8)) proceeded by the conversion of $O_3^{\bullet-}$ into $OH^\bullet$ (Eqs. (5) and (6)) [47,48].

$$HO_2^- + O_3 \rightleftharpoons HO_5^- \quad (7)$$

$$HO_5^- \rightarrow HO_2^\bullet + O_3^{\bullet-} \quad (8)$$

As a consequence, the half-life of the compound was reduced considerably compared to the ozonation alone. However, the reaction rates also show that the positive effect of H_2O_2 was less important at pH ≥ 9.0, because at the latter the decomposition of O_3 into $OH^\bullet$ radical initiated by hydroxide anions [45,46] increased significantly and, thus, the enhancement by H_2O_2 played a smaller role compared to the experiment at pH 7.0 ± 0.1. These results demonstrate that working at the optimum pH, both high 1,4-dioxane and COD removals can be achieved with a sole O_3 treatment, while the addition of hydroxyl peroxide enhances the reaction rates for the 1,4-dioxane degradation, but also increases the oxidant consumption in terms of OCC and, thus, the treatment cost.

3.3. Treatment of industrial wastewaters

Three industrial samples were treated by both O_3 (Fig. 5A) and O_3/H_2O_2 (Fig. 5B). The carbonaceous alkalinity of the wastewaters ensured working at pH > 9, which was also the optimal condition found previously. The percentage of COD removal as well as the quantity of COD removed depended highly on the initial organic load. The effluent containing only 1,4-dioxane at a concentration similar to the synthetic water (sample 1) showed an analogous behavior to the previous trials: 85% of COD was degraded by O_3 (Fig. 5A) and 98% removal was achieved by O_3/H_2O_2 (Fig. 5B).

On the other hand, samples 2 and 3 with a higher COD, containing both 1,4-dioxane and MDO (Table 1), reached a smaller COD removal percentage, but a higher total amount of COD removed. Percentage removals of 63% and 53% by O_3 (Fig. 5A), and 76% and 68% by O_3/H_2O_2 (Fig. 5B), were achieved for samples 2 and 3, respectively. Nevertheless, in terms of OCC consumed to degrade 1 g of COD, the treatment of samples 2 and 3 by ozonation was more

Table 3
Chromatography analysis. Samples 2 and 3: initial composition and composition after 1 OCC for O_3 experiments and 2.5 for O_3/H_2O_2 experiments at original pH and $[H_2O_2]_0 = 2.125 \times COD$ (mg L^{-1}). EG = ethylene glycol, VFA = volatile fatty acids.

	EG mg L^{-1}	1,4-Dioxane mg L^{-1}	MDO mg L^{-1}	VFA mg L^{-1}
Sample 2	0	228	669	0
O_3	22	<5	<15	204
Sample 3	0	300	606	0
O_3	267	65	<5	237
O_3/H_2O_2	8	0	0	50

efficient (2 and 1 OCC, respectively), while sample 1 needed more than 4 OCC per g of COD. This is probably due to the high MDO content that was degraded more readily than 1,4-dioxane [8]. However, in the combined process of O_3/H_2O_2, a similar amount of oxidants was consumed per COD for all three wastewaters (Fig. 5B). Although the overall COD removal was increased considerably by the addition of H_2O_2, the process efficiency, in terms of OCC, remained more or less the same because the higher initial COD required a greater amount of oxidant (H_2O_2), and, thus, increased the ratio $OCC/COD_{removed}$.

According to the chromatography (Table 3), a high degradation of 1,4-dioxane from the samples 2 and 3 was achieved after approximately 1 OCC. The degradation intermediates were mainly EG and volatile fatty acids, which are more biodegradable, meaning they could be removed in a traditional biological process. However, the MDO was almost completely degraded, even being in much higher quantities, which proves that it is oxidized more readily than 1,4-dioxane, and thus, it is competing for the available oxidants [8]. However, the combination of O_3/H_2O_2 allows a complete degradation of 1,4-dioxane as well as MDO from sample 3 at the same experimental time. This implies that for the complete removal of 1,4-dioxane in the presence of MDO, longer treatment times are required when using O_3 alone, or an additional oxidant, such as H_2O_2, should be added. Both options would increase the OCC per COD removal, thus, their cost-effectiveness should be studied and compared.

4. On-line FTIR monitoring of the 1,4-dioxane decomposition

For the better understanding of the differences between the ozonation of 1,4-dioxane under basic and acidic conditions, experiments were carried out, monitoring the evolution of the FTIR spectra. The 3D surface of the reaction evolution in the experiment conducted at pH < 5.7 without no pH control (Fig. 6A) shows a moderate decrease of 1,4-dioxane in time, the peak of 1118 cm^{-1} being the most illustrative, as emphasized in the graph. The slow degradation of the 4 main peaks of 1,4-dioxane in relative absorbance units is pointed out in the insert placed in the header, indicating with an arrow the foremost curvature at 1118 cm^{-1} in the spatial surface. On the other hand, much faster decrease of 1,4-dioxane can be observed in the experiment carried out at pH > 9 in the presence of bicarbonate buffer (Fig. 6B). The chromatography analysis supports this tendency: 93% of 1,4-dioxane (66% of the COD) was removed in the FTIR experiment at pH > 9, whereas only 63% removal of 1,4-dioxane (40% of the COD) was achieved in the acidic conditions.

According to the intermediate compounds identified by the ConcIRT software that associates the important organic bonds to the different organic molecules, it is clear that the basic conditions favored faster kinetics of 1,4-dioxane degradation (Fig. 7). At pH < 5.7 (Fig. 7A), the 1,4-dioxane degradation was slower and intermediates like ethylene glycol diformate (EGDF), and acetic,

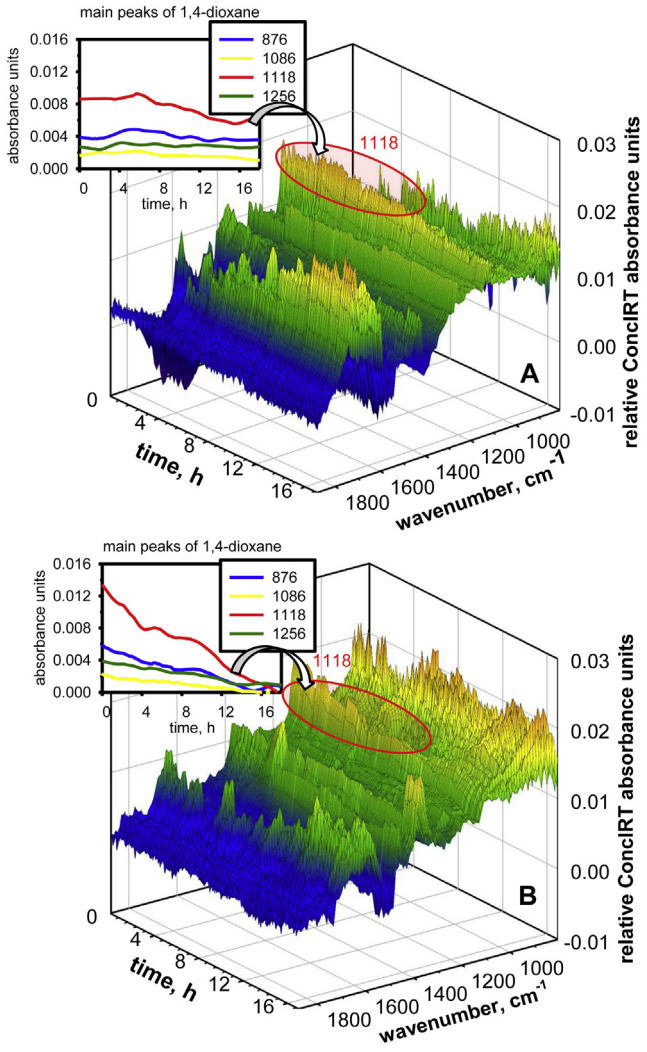

Fig. 6. Evolution of FTIR spectra (1800-800 cm^{-1}) along the ozonation treatment of 1,4-dioxane (C_0 = 6168 mg L^{-1}) under (A) basic conditions at pH > 9 in the presence of $NaHCO_3$ buffer (23.8 mM), and (B) acidic conditions at pH < 5.7. Inserts point out the evolution of the representative peaks of 1,4-dioxane along its degradation.

glycolic and glyoxylic acids, could be observed; whereas less oxalic acid was produced (this tendency is also supported by the chromatographic analyses of carboxylic acids). At pH > 9 (Fig. 7B), the major intermediate identified by ConcIRT software as well as by the chromatography analysis was EG which was subsequently degraded into oxalic acid.

Considering these results and taking into account the literature, the decomposition of 1,4-dioxane by molecular O_3 in acidic conditions (Fig. 7A) follows a pathway of EGDF formation as a primary intermediate, similarly to several UV assisted AOPs [31,32,56–58]. EGDF is generated by an oxidative ring opening mechanism through peroxyl radical [32,35]. In addition, a parallel route occurs through the formation of methoxyacetic acid [32], but in a lesser extent, since the chromatography analysis detected metoxyacetic acid only in the first quarter of the experiment. Likewise, while generated in the beginning, the concentration of EGDF decreases during the experiment, as the amount of several decomposition products increases along the reaction (Fig. 7A). According to the chromatography, the further oxidation of EGDF leads mainly to the formation of glycolic acid, in accordance with Maurino et al. and Stefan and Bolton [31,32]. In the relative absorbance profiles, glyoxylic acid appears concurrently with glycolic acid, most likely as a

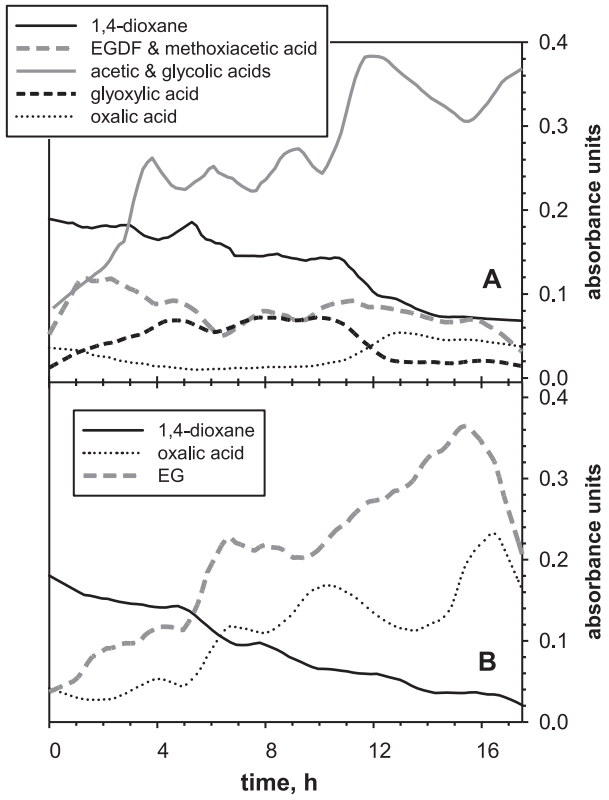

Fig. 7. FTIR-absorbance profiles of the main by-products produced during the O_3 oxidation of 1,4-dioxane (C_0 = 6168 mg L^{-1}), identified in relative absorbance units of the ConcIRT software, under (A) basic conditions at pH > 9 in the presence of $NaHCO_3$ buffer (23.8 mM), and (B) acidic conditions at pH < 5.7.

decomposition product of the latter [32], and when its concentration decreases, more oxalic acid appears (Fig. 7A). Oxalic acid could be generated from both the degradation of glycolic and glyoxylic acids [31,32]. The moderate increment of acetic acid, although visualized jointly with glycolic acid, is most certainly a decomposition product of methoxyacetic acid [32].

In basic conditions (Fig. 7B), however, the degradation of 1,4-dioxane by ozonation seems to be somewhat different. No EGDF could be detected along the reaction, but EG was identified as the primary reaction intermediate by both ConcIRT software and chromatography, simultaneously with the increment of oxalic acid as its final decomposition product [32,35]. EG is most likely produced by the hydrolysis of its formate esters [31,32,35], implicating the same initial mechanism of the EGCF formation as in the case of pH < 5.7. However, like proposed in a previous study on Fenton oxidation [35], EGDF is not detected, as it is quickly hydrolyzed to EG. Moreover, high pH conditions could also promote the fast hydrolysis of EGDF to EG, like reported for UV/TiO_2 oxidation [31]. Kishimoto [59] also reports EG as the main intermediate of 1,4-dioxane in an electrolysis/O_3 treatment, although suggesting a route through an unknown molecule "chemical I" over p-dioxanol and p-dioxanone.

Both the chromatography analysis and the relative absorbance profiles (Fig. 7B) indicate that when most of the 1,4-dioxane is consumed, the concentrations of EG and, subsequently, oxalic acid start to decrease as well. As oxalic acid is one of the last intermediates expected [31,32,35], its disappearance indicates that the reaction has reached a stage where total mineralization of the organics starts taking place. This is not the case at pH < 5.7 where the increment of oxalic acid was still very low in the end of the reaction (Fig. 7A).

5. Conclusions

O_3 was proven efficient as a sole oxidant to degrade 1,4-dioxane from wastewaters in controlled basic conditions. pH was the key parameter to make the ozonation a viable process, since the production of $OH^•$ increases at higher pH, and 1,4-dioxane and its by-products are degraded preferentially by $OH^•$. The FTIR study of decomposition pathways demonstrates that the faster degradation at pH > 9 occurs through the formation of EG as a primary intermediate; whereas the decomposition in acidic conditions consist in the formation and slow degradation of EGDF.

Working at pH 10.0 ± 0.1, close to 90% of the COD was removed and almost a complete degradation of 1,4-dioxane was reached. The presence of (bi)carbonates enhanced the process, due to their buffer effect, which kept the pH at optimal conditions. Although addition of H_2O_2 enhanced the kinetics of the 1,4-dioxane degradation process even more; this improvement was more relevant at pH 7.0 ± 0.1 than at pH over 9.

The treatment of industrial wastewater where 1,4-dioxane was the only organic contaminant showed a similar behavior to the synthetic water. 85% of COD was degraded by O_3 and 90% removal was achieved by O_3/H_2O_2. The treatment of industrial samples containing both 1,4-dioxane and MDO reached a higher reduction of COD, although smaller percentage removal. The MDO was degraded more easily than 1,4-dioxane and, therefore, its presence offered competition for the $OH^•$ radicals and reduced the efficiency of the 1,4-dioxane degradation. Adding H_2O_2 to the process, a complete elimination of 1,4-dioxane and MDO was reached; however, also a higher amount of oxidants in terms of OCC was consumed.

Acknowledgments

The research leading to these results has received funding from the European Union Seventh Framework Programme (FP7/2007-2013) under grant agreement no. 608490. The collaboration of the Gas Cromatography Service (CIB) of the Spanish National Research Council (CSIS) and the ETSI Montes of the Polytechnic University of Madrid (UPM) is fully appreciated. Archimedes Foundation (Estonia) is granting H. Barndõk's Ph.D. studies.

References

[1] European Chemicals Bureau (ECB), European Union Risk Assessment Report: 1,4-Dioxane, Second Priority List, vol. 21, Office for Official Publications of the European Communities, Luxembourg, 2002, pp. 1–29, ISBN 92-894-1252-6.
[2] U.S. Environmental Protection Agency (USEPA), Toxicological Review of 1,4-Dioxane (CAS No. 123-91-1), EPA/635/R-09/005-F, USEPA, Washington, DC, 2010.
[3] T.K.G. Mohr, Environmental Investigation and Remediation: 1,4-Dioxane and Other Solvent Stabilizers, CRC Press, Boca Raton, 2010.
[4] U.S. Environmental Protection Agency (USEPA), Treatment Technologies for 1,4-Dioxane: Fundamentals and Field Applications, EPA-542-R-06-009, USEPA, Office of Solid Waste and Emergency Response, Washington, DC, 2006.
[5] M.J. Zenker, R.C. Borden, M.A. Barlaz, Biodegradation of 1,4-dioxane using trickling filter, J. Environ. Eng. ASCE 130 (2004) 926–931.
[6] T.H. Han, J.S. Han, M.H. So, J.W. Seo, C.M. Ahn, D.H. Min, Y.S. Yoo, D.K. Cha, C.G. Kim, The removal of 1,4-dioxane from polyester manufacturing process wastewater using an up-flow Biological Aerated Filter (UBAF) packed with tire chips, J. Environ. Sci. Health Part A: Tox. Hazard. Subst. Environ. Eng. 47 (2012) 117–129.
[7] D. Shin, D.Y. Sung, H.S. Moon, K. Nam, Microbial succession in response to 1,4-dioxane exposure in activated sludge reactors: effect of inoculum source and extra carbon addition, J. Environ. Sci. Health Part A: Tox. Hazard. Subst. Environ. Eng. 45 (2010) 674–681.
[8] C.D. Adams, P.A. Scanlan, N.D. Secrist, Oxidation and biodegradability enhancement of 1,4-dioxane using hydrogen peroxide and ozone, Environ. Sci. Technol. 28 (1994) 1812–1818.
[9] H.M. Coleman, V. Vimonses, G. Leslie, R. Amal, Degradation of 1,4-dioxane in water using TiO_2 based photocatalytic and H_2O_2/UV processes, J. Hazard. Mater. 146 (2007) 496–501.
[10] P. Ghosh, A.N. Samanta, S. Ray, Oxidation kinetics of degradation of 1,4-dioxane in aqueous solution by H_2O_2/Fe(II) system, J. Environ. Sci. Health Part A: Tox. Hazard. Subst. Environ. Eng. 45 (2010) 395–399.

[11] S. Nakagawa, Y. Kenmochi, K. Tutumi, T. Tanaka, I. Hirasawa, A study on the degradation of endocrine disruptors and dioxins by ozonation and advanced oxidation processes, J. Chem. Eng. Jpn. 35 (2002) 840–847.
[12] M. Pera-Titus, V. Garcia-Molina, M.A. Banos, J. Gimenez, S. Esplugas, Degradation of chlorophenols by means of advanced oxidation processes: a general review, Appl. Catal. B 47 (2004) 219–256.
[13] A.J. Bard, R. Parsons, J. Jordan, Standard Potentials in Aqueous Solutions, International Union of Pure and Applied Chemistry, Marcel Dekker Inc, New York, 1985.
[14] W.H. Glaze, J.W. Kang, D.H. Chapin, The chemistry of water treatment processes involving ozone, hydrogen peroxide and ultraviolet radiation, Ozone: Sci. Eng. 9 (1987) 335–352.
[15] G. Bertanza, M. Papa, R. Pedrazzani, C. Repice, G. Mazzoleni, N. Steimberg, D. Feretti, E. Ceretti, I. Zerbini, E.D. Cs, estrogenicity and genotoxicity reduction in a mixed (domestic + textile) secondary effluent by means of ozonation: a full-scale experience, Sci. Total Environ. 458–460 (458) (2013) 160–170.
[16] A.M. Deegan, B. Shaik, K. Nolan, K. Urell, M. Oelgemoeller, J. Tobin, A. Morrissey, Treatment options for wastewater effluents from pharmaceutical companies, Int. J. Environ. Sci. Technol. 8 (2011) 649–666.
[17] T.A. Larsen, J. Lienert, A. Joss, H. Siegrist, How to avoid pharmaceuticals in the aquatic environment, J. Biotechnol. 113 (2004) 295–304.
[18] I. Oller, S. Malato, J.A. Sanchez-Perez, Combination of advanced oxidation processes and biological treatments for wastewater decontamination—a review, Sci. Total Environ. 409 (2011) 4141–4166.
[19] J.H. Suh, M. Mohseni, A study on the relationship between biodegradability enhancement and oxidation of 1,4-dioxane using ozone and hydrogen peroxide, Water Res. 38 (2004) 2596–2604.
[20] J.L. Acero, S.B. Haderlein, T.C. Schmidt, M.J.F. Suter, U. Von Gunten, MTBE oxidation by conventional ozonation and the combination ozone/hydrogen peroxide: efficiency of the processes and bromate formation, Environ. Sci. Technol. 35 (2001) 4252–4259.
[21] F. Beltran, B. Acedo, J. Rivas, Use of ozone to remove alachlor from surface water, Bull. Environ. Contam. Toxicol. 62 (1999) 324–329.
[22] K. Ikehata, M.G. El-Din, Aqueous pesticide degradation by ozonation and ozone-based advanced oxidation processes: a review (Part I), Ozone: Sci. Eng. 27 (2005) 83–114.
[23] K. Ikehata, M.G. El-Din, Aqueous pesticide degradation by ozonation and ozone-based advanced oxidation processes: a review (Part II), Ozone: Sci. Eng. 27 (2005) 173–202.
[24] J. Hoigne, H. Bader, The role of hydroxyl radical reactions in ozonation processes in aqueous, Water Res. 10 (1976) 377–386.
[25] S.C. Kwon, J.Y. Kim, S.M. Yoon, W. Bae, K.S. Kang, Y.W. Rhee, Treatment characteristic of 1,4-dioxane by ozone-based advanced oxidation processes, J. Ind. Eng. Chem. 18 (2012) 1951–1955.
[26] J. Hoigne, H. Bader, Rate constants of reactions of ozone with organic and inorganic compounds in water II, Water Res. 17 (1983) 11.
[27] A.B. Ross, Selected Specific Rates of Reactions of Transients from Water in Aqueous Solution: III. Hydroxyl Radical and Perhydroxyl Radical and Their Radical Ions, U. S. Department of Commerce, National Bureau of Standards, Washington, 1977.
[28] L. Bijan, M. Mohseni, Integrated ozone and biotreatment of pulp mill effluent and changes in biodegradability and molecular weight distribution of organic compounds, Water Res. 39 (2005) 3763–3772.
[29] K. Kosaka, H. Yamada, S. Matsui, K. Shishida, The effects of the co-existing compounds on the decomposition of micropollutants using the ozone/hydrogen peroxide process, Water Sci. Technol. 42 (2000) 353–361.
[30] J.H. Suh, D.J. Kang, J. Do Park, H.S. Lee, A study on the catalytic ozonation of 1,4-dioxane, in: Proceedings of the 9th Russian-Korean International Symposium on Science & Technology KORUS'2005, 2005, pp. 169–171.
[31] V. Maurino, P. Calza, C. Minero, E. Pelizzetti, M. Vincenti, Light-assisted 1,4-dioxane degradation, Chemosphere 35 (1997) 2675–2688.
[32] M.I. Stefan, J.R. Bolton, Mechanism of the degradation of 1,4-dioxane in dilute aqueous solution using the UV hydrogen peroxide process, Environ. Sci. Technol. 32 (1998) 1588–1595.
[33] V. Guzsvany, M. Kadar, Z. Papp, L. Bjelica, F. Gaal, K. Toth, Monitoring of photocatalytic degradation of selected neonicotinoid insecticides by cathodic voltammetry with a bismuth film electrode, Electroanalysis 20 (2008) 291–300.
[34] V. Guzsvany, L. Rajic, B. Jovic, D. Orcic, J. Csanadi, S. Lazic, B. Abramovic, Spectroscopic monitoring of photocatalytic degradation of the insecticide acetamiprid and its degradation product 6-chloronicotinic acid on TiO_2 catalyst, J. Environ. Sci. Health Part A: Tox. Hazard. Subst. Environ. Eng. 47 (2012) 1919–1929.
[35] N. Merayo, D. Hermosilla, L. Cortijo, Á. Blanco, Optimization of the Fenton treatment of 1,4-dioxane and on-line FTIR monitoring of the reaction, J. Hazard. Mater. 268 (2014) 102–109.
[36] M.A. Beckett, I. Hua, Elucidation of the 1,4-dioxane decomposition pathway at discrete ultrasonic frequencies, Environ. Sci. Technol. 34 (2000) 3944–3953.
[37] S.M. Kim, S.U. Geissen, A. Vogelpohl, Landfill leachate treatment by a photoassisted Fenton reaction, Water Sci. Technol. 35 (1997) 239–248.
[38] APHA, AWWA, WPCF (Eds.), Standard Methods for the Examination of Water and Wastewater, Washington, DC, 2005.
[39] H. Pobiner, Determination of hydroperoxides in hydrocarbon by conversion to hydrogen peroxide and measurement by titanium complexing, Anal. Chem. 33 (1961) 1423–1428.
[40] P. Cañizares, R. Paz, C. Saez, M.A. Rodrigo, Costs of the electrochemical oxidation of wastewaters: a comparison with ozonation and Fenton oxidation processes, J. Environ. Manage. 90 (2009) 410–420.
[41] A.M. Amat, A. Arques, F. Lopez, S. Segui, M.A. Miranda, Abatement of industrial sulfonic pollutants by ozone and UV radiation, Environ. Eng. Sci. 21 (2004) 485–492.
[42] A.M. Amat, A. Arques, M.A. Miranda, F. Lopez, Use of ozone and/or UV in the treatment of effluents from board paper industry, Chemosphere 60 (2005) 1111–1117.
[43] M.F. Sevimli, Post-treatment of pulp and paper industry wastewater by advanced oxidation processes, Ozone: Sci. Eng. 27 (2005) 37–43.
[44] R. Wang, C.L. Chen, J.S. Gratzl, Ozonation of pine kraft lignin in alkaline solution. Part 1: ozonation, characterization of kraft lignin and its ozonated preparations, Holzforschung 58 (2004) 622–630.
[45] W.H. Glaze, Reaction products of ozone – a review, Environ. Health Persp. 69 (1986) 151–157.
[46] J. Staehelin, J. Hoigne, Decomposition of ozone in water – rate of initiation by hydroxide ions and hydrogen-peroxide, Environ. Sci. Technol. 16 (1982) 676–681.
[47] A. Fischbacher, J. von Sonntag, C. von Sonntag, T.C. Schmidt, The $^{\bullet}OH$ radical yield in the $H_2O_2 + O_3$ (peroxone) reaction, Environ. Sci. Technol. 47 (2013) 9959–9964.
[48] M.M. Sein, A. Golloch, T.C. Schmidt, C. von Sonntag, No marked kinetic isotope effect in the peroxone ($H_2O_2/D_2O_2 + O_3$) reaction: mechanistic consequences, Chemphyschem 8 (2007) 2065–2067.
[49] S. Suarez, M.C. Dodd, F. Omil, U. von Gunten, Kinetics of triclosan oxidation by aqueous ozone and consequent loss of antibacterial activity: relevance to municipal wastewater ozonation, Water Res. 41 (2007) 2481–2490.
[50] M.G. El-Din, D.W. Smith, F. Al Momani, W.X. Wang, Oxidation of resin and fatty acids by ozone: kinetics and toxicity study, Water Res. 40 (2006) 392–400.
[51] M. Nakonechny, K. Ikehata, M.G. El-Din, Kinetics of estrone ozone/hydrogen peroxide advanced oxidation treatment, Ozone: Sci. Eng. 30 (2008) 249–255.
[52] W.H. Glaze, J.W. Kang, Advanced oxidation processes – description of a kinetic model for the oxidation of hazardous materials in aqueous media with ozone and hydrogen peroxide in a semibatch reactor, Ind. Eng. Chem. Res. 28 (1989) 1573–1580.
[53] J. Hoigne, H. Bader, W.R. Haag, J. Staehelin, Rate constants of reactions of ozone with organic and inorganic compounds in water. 3. Inorganic compounds and radicals, Water Res. 19 (1985) 993–1004.
[54] J. Ma, N.J.D. Graham, Degradation of atrazine by manganese-catalysed ozonation – influence of radical scavengers, Water Res. 34 (2000) 3822–3828.
[55] H. Barndõk, D. Hermosilla, L. Cortijo, C. Negro, A. Blanco, Assessing the effect of inorganic anions on TiO_2-photocatalysis and ozone oxidation treatment efficiencies, J. Adv. Oxid. Technol. 15 (2012) 125–132.
[56] R.R. Hill, G.E. Jeffs, D.R. Roberts, Photocatalytic degradation of 1,4-dioxane in aqueous solution, J. Photochem. Photobiol. A 108 (1997) 55–58.
[57] S.W. Lam, M. Hermawan, H.M. Coleman, K. Fisher, R. Amal, The role of copper(II) ions in the photocatalytic oxidation of 1,4-dioxane, J. Mol. Catal. A: Chem. 278 (2007) 152–159.
[58] T. Vescovi, H.M. Coleman, R. Amal, The effect of pH on UV-based advanced oxidation technologies-1,4-dioxane degradation, J. Hazard. Mater. 182 (2010) 75–79.
[59] N. Kishimoto, Dependency of advanced oxidation performance on the contaminated water feed mode for ozonation combined with electrolysis using a two-compartment electrolytic flow cell, J. Adv. Oxid. Technol. 10 (2007) 241–246.

PUBLICATION II

H. Barndõk, D. Hermosilla, L. Cortijo, E. Torres, A. Blanco

Electrooxidation of industrial wastewater containing 1,4-dioxane in the presence of different salts

Environmental Science and Pollution Research 21 (2014) 5701-5712

Environ Sci Pollut Res (2014) 21:5701–5712
DOI 10.1007/s11356-013-2483-2

RESEARCH ARTICLE

Electrooxidation of industrial wastewater containing 1,4-dioxane in the presence of different salts

H. Barndõk · D. Hermosilla · L. Cortijo · E. Torres · Á. Blanco

Received: 16 September 2013 / Accepted: 18 December 2013 / Published online: 16 January 2014

Abstract The treatment of 1,4-dioxane solution by electrochemical oxidation on boron-doped diamond was studied using a central composite design and the response surface methodology to investigate the use of SO_4^{2-} and HCO_3^- as supporting electrolytes considering the applied electric current, initial chemical oxygen demand (COD) value, and treatment time. Two industrial effluents containing bicarbonate alkalinity, one just carrying 1,4-dioxane (S1), and another one including 1,4-dioxane and 2-methyl-1,3-dioxolane (S2), were treated under optimized conditions and subsequently subjected to biodegradability assays with a *Pseudomonas putida* culture. Electrooxidation was compared with ozone oxidation (O_3) and its combination with hydrogen peroxide (O_3/H_2O_2). Regarding the experimental design, the optimal compromise for maximum COD removal at minimum energy consumption was shown at the maximum tested concentrations of SO_4^{2-} and HCO_3^- (41.6 and 32.8 mEq L^{-1}, respectively) and the maximum selected initial COD (750 mg L^{-1}), applying a current density of 11.9 mA cm^{-2} for 3.8 h. Up to 98 % of the COD was removed in the electrooxidation treatment of S1 effluent using 114 kWh per kg of removed COD and about 91 % of the COD from S2 wastewater applying 49 kWh per kg of removed COD. The optimal biodegradability enhancement was achieved after 1 h of electrooxidation treatment. In comparison with O_3 and O_3/H_2O_2 alternatives, electrochemical oxidation achieved the fastest degradation rate per oxidant consumption unit, and it also resulted to be the most economical treatment in terms of energy consumption and price per unit of removed COD.

Keywords Electrooxidation · 1,4-dioxane · Boron-doped diamond · Biodegradability · *Pseudomonas putida* · Central composite design · Surface response methodology

Responsible editor: Bingcai Pan

H. Barndõk · D. Hermosilla (✉) · L. Cortijo · E. Torres · Á. Blanco
Department of Chemical Engineering, Universidad Complutense de Madrid, Avda. Complutense, s/n, 28040 Madrid, Spain
e-mail: dhermosi@ucm.es

H. Barndõk
e-mail: hbarndok@quim.ucm.es

L. Cortijo
e-mail: lcortijo@quim.ucm.es

E. Torres
e-mail: cetorres@quim.ucm.es

Á. Blanco
e-mail: ablanco@quim.ucm.es

Introduction

1,4-dioxane is widely used as an industrial solvent, and it is also a common by-product of several chemical processes. Therefore, its occurrence in industrial effluents is an emerging issue that may contribute to a continuous xenobiotic contamination of groundwater and drinking water if it is not removed previously. In fact, there is a growing concern about the occurrence of 1,4-dioxane in water because of its impact on human health. 1,4-Dioxane is known to cause liver damage and kidney failure, and it has been reported to potentially promote cancer based on the evidence of carcinogenicity tests in animals, resulting in its classification as a group 2B (probable) human carcinogen (Adams et al. 1994; Choi et al. 2010; ECB 2002; USEPA 2010; Zenker et al. 2003).

Conventional wastewater treatment processes are generally inefficient for 1,4-dioxane removal, owing to its high water solubility and resistance to biodegradation (Zenker et al. 2003), although some modified biological processes have been reported viable for degrading 1,4-dioxane at a low initial concentration and at very long residence time (Han et al. 2012; Shen et al. 2008; Zenker et al. 2004).

Advanced oxidation processes (AOPs) are currently recognized as effective for the removal of biorefractory organic substances (Balcioglu et al. 2003; Coleman et al. 2007; Comninellis et al. 2008). The degradation of 1,4-dioxane has actually been carried out by several combinations of AOPs, namely sonochemical decomposition enhanced by ferrous ion (Beckett and Hua 2003), photochemical degradation enhanced by hydrogen peroxide (H_2O_2) (Maurino et al. 1997; Stefan and Bolton 1998), ozonation combined with H_2O_2 (Adams et al. 1994; Hermosilla et al. 2011), photocatalysis combined with electrooxidation (Yanagida et al. 2008), and electrooxidation (Choi et al. 2010).

The main advantage of electrooxidation over other AOPs is that this treatment does not require the presence of additional oxidants, like H_2O_2. Particularly, boron-doped diamond (BDD) is considered the most efficient electrode material for anodic oxidation due to its significant chemical and electrochemical stability, good conductivity, and very high current efficiency, resulting in increased rates of effluent mineralization; since during the treatment by BDD electrodes, most degradation is expected to occur via reaction with the OH· radicals that are generated on the anode without requiring the use of additional oxidizing agents (Comninellis et al. 2008; Rodrigo et al. 2010; Vasudevan and Oturan 2013).

On the other hand, electrolysis requires the presence of electrical conductivity. Therefore, the presence of different salts in the water matrix is an important factor to be considered. Various supporting electrolytes have been evaluated for the degradation of recalcitrant organics in synthetic solution, and sulfate has often been reported to be the most effective regarding degradation improvement (Cañizares et al. 2009a; Murugananthan et al. 2010; Velegraki et al. 2010).

However, the presence of diverse salts and bicarbonate alkalinity in industrial wastewater are often inevitable and non-optional. The use of bicarbonate as a supporting electrolyte has generally been overlooked most likely due to its radical-scavenging effect, which has been reported to occur in many AOPs (Beckett and Hua 2003). For example, Adams et al. (1994) reported that both the presence of bicarbonate and the competition by 2-methyl-1,3-dioxolane (MDO) increase the required dose of O_3/H_2O_2 for the oxidation of 1,4-dioxane in synthetic water. However, this has not been confirmed in industrial effluents yet. Although 1,4-dioxane is usually referred to as a contaminant of industrial wastewater, the studies on its degradation by AOPs (Beckett and Hua 2003; Choi et al. 2010; Maurino et al. 1997; Stefan and Bolton 1998; Yanagida et al. 2008) have almost all been performed using synthetic solutions, besides the particular exception of Fenton reaction. In this case, a considerably slower rate of organic carbon removal (11 % of the total organic carbon (TOC) in 10 h) was observed (Klecka and Gonsior 1986).

The electrochemical treatment of industrial wastewater contaminated by 1,4-dioxane and its by-products (e.g., MDO; ECB 2002) in an effluent where the presence of HCO_3^- could theoretically provide the necessary conductivity for electrolysis has not been reported yet. Therefore, the treatment of 1,4-dioxane by electrochemical oxidation on BDD electrodes was studied by a central composite design and using response surface methodology in order to assess the use of SO_4^{2-} and HCO_3^- as supporting electrolytes, considering different levels for the applied electric current, initial chemical oxygen demand (COD), and treatment time. The treatment of industrial effluents in the presence of bicarbonate alkalinity was studied under optimized conditions, and electrochemically treated industrial samples were subsequently subjected to biodegradability assay by *Pseudomonas putida*. The cost analysis of this treatment and a comparison with other AOPs (O_3 oxidation and O_3 combined with H_2O_2) were also carried out.

Materials and methods

Materials

Treatment optimization was carried out using a synthetic solution of 1,4-dioxane. This solution was prepared prior to experiments with ultrapure deionized water containing the electrolyte salts that were previously added. The final study performing electrooxidation under optimized conditions and biodegradability assessment was performed using industrial effluent samples that were supplied by a particular factory. Two industrial samples were treated (Table 1), both in the presence of bicarbonate alkalinity: one just containing 1,4-dioxane (S1) and the other one carrying both 1,4-dioxane and MDO (S2).

All used chemicals were of analytical grade. 1,4-dioxane (99.8 %) was provided by Sigma-Aldrich® Chemie GmbH (Steinheim, Germany). The supporting electrolytes that were used for electrochemical treatment were sodium sulfate (Na_2SO_4, 99.0 %) and sodium hydrogen carbonate ($NaHCO_3$, 99.7 %), supplied by Pancreac S.A. (Barcelona, Spain).

P. putida CECT 324 came from the Spanish Type Culture Collection (Colección Española de Cultivos Tipo, Valencia, Spain). Cultures were grown at pH=7 in 1 g L^{-1} of beef

Table 1 Characteristics of the industrial effluents

	S1	S2
Main contaminants	1,4-dioxane	1,4-dioxane+MDO
[COD], mg O_2 L^{-1}	450–500	1,320–1,400
[HCO_3^-], mg L^{-1}	900–1,000	900–1,000
Conductivity, μS cm^{-1}	1,900–2,100	1,900–2,100
pH	8.7–9.0	7.8–8.1

extract, 1 g L^{-1} of yeast extract, 5 g L^{-1} of peptone, and 5 g L^{-1} of NaCl and kept at −80 °C in a cryogenic solution (glycerol 87 %). The mineral solution added to the culture medium in the biodegradability assays was made of 0.5 g L^{-1} of NH_4Cl, 0.5 g L^{-1} of K_2HPO_4, 0.5 g L^{-1} of KH_2PO_4, 0.5 g L^{-1} of $MgSO_4 \cdot 7H_2O$, and 10 mL L^{-1} of trace minerals solution providing a final concentration of 0.6 mg L^{-1} of $FeSO_4 \cdot 7H_2O$, 0.2 mg L^{-1} of $CoCl_2$, 0.2 mg L^{-1} of $MnSO_4 \cdot H_2O$, and 0.2 mg L^{-1} of $CuSO_4 \cdot 5H_2O$.

Analytical methods

COD was measured, according to the Standard Methods for the Examination of Water and Wastewater (APHA 2005), by the colorimetric method at 600 nm using an AquaMate spectrophotometer (Thermos Scientific AQA 091801, Waltham, MA, USA). TOC was measured using a TOC/TN analyzer multi N/C® 3100 (Analytik Jena AG, Jena, Germany) with catalytic oxidation on cerium oxide at 850 °C. The quantitative determination of 1,4-dioxane and MDO was done by gas–liquid chromatography (GLC) on a 7980A instrument (Agilent Technologies Inc., Palo Alto, CA, USA) equipped with a flame ionization detector. Injector and detector were respectively set up at 310 and 280 °C. Samples (2 μL) were injected using the *pulsed-split* mode (*split* ratio 5:1) and analyzed in a TRB-FFAP (Teknokroma, Sant Cugat del Vallès, Spain) fused silica column (30-m×0.25-mm internal diameter×0.25-μm film thickness) with The (43 psi) as the carrier gas and the following temperature program: 80 to 240 °C after an initial hold of 9 min and at a ramp rate of 15 °C min^{-1}. Peaks were identified on the basis of sample coincidence with relative retention times of commercial standards. Quantification was performed according to peak area, corrected with the response factors calculated for each compound using 1-butanol (250 ppm) as internal standard and the software *GC-ChemStation Rev.B.04.02 (96)* from Agilent.

Electrochemical treatment

Electrochemical treatment was performed at ambient temperature (25 °C) in an undivided rectangular electrolytic flow cell (methacrylate, 10×7×15 cm^3) in a batch recirculation mode. Commercial BDD electrodes of 100 cm^2 (METAKEM GmbH, Usingen, Germany) were used as both anode and cathode and arranged parallel to each other at a distance of 2.4 cm. Experiments were carried out under galvanostatic conditions using AMEL potentiostat/galvanostat 7050 (AMEL Instruments, Milano, Italy) as the power supply. The working solution (total volume of 1.5 L) was recirculated at a constant flow rate of 0.5 L min^{-1} by a peristaltic pump (Masterflex® Console Drive, Cole-Parmer Instrument Company, IL, USA). Electrodes were fed with ordinary grade air (passed through polycarbonate filters) at a 4.5-L min^{-1} rate to facilitate mass transfer in the reactor. Na_2SO_4 and $NaHCO_3$ were added as supporting electrolytes at different concentrations. The pH of the solution was not controlled, and it increased from 8.0–8.5 up to 9.0–9.5 during the process. All the experiments were performed for 5 h.

Experimental design

Central composite design and response surface methodology were applied to optimize the treatment of 1,4-dioxane in synthetic solution. Four factors were initially chosen to evaluate the influence of operating parameters on the efficiency of electrooxidation: the concentrations (milliequivalents per liter) of the supporting electrolytes, sulfate (X_1) and bicarbonate (X_2); the initial COD of the solution (X_3, milligrams per liter); and the applied current density (X_4, milliamperes per square centimeter).

A total of 31 experiments were carried out, including a 2^4 full factorial design, augmented by eight axial points, four replications at the centre point, and three extra points chosen for a better definition of the extremes. The levels for the independent variables (Table 2) were chosen considering the local sulfate limit for effluent discharge to the municipal treatment ($[SO_4^{2-}]_{lim}$=1,000 mg L^{-1}=20.8 mEq L^{-1}, in Madrid), the actual alkalinity and COD of the real industrial effluent ($[HCO_3^-]$=900–1,000 mg L^{-1}=14.8–16.4 mEq L^{-1}; COD_{S1}=450–500 mg L^{-1}≈250 mg L^{-1} of 1,4-dioxane in S1 effluent), and preliminary experiments changing the applied current, which were performed prior to the current study, taking into account the example of Choi et al. (2010).

The studied responses were as follows: Y_1=COD removal (percent); Y_2=amount of removed COD (ΔCOD, kilograms of $COD_{removed}$ per cubic meters); Y_3=total current efficiency (TCE); and Y_4, energy consumption (EC, kilowatt-hour per kilogram of $COD_{removed}$). Particularly, TCE and EC were calculated by Eqs. 1 and 2 (Montilla et al. 2002; Panizza et al. 2001):

$$\mathrm{TCE} = 4FV\left(\frac{\mathrm{COD}_0 - \mathrm{COD}_t}{I \cdot t}\right), \quad (1)$$

where COD_0 and COD_t (moles O_2 per cubic meter) are the values of initial COD and the COD at treatment time t, respectively. I (amperes) is the applied current intensity, F (coulombs per mole) is the Faraday constant, and V (cubic meters) is the volume of the sample solution.

$$\mathrm{EC} = \frac{(t \cdot I \cdot U/V) \cdot 10^{-3}}{(\mathrm{COD}_0 - \mathrm{COD}_t) \cdot 10^{-6}}, \quad (2)$$

Table 2 Levels of the independent variables of the experimental design

	−2	−1	0	+1	+2
X_1: [SO_4^{2-}], mEq L^{-1}	0	10.4	20.8	31.2	41.6
X_2: [HCO_3^-], mEq L^{-1}	0	8.2	16.4	24.6	32.8
X_3: [COD_0, mg L^{-1}	150	300	450	600	750
X_4: j, mA cm^{-2}	2	6	10	14	18
X_5: time, h	1	2	3	4	5

where COD_0 and COD_t (moles O_2 per cubic meter), I (amperes), and V (liters) are the same variables as in Eq. 1, and U (volts) is the average cell voltage.

All the resulting responses (Y_1–Y_4) were obtained for 1, 2, 3, 4, and 5 h of the electrochemical process (complete number of process responses=4·5=20). Finally, to reduce the number of responses (20) and to obtain four comprehensive regression models, reaction time was added to the list of factors as the fifth independent variable X_5 (hours). Therefore, the final experimental design which resulted to be five times bigger in terms of the total number of experimental points became 31·5=155. This magnification of the design is described schematically in Table 3 along with the complete set of the results for COD removal (Y_1).

Regression analyses were carried out using the following quadratic model:

$$Y = b_0 + \sum_{i=1}^{k} b_i X_i + \sum_{i=1}^{k} b_{ii} X_i^2 + \sum_{i=1}^{k} \sum_{j=1}^{k} b_{ij} X_i X_j, \qquad (3)$$

where Y is the process response and $X_i \ldots X_k$ (k=5) are the above-considered independent variables.

Experimental data were analyzed using both SYSTAT 13 (SYSTAT Software Inc., Chicago, IL, USA) and Minitab 16 (Minitab Inc., State College, PA, USA).

Biodegradability assays using *P. putida*

Samples of electrochemically treated industrial effluents were subsequently subjected to biodegradability assays with *P. putida* cultures. The bacterial stock described in the methodology was previously melted at room temperature and cleaned twice with saline solution by centrifugation at 10,000 rpm for 5 min, removing the baseline medium and substituting it with a 0.9 % NaCl solution in order to remove the baseline COD provided by the organic growth medium and the glycerol solution. The sample pH was adjusted to 7.0 by the addition of 1 N HCl. A culture medium sample made up of 40 mL of sample and 10 mL of the mineral solution described above was inoculated with 200 μL of cleaned bacterial stock and incubated at 30 °C for 100 h inside 250-mL Erlenmeyer flasks placed on a rotary platform. Assays were passed through 0.20-μm syringe filters (Minisart SRP 15, Sartorius Stedim Biotech GmbH, Germany) and analyzed for COD, TOC, and 1,4-dioxane and MDO contents, taking into account the dilution ratio resulting from the addition of the mineral solution.

Results and discussion

Optimization of the electrochemical treatment of 1,4-dioxane in synthetic solution by experimental design

The complete set of experimental results for COD removal, ΔCOD, TCE, and EC is presented in Table 4. The quadratic models for the responses Y_1, Y_2, Y_3, and Y_4, based on these results, resulted to be all highly significant according to the high F and low p values resulting from the performed analysis of variance (ANOVA): $F(Y_1)$=129.53 (p<0.0001) for COD removal, $F(Y_2)$=133.23 (p<0.0001) for ΔCOD, $F(Y_3)$=134.39 (p<0.0001) for TCE, and $F(Y_4)$=213.45 (p<0.0001) for EC. The constants (b values of Eq. 3, where X_1, X_2, X_3, X_4, and X_5 are the coded independent variables) for the obtained second-order regression models for these four process responses are shown in Table 5. When plotting the experimental results against the values calculated by these quadratic models, the model prediction accuracy in terms of R^2 of the linear regression was 95.08 % for COD removal, 95.21 % for ΔCOD, 95.25 % for TCE, and 96.96 % for EC. These regression coefficients, along with the predicted and adjusted R^2 (R^2_{pred} and R^2_{adj}), are also included in Table 5.

Figures 1 and 2 report 3D response surfaces of each model as a function of two influential process parameters while keeping constant the other three process variables at their designed middle level (X_i=0; [SO_4^{2-}]=20.8 mEq L^{-1}, [HCO_3^-]=16.4 mEq L^{-1}, and [COD]$_0$=450 mg L^{-1} for Fig. 1 and [SO_4^{2-}]=20.8 mEq L^{-1}, [HCO_3^-]=16.4 mEq L^{-1}, and time=3 h for Fig. 2). Reaction time was the most important factor increasing COD removal (Fig. 1a), which agrees to the standardized effect estimates of each model component and model analyses performed by ANOVA. The percent contribution based on the portion of the sums of squares in ANOVA (Dopar et al. 2011; Yetilmezsoy et al. 2009) was 55.7 and 373 % for time (X_5) in the models of COD removal and ΔCOD, respectively. Up to 100 % COD removal could be achieved in 5 h of electrooxidation (≈130 kWh $kgCOD_{removed}^{-1}$), whereas about 85 % of the COD was already removed in 3 h (≈85 kWh $kgCOD_{removed}^{-1}$). Applied current density (j) also had an important positive influence on COD removal. The percent contribution of j to COD removal and ΔCOD in the models was 23.8 and 26.6 %, respectively. However, the surface curvature reached a plateau at around 12 mA cm^{-2}, showing that a further increase in j does not bring along a significant COD removal increase.

The response surface for TCE (Fig. 1b) shows an opposite tendency, that is, electric current efficiency was highest at the

Table 3 Experimental design and schematic addition of time as the fifth factor: example of response Y_1 (COD removal, percent) at five different treatment time intervals

						Y_1, COD removal (%)				
	X_1	X_2	X_3	X_4	X_5	*1*	*2*	*3*	*4*	*5 (h)*
28 points of CCD:					↓					
1	-1	-1	-1	-1		30.8	59.8	79.0	89.2	95.6
$\mathbf{1_1}$	-1	-1	-1	-1	-2					
$\mathbf{1_2}$	-1	-1	-1	-1	-1					
$\mathbf{1_3}$	-1	-1	-1	-1	0					
$\mathbf{1_4}$	-1	-1	-1	-1	1					
$\mathbf{1_5}$	-1	-1	-1	-1	2					
2	-1	-1	-1	1		40.6	70.6	86.9	92.8	95.2
3	-1	-1	1	-1		8.8	20.2	34.2	47.1	59.9
4	-1	-1	1	1		34.0	64.0	82.0	92.3	97.0
5	-1	1	-1	-1		28.5	54.3	74.9	86.9	92.9
6	-1	1	-1	1		30.4	55.0	72.1	82.2	90.8
7	-1	1	1	-1		19.5	41.4	63.5	82.1	93.7
8	-1	1	1	1		36.6	70.0	88.4	95.7	99.1
9	1	-1	-1	-1		31.8	60.6	79.8	89.3	94.0
10	1	-1	-1	1		44.4	73.4	86.3	95.2	98.1
11	1	-1	1	-1		17.4	34.2	47.1	55.5	66.4
12	1	-1	1	1		42.6	73.1	91.5	97.0	98.3
13	1	1	-1	-1		25.4	52.8	70.1	83.8	91.6
14	1	1	-1	1		38.5	66.8	86.5	94.2	97.9
15	1	1	1	-1		21.8	44.3	65.5	84.0	94.8
16	1	1	1	1		46.8	80.4	94.7	98.3	100.0
17	-2	0	0	0		34.6	62.2	82.0	94.4	99.4
18	2	0	0	0		34.6	64.5	82.2	94.8	99.4
19	0	-2	0	0		31.8	59.1	72.0	81.5	90.2
20	0	2	0	0		35.1	63.3	81.3	92.9	98.7
21	0	0	-2	0		34.7	53.8	71.5	76.1	81.2
22	0	0	2	0		23.5	48.0	67.2	78.8	87.9
23	0	0	0	-2		10.5	19.5	28.7	38.5	47.9
24	0	0	0	2		48.1	78.1	87.4	95.3	99.3
25	0	0	0	0		37.8	65.9	84.9	91.4	93.7
26	0	0	0	0		31.8	56.3	76.5	90.2	95.3
27	0	0	0	0		32.6	57.3	76.2	87.8	93.9
28	0	0	0	0		37.2	63.8	77.5	88.1	95.2
3 extra points:										
29	2	2	2	2		46.6	77.9	93.4	97.8	100.0
30	-2	2	2	-2		6.4	13.5	18.4	26.9	33.6
31	2	2	2	-2		8.0	14.9	21.4	28.0	33.8
Total number of design points: N = 31 · 5 = **155**										

Total number of design points: $N=31\cdot5=155$

lowest applied current density and at the shortest reaction time. As COD decreases in time, more current excess was gradually provided for its oxidation. This current did not further contribute to the degradation of such a low initial COD because the process was limited by mass transportation instead (Montilla et al. 2002; Panizza et al. 2001). For instance, TCE dropped from about 0.75 at 1 h of treatment to approximately 0.4 after 5 h when using j=12 mA cm^{-2}.

Although the percentage of COD removal was greater when performing the process using a lower initial COD, the

Table 4 Complete set of experimental results in terms of COD removal (Y_1), amount of COD removed (ΔCOD, Y_2), total current efficiency (TCE, Y_3), and energy consumption (EC, Y_4) for the electrochemical treatment of 1,4-dioxane

	Y_1	Y_2	Y_3	Y_4		Y_1	Y_2	Y_3	Y_4		Y_1	Y_2	Y_3	Y_4		Y_1	Y_2	Y_3	Y_4
1	30.8	0.10	0.68	60.0	40	99.1	0.60	0.42	117.7	79	98.3	0.60	0.53	67.5	118	87.4	0.40	0.36	151.3
2	59.8	0.19	0.67	60.6	41	31.8	0.10	0.72	34.8	80	100.0	0.62	0.43	79.3	119	95.3	0.44	0.30	185.5
3	79.0	0.25	0.53	75.1	42	60.6	0.18	0.72	35.4	81	34.6	0.17	0.80	74.5	120	99.3	0.45	0.24	228.6
4	89.2	0.29	0.51	94.4	43	79.8	0.24	0.62	41.3	82	62.2	0.30	0.72	81.6	121	37.8	0.17	0.83	43.2
5	95.6	0.31	0.49	109.3	44	89.3	0.27	0.52	51.5	83	82.0	0.39	0.61	105.0	122	65.9	0.30	0.71	50.8
6	40.6	0.13	0.46	140.3	45	94.0	0.29	0.44	63.1	84	94.4	0.45	0.51	128.1	123	84.9	0.39	0.61	60.3
7	70.6	0.23	0.39	168.7	46	44.4	0.15	0.53	78.7	85	99.4	0.48	0.46	150.1	124	91.4	0.42	0.49	76.4
8	86.9	0.28	0.32	205.4	47	73.4	0.24	0.43	97.3	86	34.6	0.16	0.81	34.2	125	93.7	0.43	0.40	94.7
9	92.8	0.30	0.26	251.1	48	86.3	0.29	0.33	128.7	87	64.5	0.30	0.74	37.7	126	31.8	0.14	0.74	47.5
10	95.2	0.31	0.22	301.7	49	95.2	0.32	0.31	161.4	88	82.2	0.38	0.64	44.7	127	56.3	0.26	0.64	55.5
11	8.8	0.05	0.72	57.2	50	98.1	0.33	0.22	199.8	89	94.8	0.44	0.53	54.8	128	76.5	0.35	0.57	63.8
12	20.2	0.13	0.73	54.6	51	17.4	0.11	0.70	40.5	90	99.4	0.46	0.45	67.0	129	90.2	0.41	0.50	75.6
13	34.2	0.21	0.71	55.1	52	34.2	0.21	0.71	39.8	91	31.8	0.14	0.63	71.1	130	95.3	0.43	0.42	92.1
14	47.1	0.29	0.70	62.8	53	47.1	0.29	0.69	39.9	92	59.1	0.27	0.59	75.7	131	32.6	0.15	0.76	47.7
15	59.9	0.37	0.67	63.3	54	55.5	0.34	0.69	40.0	93	72.0	0.33	0.48	94.5	132	57.3	0.26	0.65	56.1
16	34.0	0.21	0.76	83.6	55	66.4	0.41	0.63	44.4	94	81.5	0.37	0.41	112.0	133	76.2	0.35	0.57	66.1
17	64.0	0.39	0.70	90.4	56	42.6	0.26	0.92	40.9	95	90.2	0.41	0.37	129.7	134	87.8	0.40	0.49	80.1
18	82.0	0.50	0.59	109.5	57	73.1	0.44	0.80	48.0	96	35.1	0.16	0.82	34.6	135	93.9	0.43	0.41	97.0
19	92.3	0.56	0.47	134.9	58	91.5	0.56	0.65	59.7	97	63.3	0.29	0.73	39.8	136	37.2	0.17	0.89	40.1
20	97.0	0.59	0.41	164.6	59	97.0	0.59	0.52	76.9	98	81.3	0.37	0.62	48.6	137	63.8	0.30	0.75	48.1
21	28.5	0.09	0.75	37.8	60	98.3	0.60	0.42	97.2	99	92.9	0.43	0.52	59.3	138	77.5	0.36	0.60	61.7
22	54.3	0.17	0.71	40.7	61	25.4	0.08	0.68	34.3	100	98.7	0.46	0.44	72.0	139	88.1	0.41	0.50	75.9
23	74.9	0.24	0.64	46.7	62	52.8	0.16	0.69	33.9	101	34.7	0.06	0.33	127.1	140	95.2	0.45	0.43	90.9
24	86.9	0.27	0.55	56.3	63	70.1	0.22	0.63	37.6	102	53.8	0.10	0.26	143.2	141	46.6	0.35	0.97	37.4
25	92.9	0.29	0.47	68.1	64	83.8	0.26	0.53	45.7	103	71.5	0.13	0.24	149.5	142	77.9	0.58	0.79	46.0
26	30.4	0.10	0.27	124.6	65	91.6	0.28	0.46	53.8	104	76.1	0.14	0.20	187.7	143	93.4	0.69	0.63	59.2
27	55.0	0.17	0.25	141.5	66	38.5	0.12	0.41	86.3	105	81.2	0.14	0.17	225.1	144	97.8	0.73	0.49	78.7
28	72.1	0.23	0.19	187.5	67	66.8	0.21	0.33	105.9	106	23.5	0.18	0.93	38.5	145	100.0	0.74	0.40	99.8
29	82.2	0.26	0.19	205.2	68	86.5	0.27	0.29	122.8	107	48.0	0.37	0.93	38.3	146	6.4	0.05	1.13	16.0
30	90.8	0.28	0.19	249.6	69	94.2	0.29	0.20	166.1	108	67.2	0.52	0.85	42.4	147	13.5	0.10	1.17	15.4
31	19.5	0.12	1.00	24.3	70	97.9	0.31	0.20	188.5	109	78.8	0.61	0.74	50.3	148	18.4	0.14	1.04	17.5
32	41.4	0.26	1.05	23.5	71	21.8	0.13	0.94	24.9	110	87.9	0.68	0.65	57.8	149	26.9	0.20	1.11	16.6
33	63.5	0.39	1.05	23.6	72	44.3	0.26	0.99	23.2	111	10.5	0.05	1.12	13.5	150	33.6	0.25	1.09	17.2
34	82.1	0.51	0.98	24.9	73	65.5	0.39	0.99	23.2	112	19.5	0.09	1.09	13.7	151	5.0	0.04	0.89	16.0
35	93.7	0.58	0.90	28.1	74	84.0	0.50	0.94	24.6	113	28.7	0.13	1.00	13.6	152	11.0	0.09	1.04	17.0
36	36.6	0.22	0.85	57.4	75	94.8	0.57	0.84	28.2	114	38.5	0.18	0.96	13.3	153	17.0	0.13	0.96	17.0
37	70.0	0.42	0.78	61.3	76	46.8	0.29	1.04	32.1	115	47.9	0.22	0.97	14.2	154	24.0	0.18	0.99	18.0
38	88.4	0.53	0.65	72.9	77	80.4	0.49	0.88	39.1	116	48.1	0.22	0.61	87.2	155	30.0	0.22	0.97	19.0
39	95.7	0.58	0.52	93.8	78	94.7	0.58	0.68	52.0	117	78.1	0.36	0.49	110.0					

actual amount of COD removed in terms of kilogram per sample volume (Fig. 2a), and therefore TCE and EC as well (Fig. 2b), resulted to be greater when adding a higher initial COD value. The percent contributions of COD_0 to explain the models for ΔCOD, TCE, and EC were 15.1, 35.0, and 18.6 %, respectively. As shown in Fig. 2a, ≈0.13 kg m^{-3} (nearly a 90 %) of the COD was removed in 3 h of electrooxidation at 12 mA cm^{-2} when the initial COD was 150 mg L^{-1}, whereas a much greater amount of COD (≈0.55 kg m^{-3}) was removed under the same conditions when COD_0 was 750 mg L^{-1}. The same pattern was shown for EC (Fig. 2b). Under the same reaction conditions, ≈190 kWh was consumed per 1 kg of COD removed when COD_0 was 150 mg L^{-1}, whereas a much less EC (≈50 kWh $kgCOD_{removed}^{-1}$) was consumed when 750 mg L^{-1} of COD_0 was used. However, the positive effect of j in increasing COD removal and ΔCOD was minimal at

Table 5 Regression coefficients of the quadratic models describing the results (Y_1=COD removal, Y_2=amount of removed COD, ΔCOD; Y_3=total current efficiency, TCE; and Y_4=energy consumption, EC) for the electrochemical treatment of 1,4-dioxane

	COD removal, %		ΔCOD, $kgCOD_{removed}\ L^{-1}$		TCE		EC, kWh $kgCOD_{removed}^{-1}$	
	$b(Y_1)$	$SE(Y_1)$	$b(Y_2)$	$SE(Y_2)$	$b(Y_3)$	$SE(Y_3)$	$b(Y_4)$	$SE(Y_4)$
Model	81.29	±1.25	0.387	±0.007	0.642	±0.012	63.43	±2.03
X_1	2.67	±1.15	0.010	±0.007	0.021	±0.011	−34.00	±1.87
X_2	2.82	±1.16	0.018	±0.007	0.054	±0.011	−21.27	±1.89
X_3	−5.91	±1.16	0.165	±0.007	0.281	±0.011	−54.80	±1.89
X_4	20.40	±1.15	0.109	±0.007	−0.261	±0.011	76.27	±1.87
X_5	28.33	±0.76	0.130	±0.004	−0.145	±0.007	29.54	±1.23
X_1^2	0.65	±2.06	−0.007	±0.012	−0.035	±0.019	9.75	±3.33
X_2^2	−3.56	±2.06	−0.038	±0.012	−0.102	±0.019	5.73	±3.33
X_3^2	−11.89	±2.06	−0.067	±0.012	−0.132	±0.019	37.99	±3.33
X_4^2	−18.85	±2.06	−0.106	±0.012	0.053	±0.019	15.08	±3.33
X_5^2	−12.55	±1.25	-−0.059	±0.007	0.003	±0.012	7.20	±2.02
$X_1 \cdot X_2$	−2.93	±2.39	−0.019	±0.014	0.008	±0.023	15.48	±3.87
$X_1 \cdot X_3$	1.49	±2.39	0.020	±0.014	0.012	±0.023	8.93	±3.87
$X_1 \cdot X_4$	0.78	±2.14	0.009	±0.012	0.013	±0.020	−15.20	±3.47
$X_1 \cdot X_5$	−1.08	±1.39	−0.008	±0.008	−0.033	±0.013	−7.46	±2.26
$X_2 \cdot X_3$	14.31	±2.60	0.064	±0.015	0.140	±0.025	−8.93	±4.21
$X_2 \cdot X_4$	−10.98	±2.39	−0.049	±0.014	−0.153	±0.023	14.01	±3.87
$X_2 \cdot X_5$	−0.45	±1.47	−0.010	±0.009	−0.008	±0.014	−1.00	±2.38
$X_3 \cdot X_4$	21.79	±2.39	0.163	±0.014	0.136	±0.023	−57.49	±3.87
$X_3 \cdot X_5$	−2.27	±1.47	0.067	±0.009	−0.024	±0.014	−16.33	±2.38
$X_4 \cdot X_5$	1.85	±1.39	0.017	±0.008	−0.079	±0.013	30.41	±2.26
R^2	95.08 %		95.21 %		95.25 %		96.96 %	
R^2_{pred}	93.00 %		93.11 %		93.69 %		95.48 %	
R^2_{adj}	94.35 %		94.50 %		94.54 %		96.50 %	

low initial COD values, which means that nearly the same result could be achieved using 2 mA cm^{-2}. Therefore, EC could substantially be reduced.

Regarding the effect of the supporting electrolyte, no radical scavenging effect in terms of a negative influence on COD removal was found for either SO_4^{2-} or HCO_3^-. On the contrary, the presence of both salts rather enhanced the process. While HCO_3^- was slightly more influential than SO_4^{2-} in increasing COD removal (and ΔCOD), their positive effect (significance in terms of $p \leq 0.05$) was rather small in the studied concentration range (Fig. 3a). The percent contribution of SO_4^{2-} and HCO_3^- to the COD removal (Y_1) model was 0.7 and 1.6 %, respectively. On the other hand, both salts were important factors to be considered for decreasing the consumption in kilowatt-hours, meaning that their principal effect simply laid on providing the necessary conductivity for electrolysis. Neither the scavenging effect of bicarbonate nor the additional oxidative effect of sulfate played an important role in the oxidation process. As presented in Fig. 3b, SO_4^{2-} had a slightly greater effect on EC than HCO_3^- (percent contributions based on the sums of squares were 7.3 and 5.3 %, respectively), since the first one provides somewhat higher conductivity to the solution. However, differences were small, addressing that the natural bicarbonate alkalinity of certain wastewater may serve as a good electrolyte for performing electrochemical oxidation, just as good as SO_4^{2-} salts may be. To illustrate the discussion above, Fig. 4 shows the optimization plot for a maximum COD removal, ΔCOD, and TCE at a minimum EC. The optimal compromise is reached in the presence of the maximum concentrations of both electrolytes (41.6 mEq L^{-1} of SO_4^{2-} and 32.8 mEq L^{-1} of HCO_3^-) when the maximum initial COD of 750 mg L^{-1} was used and a current density of 11.9 mA cm^{-2} was applied for 3.8 h.

Treatment of industrial wastewater containing 1,4-dioxane

Electrochemical degradation of industrial effluents

Considering the results of the just reported experimental design, the electrochemical treatment of industrial effluents was carried out applying a current density of 12 mA cm^{-2}, in the presence of the initial bicarbonate alkalinity of the effluent

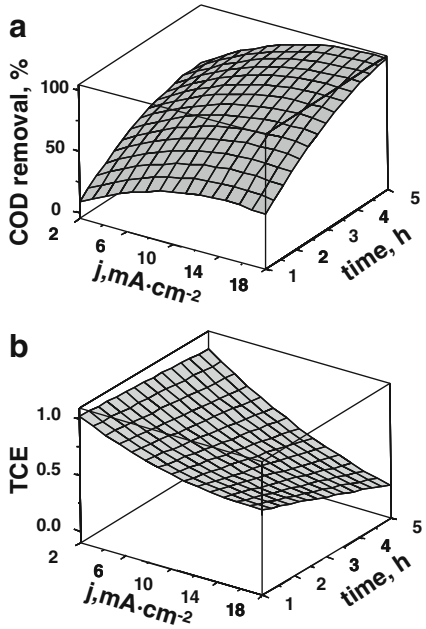

Fig. 1 3D response surfaces for **a** percent COD removal and **b** total current efficiency (TCE), built up as a function of the applied current density (j) and treatment time. Constant values at X_i=0: $[SO_4^{2-}]$= 20.8 mEq L^{-1}, $[HCO_3^-]$=16.4 mEq L^{-1}, and $[COD]_0$=450 mg L^{-1}

(16.4 mEq L^{-1}), and using 20.8 mEq L^{-1} of SO_4^{2-} as a supporting electrolyte, which is a concentration that still meets discharge limitation in force. As shown in Fig. 5, up to a 98 % COD removal was achieved for S1 effluent after 5 h of

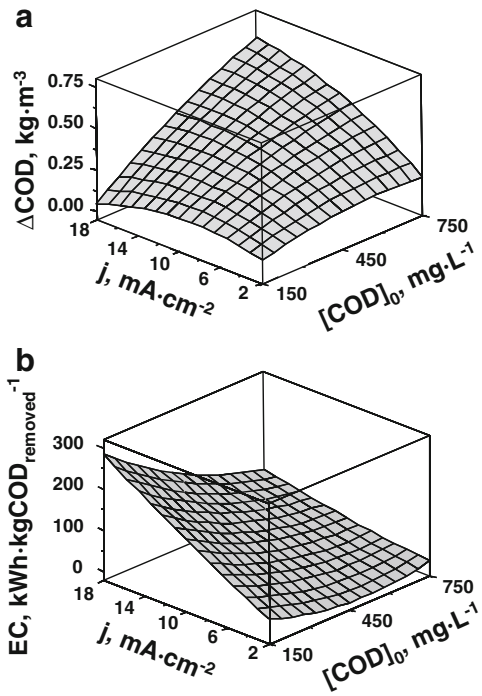

Fig. 2 3D response surfaces for **a** the amount of COD removed (ΔCOD) and **b** energetic consumption (EC), constructed as a function of the initial COD value and the applied current density. Constant values at X_i=0: $[SO_4^{2-}]$=20.8 mEq L^{-1}, $[HCO_3^-]$=16.4 mEq L^{-1}, and time=3 h

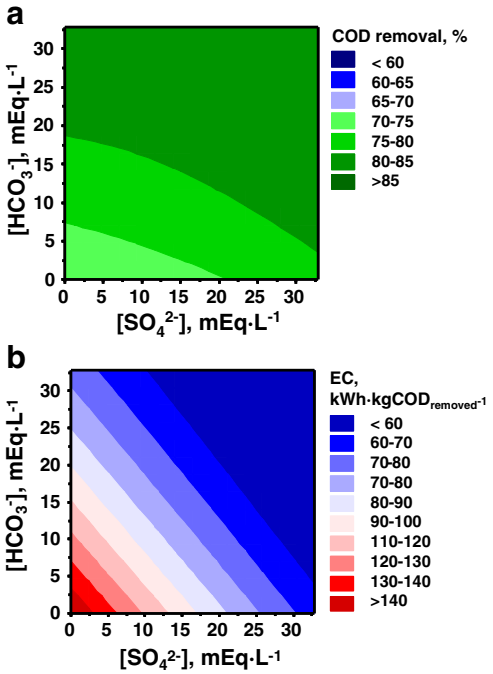

Fig. 3 Surface plots for **a** percent COD removal and **b** energetic consumption (EC), drawn as a function of the concentrations of supporting electrolytes (SO_4^{2-} and HCO_3^-). Constant values at X_i=0: $[COD]_0$= 450 mg L^{-1}, j=10 mA cm^{-2}, and time=3 h

treatment using 114 kWh $kgCOD_{removed}^{-1}$ and about a 91 % of the COD was removed from S2 effluent using 49 kWh $kgCOD_{removed}^{-1}$ (≈60 kWh m^{-3} was used in both cases). The results for the electrochemical oxidation of the S1 effluent (just containing 1,4-dioxane) resulted in a good correlation to the values predicted by the models resulting from the experimental design performed for a synthetic solution of 1,4-dioxane. After a 4-h treatment, which matches the treatment

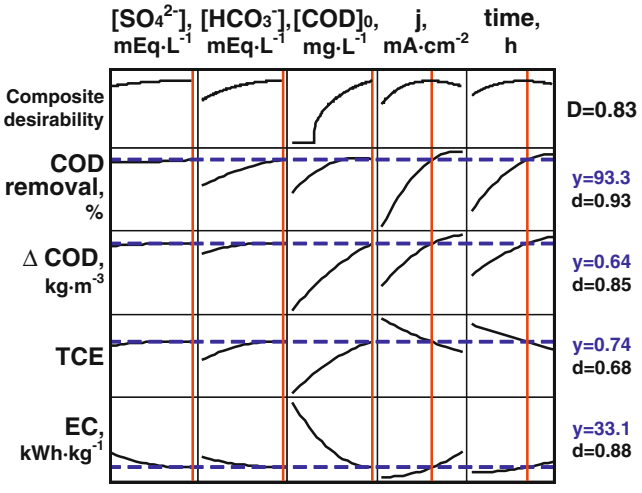

Fig. 4 Optimization plot for maximum COD removal (percent) and amount of COD removed (ΔCOD) at a maximum total current efficiency (TCE) and a minimum energetic consumption (EC) (y stands for the process response at optimal compromise, d stands for the desirability of the process response, and D stands for composite desirability)

time recommended by the model optimizer, the following results were achieved: COD removal=93 % (predicted 96 %), ΔCOD=0.48 kgCOD m^{-3} (predicted 0.50 kgCOD m^{-3}), TCE=0.48 (predicted 0.55), and EC=93 kWh $kgCOD_{removed}^{-1}$ (predicted 92 kWh $kgCOD_{removed}^{-1}$). In fact, very good regression coefficients were achieved ($R^2_{COD\ \%}$= 99.01 %, $R^2_{\Delta COD}$=99.21 %, R^2_{TCE}=99.27 %, and R^2_{EC}= 98.95 %) when plotting the experimental results using industrial effluent against the model predictions reported using synthetic 1,4-dioxane solution.

Figure 6 illustrates the evolution of the biodegradability of S1 and S2 effluents along with the degradation of COD, TOC, and 1,4-dioxane and MDO contents during their electrochemical treatment. A nearly complete mineralization was achieved in the electrochemical treatment of S1, whereas almost 90 % of the TOC was removed from S2. The major part of 1,4-dioxane (about an 85 % in both S1 and S2 effluents), as well as almost all MDO from S2 (≈90 % removal), was degraded in 2 h of electrooxidation treatment (using≈21 kWh m^{-3} for both effluents). 1,4-dioxane removal was independent of the presence of MDO, following a similar trend in both effluents (Fig. 6a, b). The degradation of 1,4-dioxane was greater at the beginning of the experiment and started slacking off in time as its concentration diminished. About 60, 85, and 90 % of the compound were degraded in 1, 2, and 3 h of treatment, respectively. The removal of MDO from S2 (Fig. 6b) otherwise appeared to be independent of its concentration, showing a linear degradation in time: about 45 and 90 % removals were achieved after 1 and 2 h of the process, respectively, and no MDO was detected after 3 h of electrooxidation treatment.

The initial biodegradability of S1 effluent (5 % of the initial COD) was significantly increased by the electrochemical process. After 1 h of electrooxidation treatment, the biodegradable part of the residual COD was 19 %. A further treatment time did not lead to a further increase of the biodegradability of the solution, meaning either that the intermediates produced afterwards resulted to be less biodegradable or that the remaining part of the organic matter was already too diluted for

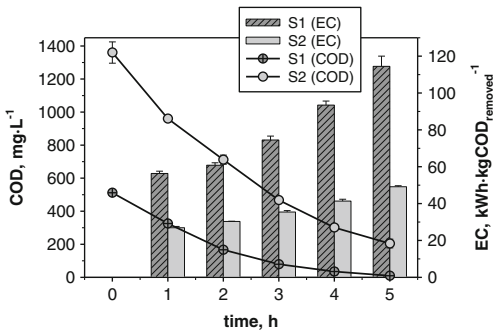

Fig. 5 COD removal and simultaneous energetic consumption (EC) increase during the electrochemical treatment of industrial effluents S1 and S2 at 12 mA cm^{-2} in the presence of its inherent initial bicarbonate alkalinity (16.4 mEq L^{-1}) using 20.8 mEq L^{-1} of SO_4^{2-} as a supporting electrolyte

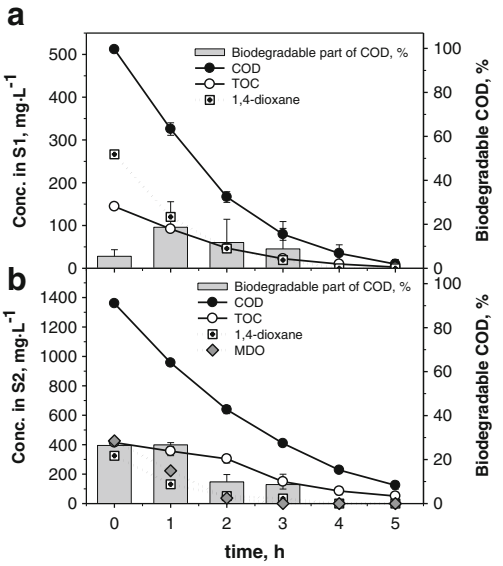

Fig. 6 Evolution of effluent biodegradability by *P. putida* (100-h bioassays) along with the degradation of COD, TOC, 1,4-dioxane, and MDO during the electrochemical treatment of **a** the 1,4-dioxane containing effluent (S1) and **b** the effluent with 1,4-dioxane and MDO (S2) at 12 mA cm^{-2} in the presence of initial bicarbonate alkalinity (16.4 mEq L^{-1}) using 20.8 mEq L^{-1} of SO_4^{2-} as a supporting electrolyte

feeding bacteria. On the other hand, the biodegradability of S2 was initially higher (26 % of the COD), which means that MDO is more susceptible to biodegradation. In fact, more than 50 % of the initial MDO content in S2 effluent was removed by the biological treatment with *P. putida*, while a negligible amount of 1,4-dioxane was degraded. As a result, the biodegradability of S2 effluent remained similar after 1 h of electrooxidation treatment (27 % of the COD). However, considering the overall results, almost 50 % of the COD, along with 85 % of the content of MDO, and 75 % of 1,4-dioxane were removed by the combined process treatment of S2 effluent. If the starting solution for biodegradation was the resulting solution of a 2-h electrooxidation process, the biodegradability of S2 effluent decreased, meaning that the resulting intermediate products were less biodegradable. Considering these results, if electrooxidation is to be used as a pretreatment for such industrial effluents prior to a biological process, the optimal time for the advanced oxidation step with the current reactor design would be approximately of 1 h applying a current density of 12 mA cm^{-2} (≈10 kWh m^{-3}). However, further research should be conducted to monitor the evolution of biodegradability determined by several methods and, using a shorter time interval, in order to determine the precise optimal time for an electrochemical pretreatment.

Comparing electrooxidation with O_3 and O_3/H_2O_2 oxidation processes

Regarding the economic assessment and feasibility of the electrochemical treatment compared with other AOPs, the

results of the current study were compared with a previous work devoted to the treatment of the same effluents S1 and S2 by O_3 and O_3 combined with H_2O_2 oxidation processes (Hermosilla et al. 2011). To compare several AOPs that use different oxidative agents, the so-called oxygen-equivalent chemical-oxidation capacity (OCC) parameter was used, as proposed by Cañizares et al. (2009b) to quantify the amount of oxidant that was added to wastewater in comparable units (Eqs. 4, 5 and 6):

$$\mathrm{OCC_{EO}}\left(\mathrm{kgO_2\ m^{-3}}\right) = Q\left(\frac{\mathrm{kAh}}{\mathrm{m^3}}\right)\frac{1\ \mathrm{kmol^-}\quad 3,600\ \mathrm{s}\,1\ \mathrm{kmolO_2}\,32\ \mathrm{kgO_2}}{96,487\ \mathrm{kAs^-}\quad 1\ \mathrm{h}\quad 4\ \mathrm{kmol^-}\quad \mathrm{kmolO_2}} = 0.298Q\left(\frac{\mathrm{kAh}}{\mathrm{m^3}}\right) \tag{4}$$

$$\mathrm{OCC_{O_3}}\left(\mathrm{kgO_2\ m^{-3}}\right) = [\mathrm{O_3}]\left(\frac{\mathrm{kgO_3}}{\mathrm{m^3}}\right)\frac{1\ \mathrm{kmolO_3}\ 6\ \mathrm{kmol^-}\ 1\ \mathrm{kmolO_2}\,32\ \mathrm{kgO_2}}{48\ \mathrm{kgO_3}\ 1\ \mathrm{kmolO_3}\ 4\ \mathrm{kmol^-}\ \mathrm{kmolO_2}} = 1.000[\mathrm{O_3}]\left(\frac{\mathrm{kgO_3}}{\mathrm{m^3}}\right) \tag{5}$$

$$\mathrm{OCC_{H_2O_2}}\left(\mathrm{kgO_2\ m^{-3}}\right) = [\mathrm{H_2O_2}]\left(\frac{\mathrm{kgH_2O_2}}{\mathrm{m^3}}\right)\frac{1\ \mathrm{kmolH_2O_2}\ 2\ \mathrm{kmol^-}\ 1\ \mathrm{kmolO_2}\,32\ \mathrm{kgO_2}}{34\ \mathrm{kgH_2O_2}\ 1\ \mathrm{kmolO_3}\ 4\ \mathrm{kmol^-}\ \mathrm{kmolO_2}} = 0.471[\mathrm{H_2O_2}]\left(\frac{\mathrm{kgH_2O_2}}{\mathrm{m^3}}\right) \tag{6}$$

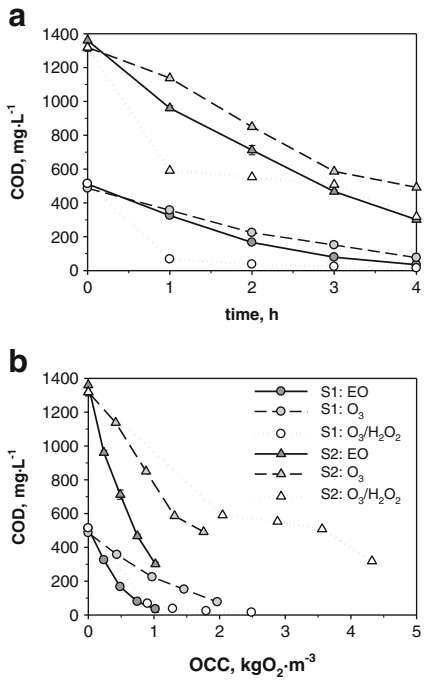

Fig. 7 The evolution of the COD during the treatment of both industrial effluents (S1 and S2) by three different AOPs [electrooxidation (EO), O_3, and O_3/H_2O_2] as a function of **a** treatment time and **b** oxygen-equivalent chemical-oxidation capacity (OCC, calculated by Eqs. 4–6; Cañizares et al. 2009b). Conditions for EO: j=12 mA cm^{-2}, [HCO_3^-]=16.4 mEq L^{-1} (initial bicarbonate alkalinity), [SO_4^{2-}]=20.8 mEq L^{-1} (supporting electrolyte). Condition for O_3: average consumption=0.40 kgO_3 h^{-1} m^{-3}. Conditions for O_3/H_2O_2: [H_2O_2]/[COD]=2.215 ([H_2O_2]$_{S1}$≈1.00 kg m^{-3}; [H_2O_2]$_{S2}$≈2.90 kg m^{-3}), average O_3 consumption was approximately 0.45 kgO_3 h^{-1} m^{-3} for S1 and 0.66 kgO_3 h^{-1} m^{-3} for S2

Panels a and b in Fig. 7 show the evolution of COD in both effluents (S1 and S2) along the application of all three different AOPs as a function of treatment time and OCC, respectively. It can be checked that the electrochemical treatment produced a faster degradation compared with ozonation, whereas O_3 oxidation combined with H_2O_2 addressed not only a much faster kinetics along the first process hour (Fig. 7a) but also an almost ineffective degradation during the following treatment time, which implies that the faster oxidation was mainly caused by the presence of H_2O_2, which was consumed in about 1 h. Figure 7b however demonstrates that the elevated amount of H_2O_2 required for the higher

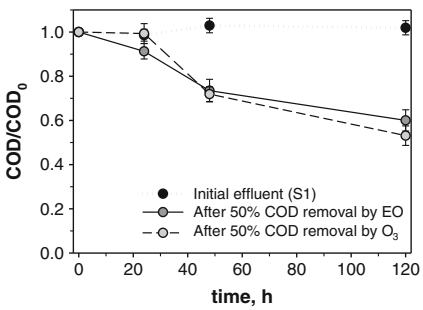

Fig. 8 Evolution of the COD in the biodegradation tests carried on by *P. putida* on the initial industrial effluent containing 1,4-dioxane (S1) and on the same S1 effluent previously treated by electrooxidation (EO) or O_3 (both performed until 50 % COD removal was achieved). Conditions for EO: j=12 mA cm^{-2}; [HCO_3^-]= 16.4 mEq L^{-1} (initial bicarbonate alkalinity), [SO_4^{2-}]=20.8 mEq L^{-1} (supporting electrolyte). Condition for O_3: average consumption= 0.40 kgO_3 h^{-1} m^{-3}

Table 6 Energetic and economic comparison of the treatment of effluents S1 (1,4-dioxane) and S2 (1,4-dioxane+MDO) by electrooxidation (EO), O_3, and O_3/H_2O_2

Process	Energetic and economical parameters for varying COD removal (%)								
	kgCOD/OCC[a]			kWh $kgCOD^{-1}$			EUR/kgCOD		
	Treatment of S1								
	50 %	70 %	90 %	50 %	70 %	90 %	50 %	70 %	90 %
EO[b]	0.9	0.7	0.5	55	63	90	7	8	11
O_3/H_2O_2[c]	0.4	0.5	0.4	69	76	164	14	13	22
O_3[d]	0.3	0.2	0.2	402	474	682	46	55	79
	Treatment of S2								
	50 %	70 %	90 %	50 %	70 %	90 %	50 %	70 %	90 %
EO[b]	1.7	1.4	0.9	30	35	50	4	4	6
O_3/H_2O_2[c]	0.3	0.2	0.1	167	322	1037	25	42	123
O_3[d]	0.5	0.4	0.3	216	268	399	25	31	46

[a] OCC denominates oxygen-equivalent chemical-oxidation capacity, calculated by Eqs. 4–6 (Cañizares et al. 2009b)

[b] j=12 mA cm^{-2}; $[HCO_3^-]$=16.4 mEq L^{-1}; $[SO_4^{2-}]$=20.8 mEq L^{-1}

[c] $[H_2O_2]/[COD]$=2.215 ($[H_2O_2]_{S1}\approx$1.00 kg m^{-3}, $[H_2O_2]_{S2}\approx$2.90 kg m^{-3}); average 0.45 kgO_3 h^{-1} m^{-3} for S1 and 0.66 kgO_3 h^{-1} m^{-3} for S2

[d] Average 0.40 kgO_3 h^{-1} m^{-3}

organic load present in the S2 effluent significantly increased the OCC for the O_3/H_2O_2 process and that the fastest degradation per consumed oxidant was really produced by the electrooxidation process.

The enhancements of biodegradability by both electrooxidation and O_3 processes were also compared performing bioassays with *P. putida* (Fig. 8). The biological treatment was applied to the industrial effluent S1 and two other effluents with the same COD (50 % of the initial COD) remaining after applying either electrooxidation or O_3 pretreatment to S1. The initial wastewater containing 1,4-dioxane had not enough biodegradability to be treated by *P. putida*, so COD remained constant after this biodegradation trial. After an electrooxidation or O_3 pretreatment, a further 25 % of the remaining COD was degraded by *P. putida* in 48 h and about 45 % after 120 h in both cases. This indicates that the degradation of 1,4-dioxane is most likely to follow a similar pathway along both AOPs, achieving a similar biodegradability if the same COD amount was previously removed. However, as COD reduction resulted faster for the electrochemical pretreatment (Fig. 7), this similar level of biodegradability was also achieved faster than in the ozonation process.

In addition, the treatment cost per unit of removed COD was estimated considering the price of industrial electric power in Spain (0.12 EUR/kWh; Eurostat 2012) and the wholesale price of industrial-grade H_2O_2 and Na_2SO_4 (0.61 and 0.09 EUR/kg, respectively; ISIC 2012). Electricity consumption was estimated considering the average consumption of a typical industrial O_3 generator (8 kWh per 1 kg of O_3 rich gas; i.e., 8 % of O_3 in oxygen), an additional energy consumption for refrigerating the O_3 generator (approximately 30 %), and the additional consumption of an Adamant PP1000industrial power supply per kilowatt-hour applied to the process (an extra 5 % from the grid). The results shown in Table 6 indicate that electrochemical oxidation was the most economical alternative in terms of energy consumption and the price per amount of removed COD, whereas O_3 oxidation may be rendered unfeasible due to its high treatment cost and slow oxidation kinetics. O_3/H_2O_2 treatment may result competitive to electrooxidation when optimizing treatment time to consume all H_2O_2, but an electrooxidation/H_2O_2 combination might be considered instead.

Conclusions

In the electrochemical treatment of synthetic 1,4-dioxane solution, the optimal compromise for achieving a maximum COD removal at a maximum current efficiency and producing the minimum energy consumption was reached using the designed highest concentrations of SO_4^{2-} (41.6 mEq L^{-1}), HCO_3^- (32.8 mEq L^{-1}), and initial COD (750 mg L^{-1}) and applying a current density of 11.9 mA cm^{-2} for 3.8 h. The regression models resulting from the experimental design for the electrooxidation treatment of a 1,4-dioxane synthetic solution accurately predicted the posterior electrooxidation treatment of an industrial sample just containing 1,4-dioxane (S1): $R^2_{COD\ \%}$=99.01 %, $R^2_{\Delta COD}$=99.21 %, R^2_{TCE}=99.27 %, and R^2_{EC}=98.95 %.

In the treatment of industrial effluents with bicarbonate alkalinity, up to 98 % of the COD was removed in the electrooxidation of the effluent just containing 1,4-dioxane

(S1), consuming 114 kWh $kgCOD_{removed}^{-1}$ and 91 % COD removal was achieved for the effluent containing both 1,4-dioxane and MDO (S2), but resulting in the consumption of 49 kWh $kgCOD_{removed}^{-1}$. Complementarily, the almost total mineralization of effluent S1 and about 90 % TOC removal in effluent S2 were achieved. In addition, the major part of 1,4-dioxane (≈85 %) was already degraded in both industrial effluents after 2 h of electrooxidation treatment (≈21 kWh m^{-3}).

The highest biodegradability enhancement was achieved in approximately 1 h of electrooxidation at 12 mA cm^{-2} (≈10 kWh m^{-3}) for both effluents. The biodegradability of the wastewater containing 1,4-dioxane and MDO (S2) was originally higher precisely due to the content of MDO, which was more susceptible to biodegradation.

In comparison with O_3 and O_3/H_2O_2, the fastest degradation per consumed oxidant was achieved by electrooxidation. This treatment also resulted to be the cheapest one in terms of kilowatt-hours and the price per amount of removed COD. Namely, energy consumption and the average price of the process to reach 90 % COD removal were 90 and 50 kWh $kgCOD_{removed}^{-1}$ and 11 and 6 EUR $kgCOD_{removed}^{-1}$, for S1 and S2 effluents, respectively.

Acknowledgments This research was funded by the European Commission (project "AQUAFIT4USE", 211534). Archimedes Foundation (Estonia) is granting H. Barndõk's Ph.D. studies. The collaboration of the Gas Chromatography Service (CIB) of the Spanish National Research Council (CSIC) is fully appreciated.

References

Adams CD, Scanlan PA, Secrist ND (1994) Oxidation and biodegradability enhancement of 1,4-dioxane using hydrogen-peroxide and ozone. Environ Sci Technol 28(11):1812–1818

Balcioglu IA, Alaton IA, Otker M, Bahar R, Bakar N, Ikiz M (2003) Application of advanced oxidation processes to different industrial wastewaters. J Environ Sci Heal A 38(8):1587–1596

Beckett MA, Hua I (2003) Enhanced sonochemical decomposition of 1, 4-dioxane by ferrous iron. Water Res 37(10):2372–2376

Cañizares P, Hernandez M, Rodrigo MA, Saez C, Barrera CE, Roa G (2009a) Electrooxidation of brown-colored molasses wastewater. Effect of the electrolyte salt on the process efficiency. Ind Eng Chem Res 48(3):1298–1301

Cañizares P, Paz R, Saez C, Rodrigo MA (2009b) Costs of the electrochemical oxidation of wastewaters: a comparison with ozonation and Fenton oxidation processes. J Environ Manag 90(1):410–420

Choi JY, Lee YJ, Shin J, Yang JW (2010) Anodic oxidation of 1,4-dioxane on boron-doped diamond electrodes for wastewater treatment. J Hazard Mater 179(1–3):762–768

Coleman HM, Vimonses V, Leslie G, Amal R (2007) Removal of contaminants of concern in water using advanced oxidation techniques. Water Sci Technol 55(12):301–306

Comninellis C, Kapalka A, Malato S, Parsons SA, Poulios L, Mantzavinos D (2008) Advanced oxidation processes for water treatment: advances and trends for R&D. J Chem Technol Biotechnol 83(6):769–776

Dopar M, Kusic H, Koprivanac N (2011) Treatment of simulated industrial wastewater by photo-Fenton process. Part I: the optimization of process parameters using design of experiments (DOE). Chem Eng J 173(2):267–279

ECB (2002) European Union risk assessment report: 1,4-dioxane. European Chemicals Bureau, Office for Official Publications of the European Communities, Luxembourg. 2nd Priority List 21: 1-129.

Eurostat (2012) Electricity prices for industrial consumers. http://epp.eurostat.ec.europa.eu/portal/page/portal/eurostat/home. Accessed 7 Sep 2012.

Han TH, Han JS, So MH, Seo JW, Ahn CM, Min DH, Yoo YS, Cha DK, Kim CG (2012) The removal of 1,4-dioxane from polyester manufacturing process wastewater using an up-flow biological aerated filter (UBAF) packed with tire chips. J Environ Sci Heal A 47(1):117–129

Hermosilla D; Cortijo L; Merayo N; Negro C; Blanco Á (2011) Removal of 1,4-dioxane by advanced oxidation processes. In: 9th green chemistry conference, Alcalá de Henares, Spain 2011.

ISIC (2012) Indicative chemical prices A-Z. www.icispricing.com. Accessed 12 Feb 2012.

Klecka GM, Gonsior SJ (1986) Removal of 1,4-dioxane from wastewater. J Hazard Mater 13(2):161–168

Maurino V, Calza P, Minero C, Pelizzetti E, Vincenti M (1997) Light-assisted 1,4-dioxane degradation. Chemosphere 35(11):2675–2688

Montilla F, Michaud PA, Morallon E, Vazquez JL, Comninellis C (2002) Electrochemical oxidation of benzoic acid at boron-doped diamond electrodes. Electrochim Acta 47(21):3509–3513

Murugananthan M, Latha SS, Raju GB, Yoshihara S (2010) Anodic oxidation of ketoprofen-An anti-inflammatory drug using boron doped diamond and platinum electrodes. J Hazard Mater 180(1–3):753–758

Panizza M, Michaud PA, Cerisola G, Comninellis C (2001) Anodic oxidation of 2-naphthol at boron-doped diamond electrodes. J Electroanal Chem 507(1–2):206–214

Rodrigo MA, Cañizares P, Sanchez-Carretero A, Saez C (2010) Use of conductive-diamond electrochemical oxidation for wastewater treatment. Catal Today 151(1–2):173–177

Shen W, Chen H, Pan S (2008) Anaerobic biodegradation of 1,4-dioxane by sludge enriched with iron-reducing microorganisms. Bioresour Technol 99:2483–2487

Stefan MI, Bolton JR (1998) Mechanism of the degradation of 1,4-dioxane in dilute aqueous solution using the UV hydrogen peroxide process. Environ Sci Technol 32(11):1588–1595

USEPA (2010) Toxicological review of 1,4-dioxane (CAS No. 123-91-1). U.S. Environmental Protection Agency, Washington, DC

Vasudevan S, Oturan MA (2013) Electrochemistry: as cause and cure in water pollution—an overview. Environ Chem Lett. doi:10.1007/s10311-013-0434-2

Velegraki T, Balayiannis G, Diamadopoulos E, Katsaounis A, Mantzavinos D (2010) Electrochemical oxidation of benzoic acid in water over boron-doped diamond electrodes: statistical analysis of key operating parameters, kinetic modeling, reaction by-products and ecotoxicity. Chem Eng J 160(2):538–548

Yanagida S, Nakajima A, Kameshima Y, Okada K (2008) Voltage swing interval effects on photocatalytic decomposition of 1,4-dioxane in aqueous media using TiO_2-coated stainless mesh. J Ceram Soc Jpn 116(1350):181–186

Yetilmezsoy K, Demirel S, Vanderbei RJ (2009) Response surface modeling of Pb(II) removal from aqueous solution by *Pistacia vera* L.: Box-Behnken experimental design. J Hazard Mater 171(1–3):551–562

Zenker MJ, Borden RC, Barlaz MA (2003) Occurrence and treatment of 1, 4-dioxane in aqueous environments. Environ Eng Sci 20(5):423–432

Zenker MJ, Borden RC, Barlaz MA (2004) Biodegradation of 1,4-dioxane using trickling filter. J Environ Eng-ASCE 130(9):926–931

PUBLICATION III

H. Barndõk, L. Blanco, D. Hermosilla, A. Blanco

Heterogeneous photo-Fenton processes using zero valent iron microspheres for the treatment of wastewaters contaminated with 1,4-dioxane

Chemical Engineering Journal 284 (2016) 112-121

Chemical Engineering Journal 284 (2016) 112–121

Contents lists available at ScienceDirect

Chemical Engineering Journal

journal homepage: www.elsevier.com/locate/cej

Heterogeneous photo-Fenton processes using zero valent iron microspheres for the treatment of wastewaters contaminated with 1,4-dioxane

Helen Barndõk, Laura Blanco, Daphne Hermosilla *, Ángeles Blanco

Departamento de Ingeniería Química, Facultad de Ciencias Químicas, Universidad Complutense de Madrid, Ciudad Universitaria s/n, 28040 Madrid, Spain

HIGHLIGHTS

- 1,4-Dioxane was successfully degraded by heterogeneous photo-Fenton on Fe^0 microspheres.
- Influences of radiation source, pH and reagent dose were studied on synthetic waters.
- Excellent results were achieved in neutral conditions without any iron leaching.
- Efficient treatment of industrial wastewaters was performed.
- Major reaction intermediates of 1,4-dioxane were identified.

GRAPHICAL ABSTRACT

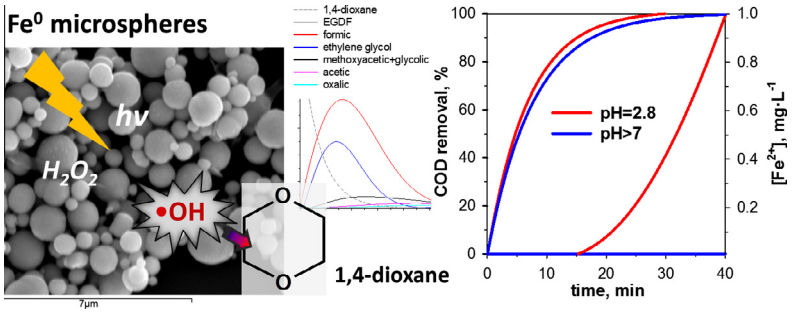

ARTICLE INFO

Article history:
Received 14 June 2015
Received in revised form 7 August 2015
Accepted 24 August 2015
Available online 31 August 2015

Keywords:
1,4-Dioxane
Fe^0 microspheres
Heterogeneous AOPs
Photo-Fenton
Pseudomonas putida

ABSTRACT

The use of zero valent iron (Fe^0) microspheres for the degradation of 1,4-dioxane by photo-Fenton processes was optimized in terms of pH and reagent dosage for the successful treatment of industrial wastewaters. In addition, reaction intermediates of 1,4-dioxane degradation were studied. In UV photo-Fenton treatment of synthetic waters, complete removal of 1,4-dioxane was reached in 5 min, significant biodegradability enhancement (up to 60%) was achieved in 10 min, and an almost total COD removal was obtained after 30 min of treatment ($\geqslant$90%), whereat the presence of bicarbonate buffer (pH $\geqslant$ 7) prevented iron leaching. At different H_2O_2/COD_0 ratios the degradation of organics by UV-catalysed Fenton was in a following order: 2.625 > 2.125 > 4 > 1.625. On the other hand, solar photo-Fenton removed above 90% of 1,4-dioxane after 180 min, whereas H_2O_2/Fe^0 ratio of 60 was found optimum. In the treatment of industrial wastewater, $\geqslant$99% and 60% of COD were removed by UV and solar photo-Fenton respectively. Ethylene glycol and formic acid were identified as primary intermediates for the 1,4-dioxane decomposition in heterogeneous photo-Fenton. The opportunity to avoid sludge production and pH adjustments makes the Fe^0 microspheres an efficient catalyst for the treatment of relatively alkaline wastewaters containing 1,4-dioxane. The solar driven process could be an important economical alternative to the UV catalysed process. When considering the consumption of energy and chemicals, if partial COD reduction for biodegradability enhancement was the purpose, both heterogeneous photo-Fenton processes appear to be more energy and cost-efficient than ozonation and electro-oxidation treatments.

* Corresponding author. Tel.: +34 91 394 4645; fax: +34 91 394 4243.
E-mail address: dhermosilla@quim.ucm.es (D. Hermosilla).

http://dx.doi.org/10.1016/j.cej.2015.08.097
1385-8947/

1. Introduction

1,4-Dioxane is a synthetic cyclic ether traditionally used as a solvent stabilizer, detected frequently at sites where chlorinated solvents are used in degreasing applications [1,2]. It is also used as an agent or solvent in the manufacture of several products, such as paints, dyes, waxes and resins; and as a reaction media in chemical synthesis [2,3]. 1,4-Dioxane is a hazardous chemical for humans and for the environment, classified as a possible human carcinogen (B2) [4,5]. 1,4-Dioxane has even been found in consumer products; however, it occurs more commonly in wastewater and landfill leachates [2].

1,4-Dioxane is fully miscible and, thus, extremely mobile and persistent in water; therefore, its removal from industrial effluents is of great importance to avoid the contamination of natural water bodies. However, conventional wastewater treatment plants tend to fail in degrading 1,4-dioxane due to its resistance to biodegradation at ambient conditions [2,6] and it cannot be efficiently treated by conventional technologies used for solvents, such as carbon adsorption, air stripping and distillation either due to its high aqueous solubility (4.31×10^5 mg/L), low vapor pressure (37 mmHg at 25 °C) and its boiling point similar to water (101 °C) [1,2]. As a consequence, a suitable technology for its treatment is demanded.

Advanced oxidation processes (AOPs) are an efficient alternative for the degradation of refractory organics, owing to its highly reactive and non-selective primary oxidant, hydroxyl radical (·OH) [7]. Removal of 1,4-dioxane has been already achieved using electro-oxidation [8], ozone based treatments [9,10], photocatalysis [11,12], ultrasonic decomposition in the presence of ferrous iron (Fe^{2+}) [13], and the combination of hydrogen peroxide (H_2O_2) and UV light [14,15]). High removals of chemical oxygen demand (COD) [3,16] and biodegradability enhancement [17] were also reported treating this compound by methods based on Fenton reaction.

Among AOPs, Fenton process has been reported as one of the fastest and most economical ones, using safe and environmentally benign reagents, Fe^{2+} and H_2O_2, to produce ·OH [18,19]. However, the production of ferric iron (Fe^{3+}) sludge and the corrosive acid pH required for the process are still important drawbacks that restrict its full scale implementation [20,21]. As an economical alternative, using solid metallic iron as a precursor of Fe^{2+} has been reported to produce less sludge, as Fe^{3+} is recycled in a so-called pseudo-catalytic zero-valent iron (Fe^0)/Fe^{2+} system [22,23]. Moreover, using Fe^0 particles in suspension would enhance the system reactivity; however, as the treatments using iron powder are usually performed in acidic conditions, like in classical Fenton reaction, the intensive iron corrosion would still result in important dissolved iron salts concentrations that would require subsequent removal [21,24]. A promising alternative was reported by Bergendahl and Thies [24], obtaining satisfactory results using heterogeneous Fe^0 under neutral pH conditions, enabling to avoid the consequent neutralization and precipitation step.

In addition, the overall efficiency of Fenton oxidation can be significantly improved by the assistance of radiation, owing to the photo-recovered catalytic Fe^{2+} and the photo-decarboxylation of the refractory ferric carboxylate complexes [23,25]. Moreover, sunlight is an economical alternative for the expensive UV radiation, and, thus, more and more research is focusing on solar photoreactors [26,27]. However, there are only few reports on the 1,4-dioxane treatment by photo-Fenton processes [17,28], and none of them considers the application of Fe^0 nor solar radiation.

Fe^0 is an advantageous material for photo-Fenton treatments, exhibiting high UV activation and excellent catalytic performances, while it is fit for environmental applications, as it allows working with a greatly lesser production of residues [22–24]. In the present investigation, we propose that Fe^0 microspheres could be used in 100% heterogeneous form at neutral pH for the treatment of refractory organics in photo-Fenton process, whereby the produced Fe^{2+} remains anchored on iron surface without any production of Fe^{2+} leaching.

Therefore, the main objective of this work was to assess the degradation of 1,4-dioxane, using Fe^0 microspheres as catalyst of photo-Fenton processes assisted both by solar and UV radiation. The effect of pH and carbonaceous alkalinity were studied and the reagent dose was optimized. The biodegradability enhancement was assessed and the 1,4-dioxane decomposition products were identified. Finally, UV and solar-driven treatments of an alkaline industrial wastewater contaminated with 1,4-dioxane were carried out and the results were compared to other AOPs in terms of process performance and operation cost.

2. Materials and methods

2.1. Materials

Industrial wastewater contaminated with 1,4-dioxane came from a chemical industry (COD = 450 mg/L; pH_0 = 8.6; alkalinity = 900 mg$CaCO_3$/L; conductivity = 810 μS/cm; [Cl^-] = 50 mg/L). Synthetic 1,4-dioxane solutions were prepared with Milli Q grade water. 248 mg/L of 1,4-dioxane (COD = 450 mg/L) was used to simulate the industrial wastewater, while a solution of higher concentration (7300 mg/L of 1,4-dioxane) was used for the chromatographic study of decomposition products. Analytical grade chemicals were supplied by MERCK KGaA (Darmstad, Germany) and PANREAC S.A. (Barcelona, Spain). For pH adjustments, $NaHCO_3$, NaOH and H_2SO_4 were used.

Fe^0 microspheres (>98.3% Fe; <1% C; <1% N; <0.7% O) with 1 μm of particle size and 800 m^2/kg of surface area were obtained from BASF (ZVI Microspheres 800, Ludwigshafen, Germany). The structure of Fe^0 microspheres was analysed by scanning electron microscopy (SEM) – energy dispersive X-ray (EDX) spectroscopy. The analysis of the images was carried out by SEM (JEOL JSM-6400) coupled with an EDX analyser (EDS system).

2.2. Photocatalytic equipment

UV photo-Fenton experiments were performed at room temperature, using a high-pressure mercury immersion lamp of 450 W from ACE-glass (Model 7825-30, Vineland, USA) placed in a quartz glass cooling jacket and located in a vertical manner in the centre of a 2 L-vessel reactor with magnetic stirring. The light intensity on the irradiated liquid surface, recorded with UV–VIS Radiometer RM-21 (UV-Elektronik, Ettlingen, Germany), was 186 mW/cm^2 at the mid-height of the UV-lamp and 1.5 cm from the light source).

Solar photo-Fenton experiments were carried out in a 0.1 L stirring reactor placed in a Solar Simulator supplied by Newport (Irvine, USA) fitted with a Xe lamp of 1000 W/m^2, a correction filter (ASTM E490–73a) to obtain the solar spectrum under ideal conditions, and a dark screen covering the device to prevent the escape of radiation. The light intensity on the irradiated liquid surface was 98.9 mW/cm^2 at the mid-surface of the Xe lamp (1 cm from the light source).

2.3. Experimental procedure

In UV photo-Fenton, the influence of H_2O_2 dose was studied at following ratios to the initial COD: 4, 2.625, 2.125 and 1.625 (H_2O_2/COD_0 = 2.125 was selected based on the stoichiometrical relation

with the COD [29]). H_2O_2/Fe^0 ratio of 60 was selected as the optimal found in a preliminary study. Different pH conditions were investigated: acid $pH_0 = 2.8$ as the optimum value found for the treatment of aromatics by Fenton and photo-Fenton processes [25]; neutral conditions ($pH_0 = 7.0$) to assess the efficiency at higher pH; and slightly basic conditions ($pH_0 = 8.2$) in the presence of 1000 mg/L of $NaHCO_3$ to evaluate the effect of carbonates usually present in industrial wastewater.

In solar photo-Fenton treatments, 1000 mg/L of $NaHCO_3$ buffer was added to the synthetic wastewater in order to assure the heterogeneous photo-Fenton process in all the solutions. Different H_2O_2/Fe^0 ratios (60, 30, 15 and 1) were assessed while maintaining the ratio $H_2O_2/COD_0 = 2.125$.

In both processes, the main parameters measured were the concentrations of 1,4-dioxane, COD, H_2O_2 and total organic carbon (TOC). In the UV enhanced process, Fe^{2+} leaching and biodegradability enhancement were studied as well. H_2O_2, Fe^{2+} and total soluble iron were measured immediately after sample withdrawal and after filtration through 0.45 μm, whereas the concentrations of COD, TOC and 1,4-dioxane were analysed in samples filtrated through 0.45 μm after quenching the reaction by increasing the pH above 9. All experiments were carried out in triplicates.

The additional experiments to study the decomposition products of 1,4-dioxane by both photo-Fenton processes were carried out in the presence of 2000 mg/L of $NaHCO_3$. In addition to 1,4-dioxane, ethylene glycol diformate (EGDF), ethylene glycol and various carboxylic acids were analysed.

2.4. Analytical methods

H_2O_2 concentration was measured using the titanium sulphate spectrophotometric method [30]. Fe^{2+} concentration was measured with the 1,10-phenanthroline colorimetric method [31], using ammonium fluoride as masking agent for Fe^{3+} to avoid its potential interference. Total soluble iron concentration was measured under acidic conditions reducing Fe^{3+} to Fe^{2+} iron adding hydroxylamine. COD was analysed by the standardized colorimetric method at 600 nm using an Aquamate-spectrophotometer (Thermo Scientific AQA 091801, Waltham, USA), and the values were corrected with the residual concentration of H_2O_2 measured according to Hermosilla et al. [25]. TOC was measured using a TOC/TN analyser Multi N/C® 3100 (Analytik Jena AG, Jena, Germany) with catalytic oxidation on cerium oxide at 850 °C. Biodegradability test using *Pseudomonas putida* CECT 324 (Spanish Type Culture Collection, Valencia, Spain) is described in detail elsewhere [8].

1,4-Dioxane and its metabolite EGDF were identified and quantified by an Agilent 6890 N gas chromatograph (GC) equipped with a quadrupole mass spectrometer (MS) Agilent 5975B (Agilent Technologies Inc., Palo Alto, CA). To extract these two volatile compounds from the water samples, an internal standard (5 mg/L of octanol) and 1,4 g of ammonium sulphate were added to 10 mL of sample, and the solution was extracted threefold with dichloromethane (40:10:10 mL). The organic fraction was dried on anhydrous sodium sulphate and concentrated to 1 mL under nitrogen flux in a Kuderna-Danish apparatus (Sigma, St. Louis, MO) and analysed by GC–MS as follows. Samples (3 μl) were injected in split mode (30:1), and volatiles were separated using a fused silica capillary column (HP-INNOWAX) (30 × 0.25 mm i.d. and 0.25-μm film thickness), supplied by Agilent (Madrid, Spain). The pressure of the GC-grade He carrier gas was 7.7 psi with a linear velocity of 1.0 mL/min; the initial oven temperature was 45 °C, first increased at 3 °C/min to 100 °C, held for 1 min, and then heated at 15 °C/min to 270 °C, and held at this temperature for an additional 5 min. The injection temperature was 230 °C. Detection was carried out by EI mode (70 eV), interphase detection temperature was 290 °C (MS source at 230 °C and MS quad at 150 °C) and scanning mass was ranged between 35 and 400 amu. Quantitative determinations were carried out by the internal standard method, using peak areas obtained from selected ion (z/m) monitoring (88, 1,4-dioxane; 60, EGDF; 45, octanol) and calibrations made with pure reference compounds analysed under the same conditions.

The analyses of 1,4-dioxane along with ethylene glycol were also done by gas–liquid chromatograph Agilent 7980A (Agilent Technologies Inc., Palo Alto, CA) equipped with a flame ionization detector. Injector and detector were respectively set up at 310 and 280 °C. Samples (2 μL) were injected using the pulsed-split mode (split ratio 5:1) and analysed in a TRB-FFAP (Teknokroma, Sant Cugat del Vallès, Spain) fused silica column (30 m × 0.25 mm internal diameter × 0.25 μm film thickness), with He (43 psi) as carrier gas, using a temperature programme from 80 °C to 240 °C (9 min initial hold, 15 °C/min ramp rate). Peaks were identified on the basis of sample coincidence with relative retention times of commercial standards. Quantification was performed according to peak area, corrected with the response factors calculated for each compound using 1-butanol (250 ppm) as the internal standard and the software GC-ChemStation Rev.B.04.02 (96) from Agilent.

Oxalic, acetic, formic, glycolic and methoxyacetic acids were identified and quantified by ion chromatography (IC) using a 940 Professional IC Vario instrument (Metrohm, Herisau, Switzerland) equipped with a conductivity detector. An isocratic gradient of Na_2CO_3 (3.6 mM) was used as eluent, keeping an eluent flow at 0.7 mL/min. The injection loop was 50 mL. Analysis was done in an ionic resin column Metrosep A Supp 7 with a guard column Metrosep A Supp 4/5 Guard.

3. Results and discussion

3.1. Fe^0-based photo-Fenton treatments: process optimization

3.1.1. Influence of pH in UV photo-Fenton process

Using Fe^0 microspheres under different pH conditions, complete degradation of 1,4-dioxane was achieved in the first 5 min of UV photo-Fenton treatment in all the experiments, working at the highest H_2O_2/COD ratio to ensure relevant degradation. The degradation of COD and TOC was slightly faster under acidic conditions (Fig. 1A and Table 1, respectively), as the Fenton oxidation is known to be enhanced at acidic pH [20]. Namely, the rate of mineralization (k_{TOC}) in different pH conditions was in the following decreasing order: $pH_0 = 2.8 > pH_0 = 8.2$ (in the presence of $NaHCO_3$) > $pH_0 = 7.0$ (in the presence of NaOH; Table 1). However, the differences were rather small: the overall TOC removals were in the range of 92–94%. Moreover, working both with an initial neutral pH and in the presence of bicarbonate alkalinity, an almost complete COD removal (98–99%) was obtained after 30 min of UV photo-Fenton as well as under acidic conditions (Fig. 1A). In fact, H_2O_2 was also consumed in a similar manner, disappearing after 30 min of oxidation reaction at all the pH conditions (Fig. 1B).

In spite of the similar performances, different tendencies of iron corrosion were observed due to the different pH patterns (Fig. 1B). Since iron salts are soluble at acidic pH conditions, relevant iron leaching ($[Fe^{2+}] = 3$ mg/L) was detected in the solution when using $pH_0 = 2.8$. For environmental applications, the concentration of Fe^{2+} in the final effluent should be reduced by posterior precipitation, which newly leads to the classical problem of Fenton operations: the production of iron sludge. On the other hand, only minor Fe^{2+} concentrations (<0.25 mg/L) were detected at the end of the experiment, working at $pH_0 = 7$; and no Fe^{2+} was found in the effluents treated in the presence of $NaHCO_3$. The milder corrosion at $pH_0 = 7$ was produced because the initial neutral pH first decreased

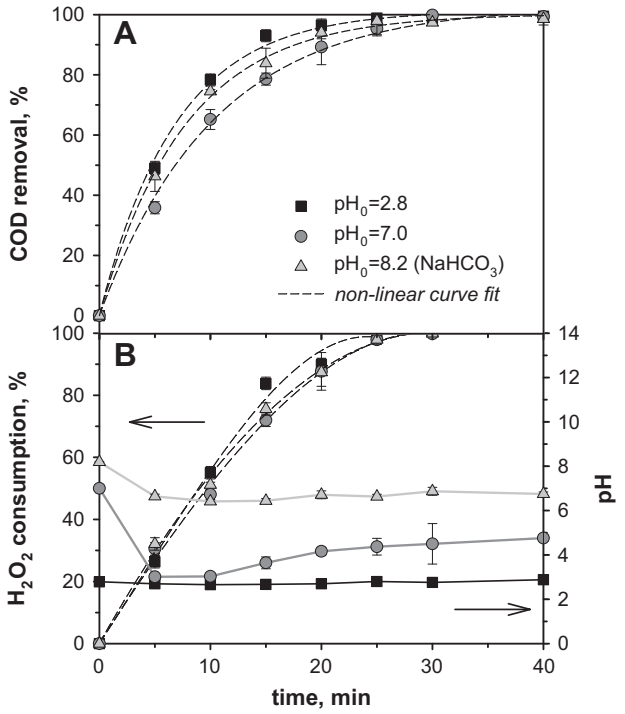

Fig. 1. COD removal (A) and H_2O_2 consumption along with the pH pattern (B) during the treatment of synthetic 1,4-dioxane solution by UV photo-Fenton process using Fe^0 at different pH. COD_0 = 450 mg/L; H_2O_2/COD = 4; H_2O_2/Fe^0 = 60.

Table 1
Pseudo-first order rate constants for TOC removal during the treatment of 1,4-dioxane solution by UV photo-Fenton processes using Fe^0 microspheres.

H_2O_2/COD	pH_0 = 2.8		pH_0 = 7		pH_0 = 8.2 $NaHCO_3$	
	$k \times 10^2$ (min^{-1})	R^2	$k \times 10^2$ (min^{-1})	R^2	$k \times 10^2$ (min^{-1})	R^2
4	8.5	0.916	7.11	0.956	7.18	0.960
2.625	–	–	8.56	0.973	8.58	0.980
2.125	–	–	7.81	0.947	7.81	0.975
1.625	–	–	6.55	0.877	6.98	0.968

to 3 (Fig. 1B) due to the formation of short chain organic acids [22], such as acetic, oxalic, glycolic, glyoxylic, methoxiacetic and formic acids [9,12,14,16]. In the course of experiment, pH increased again to a final value of 4.8, indicating a subsequent mineralization of these carboxylic acids. In the presence of $NaHCO_3$, however, the pH_0 = 8.2 only decreased about 1.5 units, remaining slightly below 7 till the end of the experiment (Fig. 1B), as the bicarbonate buffer overcame the effect of the acidic by-products, and, thus, no leaching was detected.

In a view of the similar degradation efficiencies (Fig. 1A, Table 1) and the comparable H_2O_2 consumption (Fig. 1A), it was concluded that the iron corrosion and Fe^{2+} solubilisation are not essential for the Fenton reaction on Fe^0 microspheres. In fact, it has led us to a conclusion that in heterogeneous conditions the Fe^{2+} created from metallic iron, either by reacting with H_2O_2 (Eq. (1)) or induced by UV radiation (Eq. (2)) [20,21,23,24], initially remains anchored on the surface of Fe^0 microspheres while taking part of the classical Fenton reaction without passing to the solution, whereas the produced Fe^{3+} is recycled in a so-called pseudo-catalytic Fe^0/Fe^{2+} system (Eq. (3)) [22], while the UV radiation additionally contributes to the reproduction of Fe^{2+} [21,23].

$$Fe^0 + H_2O_2 \rightarrow Fe^{2+} + 2OH^- \quad (1)$$

$$Fe^0 + h\nu \rightarrow Fe^{2+} + 2e^- \quad (2)$$

$$2Fe^{3+} + Fe^0 \rightarrow 3Fe^{2+} \quad (3)$$

In order to have a clearer insight of the fate and stability of Fe^0 microspheres in different pH conditions, SEM-EDX study was carried out on Fe^0 samples already used for photo-Fenton experiments (Fig. 2). It was observed that the morphology of microspheres remained intact after photo-Fenton treatment in neutral conditions, whereas the spherical structure of Fe^0 was terminally lost after photo-Fenton process under acidic conditions, indicating the modification and solubilisation of the material. Considering this, steady neutral pH is essential to avoid iron leaching, and, in principle, the Fe^0 microspheres should be totally recoverable, maintaining an unmodified morphology when used in heterogeneous conditions.

Moreover, the initial biodegradability of the original wastewater (10–15%) was considerably increased in the photo-Fenton process at all studied pH values as well (Fig. 3). This indicates that the reaction intermediates of 1,4-dioxane degradation are more biodegradable than the mother compound. Namely, 63% biodegradability by *P. putida* was obtained after 10 min of photo-Fenton at pH_0 = 7.0 (in the presence of NaOH), whereas 53% biodegradability was reached after 10 min of treatment at pH_0 = 2.8, and 48% biodegradability was achieved in the presence of $NaHCO_3$. Biodegradabilities of 63 and 53% were reached after 20 min photo-Fenton treatment with an initial neutral pH and in the presence of bicarbonate alkalinity, respectively. As a result, the combination of photo Fenton processes and biological treatment appears as a promising technology for the treatment of effluents containing 1,4-dioxane. UV-treatments using Fe^0 microspheres and H_2O_2 may produce a suitable effluent for being treated by biological processes or as final treatment, avoiding sludge production and pH adjustments.

3.1.2. Influence of H_2O_2 dosage in UV photo-Fenton process

Taking into account the results presented above, the influence of H_2O_2 dosage was assessed both at initial pH_0 = 7.0 and in the presence of bicarbonates. In terms of COD removal, all H_2O_2/COD ratios but 1.625 were able to degrade the organic matter almost completely in both cases (Fig. 4), whereas the fastest degradation of organic matter was reached at H_2O_2/COD = 2.625. The first order kinetic constants for TOC removal at different H_2O_2/COD_0 ratios

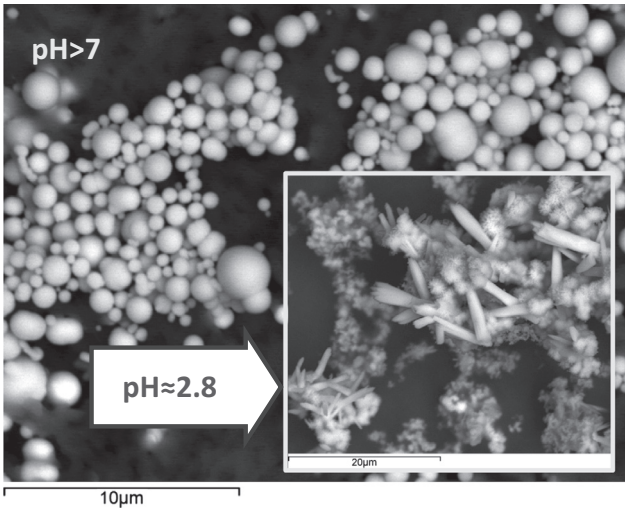

Fig. 2. SEM-EDX images of the unmodified Fe^0 microspheres after UV photo-Fenton treatment at neutral pH and the loss of spherical structure through iron leaching UV photo-Fenton process under acidic conditions.

were in a following decreasing order: 2.625 > 2.125 > 4 > 1.625 (Table 1). This mostly likely occurs because the small excess of reagent (H_2O_2/COD_0 = 2.625) promotes the Fenton-type reaction on Fe^0 as well as the direct production of ·OH from H_2O_2 and the UV radiation.

However, when further increasing the ratio H_2O_2/COD_0 to 4, the production of ·OH was scavenged by the high amount of reagent itself [25], causing slower degradation in the beginning of the reaction. Similarly, when using lower H_2O_2/COD_0 ratio (1.625), the scarcity of H_2O_2 also decreased the desirable Fenton reactions. In addition, since almost all H_2O_2 was consumed in first 20 min, some of the ·OH in the solution could be scavenged by the accumulating Fe^{2+} [25].

In terms of both COD removal (Fig. 4) and TOC reduction (Table 1), somewhat higher removal efficiencies were achieved in the presence of carbonates when compared to the experiments at initial neutral pH (adjusted by NaOH). One of the explanations is that the presence of NaOH molecules implies the adsorption of OH^- on the Fe^0 surface, reducing the available catalytic sites and hindering the oxidation–reduction reactions occurring on the microsphere surface (Merayo et al., unpublished research). Furthermore, according to Litter and Quici [32], the UV/H_2O_2 based photochemical processes are often more efficient in alkaline conditions, as the conjugate base of H_2O_2 (HO^{2-}) shows higher absorptivity (ε_{254} = 240 M^{-1} cm^{-1}), which favors light adsorption and increases ·OH production.

Regarding iron leaching (Fig. 5), some Fe^{2+} was detected in all waters treated at pH_0 = 7, whereas the iron corrosion was greater and occurred earlier when the amount of H_2O_2 was reduced (Fig. 5A). Namely, less than 1 mg/L of Fe^{2+} was found at the end of the experiment when working with H_2O_2/COD_0 = 2.625, while more than 4 mg/L was measured after 25 min when using the ratio of H_2O_2/COD_0 = 1.625. However, when working in the presence of carbonates, [Fe^{2+}] < 1 mg/L was only measured using the lowest H_2O_2/COD_0 ratio (Fig. 5B). The reason for this phenomenon is most likely the different pH pattern (Fig. 1B). As suggested before, in the presence of H_2O_2, Fe^{2+} remains anchored on the iron surface, taking part of the Fenton reaction directly on the Fe^0 microsphere. However, after the depletion of H_2O_2 at longer treatment times, the Fe^{2+} is still continuously generated on the microsphere surface by UV radiation, but not used for the Fenton process anymore. Apparently, depending on the pH conditions, it could start to transfer into the dissolved state as organic matter is not being oxidized

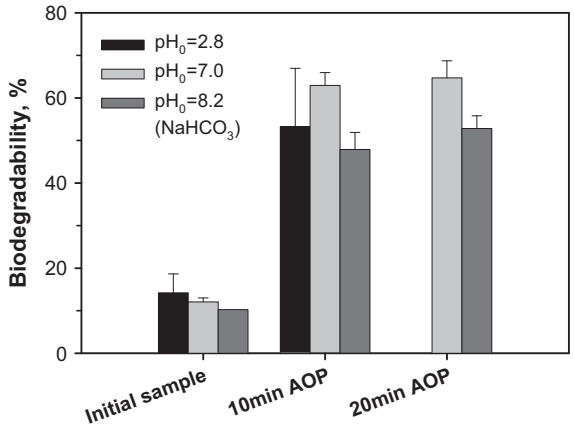

Fig. 3. Evolution of biodegradability by *Pseudomonas putida* after different reaction times of UV photo-Fenton treatment using Fe^0 on synthetic 1,4-dioxane solutions with different pH.

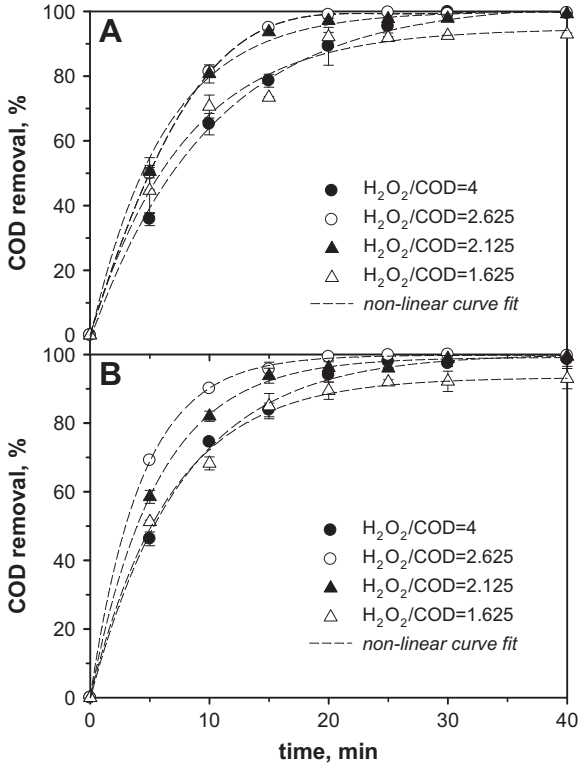

Fig. 4. COD removal during the treatment of synthetic 1,4-dioxane solution by UV photo-Fenton using Fe^0 at different H_2O_2/COD ratios (A) under initial neutral pH conditions, (B) in the presence of 1 g/L of $NaHCO_3$ (pH_0 = 8.2). COD_0 = 450 mg/L; H_2O_2/Fe^0 = 60.

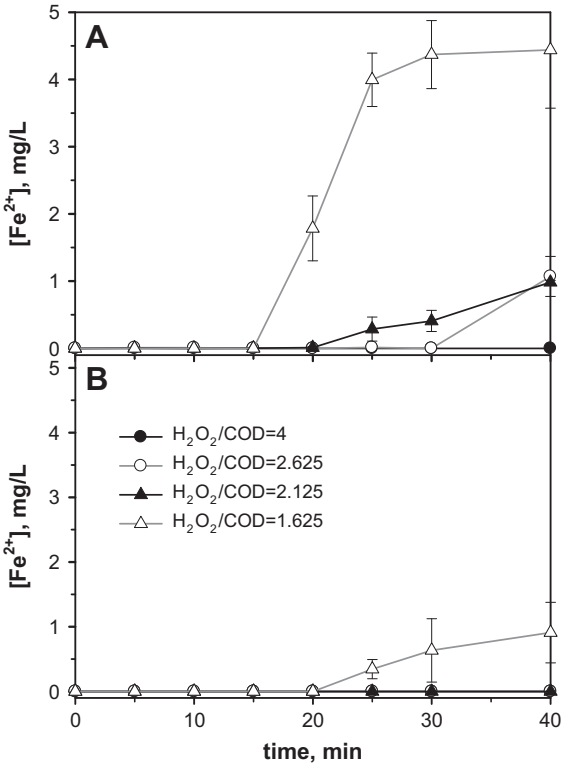

Fig. 5. Fe^{2+} leaching during the treatment of synthetic 1,4-dioxane solution by UV photo-Fenton using Fe^0 at different H_2O_2/COD ratios (A) under initial neutral pH conditions, (B) in the presence of 1 g/L of $NaHCO_3$ (pH_0 = 8.2). COD_0 = 450 mg/L; H_2O_2/Fe^0 = 60.

anymore. Thus, when working with Fe^0 microspheres, the presence of carbonaceous alkalinity can actually be desired, since it maintains the pH above 6.5 (Fig. 1B) at which the Fe^{2+} is not expected to be in soluble state [33]. Furthermore, although the pH drops and stabilizes around 4–5 when working with pH_0 = 7 without buffer, the iron leaching could still be avoided by terminating the reaction after the complete depletion of H_2O_2 and not permitting further corrosion of Fe^0 under UV radiation.

3.1.3. Solar photo-Fenton process with heterogeneous Fe^0 at different H_2O_2/Fe^0 ratios

When compared to the UV photo-Fenton process (Figs. 1 and 4, Table 1), both the H_2O_2 consumption and the degradation of organic matter were slower under solar radiation (Fig. 6, Table 2). This is mainly due to the higher ·OH production in UV photo Fenton as higher radiation was applied with the UV lamp. Furthermore, the counterproductive oxidation of Fe^{2+} to Fe^{3+} (Eq. (4)) has been reported to be faster under UV-A radiation than with UV-C radiation [21]. This could also explain why the degradation was slower under solar light because when using the UV lamp the UV-C range was measured to be greater than the UV-A (35% and 24% of the total emission, respectively), whereas with the solar simulator the emissions were different (39% and 30% for UV-A and UV-C, respectively).

$$Fe^{2+} + h\nu \rightarrow Fe^{3+} + e^- \quad (4)$$

Regardless of the slower oxidation, 1,4-dioxane removal percentages in the range of 85–91% were achieved after 3 h of solar photo-Fenton process using heterogeneous Fe^0 in the presence of bicarbonate alkalinity (Fig. 6A). Meanwhile, up to 45% of COD (Fig. 6B) and more than 20% of TOC were removed as well. Using

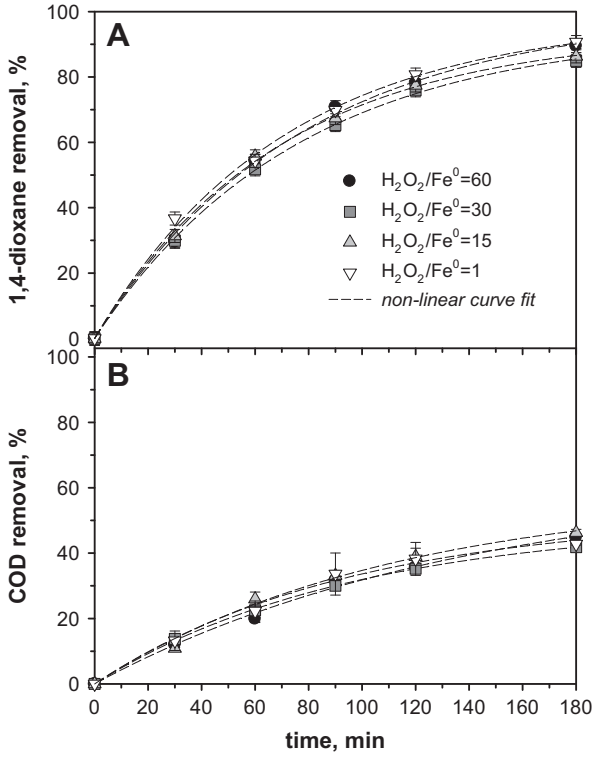

Fig. 6. Removals of COD (A) and 1,4-dioxane (B) when treating synthetic 1,4-dioxane solution by heterogeneous solar photo-Fenton in the presence of 1 g/L of $NaHCO_3$ (pH_0 = 8.2), using Fe^0 at different H_2O_2/Fe^0 ratios. COD = 450 mg/L; H_2O_2/COD = 2.125.

Table 2
Pseudo-first order rate constants for TOC removal during the treatment of 1,4-dioxane solution by heterogeneous solar photo-Fenton processes using Fe^0 microspheres in the presence of 1 g/L of $NaHCO_3$.

H_2O_2/Fe^0	$k \times 10^3$ (min^{-1})	R^2
60	1.46	0.960
30	1.50	0.978
15	1.51	0.953
1	1.62	0.935

the lowest H_2O_2/Fe^0 ratio (highest Fe^0 concentration), 1,4-dioxane removal could be increased to 96% after 4 h; thus, complete removal is expected at longer treatment times.

Although the first order kinetic constants for TOC removal at different H_2O_2/Fe^0 ratios presented a merely noticeable increase along with the concentration of Fe^0 (Table 2), no significant differences were found between different H_2O_2/Fe^0 ratios (Fig. 6). In all cases, pH was buffered at about 8 and no Fe^{2+} was detected in the medium. With all H_2O_2/Fe^0 ratios, the consumption of H_2O_2 was linear in time (R^2 = 96–98%), and after the 3 h-treatment, about 70% was used up. Therefore, the smallest amount of Fe^0 (H_2O_2/Fe^0 = 60) could be selected as the optimum for these processes.

3.2. Reaction intermediates of 1,4-dioxane decomposition in heterogeneous photo-Fenton

To confirm the mechanism of 1,4-dioxane decomposition by heterogeneous photo-Fenton, chromatographic study was carried out with a highly concentrated synthetic solution. Since 1,4-dioxane was degraded faster under UV radiation than in the solar simulator, the appearance of the primary intermediates was also faster and more pronounced with UV light. Nevertheless, mostly similar by-products appeared in the course of both AOPs (Figs. 7 and 8). Namely, ethylene glycol and formic acid were identified as the major reaction intermediates UV-catalysed (Fig. 7A) and solar photo-Fenton process (Fig. 8A). In lesser extent, various other consequent intermediates appeared in UV photo-Fenton process, such as methoxyacetic, glycolic, acetic and oxalic acids (Fig. 7B), while only methoxyacetic and glycolic acids were identified as a mixture in the end of the solar-driven experiment (Fig. 8B). In addition, it is important to note that traces of EGDF ($\leqslant$2.4 mg/L) were detected along both processes from the first minute of the experiment.

According to the literature [14,16], the initial attack of 1,4-dioxane molecule by ·OH occurs through an oxidative ring opening mechanism over 1,4-dioxan-α-oxyl radical (Fig. 9). Due to the presence of EGDF traces, it is suspected that it was produced as one of the first reaction intermediates in the degradation of this α-oxyl radical through ΔC-C splitting at the α-C position, in agreement with Stefan and Bolton [14]. However, as only low concentrations were measured, it is proposed that, due to the basic pH conditions maintained to assure the heterogeneous process, EGDF was rapidly hydrolysed to ethylene glycol, as reported for other AOPs [9,12].

As presented schematically in Fig. 9, the further decomposition of ethylene glycol leaded to the concurrent production of formic and glycolic acids [12,16]. In the more aggressive UV catalysed process (Fig. 7B), formic acid was finally oxidised directly to CO_2 and water [14,34], while oxalic acid was generated in the degradation of glycolic acid, leading eventually to a total mineralization as well [9,14,16]. The solar-driven experiment, however, was not that advanced, as the concentration profile of formic acid did not start to descend and the concentration of oxalic acid remained below the detection limit (Fig. 8B).

In addition, a secondary route of 1,4-dioxane degradation appeared (Fig. 9) through the formation of methoxyacetic acid

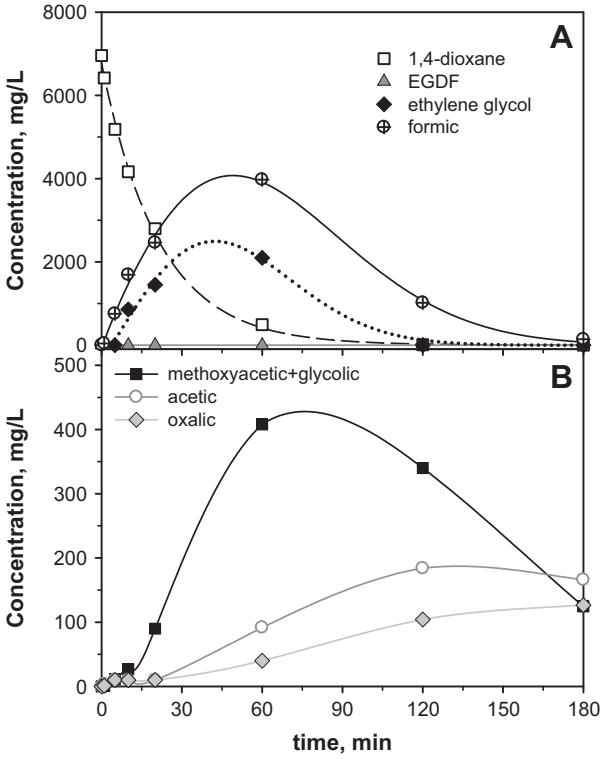

Fig. 7. 1,4-Dioxane (C_0 = 7.3 g/L) and its metabolites concentration during heterogeneous UV photo-Fenton process in the presence of 2 g/L of $NaHCO_3$ (pH_0 = 8.5): (A) evolution of 1,4-dioxane, ethylene glycol, EGDF and formic acid; (B) evolution of methoxyacetic + glycolic, acetic and oxalic acids.

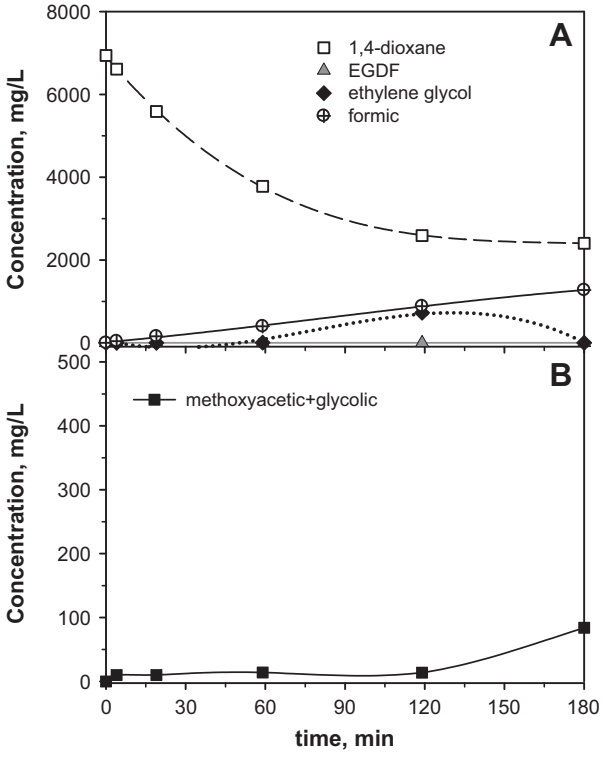

Fig. 8. 1,4-Dioxane (C_0 = 7.3 g/L) and its metabolites concentration during heterogeneous solar photo-Fenton process in the presence of 2 g/L of $NaHCO_3$ (pH_0 = 8.5): (A) evolution of 1,4-dioxane, ethylene glycol, EGDF and formic acid; (B) evolution of methoxyacetic + glycolic acids.

directly from the α-oxyl radical, as proposed by Stefan and Bolton, and Merayo et al. [14,16]. In UV-catalysed photo-Fenton (Fig. 7B), methoxyacetic acid was subsequently degraded into acetic acid [14,16], which could, in turn, be degraded into both formic and glycolic acids, whereas possible mineralization has been reported as well [14,34]. Again, the solar photo-Fenton treatment was not that advanced and, therefore, no acetic acid was detected (Fig. 8B).

3.3. Treatment of industrial wastewater

Industrial wastewater containing 1,4-dioxane was treated by both UV and solar photo-Fenton processes, taking advantage of its own relatively high alkalinity (≈900 mg $CaCO_3$/L) to maintain the Fe^0 microspheres in heterogeneous conditions (pH ≈ 8). About 98% of COD and around 90% of TOC were removed from the effluent by UV photo-Fenton oxidation (Fig. 10A), whereas solar photo-Fenton process was able to reach approximately 60% and 35% of COD and TOC removals (Fig. 10B).

As the expensive and laborious chromatography analysis is not always viable in industrial ambient, to have a better understanding of the state of oxidation and the possible intermediates of the reaction, the mean oxidation state of carbon (MOSC) of the solution for both processes (Figs. 10A and B) was calculated by Eq. (5) [25,35] where COD and TOC are given in mgO_2/L.

$$\mathrm{MOSC} = 4 - 1.5\frac{\mathrm{COD}}{\mathrm{TOC}} \quad (5)$$

Solution MOSC is a proportional average of the molecular MOSC values [35] corresponding to all the compounds present in water. MOSC can vary from −4 to +4, and the increase of this parameter throughout the process shows the oxidation of 1,4-dioxane into smaller and simpler organic products. For example, in the UV photo-Fenton (Fig. 10A), 1,4-dioxane ($MOSC_{1,4\text{-dioxane}} = -1$) was degraded quickly in the beginning of the experiment, while the final metabolites remaining in the solution were most likely simple carboxylic acids, such as formic ($MOSC_{formic} = +2$), glycolic ($MOSC_{glycolic} = +1$) and oxalic acids ($MOSC_{oxalic} = +3$) [9,14,16]. On the other hand, under solar radiation the average MOSC only increased to about +0.8 (Fig. 10B). Thus, the 1,4-dioxane degradation was not that advanced and considerable quantities of primary and intermediate oxidation products, like ethylene glycol ($MOSC_{ethylene\ glycol} = -1$) [9,16] and/or EGDF ($MOSC_{EGDF} = +1$) [14], were still present at the end of the experiment. Regardless of the slower degradation kinetics, sunlight driven photo-Fenton is still an important economical alternative to the UV catalysed process if biodegradability enhancement by the removal of 1,4-dioxane is the aim of the treatment.

Since significant results of 1,4-dioxane and COD removal from industrial wastewaters were achieved previously by anodic oxidation on boron doped diamond (BDD) electrodes [8] and ozone (O_3) oxidation in controlled basic conditions at pH > 9 [9], a brief comparative study was made with the results of heterogeneous photo-Fenton treatment. UV photo-Fenton exhibited a significantly faster treatment performance in terms of COD removal in time than the other studied AOPs (98% in 40 min; Fig. 11). Anodic oxidation on BDD and solar photo-Fenton appeared to be rather comparable in shorter treatment times (36–38% in 60 min), followed by ozonation (27%). However, it seems that O_3 oxidation as well as electro-oxidation presented more continuous degradation capacity at longer treatment times (69% and 84% in 180 min) than the solar photo-Fenton treatment that slacked off in time (60% in 180 min).

Nevertheless, for an accurate comparison of these different treatment systems, the consumption of energy and chemicals should be taken in account. Table 3 presents the energetic consumption (kWh/m^3) and the sum cost of the energy and chemicals (€/m^3) required for these four AOPs. The energy consumption in

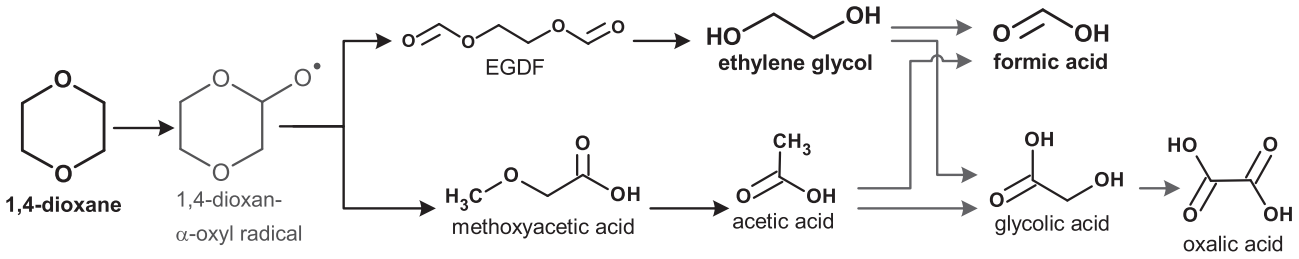

Fig. 9. Simplified schematic of 1,4-dioxane decomposition routes in heterogeneous photo-Fenton treatment.

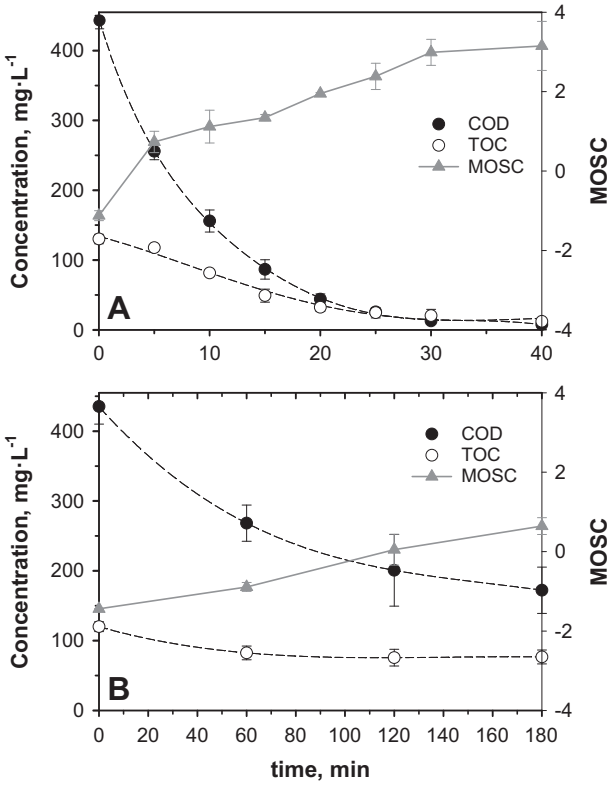

Fig. 10. Decrease of COD and TOC along with the evolution of MOSC during the (A) UV-catalysed and (B) solar photo-Fenton treatments of an industrial wastewater contaminated with 1,4-dioxane (COD = 450 mg/L; pH_0 = 8.6; alkalinity = 900 mg$CaCO_3$/L). H_2O_2/COD = 2.125; H_2O_2/Fe^0 = 60.

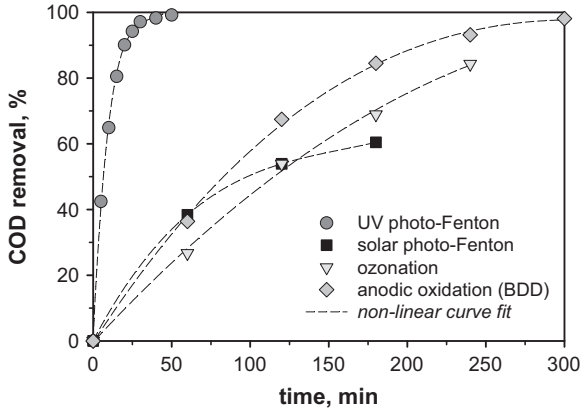

Fig. 11. COD removal in the course of different AOPs.

Table 3
Comparison of Fe^0-based photo-Fenton processes with ozonation and anodic oxidation on BDD in terms of energy consumption (kWh/m^3) and operation cost (€/m^3).

AOP	Energetic and economic parameters for varying COD removals (%)					
	kWh/m^3			€/m^3		
	25%	50%	75%	25%	50%	75%
UV photo-Fenton	6.0	20.4	68.9	1.9	5.6	16.7
Solar photo-Fenton	0.3	1.3	3.8	0.5	1.1	2.0
Ozonation	10.7	26.4	44.6	3.1	7.5	12.6
Anodic oxidation (BDD)	7.4	18.3	32.9	1.7	4.1	7.3

photo-Fenton and anodic oxidation was obtained from experimental data, whereas additional 25% was added for pumping, cooling and reagent injection operations. The total energy consumed by an industrial O_3 generator and the additional processes (including pumping, cooling, etc.) was considered to be 15 kWh/kgO_3 [36,37]. In solar photo-Fenton, the only electricity withdrawal was considered to come from pumping operation, as described by Muñoz [36]. The cost estimation was made, taking into account the prices of industrial electricity in Spain (0.22 €/kWh) [38], O_2 gas for O_3 production (85 €/t) [37], H_2O_2 of 50% (0.45 €/kg), NaOH (0.3 €/kg), Na_2SO_4 (0.09 €/kg) and industrial Fe^0 powder (5 €/kg) [39].

It is clear that the cost of energy and chemicals is the smallest in the solar photo-Fenton operation, since almost no electricity is needed. However, the process has its drawbacks in terms of space requirements and, thus, installation cost, which could complicate its industrial implementation. At lower COD removals (⩽50%), the UV photo-Fenton process is rather comparable to the anodic oxidation in terms of energy requirements, while the chemicals cost makes it slightly more expensive. Nevertheless, due to the high cost of BDD electrodes and the mass transport limitation of the anodic oxidation, the photo-Fenton unit could eventually become more viable option in industrial scale. On the other hand, to reach higher COD removals (such as 75%), both anodic oxidation and ozonation appear to be cheaper than the UV photo-Fenton process. Although the O_3 treatment is more expensive, the advantage of ozonation is its long-term know-how for large scale installations.

Therefore, the heterogeneous photo-Fenton processes appear to be more energy and cost-efficient if partial COD reduction for biodegradability enhancement was the purpose. Meanwhile, to reach high organics mineralization for final disposal, the energy or plant space required with the UV-enhanced and solar-catalysed processes, respectively, make them less feasible than the anodic oxidation and ozonation. Nevertheless, for a proper comparison of these processes, a full economic analysis should be carried out in a further study, taking into account the needed plant capacity, the installation cost, the space requirements, the maintenance and labour cost, etc.

4. Conclusions

$Fe^{0.}$ microspheres were proven an effective catalyst for photo-Fenton treatment of wastewaters with 1,4-dioxane contamination. The morphology of microspheres remained intact after treatment in neutral conditions, whereas the spherical structure of Fe^0 was terminally lost after oxidation at $pH_0 = 2.8$. Meanwhile, no significant differences were found in treatment performance at different process pH, indicating that iron solubilisation was not essential for organics degradation on Fe^0 and that photo-Fenton reaction could take place directly on the microsphere surface. Therefore, total recovery of the catalyst is expected when used in heterogeneous conditions, whereas the presence of carbonaceous alkalinity could actually result beneficial to avoid iron leaching.

According to the optimization experiments with synthetic water, the destruction of organics in UV photo-Fenton process with different H_2O_2/COD_0 ratios was in the following decreasing order: $2.625 > 2.125 > 4 > 1.625$. Complete removal of 1,4-dioxane was reached in 5 min, while an almost total removal of COD and up to 96% removal of TOC were reached in 30 min. The combination of photo-Fenton processes and biological treatment appears as a promising method, since significant biodegradability enhancement (up to 60%) was achieved by 10 min of UV photo-Fenton pre-treatment. Meanwhile, H_2O_2/Fe^0 ratio of 60 was found an optimum value for the sunlight driven photo-Fenton, which could be an important economical alternative to the UV catalysed process if biodegradability enhancement by the removal of 1,4-dioxane was the aim of the treatment. 1,4-Dioxane removals above 90% were achieved after 180 min of solar photo-Fenton.

In the treatment of industrial wastewater, the relatively high alkalinity of the effluent resulted to be an advantage, as heterogeneous conditions without any iron leaching were maintained throughout the experiment. About 98% of COD and around 90% of TOC were removed from the effluent by 40 min of UV photo-Fenton oxidation, whereby the destruction of organics was significantly faster than with anodic oxidation on BDD electrodes (84% of COD in 180 min) and ozonation in basic conditions (69% of COD in 180 min). The solar photo-Fenton appeared to be rather comparable to anodic oxidation in the beginning of experiment (36–38% of COD in 60 min), but slacked off at longer treatment times (60% in 180 min). When considering the consumption of energy and chemicals, both heterogeneous photo-Fenton processes appear to be more energy and cost-efficient if partial COD reduction for biodegradability enhancement was the purpose. The opportunity to avoid sludge production and corrosive conditions at acidic pH makes the Fe^0 microspheres a beneficial catalyst for the treatment of wastewaters containing 1,4-dioxane by photo-Fenton processes.

Acknowledgments

The research leading to these results has received funding from the European Union Seventh Framework Programme (FP7/2007-2013) under grant agreement n° 608490 (E4water). The collaboration of the Gas Chromatography Service (CIB) of the Spanish National Research Council (CSIC), the Laboratory of Geochemical and Environmental Analyses of the Complutense University of Madrid and the Laboratory of CIFOR-INIA (*Centro de Investigación Forestal, Instituto Nacional de Investigación y Tecnología Agraria y Alimentaria*) is fully appreciated. Archimedes Foundation (Estonia) is granting H. Barndõk's Ph.D. studies. The authors wish to thank BASF for microspheres supply.

References

[1] U.S. Environmental Protection Agency (USEPA), Treatment Technologies for 1,4-Dioxane: Fundamentals and Field Applications, EPA-542-R-06-009, USEPA, Office of Solid Waste and Emergency Response, Washington, DC, 2006.
[2] T.K.G. Mohr, Environmental Investigation and Remediation: 1,4-Dioxane and Other Solvent Stabilizers, CRC Press, Boca Raton, 2010.
[3] P. Ghosh, A.N. Samanta, S. Ray, Oxidation kinetics of degradation of 1,4-dioxane in aqueous solution by H_2O_2/Fe(II) system, J. Environ. Sci. Health. Part A Toxic/Hazard. Subst. Environ. Eng. 45 (2010) 395–399.
[4] European Chemicals Bureau (ECB), E.U. risk assessment report: 1,4-dioxane, ISBN 92-894-1252-6, Second Priority List 21 (2002) 1-129, Office for Official Publications of the European Communities, Luxembourg, 2002.
[5] U.S. Environmental Protection Agency (USEPA), Toxicological review of 1,4-dioxane (CAS No. 123-91-1), EPA/635/R-09/005-F, USEPA, Washington, DC, 2010.
[6] J.M. Skadsen, B.L. Rice, D.J. Meyering, The Occurence and Fate of Pharmaceuticals, Personal Care Products, and Endocrine Disrupting Compounds in a Municipal Water Use Cycle: A Case Study in the City of Ann Arbor., Water Utilities, Fleis & VendenBrink Engineering, Inc., City of Anna Arbor, 2004.
[7] W.H. Glaze, J.W. Kang, D.H. Chapin, The chemistry of water treatment processes involving ozone, hydrogen peroxide and ultraviolet radiation, Ozone Sci. Eng. 9 (1987) 335–352.
[8] H. Barndõk, D. Hermosilla, L. Cortijo, E. Torres, A. Blanco, Electrooxidation of industrial wastewater containing 1,4-dioxane in the presence of different salts, Environ. Sci. Pollut. Res. 21 (2014) 5701–5712.
[9] H. Barndõk, L. Cortijo, D. Hermosilla, C. Negro, A. Blanco, Removal of 1,4-dioxane from industrial wastewaters: routes of decomposition under different operational conditions to determine the ozone oxidation capacity, J. Hazard. Mater. 280 (2014) 340–347.
[10] J.H. Suh, M. Mohseni, A study on the relationship between biodegradability enhancement and oxidation of 1,4-dioxane using ozone and hydrogen peroxide, Water Res. 38 (2004) 2596–2604.
[11] H. Barndõk, D. Hermosilla, C. Han, D.D. Dionysiou, C. Negro, Á. Blanco, Degradation of 1,4-dioxane from industrial wastewater by solar photocatalysis using immobilized NF-TiO_2 composite with monodisperse TiO_2, Appl. Catal. B-Environ. 180 (2016) 44–52.
[12] V. Maurino, P. Calza, C. Minero, E. Pelizzetti, M. Vincenti, Light-assisted 1,4-dioxane degradation, Chemosphere 35 (1997) 2675–2688.
[13] M.A. Beckett, I. Hua, Elucidation of the 1,4-dioxane decomposition pathway at discrete ultrasonic frequencies, Environ. Sci. Technol. 34 (2000) 3944–3953.
[14] M.I. Stefan, J.R. Bolton, Mechanism of the degradation of 1,4-dioxane in dilute aqueous solution using the UV hydrogen peroxide process, Environ. Sci. Technol. 32 (1998) 1588–1595.
[15] C.-G. Kim, H.-J. Seo, B.-R. Lee, Decomposition of 1,4-dioxane by advanced oxidation and biochemical process, J. Environ. Sci. Health. Part A Toxic/Hazard. Subst. Environ. Eng. 41 (2006) 599–611.
[16] N. Merayo, D. Hermosilla, L. Cortijo, Á. Blanco, Optimization of the Fenton treatment of 1,4-dioxane and on-line FTIR monitoring of the reaction, J. Hazard. Mater. (2014).
[17] M.H. So, J.S. Han, T.H. Han, J.W. Seo, C.G. Kim, Decomposition of 1,4-dioxane by photo-Fenton oxidation coupled with activated sludge in a polyester manufacturing process, Water Sci. Technol. 59 (2009) 1003–1009.
[18] D. Hermosilla, N. Merayo, R. Ordonez, A. Blanco, Optimization of conventional Fenton and ultraviolet-assisted oxidation processes for the treatment of reverse osmosis retentate from a paper mill, Waste Manage. 32 (2012) 1236–1243.
[19] C.P. Huang, C. Dong, Z. Tang, Advanced chemical oxidation: its present role and potential future in hazardous waste treatment, Waste Manage. 13 (1993) 361–377.
[20] J.J. Pignatello, E. Oliveros, A. MacKay, Advanced oxidation processes for organic contaminant destruction based on the Fenton reaction and related chemistry, Crit. Rev. Environ. Sci. Technol. 36 (2006) 1–84.
[21] H.-S. Son, J.-K. Im, K.-D. Zoh, A Fenton-like degradation mechanism for 1,4-dioxane using zero-valent iron (Fe-0) and UV light, Water Res. 43 (2009) 1457–1463.
[22] M. Kallel, C. Belaid, T. Mechichi, M. Ksibi, B. Elleuch, Removal of organic load and phenolic compounds from olive mill wastewater by Fenton oxidation with zero-valent iron, Chem. Eng. J. 150 (2009) 391–395.
[23] J. Prousek, E. Palackova, S.A. Priesolova, L. Markova, A. Alevova, Fenton- and fenton-like AOPs for wastewater treatment: From Laboratory-to-plant-scale application, Sep. Sci. Technol. 42 (2007) 1505–1520.
[24] J.A. Bergendahl, T.P. Thies, Fenton's oxidation of MTBE with zero-valent iron, Water Res. 38 (2004) 327–334.
[25] D. Hermosilla, M. Cortijo, C.P. Huang, The role of iron on the degradation and mineralization of organic compounds using conventional Fenton and photo-Fenton processes, Chem. Eng. J. 155 (2009) 637–646.
[26] S. Malato, P. Fernandez-Ibanez, M.I. Maldonado, J. Blanco, W. Gernjak, Decontamination and disinfection of water by solar photocatalysis: Recent overview and trends, Catal. Today 147 (2009) 1–59.
[27] P.A. Soares, T.F.C.V. Silva, D.R. Manenti, S.M.A.G.U. Souza, R.A.R. Boaventura, V. J.P. Vilar, Insights into real cotton-textile dyeing wastewater treatment using solar advanced oxidation processes, Environ. Sci. Pollut. Res. 21 (2014) 932–945.

[28] H.-S. Kim, B.-H. Kwon, S.-J. Yoa, I.-K. Kim, Degradation of 1,4-dioxane by photo-fenton processes, J. Chem. Eng. Jpn. 41 (2008) 829–835.
[29] S.M. Kim, S.U. Geissen, A. Vogelpohl, Landfill leachate treatment by a photoassisted Fenton reaction, Water Sci. Technol. 35 (1997) 239–248.
[30] H. Pobiner, Determination of hydroperoxides in hydrocarbon by conversion to hydrogen peroxide and measurement by titanium complexing, Anal. Chem. 33 (1961) 1423–1428.
[31] H. Tamura, K. Goto, T. TYotsuyanagi, M. Nagayama, Spectrophotometric determination of iron(II) with 1,10-phenanthroline in the presence of large amounts of iron(III), Talanta 21 (1974) 314–318.
[32] M.I. Litter, N. Quici, Photochemical advanced oxidation processes for water and wastewater treatment, Recent Pat. Eng. 4 (2010) 217–241.
[33] D.H.F. Liu, B.G. Liptak, Environmental Engineers' Handbook, 2nd ed., CRC Press LLC, Boca Raton, 1997.
[34] W.J. Cooper, C.J. Cramer, N.H. Martin, S.P. Mezyk, K.E. O'Shea, C. von Sonntag, Free radical mechanisms for the treatment of methyl tert-butyl ether (MTBE) via advanced oxidation/reductive processes in aqueous solutions, Chem. Rev. 109 (2009) 1302–1345.
[35] F. Vogel, J. Harf, A. Hug, P.R. von Rohr, The mean oxidation number of carbon (MOC) – a useful concept for describing oxidation processes, Water Res. 34 (2000) 2689–2702.
[36] I. Muñoz, Life cycle assessment as a tool for green chemistry: application to different advanced oxidation processes for wastewater treatment (Ph.D. thesis). Autonomous University of Barcelona, Bellaterra, 2006.
[37] I. Karat, Advanced oxidation processes for removal of COD from pulp and paper mill effluents. A technical, economical and environmental evaluation (M.Sc. thesis). Royal Institute of Technology, Stockholm, 2013.
[38] Eurostat, Electricity prices components for industrial consumers – annual data, <http://appsso.eurostat.ec.europa.eu/nui/show.do?dataset=nrg_pc_205_c&lang=en>, 2015 (accessed: July 24, 2015).
[39] Alibaba Chemicals Market, <http://www.alibaba.com>, 2015 (accessed: June 5, 2015).

PUBLICATION IV

H. Barndõk, M. Pelaez, C. Han, W.E. Platten, III, P. Campo, D. Hermosilla, A. Blanco, D.D. Dionysiou

Photocatalytic degradation of contaminants of concern with composite NF-TiO_2 films under visible and solar light

Environmental Science and Pollution Research 20 (2013) 3582-3591

Environ Sci Pollut Res
DOI 10.1007/s11356-013-1550-z

Photocatalytic degradation of contaminants of concern with composite NF-TiO_2 films under visible and solar light

H. Barndõk · M. Peláez · C. Han · W. E. Platten III · P. Campo · D. Hermosilla · A. Blanco · D. D. Dionysiou

Received: 20 November 2012 / Accepted: 4 February 2013

Abstract This study reports the synthesis and characterization of composite nitrogen and fluorine co-doped titanium dioxide (NF-TiO_2) for the removal of contaminants of concern in wastewater under visible and solar light. Monodisperse anatase TiO_2 nanoparticles of different sizes and Evonik P25 were assembled to immobilized NF-TiO_2 by direct incorporation into the sol–gel or by the layer-by-layer technique. The composite films were characterized with X-ray diffraction, high-resolution transmission electron microscopy, environmental scanning electron microscopy, and porosimetry analysis. The photocatalytic degradation of atrazine, carbamazepine, and caffeine was evaluated in a synthetic water solution and in an effluent from a hybrid biological concentrator reactor (BCR). Minor aggregation and improved distribution of monodisperse titania particles was obtained with NF-TiO_2-monodisperse (10 and 50 nm) from the layer-by-layer technique than with NF-TiO_2+monodisperse TiO_2 (300 nm) directly incorporated into the sol. The photocatalysts synthesized with the layer-by-layer method achieved significantly higher degradation rates in contrast with NF-TiO_2-monodisperse titania (300 nm) and slightly faster values when compared with NF-TiO_2-P25. Using NF-TiO_2 layer-by-layer with monodisperse TiO_2 (50 nm) under solar light irradiation, the respective degradation rates in synthetic water and BCR effluent were 14.6 and $9.5\times10^{-3}\,min^{-1}$ for caffeine, 12.5 and $9.0\times10^{-3}\,min^{-1}$ for carbamazepine, and 10.9 and $5.8\times10^{-3}\,min^{-1}$ for atrazine. These results suggest that the layer-by-layer technique is a promising method for the synthesis of composite TiO_2-based films compared to the direct addition of nanoparticles into the sol.

Keywords NF-TiO_2 · Monodisperse · Sol–gel method · Carbamazepine · Atrazine · Caffeine · TiO_2 photocatalysis · Solar · Visible light · Contaminants · Emerging · Concern · Water · Reuse

Responsible editor: Philippe Garrigues

H. Barndõk · D. Hermosilla · A. Blanco
Department of Chemical Engineering,
Complutense University of Madrid, Avda. Complutense, s/n,
28040 Madrid, Spain

H. Barndõk
e-mail: hbarndok@quim.ucm.es

D. Hermosilla
e-mail: dhermosilla@quim.ucm.es

A. Blanco
e-mail: ablanco@quim.ucm.es

M. Peláez · C. Han · W. E. Platten III · P. Campo · D. D. Dionysiou
Environmental Engineering and Science Program,
University of Cincinnati, Cincinnati, OH, USA

M. Peláez
e-mail: pelaezma@mail.uc.edu

C. Han
e-mail: hanck@mail.uc.edu

W. E. Platten III
e-mail: plattewe@mail.uc.edu

P. Campo
e-mail: campomp@ucmail.uc.edu

D. D. Dionysiou (✉)
Nireas-International Water Research Centre,
University of Cyprus, 20537 Nicosia, Cyprus
e-mail: dionysios.d.dionysiou@uc.edu

Introduction

Contaminants of concern (COCs), especially pharmaceuticals and pesticides, are routinely detected in the effluents of municipal wastewater treatment plants (WTPs), which presents a risk for the environment and human health

Published online: 24 February 2013

(Andreozzi et al. 2003; Belgiorno et al. 2007; Bernabeu et al. 2011; Castiglioni et al. 2006; Glassmeyer et al. 2005; Ho et al. 2011; Joss et al. 2005). Carbamazepine (CMP), a widely used anticonvulsant and mood-stabilizing drug (WHO 2002), is frequently identified downstream of sewage treatment plants in several European countries (Andreozzi et al. 2003; Bernabeu et al. 2011; Castiglioni et al. 2006; Joss et al. 2005) as well as in the USA (Glassmeyer et al. 2005). Likewise, atrazine (ATR) is a commonly found herbicide in WTP effluents around the USA (Glassmeyer et al. 2005; USEPA 2003) and Australia (Ho et al. 2011). According to the U.S. Environmental Protection Agency, ATR has a suspected impact on gonadal development in amphibians. Moreover, the European Union (EU) considers it an endocrine disruptor and, therefore, a priority substance in the EU Water Framework Directive 2008/105/EC (EC 2008). The treatment of these compounds by conventional biological methods, such as activated sludge process, trickling filter, membrane bioreactor, and suspended-biofilm reactor, achieves only partial removal of these chemicals (Andreozzi et al. 2003; Belgiorno et al. 2007; Bernabeu et al. 2011; Castiglioni et al. 2006; Glassmeyer et al. 2005; Ho et al. 2011; Joss et al. 2005). For this reason, the integrated use of advanced oxidation processes (AOPs) with biological treatment is of great interest as they have shown the capability to polish effluent streams containing biorefractory organics (Andreozzi et al. 2003; Belgiorno et al. 2007; Bernabeu et al. 2011; Rizzo et al. 2009). Titanium dioxide (TiO_2)-based nanotechnology has gained recognition as a promising AOP for water remediation due to the process high decomposition efficiency and TiO_2 green characteristics, e.g., low toxicity, inert nature, and relatively low cost (Antoniou et al. 2008; Choi et al. 2007; Fujishima et al. 2000). This non-selective treatment even degrades trace level concentrations that are difficult or expensive to remove with conventional methods (Balasubramanian et al. 2004; Lin et al. 2006).

Photocatalytic degradation employing TiO_2-based nanomaterials in slurry suspension or colloidal solution has been carried out successfully for both ATR (Hincapie et al. 2005; Li et al. 2012; Mourao et al. 2010; Parra et al. 2004) and CMP (Bernabeu et al. 2011; Chong and Jin 2012; Doll and Frimmel 2004; Laera et al. 2011). However, TiO_2 immobilization to avoid a filtration step could appreciably improve the cost-effectiveness of the operation (Balasubramanian et al. 2004; Goetz et al. 2009; Han et al. 2011; Miranda-Garcia et al. 2011; Pelaez et al. 2010). Hence, among current challenges of the TiO_2-based nanotechnology for environmental applications include enhancement of the structural and the photocatalytic properties of the immobilized catalysts.

Satisfactory removals of ATR, as a sole contaminant in synthetic solutions, have been achieved with TiO_2 immobilized on a supporting media under UV or solar light irradiation (Goetz et al. 2009; McMurray et al. 2006; Parra et al. 2004). However, COCs are usually not the only substances present in effluents, so their photocatalytic degradation may be hampered by the presence of other organic and inorganic constituents that exert a stronger selectivity towards the catalyst or the oxidant species (Chong et al. 2011; Klamerth et al. 2009; Laera et al. 2011). Very few papers deal with supported photocatalysts for the treatment of COCs in mixtures. Miranda-Garcia et al. (2011) studied the degradation of 15 COCs in simulated and real municipal wastewater with TiO_2 immobilized on glass spheres under solar irradiation. ATR and CMP demonstrated to be the most recalcitrant since they presented the lowest degradation rates among the studied compounds.

The UV-restricted photoactivation of TiO_2 limits the utilization of a higher portion of the solar spectrum (i.e., visible light) to generate reactive oxidizing species. Several approaches, including metal and non-metal doping, dye-sensitization, and coupled semiconductors, have been applied to overcome this 3.2-eV band gap energy (Pelaez et al. 2012b). For drinking water treatment, non-metallic dopants (e.g., nitrogen, sulfur, fluorine, or carbon) are preferable because these elements do not show leakage as metals or other semiconductors do (Asahi et al. 2001; Choi et al. 2007; Lin et al. 2006; Rengifo-Herrera et al. 2009; Subagio et al. 2010). Nitrogen and fluorine co-doped TiO_2 (NF-TiO_2) films with enhanced structural properties have been synthesized using a modified sol–gel procedure and successfully applied to the photocatalytic degradation of cyanobacterial toxins in water (Pelaez et al. 2009; Pelaez et al. 2010). Additionally, the incorporation of Evonik® P25-TiO_2 nanoparticles into the sol–gel improved the physicochemical and optical properties of the TiO_2 film (Chen and Dionysiou 2008; Pelaez et al. 2011). Therefore, studying the effect of different nanoparticles added into the NF-TiO_2 sol–gel to improve its photocatalytic efficiency is of great interest.

In this work, monodisperse anatase TiO_2 nanoparticles of various particle sizes (Han et al. 2012) were assembled to the immobilized NF-TiO_2 films by direct incorporation into the NF-TiO_2 sol–gel or by employing the layer-by-layer technique. The performance of these composite films in the degradation of a mixture of COCs in both synthetic water and wastewater was evaluated under visible and solar irradiation, and compared with the performance of NF-TiO_2-P25. The tested COCs were CMP and ATR as the representatives of the most persistent pharmaceuticals and pesticides typically present in WTP effluents. In addition, caffeine (CAF) was included as one of the most commonly detected contaminants in wastewater streams worldwide (Bernabeu et al. 2011; Glassmeyer et al. 2005; Kolpin et al. 2002).

Materials and methods

Reagents and sample preparation

ATR, CAF, and CMP were obtained from Sigma-Aldrich (USA). NF-TiO_2 was prepared using a modified sol–gel method reported by Pelaez et al. (2010). Briefly, a flurosurfacant (Zonyl FS 300, Fluka), which served as a pore template and fluorine dopant, was dissolved in isopropyl alcohol (Fisher, USA). After the addition of glacial acetic acid (Fisher, USA), ethylenediamine (Fisher, USA) was added as a nitrogen precursor. Titanium tetraisopropoxide (TTIP; Sigma-Aldrich, USA, 97 %) was added dropwise to the sol, followed by additional acetic acid for peptidization. Monodisperse anatase titania was synthesized by a sol–gel method described by Han et al. (2012). In brief, $CaCl_2$ solutions of varying concentrations (to provide different ionic strength for the particle size control) were added to methanol (Tedia, USA). After mixing, TTIP was added dropwise as the titanium precursor.

Two different ways of incorporating the nanoparticles into the composite NF-TiO_2 films were implemented. In the first method, Evonik® P25-TiO_2 or monodisperse titania nanoparticles (300 nm) were incorporated directly into the NF-TiO_2 sol–gel at 5 gL^{-1} and sonicated. Subsequently, the sol was deposited on the substrate by dip-coating and immobilized as described elsewhere (Pelaez et al. 2012a). The second approach consisted in a layer-by-layer technique employing a separate solution of monodisperse titania with a particle size of 10 or 50 nm. The first coating consisted of a NF-TiO_2 film followed by monodisperse titania one. This process of merging NF-TiO_2 with monodisperse titania on top of it was repeated three times layer-by-layer until a final layer of monodisperse titania was achieved (six layers in total). The procedure of immobilization of the composite films is described elsewhere (Pelaez et al. 2012a).

Characterization of the films

A Tristar 3000 (Micromeritics) porosimeter analyzer was employed for the determination of BET surface area, pore volume, porosity, and BJH pore size distribution of the composite NF-TiO_2 films. The films were scraped, and the samples were collected as powder and purged with N_2 for 2 h at 150 °C using Flow prep 060 (Micromeritics). The film morphology was characterized with an environmental scanning electron microscope (ESEM, Philips XL 30 ESEM-FEG). The crystallographic structure of the synthesized TiO_2 films was determined with a X'Pert PRO (Philips) XRD diffractometer with Cu Kα (λ=1.5406 Å) radiation. Optoelectronic properties were derived from diffuse reflectance spectra obtained on a UV–vis spectrophotometer (Shimadzu 2501 PC) equipped with an integrated sphere attachment (ISR 1200) with $BaSO_4$ reference standard.

Photocatalytic experiments

The photocatalytic degradation of ATR, CAF, and CMP was carried out both in a synthetic water solution (MilliQ-grade water) and in the effluent of a hybrid biomass concentrator reactor (BCR; Scott 2012), which treated a medium strength synthetic municipal wastewater (see Table 3 for effluent characteristics prior to spiking). Stock solutions of the analytes were prepared in MilliQ-grade water, and all the analytes were added together in aforementioned matrices at 4 $\mu molL^{-1}$. A borosilicate glass vessel reactor (i.d. 4.7 cm) containing 10 mL of spiked solution (0.58 cm of aqueous irradiated layer) and a composite film was sealed with parafilm and cooled down with a fan to prevent evaporation. The solution was irradiated with a 500-W solar simulator (Newport Corporation) equipped with AM 1.5 and infrared filters. The light intensity was 70 Wcm^{-2} and was measured with a radiant power meter (Newport Corporation). When the experiments were performed in the visible range (420–700 nm), the measured light intensity was 40 Wcm^{-2}. The experiments were carried out in duplicates.

The COCs were analyzed by liquid chromatography–electrospray ionization–tandem mass spectrometry with a 1200 Series rapid resolution liquid chromatograph and 6410A triple quadrupole mass spectrometer equipped with a G1948B electrospray ionization source (Agilent, Palo Alto, CA, USA). The ESI was operated in positive mode. The analytes were separated with a Zorbax Eclipse XDB-C18 (2.1×50 mm, 3.5 um) column (Agilent, Palo Alto, CA, USA). The flow was 0.5 mL/min. The mobile phase was comprised of water (A) and methanol (B), both containing ammonium formate (5 mM). At time 0, the eluent composition was 90 % (A) and 10 % (B), being 36 % (A) and 64 % (B) after 12 min. The analytes were detected in the following selected reactions: ATR m/z 216→m/z 174, CAF m/z 195→m/z 138, and CMP m/z 237→m/z 194.

Results and discussion

Morphology and microstructure of the composite NF-TiO_2 films

The overall surface morphology of the NF-TiO_2 composite materials was examined by ESEM. Rough and porous surfaces were observed in all of the studied composite films (Figs. 1 and 2). The high surface roughness is a characteristic of NF-TiO_2 films synthesized with the abovementioned sol–gel method. Nevertheless, a rougher surface could

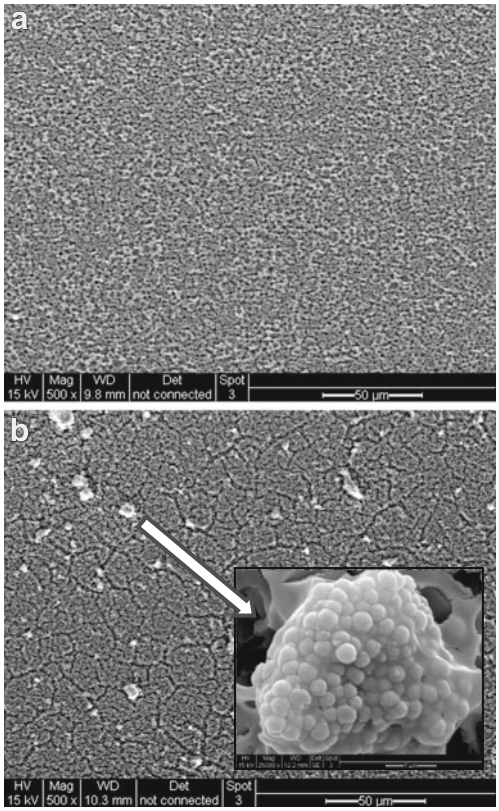

Fig. 1 ESEM images of **a** NF-TiO_2-P25, **b** NF-TiO_2+monodisperse titania (300 nm) added directly to the sol

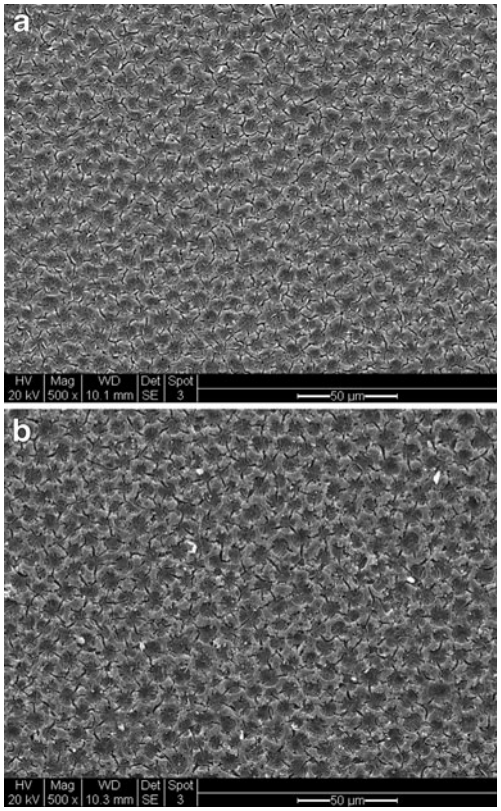

Fig. 2 ESEM images of the catalysts from the layer-by-layer method: **a** NF-TiO_2-monodisperse TiO_2 (50 nm). **b** NF-TiO_2-monodisperse TiO_2 (10 nm)

provide a larger surface area for the photocatalytic reactions and more effective light absorbance than smoother surfaces (Pelaez et al. 2010; Provata et al. 1998). Based on Figs. 1 and 2, the difference among films was mainly due to the surface coverage. Higher surface coverage and more uniform distribution of nanoparticle additives were achieved in those films composed with P25 (Fig. 1a) than with the composite film containing monodisperse nanoparticles of 300 nm (Fig. 1b). In the latter, the surface coverage was greatly decreased due to the extensive aggregation of nanoparticles. Although the presence of aggregates was observed in all the catalysts cases (Figs. 1 and 2), much larger nanoparticle clusters were formed when monodisperse anatase titania was directly added into the sol–gel (Fig. 1b). Nevertheless, with the layer-by-layer technique, when the initially fairly well-distributed sol of the monodisperse TiO_2 was deposited as an even layer on top of the NF-TiO_2 by dip-coating, fewer aggregates and improved distribution of monodisperse titania was obtained (Fig. 2). It can be concluded that the dispersion of the monodisperse particles is higher when employing the layer-by-layer method than when added directly into the NF-TiO_2 sol in a powdered form after recovering the monodisperse particles from the initial solution. The smaller particle size (50 and 10 nm) could probably also enhance the distribution of monodisperse titania. However, no notable difference was found in the ESEM images when using the particle size of 50 nm (Fig. 2a) or 10 nm (Fig. 2b), showing that the uniformity of the distribution of monodisperse particles is similar in the size range of 10 to 50 nm. Since the COCs degradation preferentially occurs on the catalyst surface, a higher interaction is expected with the film that has the highest surface area coverage (Linsebigler et al. 1995). Therefore, since fewer aggregates and improved

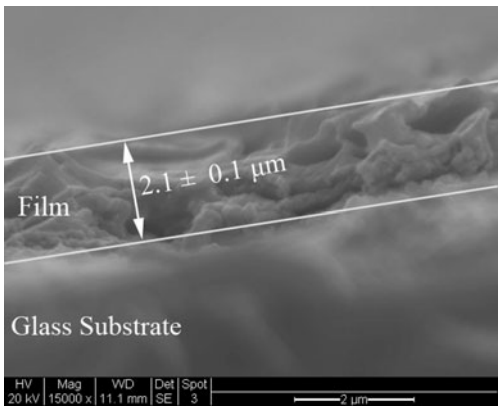

Fig. 3 Cross-section ESEM image of the film thickness of the composite NF-TiO_2 with monodisperse TiO_2 by the layer-by-layer technique

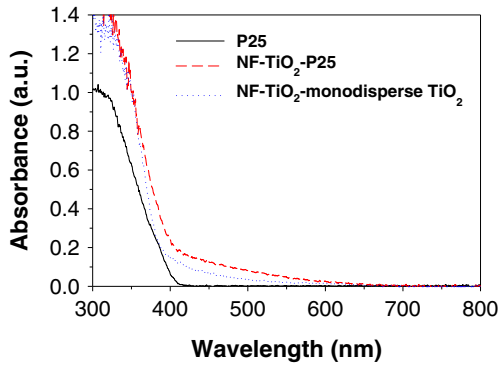

Fig. 4 Absorbance spectra of P25, composite NF-TiO_2-P25, and NF-TiO_2-monodisperse TiO_2

distribution of monodisperse titania were obtained by the layer-by-layer method, improved degradation similar to, or higher than, the NF-TiO_2-P25 could be expected.

In spite of the doubled number of layers, the films prepared by the layer-by-layer method had a slightly lower film thickness (Fig. 3) than the composite NF-TiO_2-P25 (Pelaez et al. 2012a) where nanoparticle additives were incorporated directly into the sol. This, however, did not lead to lower photocatalytic activity for the NF-TiO_2-monodisperse compared to NF-TiO_2-P25 (see "Photocatalytic evaluation of the composite NF-TiO_2 films synthesized layer-by-layer with the monodisperse TiO_2" section).

According to XRD analysis, NF-TiO_2-P25 films exhibited two crystal phases, anatase and rutile (confirming the presence of P25 nanoparticles). On the other hand, anatase was the only form detected for NF-TiO_2-monodisperse (300 nm) and NF-TiO_2 layer-by-layer with monodisperse TiO_2 (10 and 50 nm). Dopant-related crystal phases were not observed since the amount of nitrogen and fluorine does not produce significant changes in the TiO_2 structure (Pelaez et al. 2010).

The absorbance spectra of the Evonik P25, the composite NF-TiO_2-P25, and the NF-TiO_2-monodisperse TiO_2 are shown in Fig. 4. While the reference sample of P25 showed no absorption towards visible light, the composite NF-TiO_2 exhibited absorption spectra extended to the visible range of 400–500 nm to a small degree. This is due to the N and F doping, whereas the P25 and monodisperse titania additives most likely reduce the visible light absorption capacity of the NF-TiO_2 (Pelaez et al. 2012a).

Porosimetry analysis was carried out for further characterization of the films. Table 1 summarizes the structural characteristics of all the composite NF-TiO_2 films. The BET surface area increased with the direct addition of monodisperse titania (300 nm) into the NF-TiO_2 sol, compared to the NF-TiO_2-P25 composite film. The formation of different aggregate sizes due to the specific properties of the monodisperse titania and P25 can lead to the different values of BET area obtained. The films with monodisperse titania added by the layer-by-layer method presented BET surface area similar to or even smaller than the NF-TiO_2-P25 (monodisperse titania of 50 and 10 nm, respectively). The smaller monodisperse particles of 10 nm could smoothen the surface roughness of the TiO_2 film, but doing so also decreases the available surface area. Fairly similar pore size distribution was observed in all studied composite films.

Photocatalytic evaluation of the composite films

The photocatalytic degradation of the studied COCs followed pseudo-first-order kinetics. Regardless of the catalyst used or the aqueous matrix, CAF presented the highest degradation rate followed by CMP and ATR (see Table 2). ATR seemed to be more resistant at the early stages of the photocatalytic reaction (see Figs. 5, 6, 7, and 8), probably because of the higher persistence of ATR due to its chemical structure and/or because of the competitive adsorption on the catalyst surface by the other compounds in the mixture (Zahraa et al. 2003). However, the final concentrations of all the compounds were not substantially different after 7 h of degradation, which shows the high efficiency of the treatment under the experimental conditions.

Photocatalytic evaluation of the composite films with nanoparticle additives directly incorporated to the NF-TiO_2 sol

Preliminary studies were carried out in synthetic water, comparing the two composite catalysts with nanoparticle additives directly incorporated into the NF-TiO_2 sol both

Table 1 Structural characteristics of NF-TiO_2 films with different nanoparticle additives

Material	S_{BET} ($m^2 g^{-1}$)	Pore volume ($cm^3 g^{-1}$)	Porosity (%)	Crystal phase
NF-TiO_2-monodisperse (50 nm)[a]	110.6	0.189	42.4	Anatase
NF-TiO_2-monodisperse (10 nm)[a]	99.4	0.173	40.3	Anatase
NF-TiO_2-P25	111.5	0.154	37.5	Anatase/Rutile
NF-TiO_2-monodisperse (300 nm)[b]	147.7	0.189	42.5	Anatase

[a] Monodisperse titania incorporated by the layer-by-layer method

[b] Monodisperse titania added directly to the sol–gel

under visible and solar light (Fig. 5). Limited visible light degradation of all COCs was observed with NF-TiO_2-P25 and NF-TiO_2+monodisperse titania (300 nm), indicating the persistence of the COCs under the conditions tested.

Nevertheless, the COCs were effectively degraded under solar light with both composite films in synthetic solution. Higher degradation efficiency in terms of higher kinetic constant k (minutes; Table 2) was obtained with NF-TiO_2-P25 (see Fig. 5a) when compared with NF-TiO_2+monodisperse titania (300 nm; Fig. 5b). ATR had the lowest reaction kinetics, the k values in the case of using P25 additive or monodisperse TiO_2 (300 nm) were 8.8 and $2.5\times10^{-3}\,min^{-1}$, respectively (Table 2). In terms of removal, after 2 h of solar light irradiation, 77 % of CAF, 72 % of CMP, and 56 % of ATR were degraded by NF-TiO_2-P25, while with NF-TiO_2+monodisperse titania of 300 nm, the percentages were 54, 50, and 24 %, respectively.

The degradation of COCs was slower in the BCR effluent than in the synthetic water solution (Fig. 6). With NF-TiO_2-P25, the k value for the CMP degradation in synthetic water ($12.6\times10^{-3}\,min^{-1}$) decreased to $8.4\times10^{-3}\,min^{-1}$ (by about 30 %; see Table 2). This decrease of degradation rates compared to the synthetic water is explained by the fact that the BCR effluent is a complex matrix containing several inorganic constituents that may compete with the analytes during the photocatalytic process (Table 3). The presence of SO_4^{2-} and Cl^- (316 and 59 $mg\,L^{-1}$, respectively) and a total alkalinity of 156 $mg\,L^{-1}$ (usually caused by the bicarbonates in great extent) were most likely the reason for the decrease in the degradation rates. Those inorganic species are reported to inhibit the TiO_2 photocatalysis, principally as competitors for the adsorption on the catalyst surface or as the scavengers of $^{\bullet}OH$ radical (Burns et al. 1999; Yalap and Balcioglu 2009). Furthermore, the higher pH of the BCR effluent (7.9) compared to the synthetic solution at 5.7 could also affect the photocatalytic reactions (Barndõk et al. 2012). As the surface of NF-TiO_2 is negatively charged at pH values above ~6.0 as well as CMP (Achilleos et al. 2010; Pelaez et al. 2009), the adsorption of the compound on the surface of the catalyst is hindered by the action of repulsive electrostatic forces.

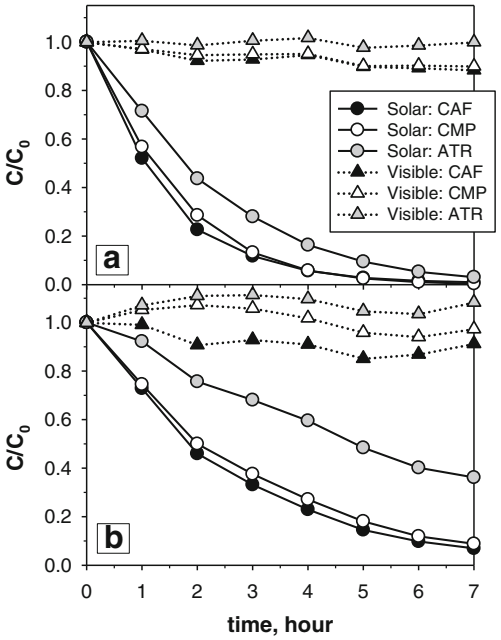

Fig. 5 Photocatalytic degradation of COCs in synthetic solution under visible and solar irradiation by **a** NF-TiO_2-P25, **b** NF-TiO_2+monodisperse titania (300 nm) added directly to the sol

The negative effect of the BCR effluent on the degradation was even greater when monodisperse TiO_2 (300 nm) was directly incorporated to the sol (Table 2). For CAF, that exhibited the highest degradation kinetics in both water matrices, the k values in the synthetic water decreased in the BCR effluent by about 20 % when using P25 additive, but more than 50 % when employing TiO_2 (300 nm). In terms of

Table 2 First-order kinetic constants of the photocatalytic degradation of COCs under solar light irradiation in (a) synthetic solution and (b) BCR effluent

Catalyst	NF-TiO_2-monodisperse(50 nm)[a]			NF-TiO_2-monodisperse (10 nm)[b]			NF-TiO_2-P25			NF-TiO_2-monodisperse (300 nm)[b]		
Compound	$t_{1/2}$ min	$k\cdot10^3\,min^{-1}$	R^2	$t_{1/2}$ min	$k\cdot10^3\,min^{-1}$	R^2	$t_{1/2}$ min	$k\cdot10^3\,min^{-1}$	R^2	$t_{1/2}$ min	$k\cdot10^3\,min^{-1}$	R^2
Synthetic solution												
CAF	47.4	14.6	1.00	54.8	12.6	1.00	60.9	11.4	0.99	105.7	6.56	1.00
CMP	55.5	12.5	0.99	59.1	11.7	1.00	55.1	12.6	0.99	116.9	5.93	1.00
ATR	63.6	10.9	1.00	70.2	9.9	0.99	78.7	8.8	0.97	275.4	2.52	0.99
BCR effluent												
CAF	72.8	9.52	1.00	70.8	9.79	1.00	76.1	9.11	0.99	199.4	3.48	1.00
CMP	77.3	8.97	0.95	79.4	8.73	0.93	82.4	8.42	0.99	245.2	2.83	0.99
ATR	118.8	5.83	0.99	104.8	6.61	0.99	134.2	5.17	0.99	685.2	1.01	1.00

[a] Monodisperse titania incorporated by the layer-by-layer method

[b] Monodisperse titania added directly to the sol–gel

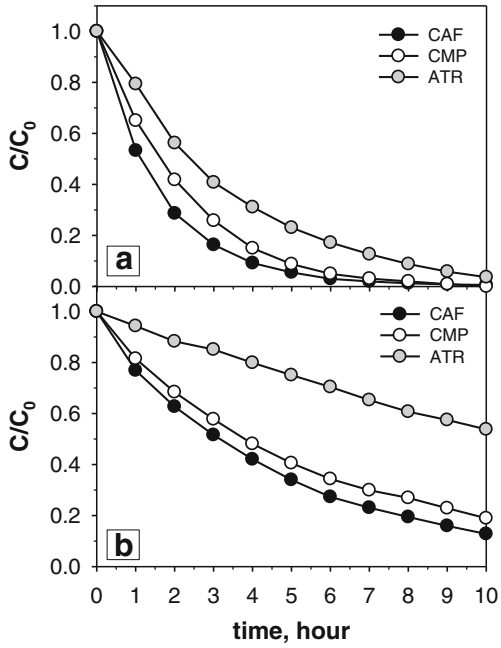

Fig. 6 Photocatalytic degradation of COCs in BCR effluent under solar light employing **a** NF-TiO_2-P25, **b** NF-TiO_2+monodisperse titania (300 nm) added directly to the sol

removal efficiency, after 2 h of degradation, 71 % of CAF, 59 % of CMP, and 44 % of ATR were removed with NF-TiO_2-P25 (Fig. 6a); however, with NF-TiO_2+monodisperse TiO_2 (300 nm), the removal percentages were only 37, 32, and 12 % for CAF, CMP, and ATR, respectively (Fig. 6b). The superior photocatalytic performance by NF-TiO_2-P25 compared to NF-TiO_2+monodisperse titania (300 nm) was mainly due to the different properties of the material. Although the composite film containing monodisperse nanoparticles of 300 nm presented a higher surface area than those prepared with P25 (Table 1), a higher surface coverage was achieved in the film composed with P25 (Fig. 1a). The more uniform dispersion of P25 was a reason for the better photocatalytic activity of NF-TiO_2-P25, while the highly aggregated monodisperse particles brought along poor surface area coverage and, thus, inferior photocatalytic efficiency. Such lower activity in photocatalytic degradation was accentuated in the more complex nature of the BCR effluent.

Table 3 Characterization of the BCR effluent

Effluent characteristic	Measure	Unit
pH	7.9	
Total alkalinity	156	mgL^{-1}
Total hardness	64	mgL^{-1}
Turbidity	0.13	NTU
Conductivity	1,055	μS
COD	<3	mgL^{-1}
TOC	4.1	mgL^{-1}
Cl^-	59	mgL^{-1}
NO_3^-	14	mgL^{-1}
PO_4^{3-}	2.8	mgL^{-1}
SO_4^{2-}	316	mgL^{-1}

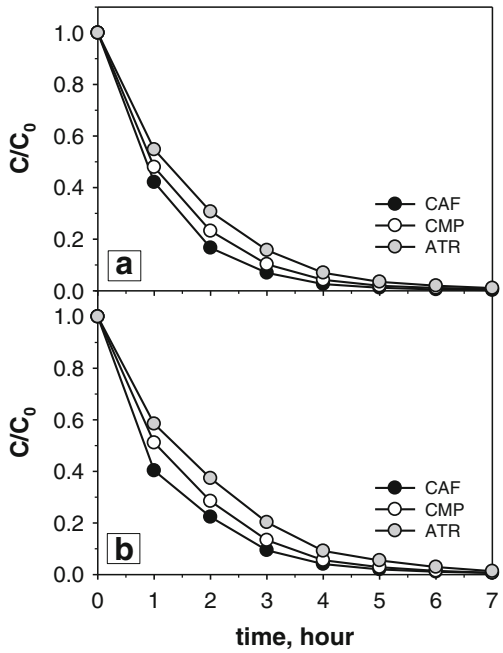

Fig. 7 Photocatalytic degradation of COCs in synthetic solution under solar irradiation by catalysts from the layer-by-layer method: **a** NF-TiO_2-monodisperse TiO_2 (50 nm), **b** NF-TiO_2-monodisperse TiO_2 (10 nm)

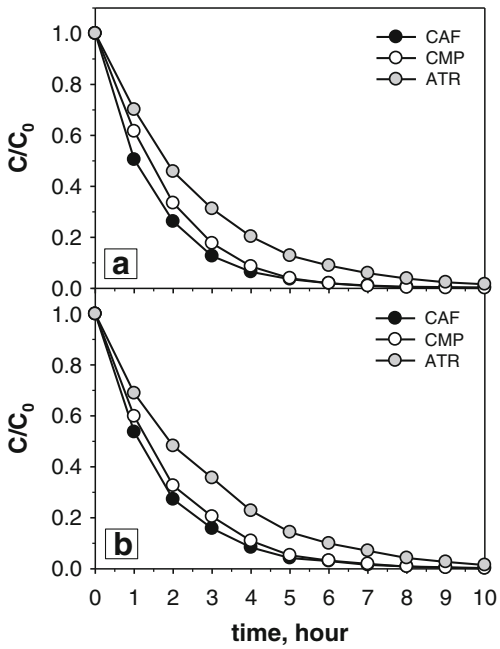

Fig. 8 Photocatalytic degradation of COCs in BCR effluent under solar light employing catalysts from the layer-by-layer method: **a** NF-TiO_2-monodisperse TiO_2 (50 nm), **b** NF-TiO_2-monodisperse TiO_2 (10 nm)

Photocatalytic evaluation of the composite NF-TiO_2 films synthesized layer-by-layer with the monodisperse TiO_2

The catalysts synthesized with the layer-by-layer method achieved higher degradation rates than those where nanoparticle additives were directly incorporated into the NF-TiO_2 sol. As shown in Fig. 7, in the synthetic water solution, the photocatalysts comprising of monodisperse titania of 50 and 10 nm (Fig. 7a and b, respectively) yielded slightly higher degradation than NF-TiO_2-P25 (see Table 2). The k values for ATR were 10.9 and $9.9\times10^{-3}\,min^{-1}$ using NF-TiO_2 layer-by-layer with monodisperse TiO_2 of 50 and 10 nm, respectively. In terms of removal, after 2-h period of exposure, 83 % of CAF, 77 % of CMP, and 69 % of ATR were removed when using monodisperse particles of 50 nm (Fig. 7a), and 78 % of CAF, 72 % of CMP, and 63 % of ATR were removed when using monodisperse particles of 10 nm (Fig. 7b).

With the catalysts from the layer-by-layer method, the degradation of COCs was also slower in the BCR effluent compared to the synthetic water solution (Table 2). With NF-TiO_2-monodisperse TiO_2 (10 nm), the k value for the COCs degradation was decreased by about $3\times10^{-3}\,min^{-1}$ when compared with the kinetics in synthetic water. In terms of removal efficiency, after 2 h, 73 % of CAF, 67 % of CMP, and 52 % of ATR were removed when adding monodisperse particles of 10 nm by the layer-by-layer technique and 67 % of CAF, 68 % of CMP, and 48 % of ATR were removed using monodisperse particles of 50 nm (Fig. 8a, b). As witnessed in the characterization of the composite films ("Morphology and microstructure of the composite NF-TiO_2 films" section), the difference between the catalyst materials was mainly due to the surface area coverage. Based on the ESEM images (Fig. 2), there was no remarkable variation in the surface coverage between the films made by the layer-by-layer technique. In the 10- to 50-nm range, a change in size of the monodisperse particles did not induce a relevant modification in the distribution of nanoparticles and, thus, in the coverage of the merged catalyst surface. Hence, NF-TiO_2 films synthesized by the layer-by-layer method with monodisperse TiO_2 with either 10 or 50 nm of particle size possess similar photocatalytic activities.

Conclusions

The incorporation method of the monodisperse titania to NF-TiO_2 played a significant role in the final physicochemical and photocatalytic properties of the composite film. Fewer nanoparticle aggregates and improved distribution of monodisperse TiO_2 were obtained with the layer-by-layer technique compared to the direct addition of monodisperse particles into the sol. The COCs were effectively degraded under solar light with NF-TiO_2-monodisperse (10 and 50 nm size) from the layer-by-layer technique as well as with NF-TiO_2-P25, whereas monodisperse TiO_2 of 300 nm directly incorporated into the NF-TiO_2 sol only achieved partial COCs degradation. Due to the presence of several inorganic components and higher pH, slower degradation was observed in the BCR effluent than in the synthetic solution (k values decreased by about $3–4\times10^{-3}\,min^{-1}$). NF-$TiO_2$-monodisperse (10 and 50 nm) presented the best performance in both aqueous matrices (in the first 2 h, about 80, 75, and 70 % removal in synthetic water and about 70, 70, and 50 % removal in the BCR effluent was obtained for CAF, CMP, and ATR, respectively). These results imply that the layer-by-layer technique is a promising technique for the synthesis of composite TiO_2-based films as opposed to the direct addition of nanoparticles into the prepared sol–gel, and further optimization of the method is warranted.

Acknowledgments This research was funded by the Cyprus Research Promotion Foundation through Desmi 2009–2010, which is co-funded by the Republic of Cyprus and the European Regional Development Fund of the EU (contract NEA IPODOMI/STRATH/0308/09); the Ministry of Science and Innovation of Spain (project "AGUA Y ENERGÍA", CTM2008-06886-C02-01); the European Commission (project "AQUAFIT4USE", 211534); and the Archimedes Foundation (Estonia), which is granting Helen Barndõk's Ph.D. studies.

References

Achilleos A, Hapeshi E, Xekoukoulotakis NP, Mantzavinos D, Fatta-Kassinos D (2010) UV-A and solar photodegradation of ibuprofen and carbamazepine catalyzed by TiO_2. Separ Sci Technol 45(11):1564–1570. doi:10.1080/01496395.2010.487463

Andreozzi R, Raffaele M, Nicklas P (2003) Pharmaceuticals in STP effluents and their solar photodegradation in aquatic environment. Chemosphere 50(10):1319–1330. doi:10.1016/s0045-6535(02)00769-5

Antoniou MG, Shoemaker JA, De La Cruz AA, Dionysiou DD (2008) Unveiling new degradation intermediates/pathways from the photocatalytic degradation of microcystin-LR. Environ Sci Technol 42(23):8877–8883. doi:10.1021/es801637z

Asahi R, Morikawa T, Ohwaki T, Aoki K, Taga Y (2001) Visible-light photocatalysis in nitrogen-doped titanium oxides. Science 293(5528):269–271. doi:10.1126/science.1061051

Balasubramanian G, Dionysiou DD, Suidan MT, Baudin I, Audin B, Laine JM (2004) Evaluating the activities of immobilized TiO_2 powder films for the photocatalytic degradation of organic contaminants in water. Appl Catal B-Environ 47(2):73–84. doi:10.1016/j.apcatb.2003.04.002

Barndõk H, Hermosilla D, Cortijo L, Negro C, Blanco A (2012) Assessing the effect of inorganic anions on TiO_2-photocatalysis and ozone oxidation treatment efficiencies. J Adv Oxid Technol 15(1):125–132

Belgiorno V, Rizzo L, Fatta D, Della Rocca C, Lofrano G, Nikolaou A, Naddeo V, Meric S (2007) Review on endocrine disrupting-emerging compounds in urban wastewater: occurrence and removal by photocatalysis and ultrasonic irradiation for wastewater reuse. Desalination 215(1–3):166–176. doi:10.1016/j.desal.2006.10.035

Bernabeu A, Vercher RF, Santos-Juanes L, Simon PJ, Lardin C, Martinez MA, Vicente JA, Gonzalez R, Llosa C, Arques A, Amat AM (2011)

Solar photocatalysis as a tertiary treatment to remove emerging pollutants from wastewater treatment plant effluents. Catal Today 161(1):235–240. doi:10.1016/j.cattod.2010.09.025

Burns RA, Crittenden JC, Hand DW, Selzer VH, Sutter LL, Salman SR (1999) Effect of inorganic ions in heterogeneous photocatalysis of TCE. J Environ Eng-Asce 125(1):77–85. doi:10.1061/(asce)0733-9372(1999)125:1(77)

Castiglioni S, Bagnati R, Fanelli R, Pomati F, Calamari D, Zuccato E (2006) Removal of pharmaceuticals in sewage treatment plants in Italy. Environ Sci Technol 40(1):357–363. doi:10.1021/es050991m

Chen Y, Dionysiou DD (2008) Bimodal mesoporous TiO2-P25 composite thick films with high photocatalytic activity and improved structural integrity. Appl Catal B-Environ 80(1–2):147–155. doi:10.1016/j.apcatb.2007.11.010

Choi H, Antoniou MG, Pelaez M, De la Cruz AA, Shoemaker JA, Dionysiou DD (2007) Mesoporous nitrogen-doped TiO2 for the photocatalytic destruction of the cyanobacterial toxin microcystin-LR under visible light irradiation. Environ Sci Technol 41(21):7530–7535. doi:10.1021/es0709122

Chong MN, Jin B (2012) Photocatalytic treatment of high concentration carbamazepine in synthetic hospital wastewater. J Hazard Mater 199:135–142. doi:10.1016/j.jhazmat.2011.10.067

Chong MN, Jin B, Laera G, Saint CP (2011) Evaluating the photodegradation of carbamazepine in a sequential batch photoreactor system: impacts of effluent organic matter and inorganic ions. Chem Eng J 174(2–3):595–602. doi:10.1016/j.cej.2011.09.065

Doll TE, Frimmel FH (2004) Kinetic study of photocatalytic degradation of carbamazepine, clofibric acid, iomeprol and iopromide assisted by different TiO_2 materials—determination of intermediates and reaction pathways. Water Res 38(4):955–964. doi:10.1016/j.watres.2003.11.009

EC (2008) Directive 2008/105/EC of the European Parliament and of the Council on the environmental quality standards in the field of water policy, amending and subsequently repealing Council Directives 82/176/EEC, 83/513/EEC, 84/156/EEC, 84/491/EEC and amending Directive 2000/60/EC. Official Journal L348:84–97

Fujishima A, Rao TN, Tryk DA (2000) Titanium dioxide photocatalysis. J Photoch Photobio C 1:1–21. doi:10.1016/S1389-5567(00)00002-2

Glassmeyer ST, Furlong ET, Kolpin DW, Cahill JD, Zaugg SD, Werner SL, Meyer MT, Kryak DD (2005) Transport of chemical and microbial compounds from known wastewater discharges: potential for use as indicators of human fecal contamination. Environ Sci Technol 39(14):5157–5169. doi:10.1021/es048120k

Goetz V, Cambon JP, Sacco D, Plantard G (2009) Modeling aqueous heterogeneous photocatalytic degradation of organic pollutants with immobilized TiO_2. Chem Eng Process 48(1):532–537. doi:10.1016/j.cep.2008.06.013

Han C, Luque R, Dionysiou DD (2012) Facile preparation of controllable size monodisperse anatase titania nanoparticles. Chem Commun 48(13):1860–1862. doi:10.1039/c1cc16050h

Han C, Pelaez M, Likodimos V, Kontos AG, Falaras P, O'Shea K, Dionysiou DD (2011) Innovative visible light-activated sulfur doped TiO_2 films for water treatment. Appl Catal B-Environ 107(1–2):77–87. doi:10.1016/j.apcatb.2011.06.039

Hincapie M, Maldonado MI, Oller I, Gernjak W, Sanchez-Perez JA, Ballesteros MM, Malato S (2005) Solar photocatalytic degradation and detoxification of EU priority substances. Catal Today 101(3–4):203–210. doi:10.1016/j.cattod.2005.03.004

Ho L, Grasset C, Hoefel D, Dixon MB, Leusch FDL, Newcombe G, Saint CP, Brookes JD (2011) Assessing granular media filtration for the removal of chemical contaminants from wastewater. Water Res 45(11):3461–3472. doi:10.1016/j.watres.2011.04.005

Joss A, Keller E, Alder AC, Gobel A, McArdell CS, Ternes T, Siegrist H (2005) Removal of pharmaceuticals and fragrances in biological wastewater treatment. Water Res 39(14):3139–3152. doi:10.1016/j.watres.2005.05.031

Klamerth N, Miranda N, Malato S, Agueera A, Fernandez-Alba AR, Maldonado MI, Coronado JM (2009) Degradation of emerging contaminants at low concentrations in MWTPs effluents with mild solar photo-Fenton and TiO_2. Catal Today 144(1–2):124–130. doi:10.1016/j.cattod.2009.01.024

Kolpin DW, Furlong ET, Meyer MT, Thurman EM, Zaugg SD, Barber LB, Buxton HT (2002) Pharmaceuticals, hormones, and other organic wastewater contaminants in US streams, 1999–2000: a national reconnaissance. Environ Sci Technol 36(6):1202–1211. doi:10.1021/es011055j

Laera G, Jin B, Zhu H, Lopez A (2011) Photocatalytic activity of TiO2 nanofibers in simulated and real municipal effluents. Catal Today 161(1):147–152. doi:10.1016/j.cattod.2010.10.037

Li K, Huang Y, Yan L, Dai Y, Xue K, Guo H, Huang Z, Xiong J (2012) Simulated sunlight photodegradation of aqueous atrazine and rhodamine B catalyzed by the ordered mesoporous graphene-titania/silica composite material. Catal Commun 18:16–20. doi:10.1016/j.catcom.2011.11.008

Lin YM, Tseng YH, Huang JH, Chao CC, Chen CC, Wang I (2006) Photocatalytic activity for degradation of nitrogen oxides over visible light responsive titania-based photocatalysts. Environ Sci Technol 40(5):1616–1621. doi:10.1021/es051007p

Linsebigler AL, Lu GQ, Yates JT (1995) Photocatalysis on TiO_2 surfaces—principles, mechanisms, and selected results. Chem Rev 95(3):735–758. doi:10.1021/cr00035a013

McMurray TA, Dunlop PSM, Byrne JA (2006) The photocatalytic degradation of atrazine on nanoparticulate TiO_2 films. J Photoch Photobio A 182(1):43–51. doi:10.1016/j.jphotochem.2006.01.010

Miranda-Garcia N, Suarez S, Sanchez B, Coronado JM, Malato S, Ignacio Maldonado M (2011) Photocatalytic degradation of emerging contaminants in municipal wastewater treatment plant effluents using immobilized TiO_2 in a solar pilot plant. Appl Catal B-Environ 103(3–4):294–301. doi:10.1016/j.apcatb.2011.01.030

Mourao HAJL, Malagutti AR, Ribeiro C (2010) Synthesis of TiO2-coated CoFe2O4 photocatalysts applied to the photodegradation of atrazine and rhodamine B in water. Appl Catal A-Gen 382(2):284–292. doi:10.1016/j.apcata.2010.05.007

Parra S, Stanca SE, Guasaquillo I, Thampi KR (2004) Photocatalytic degradation of atrazine using suspended and supported TiO_2. Appl Catal B-Environ 51(2):107–116. doi:10.1016/j.apcatb.2004.01.021

Pelaez M, de la Cruz AA, Stathatos E, Falaras P, Dionysiou DD (2009) Visible light-activated N-F-codoped TiO_2 nanoparticles for the photocatalytic degradation of microcystin-LR in water. Catal Today 144(1–2):19–25. doi:10.1016/j.cattod.2008.12.022

Pelaez M, Falaras P, Kontos AG, de la Cruz AA, O'Shea K, Dunlop PSM, Byrne JA, Dionysiou DD (2012a) A comparative study on the removal of cylindrospermopsin and microcystins from water with NF-TiO_2-P25 composite films with visible and UV–vis light photocatalytic activity. Appl Catal B-Environ 121:30–39. doi:10.1016/j.apcatb.2012.03.010

Pelaez M, Falaras P, Likodimos V, Kontos AG, de la Cruz AA, Dionysiou DD (2011) Novel NF-TiO_2-P25 composite photocatalyst for the removal of microcystins and cylindrospermopsin under visible and solar light. Abstr Pap Am Chem S 241 (41-IEC)

Pelaez M, Falaras P, Likodimos V, Kontos AG, de la Cruz AA, O'Shea K, Dionysiou DD (2010) Synthesis, structural characterization and evaluation of sol–gel-based NF-TiO_2 films with visible light-photoactivation for the removal of microcystin-LR. Appl Catal B-Environ 99(3–4):378–387. doi:10.1016/j.apcatb.2010.06.017

Pelaez M, Nolan NT, Pillai SC, Seery MK, Falaras P, Kontos AG, Dunlop PSM, Hamilton JWJ, Byrne JA, O'shea K, Entezari MH, Dionysiou DD (2012b) A review on the visible light active titanium dioxide photocatalysts for environmental applications. Appl Catal B: Environ 125:331–349

Provata A, Falaras P, Xagas A (1998) Fractal features of titanium oxide surfaces. Chem Phys Lett 297(5–6):484–490. doi:10.1016/s0009-2614(98)01127-0

Rengifo-Herrera JA, Pierzchala K, Sienkiewicz A, Forro L, Kiwi J, Pulgarin C (2009) Abatement of organics and *Escherichia coli* by N, S co-doped TiO_2 under UV and visible light. Implications of the formation of singlet oxygen ($^1O_2$) under visible light. Appl Catal B-Environ 88(3–4):398–406. doi:10.1016/j.apcatb.2008.10.025

Rizzo L, Meric S, Guida M, Kassinos D, Belgiorno V (2009) Heterogenous photocatalytic degradation kinetics and detoxification of an urban wastewater treatment plant effluent contaminated with pharmaceuticals. Water Res 43(16):4070–4078. doi:10.1016/j.watres.2009.06.046

Scott D et al (2012) Biological nitrogen and carbon removal in a gravity flow biomass concentrator reactor for municipal sewage treatment. Chemosphere. doi:10.1016/j.chemosphere.2012.08.045

Subagio DP, Srinivasan M, Lim M, Lim T-T (2010) Photocatalytic degradation of bisphenol-A by nitrogen-doped TiO_2 hollow sphere in a vis-LED photoreactor. Appl Catal B-Environ 95(3–4):414–422. doi:10.1016/j.apcatb.2010.01.021

USEPA (2003) Interim Reregistration Eligibility Decision for Atrazine (Report of the United States Environmental Protection Agency). USEPA, Washington Case No. 0062

WHO (2002) WHO model list of essential medicines. World Health Organization Drug Information 16(2):139–150

Yalap KS, Balcioglu IA (2009) Effects of inorganic anions and humic acid on the photocatalytic and ozone oxidation of oxytetracycline in aqueous solution. J Adv Oxid Technol 12(1):134–143

Zahraa O, Sauvanaud L, Hamard G, Bouchy M (2003) Kinetics of atrazine degradation by photocatalytic process in aqueous solution. Int J Photoenergy 5(2):87–93. doi:10.1155/s1110662x03000187

PUBLICATION V

H. Barndõk, D. Hermosilla, C. Han, D.D. Dionysiou, C. Negro, A. Blanco

Degradation of 1,4-dioxane from industrial wastewater by solar photocatalysis using immobilized NF-TiO_2 composite with monodisperse TiO_2 nanoparticles

Applied Catalysis B: Environmental 180 (2016) 44-52

Applied Catalysis B: Environmental 180 (2016) 44–52

Contents lists available at ScienceDirect

Applied Catalysis B: Environmental

journal homepage: www.elsevier.com/locate/apcatb

Degradation of 1,4-dioxane from industrial wastewater by solar photocatalysis using immobilized NF-TiO_2 composite with monodisperse TiO_2 nanoparticles

Helen Barndõk[a], Daphne Hermosilla[a,*], Changseok Han[b], Dionysios D. Dionysiou[b], Carlos Negro[a], Ángeles Blanco[a]

[a] Department of Chemical Engineering, Universidad Complutense de Madrid, Avda. Complutense, s/n, 28040 Madrid, Spain.
[b] Environmental Engineering and Science Program, Department of Biomedical, Chemical and Environmental Engineering (DBCEE), University of Cincinnati, Cincinnati, OH, USA.

ARTICLE INFO

Article history:
Received 24 February 2015
Received in revised form 24 May 2015
Accepted 11 June 2015
Available online 16 June 2015

Keywords:
NF-TiO_2
Monodisperse titania
Immobilized catalyst
Photocatalysis
1,4-Dioxane

ABSTRACT

The degradation of 1,4-dioxane was accomplished by solar photocatalysis using an immobilized nitrogen and fluorine co-doped titanium dioxide (NF-TiO_2) composite with monodisperse TiO_2 nanoparticles. The effect of different wastewater matrices was studied, and the treatment of an industrial effluent contaminated with 1,4-dioxane was carried out. Compared to the degradation rate in a synthetic solution ($k_{dioxane} = 0.34 \pm 0.02\ h^{-1}$), 1,4-dioxane removal decreased in the industrial wastewater ($k_{dioxane} = 0.27 \pm 0.01\ h^{-1}$) due to the presence of inorganic constituents, whereas, the increase of the effluent pH to 6.9 produced only a slight decrease of the photocatalytic efficiency ($k_{dioxane} = 0.31 \pm 0.01\ h^{-1}$). In the photocatalytic treatment of the industrial effluent, almost complete degradation of 1,4-dioxane (≤100%) was achieved along with 65% and 50% removal of COD and TOC, respectively. Moreover, remarkably similar results (about 50% of COD removal in 6 h) were achieved using both the immobilized lab-made catalyst and the commercial P25-TiO_2. In the chromatographic study of metabolites, ethylene glycol diformate, ethylene glycol monoformate, and formic acid were identified as major reaction intermediates, and thereby, the main reaction pathways have been proposed. The progressive decrease of the partial oxidation efficiency down to about 0.2 and the moderate increase of the mean oxidation state of carbon in the solution (up to +0.5) indicate that a complete mineralization of the contamination from the current industrial effluent could be feasible using this supported catalyst.

1. Introduction

Continuous xenobiotic contamination of water by 1,4-dioxane is an emerging problem due to its adverse impact on human health. This widely used industrial solvent and common by-product from several chemical processes is known to induce kidney failure and liver damage. Furthermore, since animal studies reported its tumour promoter properties, it has been classified as a probable human carcinogen (Group 2B) [1–5].

Although several modified biological processes have attained the biodegradation of 1,4-dioxane at low concentrations and long residence times [6–8], 1,4-dioxane is easily found in the downstream of industrial effluents, which indicate the inefficiency of traditional secondary treatments for complete removal of this compound [5,9,10].

As it is well known, advanced oxidation processes (AOPs) are able to effectively decontaminate effluent streams containing biorefractory organic substances [11–14]. In particular, titanium dioxide (TiO_2)-based photocatalysis offers several potential advantages with respect to typical Fenton-based AOPs such as milder reaction conditions, more flexibility in operation variables, and no waste/sludge production [15]. TiO_2 is suitable for water treatment purposes since it is an inert and rather inexpensive material [16,17]. Moreover, solar light is an economical alternative for the UV radiation, as the expense of electricity constitutes one of the major drawbacks for the implementation of photocatalytic water treatment and, thus, more and more research is focusing on sunlight-driven photo-reactors [18–21].

* Corresponding author. Fax: +34 91 394 4243.
E-mail addresses: hbarndok@quim.ucm.es (H. Barndõk), dhermosilla@quim.ucm.es (D. Hermosilla), hanck@mail.uc.edu (C. Han), dionysios.d.dionysiou@uc.edu (D.D. Dionysiou), cnegro@quim.ucm.es (C. Negro), ablanco@quim.ucm.es (Á. Blanco).

http://dx.doi.org/10.1016/j.apcatb.2015.06.015
0926-3373/

The traditional TiO_2-based photocatalysis in slurry suspension [13,22–28] requires a subsequent filtration step to remove TiO_2 particles from water, increasing the treatment cost. The immobilization of the photocatalyst is of great interest to enhance the process engineering since it allows a straight-forward separation and recovery of the catalyst from the process stream [13,26,29–31]. Immobilization, on the other hand, could restrict the reactant mass transfer [13,26], which is the main obstacle to overcome in the ongoing research regarding the industrial viability of supported photocatalysts.

Several methods have been reported to enhance the photocatalytic properties of titania, including doping, dye-sensitization, noble metal deposition, and coupled semiconductors [16,32–36]. For instance, the addition of gold nanoparticles on the surface of TiO_2 powder has been reported to increase the photocatalytic degradation of 1,4-dioxane in a slurry [25], yielding removals close to 60% in 4 h. With regard to immobilized TiO_2, however, very few studies deal with the photodegradation of 1,4-dioxane on modified TiO_2. Nakajima et al. [37] reported a 30% removal of the compound in 4 h of UV radiation using TiO_2–$Cs_{2.5}H_{0.5}PW_{12}O_{40}$ hybrid films.

Among the various approaches, non-metal doping is an advantageous technique to improve the photoactivation of TiO_2 at a broader range of solar spectrum compared to metal-doped TiO_2, since the possible toxicity emission associated to metal leaching diminishes its potential for environmental applications. Successful water remediation was obtained by nitrogen and fluorine doped titania (NF-TiO_2) [38], and the immobilization of this catalyst resulted in active and mechanically stable photocatalytic films [31]. Moreover, the optical and physicochemical properties of the film for NF-TiO_2 photocatalysis were improved by adding P25-TiO_2 nanoparticles into the NF-TiO_2 sol–gel [39]. In a recent study [40], the incorporation of lab-made monodisperse titania nanoparticles [29] layer-by-layer on NF-TiO_2, instead of the direct addition of P25-TiO_2, further improved the catalyst, resulting in an effective degradation of various wastewater contaminants. However, the performance of immobilized NF-TiO_2 composite with monodisperse TiO_2 (NF-TiO_2-monodisp.TiO_2) has not been tested on heavily loaded industrial effluents containing contaminants such as 1,4-dioxane.

In fact, photocatalytic degradation studies of 1,4 dioxane have all been performed in synthetic solutions with ultrapure water [13,22–28,37,41,42], whereas, usually very low initial concentrations are treated. Thus, although the substantial concentrations of salts and alkalinity often present in wastewaters could abate the effectiveness of the photocatalysis [24,43,44], their effect on the removal of 1,4-dioxane from heavily loaded industrial effluents by photocatalysis has not been assessed yet.

Therefore, in this study, the treatment of wastewaters containing 1,4-dioxane by solar photocatalysis using an immobilized NF-TiO_2-monodisp.TiO_2 as photocatalyst was studied. The effect of various wastewater matrices on the removal of 1,4-dioxane was studied and a treatment of an industrial wastewater contaminated with 1,4-dioxane was carried out. Comparative experiments were also conducted with commercial P25-TiO_2 in suspension. Furthermore, the main reaction pathways were proposed by identifying the major reaction intermediates of solar light-induced NF-TiO_2 photocatalysis of 1,4-dioxane.

2. Materials and methods

2.1. Wastewater samples

Industrial wastewater contaminated by 1,4-dioxane outflowing a biological treatment was supplied by a chemical factory. A synthetic solution (140 mg L^{-1}) of 1,4-dioxane (Sigma–Aldrich® Chemie GmbH, Steinheim, Germany) was also prepared with ultrapure deionized water. The initial pH of the synthetic solution was 5.7. Since the industrial wastewater under concern had a relatively high bicarbonate alkalinity and concentration of inorganic salts (Table 1) as well as a pH higher than the one of a synthetic solution, the effect of these characteristics on the degradation of 1,4-dioxane by solar light-induced NF-TiO_2 photocatalysis was investigated. Therefore, the experiments were run at pH 6.9, analogous to the industrial effluent, achieved either by adding sodium hydroxide (Panreac S.A., Barcelona, Spain) or by simulating the inorganic content of the industrial wastewater with calcium chloride, magnesium heptahydrate, sodium bicarbonate, and sulphuric acid, supplied by Panreac S.A. (Barcelona, Spain).

Table 1
Main characteristics of the industrial effluent.

Characteristic	Value
1,4-Dioxane, mg$C_4H_8O_2$ L^{-1}	135–140
COD, mgO_2 L^{-1}	245–255
TOC, mgC L^{-1}	76–80
pH	6.9
Conductivity, mS cm^{-1}	2.44
Alkalinity, mg$CaCO_3$ L^{-1}	270–280
Chlorides, mgCl^- L^{-1}	500–550
Sulphates, mgSO_4^{2-} L^{-1}	240–260

2.2. Photocatalysts

Aeroxide® P25-TiO_2 photocatalyst with a specific surface area (BET) of 50 ± 15 m^2 g^{-1}, pore volume of 0.25 m^3 g^{-1} and an average primary particle size of 21 nm was supplied by Evonik (Essen, Germany). The composite NF-TiO_2-monodisp.TiO_2 films were prepared by a modified method reported by Barndõk et al. [40]. Briefly, two different TiO_2 solutions were alternately deposited on a borosilicate substrate by dip-coating using a so-called layer-by-layer method (6 layers in total). The NF-TiO_2 sol was prepared using a modified sol–gel method similar to that reported by Pelaez et al. [31], and the solution of monodisperse anatase titania with a particle size of 50 nm was synthesized by a method described by Han et al. [29]. Shortly, the NF-TiO_2 sol was made up of fluorosurfactant Zonyl FS 300 (Fluka, Steinheim, Germany), isopropyl alcohol (Panreac S.A., Barcelona, Spain), glacial acetic acid (Panreac, S.A., Barcelona, Spain), ethlyenediamine (Fluka, Steinheim, Germany), and titanium tetraisopropoxide (TTIP; Sigma–Aldrich® Chemie GmbH, Steinheim, Germany). Monodisperse anatase titania sol was prepared by adding TTIP to methanol (Panreac S.A., Barcelona, Spain) in the presence of $CaCl_2$. Each layer was prepared using a home dip-coating apparatus with an average dipping-withdrawal speed of 12.5 cm min^{-1}, whereas, after each coating, the film was dried with an infrared lamp for 20 min and subsequently calcined at 400 °C during 30 min and cooled down naturally.

2.3. Characterization of the films

The crystallographic structure of the synthesized TiO_2 films was determined by X-ray diffractometry (XRD) using a Grazing incident method in a Philips X'pert pro MRD instrument with a parabolic mirror in the primary optic and a parallel plate collimator with a secondary monochromator in the secondary optic. The radiation used was Cu K–α (λ = 1.54 Å). The Brunauer–Emmett–Teller (BET) surface area, pore volume, porosity, Barret–Joyner–Halenda (BJH) pore size and distribution were determined by ASAP 2020 physisorption analyzer (Micromeritics). Before the analysis, the samples were purged with N_2 for 2 h at 150 °C. The morphology of the catalytic film was characterized with a JEOL 7600F scanning electron microscope (SEM). For SEM analysis, the films were coated

with carbon. To obtain detail information of the crystal size and structure at nanoscale, transmission electron microscopy (TEM) was carried out with a JEM 3000F microscope (point resolution of 0.17 nm). For TEM analysis, the samples were ultrasonically dispersed in butanol (99.5%, Panreac, Spain) and then deposited on a copper grid covered with a holey carbon film. For BET, XRD and TEM analyses, powdered samples were obtained by scraping the TiO_2 films.

2.4. Dark adsorption experiments

20 mL of 1,4-dioxane solution of various initial concentrations (25, 50, 100, 150 and 200 mg L^{-1}) were kept for 24 h in contact with two immobilized NF-TiO_2-monodisp.TiO_2 films with a total coated area of 25 cm^2 on the substrates inside sealed plastic vessels under dark conditions. Blank control reactors containing 1,4-dioxane without the photocatalyst were also left in the dark for 24 h. The experiments were carried out in triplicates, and TOC was used as an analytical parameter to assess the change in the concentration of 1,4-dioxane in the solution.

2.5. Photocatalytic experiments

The photocatalytic degradation of 1,4-dioxane was carried out in a borosilicate glass vessel reactor (i.d. 11.5 cm) containing 50 mL of actual or synthetic wastewater (approx. 0.50 cm of aqueous irradiated layer) and 5 photocatalytic films with a total coated area of 75 cm^2. The quartz cover of the reactor was sealed with parafilm and a fan was used to cool the air and prevent evaporation. The solution was irradiated with a Solar Simulator supplied by Newport (Irvine, USA) equipped with a Xe lamp (1000 W m^{-2}) and a correction filter (ASTM E490-73a) to obtain the solar spectrum under ideal conditions. The total power radiated in the visible and UV region was 106.5 W (51.7% and 48.3%, respectively). Major emission bands (>3%) were located at 578.0 nm (17.4%); 546.1 nm (16.0%); 435.8 nm (10.9%); 404.5 nm (7.5%); 366.0 nm (6.3%); 334.1 nm (4.4%); 313.0 nm (3.9%); 302.5 nm (3.7%); 296.7 nm (3.6%); 289.4 nm (3.2%); 280.4 nm (3.0%); and 253.7 nm (3.6%). The light intensity on the illuminated liquid surface was 80 mW cm^{-2} within 315–400 nm at the mid-surface of the Xe lamp, measured with a radiant power meter RM21 (Dr. Göbel UV-elektronik GmbH, Ettlingen, Germany). The experiments were carried out in triplicates.

When the experiments were conducted using the P25-TiO_2 in suspension instead of immobilized films, a loading of 1.24 g L^{-1} of photocatalyst was chosen, corresponding to the available specific catalytic surface that was equal to the one available using immobilized catalysts, taking into account the BET surface area of both photocatalysts.

2.6. Analytical methods

All the analyses were performed according to the standard methods for the examination of water and wastewater [45]. Chemical oxygen demand (COD) was measured by the colorimetric method at 600 nm using an Aquamate-spectrophotometer (Thermos Scientific AQA 091801, Waltham, USA). Total organic carbon (TOC) was measured using a TOC/TN analyzer multi N/C® 3100 (Analytik Jena AG, Jena, Germany) with catalytic oxidation on cerium oxide at 850 °C. Conductivity was measured with a non ionic-selective conductivity probe GLP 31 (Crison, S.A., Barcelona, Spain). The pH was measured using a model GLP 21 pH-meter (Crison, S.A., Barcelona, Spain) and alkalinity was measured by titration with sulphuric acid 0.1N using a pH electrode connected to an automatic titrator Compact I (Crison, S.A., Barcelona, Spain). Sulphate content was determined by turbidimetric method and chloride concentration was measured colorimetrically by Spectroquant® Chloride Test (Merck KGaA, Darmstadt, Germany).

1,4-Dioxane and its metabolites, ethylene glycol diformate (EGDF), and ethylene glycol monoformate (EGMF) were identified and quantified by an Agilent 6890N gas chromatograph (GC, Palo Alto, CA) equipped with a quadrupole mass spectrometer (MS) Agilent 5975B. To extract these two volatile compounds from the water samples, an internal standard (5 mg L^{-1} of octanol) and 1.4 g of ammonium sulphate were added to 10 mL of sample, and the solution was extracted threefold with dichloromethane (40:10:10 mL). The organic fraction was dried on anhydrous sodium sulphate and concentrated to 1 mL under nitrogen flux in a Kuderna–Danish apparatus (Sigma, St. Louis, MO) and analysed by GC–MS as follows. Samples (3 μL) were injected in split mode (30:1), and volatiles were separated using a fused silica capillary column (HP-INNOWAX) (30 × 0.25 mm i.d. and 0.25 μm film thickness), supplied by Agilent (Madrid, Spain). The pressure of the GC-grade He carrier gas was 7.7 psi with a linear velocity of 1.0 mL min^{-1}; the initial oven temperature was 45 °C, first increased at 3 °C min^{-1}–100 °C, held for 1 min, and then heated at 15 °C min^{-1}–270 °C, and held at this temperature for an additional 5 min. The injection temperature was 230 °C. Detection was carried out by electron ionization (EI) mode (70 eV), interphase detection temperature was 290 °C (MS source at 230 °C and MS quad at 150 °C) and scanning mass was ranged between 35 and 400 amu. Quantitative determinations were carried out by the internal standard method, using peak areas obtained from selected ion monitoring (88, 1,4-dioxane; 60, EGDF/EGMF; 45, octanol) and calibrations made with pure reference compounds analyzed under the same conditions.

1,4-Dioxane was also quantified together with ethylene glycol as its possible degradation product, using gas–liquid chromatography (GLC) on a 7980A instrument (Agilent Technologies Inc., Palo Alto, CA) equipped with a flame ionization detector. The temperatures of the injector and detector were 310 °C and 280 °C, respectively. Samples (2 μL) were injected using the pulsed-split mode (split ratio 5:1) and analyzed in a TRB-FFAP (Teknokroma, Sant Cugat del Vallès, Spain) fused silica column (30 m × 0.25 mm internal diameter × 0.25 μm film thickness) with He (43 psi) as carrier gas and the following temperature programm: 80 °C–240 °C after 9 min initial hold and at a 15 °C min^{-1} ramp rate. Peaks were identified according to the relative retention times of commercial standards. Quantification was performed according to peak area, corrected with the response factors calculated for each compound using 1-butanol (250 ppm) as internal standard, and the software GC-ChemStation Rev.B.04.02 (96) from Agilent.

Oxalic, acetic, formic, glycolic, and methoxyacetic acids were identified and quantified by ion chromatography (IC) using a 940 Professional IC Vario instrument (Metrohm, Herisau, Switzerland) equipped with a conductivity detector. An isocratic gradient of Na_2CO_3 (3.6 mM) was used as eluent, keeping an eluent flow at 0.7 mL min^{-1}. The injection loop was 50 mL. Analysis was done in an ionic resin column Metrosep A Supp 7 with a guard column Metrosep A Supp 4/5 Guard.

2.7. Determination of the mean oxidation state of carbon and the partial oxidation efficiency

The mean oxidation state of carbon (MOSC) for a single organic molecule was calculated using Eq. (1) [46]:

$$\mathrm{MOSC}_{\mathrm{compound}} = \frac{\sum_{i=n}^{n} \mathrm{OSC}_i}{n} \quad (1)$$

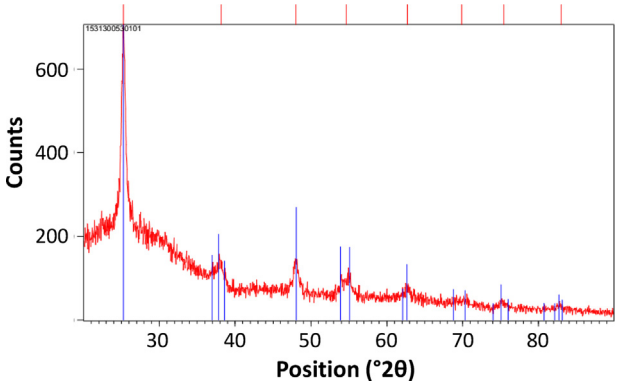

Fig. 1. XRD pattern of NF-TiO_2-monodisp.TiO_2 catalytic film.

where n is the number of carbon (C) atoms and OSC_i is the oxidation state of the ith C atom in the molecule. The determination of OSC_i is illustratively described by Ashenhurst [47].

The MOSC of wastewater was calculated from the values of TOC and COD, using Eq. (2) [46,48–50]:

$$MOSC_{wastewater} = 4 - 1.5\frac{COD}{TOC} \quad (2)$$

where COD and TOC are given in $mgO_2\ L^{-1}$.

Partial oxidation efficiency ($\mu_{CODpartox}$) was calculated by Eq. (3), where the COD of partial oxidation (COD_{partox}) was defined by Eq. (4) [48,49]:

$$\mu_{COD_{partox}} = \frac{COD_{partox}}{COD_0 - COD} \quad (3)$$

$$COD_{partox} = \frac{COD_0 \times TOC}{TOC_0} - COD \quad (4)$$

3. Results and discussion

3.1. Structural characteristics of the composite films

According to the XRD pattern of the prepared films (Fig. 1), all peaks corresponding to anatase phase at $2\theta = 25.3$, 38.0, 48.1, 54.6, 62.6, 70.5, 75.2 and 82.9, were detected by XRD analysis (JCPDF card no 00-021-1272). This indicates that anatase, the most active phase among TiO_2 phases, was synthesized with this method. Dopant-related crystal phases were not observed since the amount of N and F does not produce significant changes in the TiO_2 structure [31]. Based on the rough estimation obtained from XRD data, the crystalline size was calculated to be 8.62 nm (Table 2).A defined crystalline interconnected network can be observed from TEM images (Fig. 2), whereas, the lattice spacing of 0.352 nm, corresponding to the 1 0 1 plane of TiO_2, is well observed by the higher magnification, providing evidence on high crystallinity. According to the TEM images, there were two different size groups of particles, one with the size around 20 nm and the other one smaller than 10 nm since two different methods were used to prepare these catalyst films. With regard to monodisperse particles, it is not easy to observe their unique structure with TEM analysis because they are actually aggregates of smaller nanosized particles. The discrepancy between the crystallite sizes obtained from BET and XRD data (the degree of agglomeration, D_{BET}/D_{XRD}) indicates that the titania particles were quite highly aggregated. Considering the SEM analysis (Fig. 3), the films had a rough and porous surface quite similar to the previous findings [40]. According to the porosimetry analysis, the immobilized catalyst had a relatively moderate BET surface of $69.5\ m^2\ g^{-1}$ and porosity of 33.6%. All the main physicochemical properties are listed in Table 2.

Table 2
Physicochemical properties of NF-TiO_2-monodisp.TiO_2.

Characteristic	Value
Crystal phase	Anatase
Crystal size (D_{XRD})[a](nm)	8.62
$D_{(101)}$[b](nm)	0.352
BET surface, $m^2\ g^{-1}$	69.5
Crystal size (D_{BET})[c](nm)	22.1
Pore volume, $cm^3\ g^{-1}$	0.133
Porosity[d], %	33.6
Agglomeration (D_{BET}/D_{XRD})	2.57

[a] Based on XRD, using Scherrer equation: $D = 0.9\lambda/(B \times \cos\theta)$; B = full width at half maximum (FWHM) of the highest peak, $\lambda = 0.154$ nm.
[b] Based on Bragg's Law: $D = \lambda/(2 \times \sin\theta)$.
[c] Obtained from BET, using $D = 6000/(\rho_{anatase} \times S_{BET})$; $\rho_{anatase} = 3.9\ g^3$ cm.
[d] Based on pore volume and $\rho_{anatase}$.

Table 3
First order kinetic constants of 1,4-dioxane degradation and the linear removal rates of TOC in the solar photocatalytic treatment of 1,4-dioxane using NF-TiO_2-monodisperse TiO_2 films under different wastewater conditions.

	$k_{dioxane}$ (1st order)	k_{TOC} (linear)
Wastewater matrix	h^{-1}	$mg\ L^{-1}\ h^{-1}$
pH 5.7 (as it is)	0.34 ± 0.02	5.65 ± 0.10
pH 6.9 (+NaOH)	0.31 ± 0.01	5.62 ± 0.34
Simulated salt content	0.26 ± 0.02	4.70 ± 0.36
Industrial effluent	0.27 ± 0.01	4.16 ± 0.34

3.2. Dark adsorption

No significant adsorption of 1,4-dioxane on the supported catalyst was found during the experiments under dark conditions at different initial concentrations. The different solution pH (5.7 and 6.9) and the presence of inorganic salt content, simulating the industrial effluent, did not affect the adsorption of 1,4-dioxane either. The differences in final TOC compared with blank experiments without NF-TiO_2-monodisp.TiO_2 catalyst were statistically insignificant ($p > 0.05$) in all wastewater matrices.

3.3. Photocatalytic degradation

3.3.1. Kinetics of 1,4-dioxane degradation in different wastewater matrices

The photocatalytic treatment of 1,4-dioxane in various wastewater matrices resulted in the linear removal of TOC in time, whereas, 1,4-dioxane removal was concentration dependent, decreasing in time (Table 3). First order kinetic models for 1,4-dioxane degradation in various wastewater matrices (Fig. 4) and the corresponding kinetic constants ($k_{dioxane}$, Table 3) indicate that 1,4-dioxane removal diminished in the industrial wastewater compared to synthetic water. The degradation rate in terms of the half-life of 1,4-dioxane was in the following decreasing order for different wastewater conditions: pH 5.7 ($t_{1/2} = 124$ min) > pH 6.9 ($t_{1/2} = 134$ min) > pH 6.9, industrial effluent ($t_{1/2} = 156$ min) > pH 6.9, simulated salt content ($t_{1/2} = 161$ min). However, the difference between the overall 1,4-dioxane removals at pH 5.7 and 6.9 (90% and 88%, respectively) were insignificant, which implies that the decrease in photocatalytic degradation rates was caused by the presence of inorganic constituents.

In fact, when considering the mineralization of organics in terms of TOC removal (k_{TOC}, Table 3), no significant differences were found, neither between the experiments at pH 5.7 and pH 6.9, nor between the experiments comparing industrial effluent and synthetic water with simulated salt content. The degradation of TOC per unit area of the coated catalyst surface (Fig. 5) was about $3.4\ \mu gC\ cm^{-2}\ h^{-1}$ in synthetic wastewaters at both pH 5.7 and pH 6.9; whereas, about $2.8\ \mu gC\ cm^{-2}\ h^{-1}$ was degraded in both the

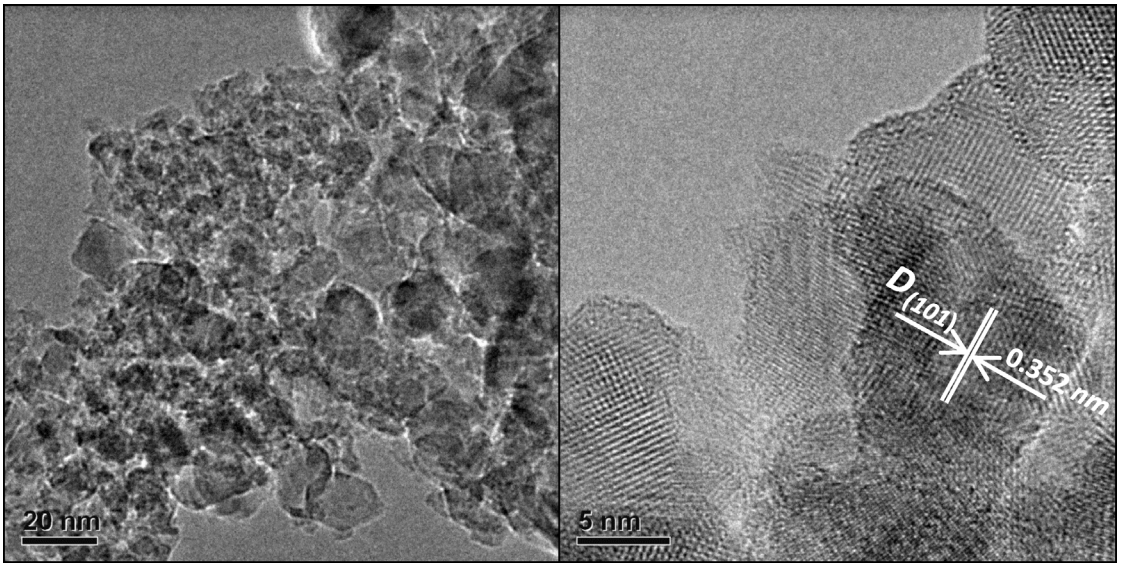

Fig. 2. TEM image of NF-TiO_2-monodisp.TiO_2 catalytic film.

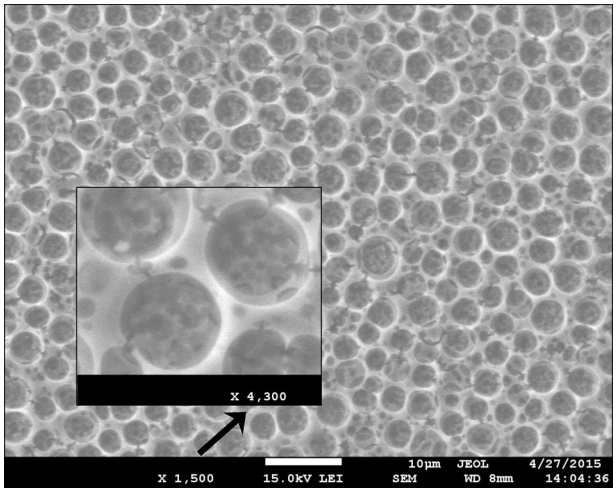

Fig. 3. SEM image of NF-TiO_2-monodisp.TiO_2 catalytic film.

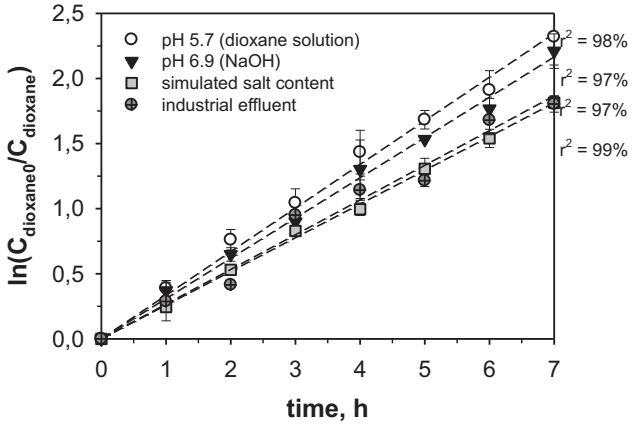

Fig. 4. First order kinetic model for the solar photocatalytic degradation of 1,4-dioxane on immobilized NF-TiO_2-monodisp.TiO_2 under different wastewater conditions.

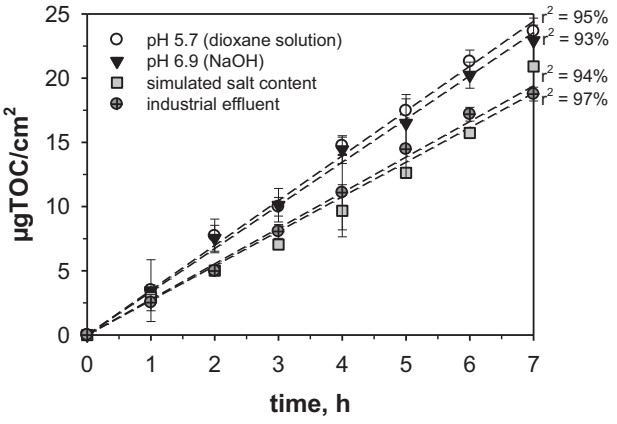

Fig. 5. Decomposition amount of TOC per unit of film area in the solar photocatalytic degradation of 1,4-dioxane on immobilized NF-TiO_2-monodisp.TiO_2 under different wastewater conditions.

industrial effluent and synthetic water with previously added salt content.

Since the surface of NF-TiO_2 is negatively charged at pH above ≈6 [38] and the molecule of 1,4-dioxane acts as an electron donor by its definition as a Lewis base [51], an inhibition in the photocatalytic degradation of 1,4-dioxane at pH above 6 could be expected due to the repulsive electrostatic forces between the catalyst and the contaminant. However, the results of this study show that this effect is not pronounced in a great extent at the pH of the real industrial effluent (pH 6.9).

On the other hand, when the inorganic content was present, either initially in the industrial effluent or in a form of added salts, the photocatalytic degradation of both 1,4-dioxane and TOC decreased (Figs. 5 and 6). The negative effect of inorganic anions on the efficiency of photocatalytic oxidation has been attributed to various mechanisms, such as •OH radical and "hole" scavenging [43], and competitive adsorption [44]. Although the adsorption of 1,4-dioxane on the surface of NF-TiO_2-monodisperse TiO_2 was found to be negligible for all the wastewater matrices (Section 3.2.), there is always a concentration gradient through a molecular transfer toward the catalyst surface because the photocatalytic degradation is expected to occur at the liquid–solid interface [52,53]. Therefore, the concentration and adsorption of inorganic

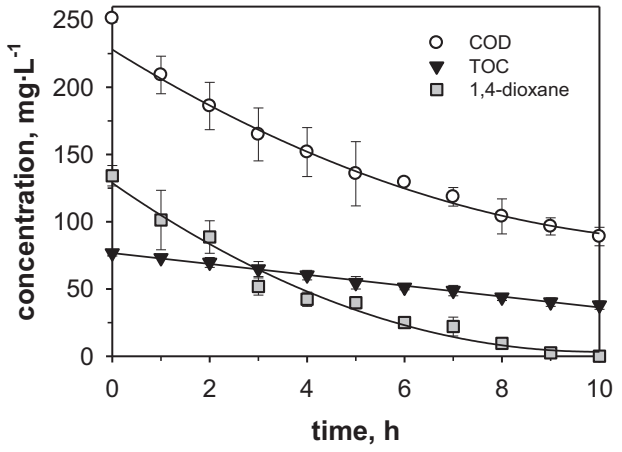

Fig. 6. The evolution of the concentrations of 1,4-dioxane, COD and TOC in the treatment of an industrial effluent containing 1,4-dioxane by solar photocatalysis using NF-TiO_2-monodisp.TiO_2 films.

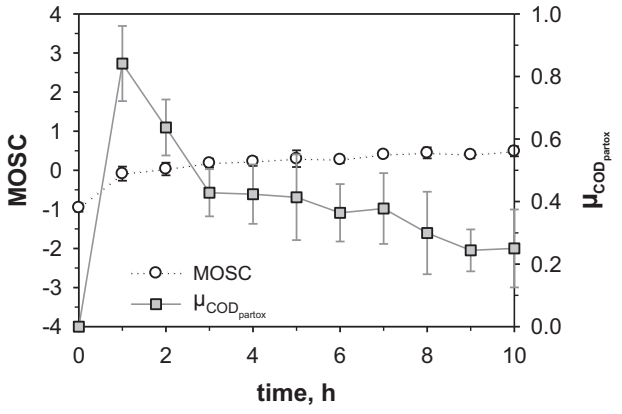

Fig. 7. The evolution of the mean oxidation state of carbon (MOSC) and the partial oxidation efficiency ($\mu_{CODpartox}$) in the treatment of an industrial effluent containing 1,4-dioxane by solar photocatalysis using NF-TiO_2-monodisp.TiO_2 films.

anions on the surface of TiO_2 could result in a loss of active sites for the oxidation of organic molecules [43,44].

On the other hand, our previous research [54] and the investigation performed by Merayo et al. (2013, unpublished research) shows that the inorganic content could reduce the photocatalytic efficiency simply due to the increase of ionic strength or by modifying the solution pH. According to a previous study, neither sulphates nor chlorides affect the UV/TiO_2 oxidation of phenol, whereas, carbonates decrease its removal along with the increasing pH [54]. However, no important negative effect on the 1,4-dioxane degradation was found under the higher pH conditions of the industrial wastewater, as discussed above (Figs. 4 and 5).

3.3.2. *Photocatalytic treatment of industrial wastewater containing 1,4-dioxane*

In the photocatalytic treatment of an industrial effluent, the degradation of 1,4-dioxane (≤100%) was almost completed along with the 65% and 50% removal of COD and TOC, respectively (Fig. 6). While the concentration of TOC decreased in a linear manner, the degradation of COD followed a trend similar to that of 1,4-dioxane removal (the first order rate constant was $k_{COD} = 0.11\ h^{-1}$, $r^2 = 97\%$), which implies the accumulation and slower degradation of reaction intermediates produced during the photocatalysis.

Both the identification and quantification of the multiple reaction products by chromatographic analyses can be extremely laborious and expensive for the complex industrial wastewater.

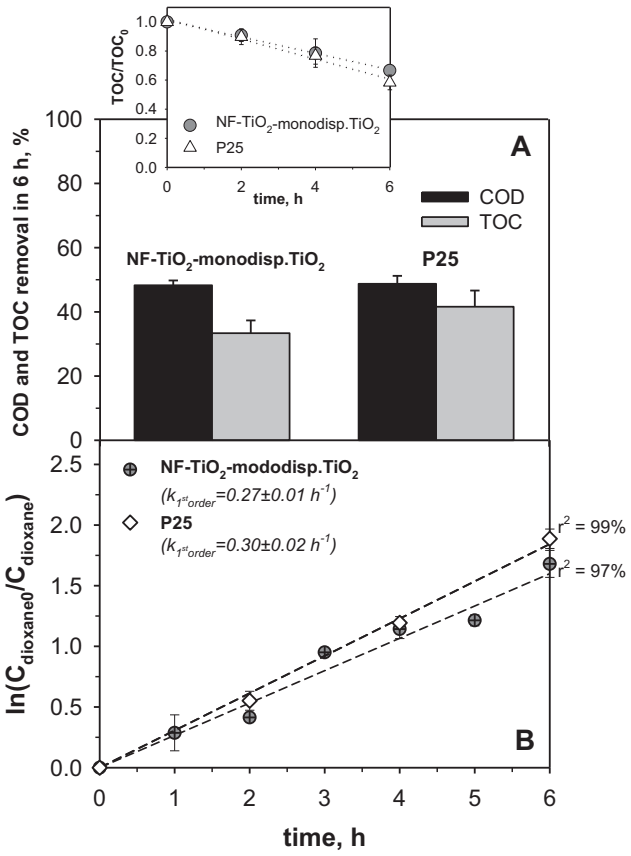

Fig. 8. Comparison of COD and TOC removals after 6 h of solar photocatalytic degradation of an industrial effluent containing 1,4-dioxane using an immobilized film of NF-TiO_2-monodisp.TiO_2 and commercial TiO_2-P25 (Aeroxide®) in suspension.

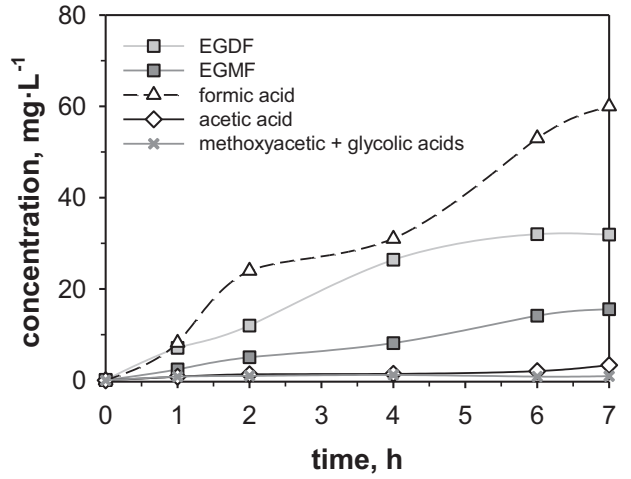

Fig. 9. Primary reaction intermediates in the photocatalytic degradation of 1,4-dioxane under solar light using immobilized NF-TiO_2-monodisp.TiO_2.

Nevertheless, the MOSC (Eqs. (1) and (2)) can be a useful parameter to understand reaction development during wastewater treatment, providing valuable information about the possible oxidative transformations [46,48–50]. MOSC can vary from −4 (e.g., CH_4) to +4 (e.g., CO_2); however, as CO_2 is released from the solution, it does no account for the solution MOSC, which is a proportional average of the molecular MOSC values of all the compounds present in the effluent. The $\mu_{CODpartox}$ (Eq. (3)) provides a better understanding of the mineralization capacity of an oxidative system, indicating

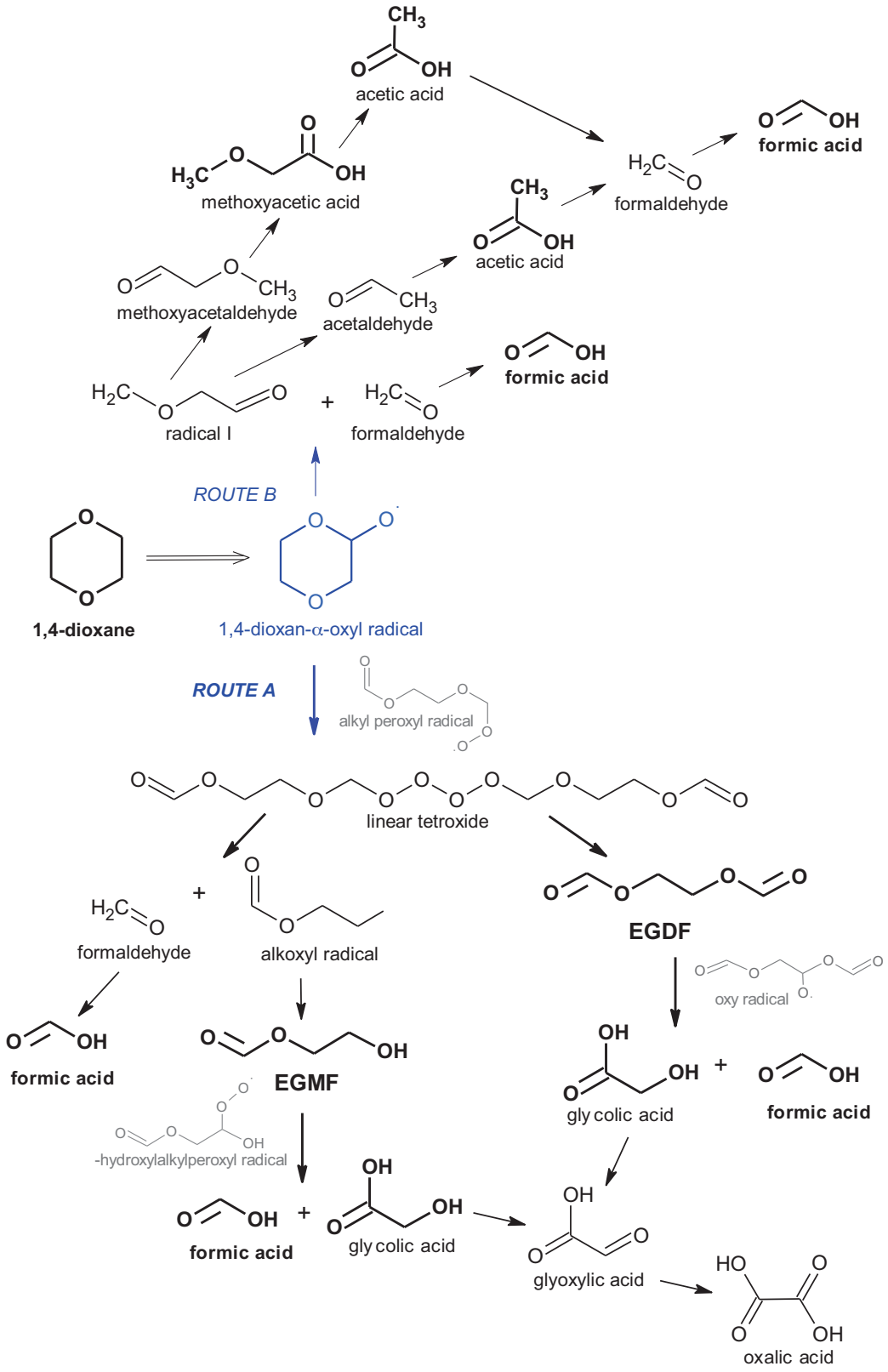

Fig. 10. Simplified schematic of the major reaction pathways proposed for 1,4-dioxane degradation

the percentage of COD decrease that does not lead to mineralization, but result in oxygenated products other than CO_2 and H_2O (COD_{partox}).

In the photocatalytic treatment of the industrial effluent using immobilized NF-TiO_2-monodisp.TiO_2, the MOSC of the wastewater increased from about −1 to 0 in the first 60 min, as 1,4-dioxane molecule ($MOSC_{dioxane} = -1$) was being oxidized; and continued to increase more slowly during the rest of the experiment, indicating an accumulation of reaction intermediates with an average MOSC of about +0.5 (Fig. 7). This is in accordance with the following chro-

matographic study (section 3.3.3) where EGDF ($MOSC_{EGDF}$ = +1) and EGMF ($MOSC_{EGMF}$ = 0) were found as major primary metabolites. Although the solution MOSC remained relatively low, the $\mu_{CODpartox}$ progressively decreased to about 0.2, as expected when organics are degraded to CO_2 and water [48,49]. Therefore, rapid mineralization of simpler carboxylic acids is suspected.

According to Nakajima et al. [37], the low decomposition of EGDF during photocatalysis is due to its poor affinity with TiO_2. In the photocatalytic treatment of waters contaminated by 1,4-dioxane, the fastest removal rates are usually reported using commercial P25-TiO_2 in suspension [24,26]. To improve the cost-effectiveness of the process, immobilization of the photocatalysts is of great interest, as the separation and recovery of the catalyst from the process stream is straight-forward [13,26,29–31]. In order to compare the performance of the immobilized NF-TiO_2-monodisp.TiO_2 catalyst with the P25-TiO_2 slurry suspension, experiments were carried out using a concentration of P25 that corresponds to the available specific catalytic surface that was equal to the one available using the immobilized catalysts, taking into account the BET surface area of both photocatalysts. These experiments, however, resulted in COD and TOC removals remarkably similar to the ones obtained by the immobilized catalyst (Fig. 8A). Namely, in the same treatment period of 6 h, 49% and 50% COD, and 34% and 40% TOC were respectively removed when using NF-TiO_2-monodisp.TiO_2 films and P25 suspension. In fact, differences were statistically insignificant ($P > 0.05$). The first order rate constant for the degradation of 1,4-dioxane was only slightly higher with P25 suspension (Fig. 8B). Obtaining results by an immobilized catalyst which are similar as those obtained by P25 in suspension is an encouraging result. Generally, the superiority of P25 catalyst is well-known and higher removals are always reported when working with slurry systems [13,26].

The slow but persistent removal of carbon in the experiments with the supported catalyst reflects that a complete mineralization of contamination from the real industrial effluent could be feasible using immobilized NF-TiO_2-monodisp.TiO_2. Total mineralization could be reached either by elongating the reaction time or, preferably, by increasing the catalyst surface. Thus, a further study on optimizing the reactor design would be of great interest. Using an immobilized catalyst would permit working without the need of an additional costly filtration step, which would greatly enhance the engineering of the process [13,26,29–31].

3.3.3. *Reaction intermediates of 1,4-dioxane photocatalytic decomposition*

In the study of decomposition routes along with the removal of 1,4-dioxane in the course of photocatalytic oxidation, various degradation products appeared (Fig. 9). EGDF, EGMF and formic acid were identified as major reaction intermediates. In lesser extent ($\leq 4.0 \pm 0.1\ mg\ L^{-1}$), some acetic acid was produced along the process, while traces of methoxyacetic and glycolic acids were detected as mixture at concentrations below $1.16 \pm 0.06\ L^{-1}$.

Fig. 10 presents a simplified schematic of the major reaction pathways proposed for 1,4-dioxane degradation. According to the literature, EGDF and EGMF are produced concurrently in an oxidative ring opening mechanism initiated by •OH radical, whereat 1,4-dioxan-α-oxyl radical has been suggested to be the precursor, as described in detail by [41,55]. This α-oxyl radical can be degraded either through ΔC–C splitting at the *α–C* position (route A) or through an intramolecular reaction (H abstraction from the *αí–C* position) followed by fragmentation (route B).

Considering the chromatography analysis, route A was the primary degradation pathway in which, in accordance with the literature, it is suggested that the linear tetroxide generated over alkyl peroxyl radicals decomposed either to EGDF or to alkoxyl radical that lead to EGMF and formaldehyde [41]. Formaldehyde is readily oxidized to formic acid [56], and, in addition, formic acid is also produced along with glycolic acid in the further decomposition of both EGDF and EGMF [24,41]. However, the low concentrations of glycolic acid detected and the continuous decrease of TOC measured most likely refer to its very fast subsequent mineralization over oxalic acid [41]. In addition, it is important to note that, although reported as possible route for 1,4-dioxane degradation in different AOPs [24,55,57], ethylene glycol was not detected during the experiment, showing that no hydrolysis of the EGDF and EGMF took place in this photocatalytic process.

In the alternative route B (Fig. 10), formaldehyde and, thus, formic acid are also produced along with the *C*-centered radical I, which in turn supports the higher concentrations of formic acid in the system (Fig. 9). Radical I is either reduced to methoxyacetaldehyde, which is subsequently oxidized to methoxyacetic and acetic acids, or it proceeds through β-scission yielding acetaldehyde and, consequently, acetic acid [41,55,56]. Nevertheless, taking into account the low concentrations of methoxyacetic and acetic acids, the mechanism through EGDF and EGMF formation must have been predominant. In fact, similar pathway, mainly through the formation of the EGDF concurrently with a minor route for the formation of methoxiacetic acid, was observed by FTIR monitoring in a recent study on ozone oxidation of 1,4-dioxane under acidic conditions [57].

Despite the fact that the concentration of formic acid ($MOSC_{formic}$ = +2) increased throughout the experiment, indicating its continuous production, the relatively low solution MOSC (0. . .+0.5; Fig. 7) also implied its continuous mineralization, considering its high rate constant with •OH radical ($3.2 \times 10^9\ M^{-1}\ s^{-1}$ [58]). Moreover, the progressive decrease of the partial oxidation efficiency down to about 0.2 (Fig. 7) and the linear removal of TOC from the system (Fig. 6) also account for the continuous production of CO_2 and water.

4. Conclusions

Wastewaters containing 1,4-dioxane were successfully treated by solar photocatalysis using an immobilized NF-TiO_2 composite with monodisperse TiO_2 nanoparticles. Degradation of 1,4-dioxane decreased in the industrial effluent mainly due to its inorganic constituents, whereas, the change in effluent pH only produced a slight decrease in the degradation efficiency. Removal decreased for different wastewater conditions in the following order: pH 5.7 ($k = 0.34 \pm 0.02\ h^{-1}$) > pH 6.9 ($k = 0.31 \pm 0.01\ h^{-1}$) > industrial effluent ($k = 0.27 \pm 0.01\ h^{-1}$) > simulated salt content ($k = 0.26 \pm 0.01\ h^{-1}$). The mineralization was about $3.4\ \mu gC\ cm^{-2}\ h^{-1}$ in synthetic waters at both pH 5.7 and pH 6.9; whereas, about $2.8\ \mu gC\ cm^{-2}\ h^{-1}$ were degraded in both the industrial effluent and the solution with a simulated inorganic content.

Despite the salt content, the complete removal of 1,4-dioxane (≤100%) from the industrial wastewater was achieved along with a 65% and 50% of COD and TOC, respectively. Similar results ($P > 0.05$) were achieved by the immobilized lab-made catalyst and by the commercial P25-TiO_2. Namely, 49% and 50% COD, and 34% and 40% TOC were removed after 6 h of treatment with NF-TiO_2-monodisp. TiO_2 films and the P25 suspension, respectively.

The solar photocatalysis of 1,4-dioxane on NF-TiO_2-monodisp.TiO_2 was predominantly dependent on the slow degradation of primary intermediates, EGDF and EGMF, produced concurrently in an oxidative ring opening mechanism initiated by •OH. In addition, formic acid was continuously generated in various simultaneous degradation reactions, whereas, its steady removal from the system is also suggested alongside with the other simple carboxylic acids. Such a slow but persistent removal of

organic carbon throughout the experiment reflects that a complete mineralization of contamination from actual industrial effluents could be feasible using this supported catalyst. Immobilization, in turn, would greatly enhance the process engineering and, thus, increase the cost-effectiveness of the treatment.

Acknowledgements

The research leading to these results has received funding from the European Union's Seventh Framework Programme (FP7/2007-2013) under the grant agreement no 608490, E4Water project. The collaboration of the Gas Chromatography Service (CIB) of the Spanish National Research Council (CSIC), the Laboratory of Geochemical and Environmental Analyses of the Complutense University of Madrid and the Laboratory of CIFOR-INIA (Centro de Investigación Forestal, Instituto Nacional de Investigación y Tecnología Agraria y Alimentaria) is fully appreciated. The Archimedes Foundation (Estonia) is acknowledged for support to Helen Barndõk's Ph.D. studies.

References

[1] C.D. Adams, P.A. Scanlan, N.D. Secrist, Environ. Sci. Technol. 28 (1994) 1812–1818.
[2] J.Y. Choi, Y.J. Lee, J. Shin, J.W. Yang, J. Hazard. Mater. 179 (2010) 762–768.
[3] European Chemicals Bureau (ECB), E.U. Risk Assessment Report: 1,4-Dioxane, ISBN 92-894-1252-6, Second Priority List 21 (2002) 1-129, Office for Official Publications of the European Communities, Luxembourg, 2002.
[4] U.S Environmental Protection Agency (USEPA), Toxicological Review of 1,4-Dioxane (CAS No. 123-91-1), EPA/635/R-09/005-F, USEPA, Washington, DC, 2010.
[5] M.J. Zenker, R.C. Borden, M.A. Barlaz, Environ. Eng. Sci. 20 (2003) 423–432.
[6] T.-H. Han, J.-S. Han, M.-H. So, J.-W. Seo, C.-M. Ahn, D.H. Min, Y.S. Yoo, D.K. Cha, C.G. Kim, J. Environ. Sci. Health, Part A: Toxic/Hazard. Subst. Environ. Eng. 47 (2012) 117–129.
[7] W. Shen, H. Chen, S. Pan, Bioresour. Technol. 99 (2008) 2483–2487.
[8] M.J. Zenker, R.C. Borden, M.A. Barlaz, J. Environ. Eng. 130 (2004) 926–931.
[9] T.K.G. Mohr, Environmental Investigation and Remediation: 1,4-Dioxane and Other Solvent Stabilizers, CRC, Press, Boca Raton, 2010.
[10] J.M. Skadsen, B.L., Rice, D.J. Meyering, A case study in the City of Ann Arbor, Water Utilities, City of Anna Arbor, and Fleis & VendenBrink Engineering, Inc., 2004.
[11] I.A. Balcioglu, I.A. Alaton, M. Otker, R. Bahar, N. Bakar, M. Ikiz, J. Environ. Sci. Health Part A-Toxic/Hazard. Subst. Environ. Eng. 38 (2003) 1587–1596.
[12] V. Belgiorno, L. Rizzo, D. Fatta, C. Della Rocca, G. Lofrano, A. Nikolaou, V. Naddeo, S. Meric, Desalination 215 (2007) 166–176.
[13] H.M. Coleman, V. Vimonses, G. Leslie, R. Amal, Water Sci. Technol. 55 (2007) 301–306.
[14] C. Comninellis, A. Kapalka, S. Malato, S.A. Parsons, L. Poulios, D. Mantzavinos, J. Chem. Technol. Biotechnol. 83 (2008) 769–776.
[15] S. Perathoner, ChemH_2O, in: Leading-Edge Conference on Sustainable Water Management, 1–2 October 2013 Madrid, 2013.
[16] H. Choi, M.G. Antoniou, M. Pelaez, A.A. De la Cruz, J.A. Shoemaker, D.D. Dionysiou, Environ. Sci. Technol. 41 (2007) 7530–7535.
[17] A. Fujishima, T.N. Rao, D.A. Tryk, J. Photochem. Photobiol. C 1 (2000) 1–21.
[18] R.J. Braham, A.T. Harris, Ind. Eng. Chem. Res. 48 (2009) 8890–8905.
[19] S. Malato, P. Fernandez-Ibanez, M.I. Maldonado, J. Blanco, W. Gernjak, Catal. Today 147 (2009) 1–59.
[20] C. Singh, R. Chaudhary, K. Gandhi, J. Renew. Sustain. Energy 5 (2013).
[21] P.A. Soares, T.F.C.V. Silva, D.R. Manenti, S.M.A.G.U. Souza, R.A.R. Boaventura, V.J.P. Vilar, Environ. Sci. Pollut. Res. 21 (2014) 932–945.
[22] R.R. Hill, G.E. Jeffs, D.R. Roberts, J. Photochem. Photobiol. A 108 (1997) 55–58.
[23] S.W. Lam, M. Hermawan, H.M. Coleman, K. Fisher, R. Amal, J. Mol. Catal. A-Chem. 278 (2007) 152–159.
[24] V. Maurino, P. Calza, C. Minero, E. Pelizzetti, M. Vincenti, Chemosphere 35 (1997) 2675–2688.
[25] B.K. Min, J.E. Heo, N.K. Youn, O.S. Joo, H. Lee, J.H. Kim, H.S. Kim, Catal. Commun. 10 (2009) 712–715.
[26] T. Vescovi, H.M. Coleman, R. Amal, J. Hazard. Mater. 182 (2010) 75–79.
[27] K. Yasui, T. Isobe, S. Matsushita, A. Nakajima, J. Mater. Sci. 48 (2013) 2290–2298.
[28] N.K. Youn, J.E. Heo, O.S. Joo, H. Lee, J. Kim, B.K. Min, J. Hazard. Mater. 177 (2010) 216–221.
[29] C. Han, R. Luque, D.D. Dionysiou, Chem. Commun. 48 (2012) 1860–1862.
[30] N. Miranda-Garcia, S. Suarez, B. Sanchez, J.M. Coronado, S. Malato, M. Ignacio Maldonado, Appl. Catal. B-Environ. 103 (2011) 294–301.
[31] M. Pelaez, P. Falaras, V. Likodimos, A.G. Kontos, A.A. de la Cruz, K. O'Shea, D.D. Dionysiou, Appl. Catal. B-Environ. 99 (2010) 378–387.
[32] C. Han, V. Likodimos, J.A. Khan, M.N. Nadagouda, J. Andersen, P. Falaras, P. Rosales-Lombardi, D.D. Dionysiou, Environ. Sci. Pollut. Res. 21 (2014) 11781–11793.
[33] C. Han, M. Pelaez, V. Likodimos, A.G. Kontos, P. Falaras, K. O'Shea, D.D. Dionysiou, Appl. Catal. B-Environ. 107 (2011) 77–87.
[34] M. Pelaez, N.T. Nolan, S.C. Pillai, M.K. Seery, P. Falaras, A.G. Kontos, P.S.M. Dunlop, J.W.J. Hamilton, J.A. Byrne, K. O'shea, M.H. Entezari, D.D. Dionysiou, Appl. Catal. B-Environ. 125 (2012) 331–349.
[35] G.S. Pozan, A. Kambur, Appl. Catal. B-Environ. 129 (2013) 409–415.
[36] X. Shang, B. Li, C. Li, X. Wang, T. Zhang, S. Jiang, Dyes Pigm. 98 (2013) 358–366.
[37] A. Nakajima, S. Matsui, S. Yanagida, Y. Kameshima, K. Okada, Surf. Coat. Technol. 203 (2009) 1133–1137.
[38] M. Pelaez, A.A. de la Cruz, E. Stathatos, P. Falaras, D.D. Dionysiou, Catal. Today 144 (2009) 19–25.
[39] M. Pelaez, P. Falaras, A.G. Kontos, A.A. de la Cruz, K. O'Shea, P.S.M. Dunlop, J.A. Byrne, D.D. Dionysiou, Appl. Catal. B-Environ. 121 (2012) 30–39.
[40] H. Barndõk, M. Pelaez, C. Han, W.E. Platten III, P. campo, D. Hermosilla, A. Blanco, D.D. Dionysiou, Environ. Sci. Pollut. Res. 20 (2013) 3582–3591.
[41] M.I. Stefan, J.R. Bolton, Environ. Sci. Technol. 32 (1998) 1588–1595.
[42] S. Yamazaki, N. Yamabe, S. Nagano, A. Fukuda, J. Photochem. Photobiol. A 185 (2007) 150–155.
[43] R.A. Burns, J.C. Crittenden, D.W. Hand, V.H. Selzer, L.L. Sutter, S.R. Salman, J. Environ. Eng. 125 (1999) 77–85.
[44] H.Y. Chen, O. Zahraa, M. Bouchy, J. Photochem. Photobiol. A 108 (1997) 37–44.
[45] APHA, AWWA, W.P.C.F, Standard Methods for the Examination of Water and Wastewater, APHA, AWWA, WPCF, Washington, DC, 2005.
[46] F. Vogel, J. Harf, A. Hug, P.R. von Rohr, Water Res. 34 (2000) 2689–2702.
[47] J.A. Ashenhurst, Calculating the oxidation state of a carbon, http://www.masterorganicchemistry.com/2011/07/25/calculating-the-oxidation-state-of-a-carbon (2011), (accessed 07.01.14).
[48] M. Carbajo, F.J. Beltran, O. Gimeno, B. Acedo, F.J. Rivas, Appl. Catal. B-Environ. 74 (2007) 203–210.
[49] D. Hermosilla, M. Cortijo, C.P. Huang, Chem. Eng. J. 155 (2009) 637–646.
[50] N. Merayo, D. Hermosilla, C. Negro, A. Blanco, Chem. Eng. J. 232 (2013) 519–526.
[51] W. DiGuiseppi, C. Whitesides, T.K.G. Mohr, In Situ and on-site bioremediation, in: Proceedings of the 9th International In Situ Bioremediation Symposium Paper M-05, 7–10 May 2007, Baltimore, 2007.
[52] V. Augugliaro, V. Loddo, G. Marci, L. Palmisano, M. Schiavello, Chem. Biochem. Eng. Q. 9 (1995) 133–139.
[53] A.L. Linsebigler, G.Q. Lu, J.T. Yates, Chem. Rev. 95 (1995) 735–758.
[54] H. Barndõk, D. Hermosilla, L. Cortijo, C. Negro, A. Blanco, J. Adv. Oxid. Technol. 15 (2012) 125–132.
[55] N. Merayo, D. Hermosilla, L. Cortijo, Á. Blanco, J. Hazard. Mater. 268 (2014) 102–109.
[56] H.-S. Kim, B.-H. Kwon, S.-J. Yoa, I.-K. Kim, J. Chem. Eng. Jpn. 41 (2008) 829–835.
[57] H. Barndõk, L. Cortijo, D. Hermosilla, C. Negro, A. Blanco, J. Hazard. Mater. 280 (2014) 340–347.
[58] G.V. Buxton, C.L. Greenstock, W.P. Helman, A.B. Ross, J. Phys. Chem. Ref. Data 17 (1988) 513–886.

PUBLICATION VI

H. Barndõk, N, Merayo, L. Blanco, D. Hermosilla, A. Blanco

Application of on-line FTIR methodology to study the mechanisms of heterogeneous advanced oxidation processes

Sent to: *Applied Catalysis B: Environmental*

Elsevier Editorial System(tm) for Applied Catalysis B: Environmental
Manuscript Draft

Manuscript Number:

Title: Application of on-line FTIR methodology to study the mechanisms of heterogeneous advanced oxidation processes

Article Type: Research Paper

Keywords: 1,4-dioxane; heterogeneous AOPs; Fe0 microspheres; photo-Fenton; TiO2 photocatalysis

Corresponding Author: Prof. Daphne Hermosilla, PhD

Corresponding Author's Institution: Complutense University of Madrid

First Author: Helen Barndõk, MsC

Order of Authors: Helen Barndõk, MsC; Noemi Merayo, PhD; Laura Blanco, MsC; Daphne Hermosilla, PhD; Ángeles Blanco, PhD

GRUPO DE CELULOSA Y PAPEL
Departamento de Ingeniería Química
Facultad de Ciencias Químicas. Universidad Complutense de Madrid
Avda. Complutense, s/n 28040 Madrid

Daphne Hermosilla
Department of Chemical Engineering
Complutense University of Madrid,
Avda Complutense s/n, 28040 Madrid, Spain
Tlf: +34 91 394 4245; Fax: +34 91 394 4243
dhermosilla@quim.ucm.es

July 7th, 2015

Editor-in-Chief
Applied Catalysis B: Environmental

Please find herewith the manuscript titled "Application of on-line FTIR methodology to study the mechanisms of heterogeneous advanced oxidation processes" written by Barndõk, Merayo, Blanco, Hermosilla and Blanco.
This study provides a comprehensive understanding of the advanced catalytic oxidation of an emerging environmental pollutant, 1,4-dioxane, by heterogeneous photo-Fenton with zero valent iron (Fe^0) in neutral conditions and heterogeneous photocatalysis with titanium dioxide (TiO_2). Fourier transform infrared (FTIR) spectroscopy served as a powerful tool for on-line reaction monitoring and process optimization. The effect of different radiation sources and iron precursors was studied and the influence of H_2O_2 addition profile was assessed. An extensive chromatography analysis supported by FTIR monitoring allowed the establishment and comparison of the major decomposition pathways of 1,4-dioxane in both advanced oxidation processes. While very few and outdated reports exist on 1,4-dioxane decomposition by TiO_2-photocatalysis, to the best of our knowledge, this manuscript is the first literature example of photo-Fenton operation in heterogeneous conditions at neutral pH avoiding iron leaching.

Therefore, we would appreciate your consideration of this manuscript for publication as an original paper in Applied Catalysis B: Environmental.

Thank you for your precious time and assistance. I kindly remain at your disposal for any question regarding this submission.

Looking forward for your reply, yours sincerely,

Prof. Daphne Hermosilla, Ph.D.

***List of Three (3) Potential Reviewers**

Rui Alfredo da Rocha Boaventura

Universidade do Porto

Faculdade de Engenharia

Departamento de Engenharia Química

E-mail: bventura@fe.up.pt

Wanpen Wirojanagud

Research Director of Research Center of Environmental and Hazardous Substance Management

Khon Kaen University

Department of Environmental Engineering

wanpen@kku.ac.th

Yang Deng

Montclaire State University

Associate Professor, Earth and Environmental Studies

dengy@mail.montclair.edu

Application of on-line FTIR methodology to study the mechanisms of heterogeneous advanced oxidation processes

Helen Barndõk, Noemi Merayo, Laura Blanco, Daphne Hermosilla, Ángeles Blanco

[a]Department of Chemical Engineering, Universidad Complutense de Madrid, Avda. Complutense, s/n, 28040 Madrid. E-mail addresses (in order of appearance): hbarndok@quim.ucm.es, nmerayo@quim.ucm.es, lblanco@quim.ucm.es, dhermosilla@quim.ucm.es, ablanco@quim.ucm.es

[*] Corresponding author:
Daphne Hermosilla
Tel.: (+34) 913944247; email: dhermosilla@quim.ucm.es

ABSTRACT

On-line Fourier transform infrared (FTIR) spectroscopy was used to study the 1,4 dioxane degradation mechanism by heterogeneous photocatalysis with titanium dioxide (TiO_2) and heterogeneous photo-Fenton with zero valent iron (Fe^0). The effect of different radiation sources and iron precursors was studied and the influence of H_2O_2 addition profile was assessed. Complete removal of 1,4-dioxane and 85% mineralization of TOC were achieved by UV photo-Fenton with Fe^0, while solar light could work as cost-effective alternative, achieving 65% removal of 1,4-dioxane. Although constant addition of H_2O_2 was crucial for the rapid oxidation, significant degradation was reached by only half of the stoichiometric amount of H_2O_2. Meanwhile, almost 60% of 1,4-dioxane was degraded in TiO_2-photocatalysis. The degradation routes for 1,4-dioxane in both advanced oxidation processes were established and compared based on extensive chromatography analysis, whereas FTIR monitoring served as a powerful tool for on-line reaction monitoring. Ethylene glycol diformate was detected as the major primary intermediate in TiO_2-photocatalysis, whereas ethylene glycol was found as the main initial by-product in Fe^0-based photo-Fenton. An alternative route of 1,4-dioxane degradation through methoxyacetic and acetic acids was observed, being more pronounced in photo-Fenton processes and accentuated further in the presence of Fe^0.

Keywords: 1,4-dioxane; heterogeneous AOPs; Fe^0 microspheres; photo-Fenton; TiO_2 photocatalysis.

1. Introduction

1,4-Dioxane is a common organic solvent, generated also as a by-product in many industrial processes [1]. This cyclic ether is classified as a B2 carcinogen due to its negative health effects [2-4], whereas its biorefractory and persistent nature render difficult its removal by conventional technologies [1,5-7]. Advanced oxidation processes (AOPs) are reported to effectively degrade 1,4-dioxane [8-11] through the formation of more biodegradable compounds that can be treated by traditional biological methods, thus, reducing the overall cost of the process [12].

One of the most common AOPs, TiO_2-photocatalysis, is based on the combination of UV light and a semiconductor catalyst, offering several advantages like minimal production of residues and mild operation conditions suitable for environmental applications [13,14]. In contrast, another typical AOP, Fenton oxidation, is based on the electron transfer between hydrogen peroxide (H_2O_2) and ferrous ion (Fe^{2+}), and it appears as one of the most rapid and aggressive treatments suitable for heavily loaded industrial effluents [15,16]. During the last decade, however, combining both UV light and Fenton reaction in a so-called photo-Fenton process has become popular as an advantageous method, owing to the photo-recovery of catalytic Fe^{2+} and the photo-decarboxylation of the refractory ferric carboxylate complexes [17-23].

TiO_2-photocatalysis can achieve complete mineralization of 1,4-dioxane from diluted synthetic solutions [24,25]; however, elevated concentrations of this compound and other organic matter would require elevated concentrations of photocatalyst [26,27], causing a turbidity that could ultimately inhibit the penetration of light and, thus, the activation of TiO_2. On the other hand, Fenton and photo-Fenton processes are limited by its optimal pH range (usually set at pH≈3) [28,29] and final production of iron sludge that requires ultimate disposal [30]. Nevertheless, according to previous research, the

use of zero valent iron (Fe^0) microspheres instead of Fe^{2+} salts can solve the drawbacks of photo-Fenton when working in heterogeneous conditions at neutral pH. Under neutral pH conditions the produced Fe^{2+} remains anchored on the surface of Fe^0 microspheres without Fe^{2+} leaching and avoiding the subsequent generation of iron sludge (Barndõk et al., unpublished research).

Considering these heterogeneous AOPs, very few reports exist on the decomposition mechanisms of 1,4-dioxane during TiO_2-photocatalysis [31], and there is no literature on the identification of degradation routes and reaction intermediates formed along the treatment of 1,4-dioxane by heterogeneous photo-Fenton process using Fe^0, although some by-products have been identified [32,33]. Stefan and Bolton [34] proposed a degradation mechanism for 1,4-dioxane in UV/H_2O_2 oxidation, and Kim et al. [35] suggested a reaction pathway for homogeneous photo-Fenton reaction, both by exhaustive series of chromatographic methods.

As an alternative to the expensive and time-consuming chromatographic analysis, on-line Fourier transform infrared (FTIR) spectroscopy has been successfully applied for the *in situ* control of the intermediate chemical species during the oxidation of 1,4-dioxane by classical Fenton [10] and ozonation [8] processes. Since the heterogeneous photocatalytic and photo-Fenton processes involve multiple possible transformations of catalyst and reactive radical species, different degradation routes could be expected, depending on the treatment. Moreover, on-line information of the whole reaction during the experiment would not only provide a straightforward understanding of the reaction mechanism, but also an accurate optimization of the reagent doses and reaction time, thus reducing the treatment cost.

Therefore, the main objective of this research was to establish the degradation routes for 1,4-dioxane treated by both heterogeneous photocatalysis with TiO_2 and

heterogeneous photo-Fenton with Fe^0 and to study the mechanism of these processes under different radiation sources, using the on-line FTIR-methodology supported by extensive chromatography analysis. Furthermore, the FTIR tool was also applied for the optimization of the H_2O_2 required for the photo-Fenton process using Fe^0.

2. Materials and methods

2.1. Materials and analytical methods

All used reagents were of analytical grade and supplied by PANREAC S.A. (Barcelona, Spain) or Sigma-Aldrich (Highland, USA). Synthetic wastewater was prepared with 7050 mg L^{-1} of 1,4-dioxane in deionized water. AEROXIDE® P25-TiO_2 (BET surface area = 50 m^2 g^{-1}; pore volume = 0.25 m^3 g^{-1}, and mean particle size of ca. 21 nm) was supplied by Evonik (Essen, Germany). Fe^0 microspheres (>98.3% Fe; <1% C; <1% N; <0.7% O) with 1 µm of particle size and 800 m^2 kg^{-1} of surface area were obtained from BASF (ZVI Microspheres 800, Ludwigshafen, Germany).

All the analyses were made according to the standard methods for the examination of water and wastewaters [36]. Chemical oxygen demand (COD) was measured by the colorimetric method at 600 nm using an Aquamate-spectrophotometer (Thermo Scientific AQA 091801, Waltham, USA). Total organic carbon (TOC) was measured by the combustion-infrared method using a TOC/TN analyser multi N/C® 3100 (Analytik Jena AG, Jena, Germany) with catalytic oxidation on cerium oxide at 850 ºC. H_2O_2 concentration was analysed by the titanium sulphate spectrophotometric method [37]. Light intensity was recorded using a radiometer (UV-Elektronik, UV-VIS Radiometer RM-21, Ettlingen, Germany).

The FTIR analytical spectrometer ReacIR iC10 (Mettler-Toledo, Columbia, USA) was used to monitor chemical species as they react over a period of time as described by Merayo et al. [38]. In order to confirm the FTIR results, 1,4-dioxane and its metabolites, ethylene glycol diformate (EGDF) and ethylene glycol monoformate (EGMF), were identified and quantified by an Agilent 6890N gas chromatograph (GC, Palo Alto, CA) equipped with a quadrupole mass spectrometer (MS) Agilent 5975B. To extract these two volatile compounds from the water samples, an internal standard (5 mg L^{-1} of octanol) and 1.4 g of ammonium sulphate were added to 10 mL of sample, and the solution was extracted threefold with dichloromethane (40:10:10 mL). The organic fraction was dried on anhydrous sodium sulphate and concentrated to 1 mL under nitrogen flux in a Kuderna-Danish apparatus (Sigma, St. Louis, MO) and subsequently analysed by GC-MS as follows. Samples (3 µl) were injected in split mode (30:1) and volatiles were separated using a fused silica capillary column (HP-INNOWAX) (30 × 0.25 mm i.d. and 0.25-µm film thickness), supplied by Agilent (Madrid, Spain). The pressure of the GC-grade He carrier gas was 7.7 psi with a linear velocity of 1.0 mL min^{-1}; the initial oven temperature was 45 °C, which was first increased at 3 °C min^{-1} up to 100 °C, held for 1 min, and then heated at 15 °C min^{-1} up to 270 °C, and held at this temperature for an additional 5 min. The injection temperature was 230 °C. Detection was carried out by electron ionization (EI) mode (70 eV), interphase detection temperature was 290 °C (MS source at 230 °C and MS quad at 150 °C) and scanning mass was ranged between 35 and 400 amu. Quantitative determinations were carried out by the internal standard method, using peak areas obtained from selected ion (m/z) monitoring (88, 1,4-dioxane; 60, EGDF/EGMF; 45, octanol) and calibrations made with pure reference compounds analysed under the same conditions.

1,4-Dioxane was also quantified together with ethylene glycol as its possible degradation product, using gas−liquid chromatography (GLC) on a 7980A instrument (Agilent Technologies Inc., Palo Alto, CA) equipped with a flame ionization detector. The temperatures of the injector and detector were 310 °C and 280 °C, respectively. Samples (2 μL) were injected using the pulsed-split mode (split ratio 5:1) and analysed in a TRB-FFAP (Teknokroma, Sant Cugat del Vallès, Spain) fused silica column (30 m x 0.25 mm internal diameter x 0.25 μm film thickness) with He (43 psi) as carrier gas and the following temperature programme: 80 °C to 240 °C after 9 min initial hold and at 15 °C min^{-1} ramp rate. Peaks were identified according to the relative retention times of commercial standards. Quantification was performed according to peak area, corrected with the response factors calculated for each compound using 1-butanol (250 ppm) as internal standard, and the software GC-ChemStation Rev.B.04.02 (96) from Agilent.

Oxalic, acetic, formic, glycolic, and methoxyacetic acids were identified and quantified by ion chromatography (IC) using a 940 Professional IC Vario instrument (Metrohm, Herisau, Switzerland) equipped with a conductivity detector. An isocratic gradient of Na_2CO_3 (3.6 mM) was used as eluent, keeping an eluent flow at 0.7 mL min^{-1}. The injection loop was 50 mL. Analysis was done in an ionic resin column Metrosep A Supp 7 with a guard column Metrosep A Supp 4/5 Guard.

2.2. Experimental procedures

2.2.1. TiO_2 photocatalytic processes

Experiments were performed with P25-TiO_2 suspension of 10 g L^{-1} [26,27] stirred on a magnetic mixing device. The initial pH of the 1,4-dioxane solution (≈5.7) was not modified. For the analyses, samples were withdrawn from the reactor and centrifuged

for 15 min at 335 g, and then the supernatant was filtrated through 0.45 µm to measure COD and TOC.

2.2.2. Fenton and photo-Fenton processes

Heterogeneous experiments with Fe^0 were performed in the presence of 1000 mg L^{-1} $NaHCO_3$ buffer ($pH_0 \approx 8.5$), whereas the acidic conditions for homogeneous process with Fe^{2+} were obtained by adjusting the initial pH to 2.8 with 1M H_2SO_4. In all the studied cases, pH was monitored along the process. After the initial pH adjustment, iron was added to the 1,4-dioxane solution either in the form of Fe^0 microspheres at the optimum molar ratio $[H_2O_2]/[Fe^0]$ = 60 found in preliminary experiments (Barndõk et al., unpublished research) or in the form of $FeSO_4$ at the optimum ratio of 5 found for the conventional Fenton process [10]. Batches of H_2O_2 (35% w/v) were then added in sequence until the total amount based on the stoichiometric ratio of $[H_2O_2]_0/[COD]_0$=2.125 was reached. After every sample withdrawal, an initial measurement of the H_2O_2 in the samples was made. Immediately afterward, the samples were adjusted to pH≈9.0 by adding 40% NaOH, and then filtered through 0.45 µm to measure COD, TOC and remaining H_2O_2 concentrations. H_2O_2 concentration values were used to correct COD values according to Hermosilla et al. [28].

2.2.3. UV lamp and solar simulator

Experiments of UV/TiO_2 photocatalysis and UV photo-Fenton were performed at 25°C, using a high-pressure mercury immersion lamp of 450 W from ACE-glass (Model 7825-30, Vineland, USA) placed in a quartz glass cooling jacket and located in a vertical manner in the centre of the glass reactor. Total volume of 1000 mL was treated, whereas the irradiated liquid surface per sample was 240 cm^2 L^{-1}. The total photon flux of $1.1 \cdot 10^{20}$ photon s^{-1} was calculated to flow inside the photochemical reactor as

described by Liang et al. [39]. Light intensity on the irradiated liquid surface was 788 W m^{-2} at the mid-height of the UV-lamp (1.5 cm from the light source).

Solar TiO_2 photocatalysis and photo-Fenton trials were carried out in a Solar Simulator supplied by Newport (Irvine, USA), equipped with a Xe lamp (300 W) with a correction filter (ASTM E490-73a) to obtain the solar spectrum under ideal conditions. Total volume of 100 mL was treated, whereas the irradiated liquid surface per sample was 980 cm^2 L^{-1}. The total photon flux was $6.8 \cdot 10^{19}$ photon s^{-1}. Light intensity was 444 W m^{-2} at 8 cm from the light source, which was the distance between the sample surface and the lamp.

In the experiments with TiO_2, the intensity of light in a depth of 1 cm inside the turbid catalyst suspension was only 5% of the radiation on the liquid surface. Thus, activation of TiO_2 particles was expected to occur mainly on the irradiated liquid surface, which was much higher per reactor volume using the solar simulator than using the UV lamp. Therefore, for a better comparison of these two processes, the results were presented taking into account the liquid surface:volume ratio.

3. Results and discussion

3.1.Heterogeneous photocatalysis with TiO_2

Although the UV lamp with much greater potential than the solar simulator should lead to greater TiO_2 activation and, thus, faster degradation kinetics, in this particular case, the configuration of the solar simulator above the surface of a rather thin water layer was more beneficial than the UV lamp immersed in a much larger water bulk. Therefore, apparently similar treatment efficiencies were observed in both UV-assisted and solar photocatalysis (Fig 1). About 45% of 1,4-dioxane was degraded when

applying around 350 kJ L^{-1} of either solar or UV radiation, whereas almost 60% removal could be obtained in further irradiation in solar simulator (500 kJ L^{-1}). With both radiation sources, almost a linear degradation of 1,4-dioxane was observed (≈7.5 mg kJ^{-1}), according to both the chromatographic sample analysis and the *on-line* FTIR spectrometry, monitoring the peak at 1120 cm^{-1} characteristic to 1,4-dioxane spectra. This indicates that in both cases further removal of 1,4-dioxane is possible under longer radiation times.

Regardless of the radiation source, both photocatalytic processes led to very similar decomposition of 1,4-dioxane. Metabolites of 1,4-dioxane were observed in greater detail in the UV-catalysed process (Fig. 2), in which EGDF and formic acid were identified as major reaction intermediates, generated alongside since the beginning of the reaction. Their evolution along the degradation process is well observed by chromatography after certain time-intervals (Fig. 2A); however, the on-line monitoring of the major characteristic peaks of FTIR spectra allows even clearer appreciation of the real trends of EGDF appearance and decay accompanied by the accumulation of formic acid (Fig. 2B). In lesser extent, some acetic acid was produced along the process, while methoxyacetic and glycolic acids were detected as mixture at concentrations below 5.6±0.2 mg L^{-1}. Such a low concentrations could not be detected with a certainty in the FTIR spectra. In addition, traces of EGMF (≤0.03±0.01 mg L^{-1}) were observed by GC-MS (not presented in the graph).

3.2. Heterogeneous photo-Fenton processes with Fe^0

3.2.1. Fenton vs. photo-Fenton

Radiation significantly contributed to the activation of the Fe^0 microspheres and, thus, to the treatment efficiency, as shown in Fig. 3. Without radiation, up to 25% of COD

and 45% of 1,4-dioxane were removed by the heterogeneous Fenton oxidation with Fe^0 microspheres, which could be sufficient reduction for certain applications. On the other hand, complete degradation of the compound, 90% of COD and 85% of TOC removals were achieved in Fe^0/H_2O_2/UV process. Solar light also significantly improved the Fe^0/H_2O_2 treatment, but to a lesser extent than UV radiation, resulting in 65% of 1,4-dioxane degradation along with 50 and 45% of COD and TOC removals, respectively.

Unlike in TiO_2-based photocatalysis, the ratio of irradiated surface to reactor volume did not strongly affect the treatment efficiencies, since the addition of Fe^0 microspheres did not cause such a significant turbidity that would suppress the light penetration. Therefore, the activation of Fe^0 was expected to occur similarly in the whole bulk of the treated sample, and the process was only dependent on the nature and intensity of the light. Namely, it took about 280 J cm^{-2} of UV light and around 520 J cm^{-2} of solar radiation (measured at 315-400 nm on irradiated liquid surface) to degrade 50% of the COD. Such an increase in the required radiation by solar simulator to degrade the same pollutant load as with the UV lamp, is due to the differences in lamp power and the range of the emitted light spectrum.

Among the decomposition products of 1,4-dioxane, very low concentrations of EGDF ($\leq 1.1 \pm 0.1$ mg L^{-1}) were detected throughout the Fe^0-based Fenton processes. In contrast with TiO_2-photocatalysis, significant concentrations of ethylene glycol were measured in both light-enhanced Fenton experiments (Fig. 4). Apparently, the type of radiation does not affect the degradation mechanism in heterogeneous photo-Fenton, since similar metabolites were detected with both UV and solar light. Namely, ethylene glycol and formic acid were found to be the major reaction intermediates, as shown for the Fe^0/H_2O_2/UV process in Fig. 5. In addition to formic acid, several other carboxylic acids were identified and monitored both by chromatographic analysis and FTIR

spectrometry (Figs. 5A and 5B, respectively). Namely, methoxyacetic and glycolic acids were generated since the beginning of the reaction, reaching its maximum concentration at 60 min and degrading slowly onwards, while acetic and oxalic acids appeared later, accumulating to a lesser extent till the end of the reaction. The earlier appearance and faster degradation of the reaction intermediates (e.g. ethylene glycol; Fig. 4) in UV-enhanced process than in Fe^0/H_2O_2/solar is most likely due to the greater activation of Fe^0 microspheres in UV region than under solar radiation, which eventually results in greater OH• production and shorter reaction times.

3.2.2. Influence of iron source

For the sake of comparison, classical photo-Fenton with Fe^{2+} at highly acidic pH was also performed along with the heterogeneous photo-Fenton in basic conditions. With both iron sources ($FeSO_4$ and Fe^0), ethylene glycol and formic acid were the major reaction intermediates of 1,4-dioxane decomposition (Figs. 5 and 6, respectively). Although same carboxylic acid by-products were detected using either $FeSO_4$ or Fe^0, much earlier and higher production of acetic acid was observed in heterogeneous photo-Fenton with Fe^0. Apart from that, the main differences between classical and Fe^0-based photo-Fenton appear to lie in the reaction rate and the mineralization efficiency. Namely, the degradation of 1,4-dioxane was somewhat slower, the appearance of ethylene glycol later and the accumulation of formic acid greater with Fe^{2+}/H_2O_2/UV (Fig. 6) than with Fe^0/H_2O_2/UV (Fig. 5). In general, the final step of mineralization of the short chain carboxylic acids, e.g. oxalic acid, was slower with Fe^{2+} (75% of TOC removal) compared to the heterogeneous Fe^0-based treatment (85% of TOC removal).

The higher rates of 1,4-dioxane degradation and faster mineralization of the rest of the organics are most likely due to the Fe^{3+} recycle step in a so-called "pseudo-catalytic Fe^0/Fe^{2+} system", as reported previously by Bremner et al., Kallel et al. and Prousek et

al. [40-43]. In agreement with other authors [30,33,44], Fe^0 is oxidized to Fe^{2+} in the presence of H_2O_2 and/or UV light, leading to the traditional Fenton reaction, producing ferric iron (Fe^{3+}). Fe^{3+} tends to form refractory ferric carboxylate complexes that, although eventually photo-decarboxylated by UV-light, can slow down the overall mineralization process [23,43,45]. Thus, Fe^0 microspheres present an advantage because, apart from the photo-recovery of catalytic Fe^{2+} similar to classical photo-Fenton, the produced Fe^{3+} also reacts with Fe^0, additionally regenerating Fe^{2+} which will newly proceed with the Fenton reaction, producing more available •OH [40-43].

3.2.4. Influence of reagent dose

Fe^0-based photo-Fenton experiments using different patterns of H_2O_2 addition, demonstrated that the presence of an excess H_2O_2 is crucial for the oxidation on Fe^0 microspheres to take place at acceptable velocity. Namely, the best results were achieved with continuous H_2O_2 additions up to the stoichiometric ratio of H_2O_2/COD_0=2.125, whereby most of the 1,4-dioxane (>99%) was degraded in 2 h and the subsequent degradation of the primary intermediate, ethylene glycol, was also almost completed. H_2O_2 was consumed slowly (about 53 mg L^{-1} per minute) while most of the oxidant was accumulated in the solution during the experiment (Fig. 7A). Therefore, more than 15,000 mg L^{-1} of H_2O_2 was still present in the water at the end of the experiment, which would not be acceptable in industrial application.

As a consequence, a different pattern for the addition of H_2O_2 was studied. In this case, each new addition of H_2O_2 was performed only when the previous dosage was consumed, obtaining a rate of H_2O_2 disappearance of just 13 mg L^{-1} min^{-1} and only 30% of 1,4-dioxane degradation in 3 h. Thus, it was concluded that at least an initial excess of H_2O_2 was needed and a compromise was done, as shown in Fig. 7B. H_2O_2 was added continuously in short intervals up to the ratio of H_2O_2/COD_0=1.0625 (50% of the

stoichiometric ratio) during the first hour of experimentation, but oxidant addition was cut afterwards to estimate whether the excess of H_2O_2 accumulated in the system by that point was sufficient to proceed with the oxidation of organics at similar rate compared to working at stoichiometric ratio.

The on-line FTIR monitoring of both 1,4-dioxane and ethylene glycol indicated that the process with lower amount of H_2O_2 was less effective, as the ethylene glycol started to accumulate when oxidant additions stopped and it was not consumed (Fig. 7B). Nevertheless, nearly 97% of 1,4-dioxane, 65% of COD and 50% of TOC was still removed along with the total consumption of the leftover H_2O_2. Moreover, the residual ethylene glycol is a biodegradable compound that should not imply any complications for further treatment by conventional methods [46]. Therefore, nearly complete removal of 1,4-dioxane accompanied with the generation of biodegradable compounds could be reached by using only half of the stoichiometric amount of H_2O_2 required.

3.2. Comparison of degradation routes

The major routes proposed for 1,4-dioxane degradation with the studied treatments are presented in a simplified schematic (Scheme 1). Most of the intermediate degradation steps omitted in Scheme 1 occur through radical intermediates following the mechanism of tetroxide formation over peroxyl radical, as described in detail by Cooper et al. and by von Sonntag and Schuchmann [47,48]. In principle, all the reactions with organics initiated by free radicals (e.g. •OH) lead to the formation of carbon-centered radicals [47]. These radicals (e.g. $RH_2C^{\bullet}$) may react with dissolved O_2 to form peroxyl radicals (Eq. 1), which normally undergo bimolecular decay to form tetroxide intermediates (Eq. 2) [47,48]. The production of two oxyl radicals and O_2 (Eq. 3) and the generation of two

carbonyl compounds and H_2O_2 (Eq. 4) are two of the typical pathways suggested for the subsequent tetroxide decomposition [48,49].

$$RH_2C\bullet + O_2 \rightarrow RH_2CO_2\bullet \quad (1)$$

$$2RH_2CO_2\bullet \rightarrow RH_2C\text{-}O_4\text{-}CH_2R \quad (2)$$

$$RH_2C\text{-}O_4\text{-}CH_2R \rightarrow 2RCH_2CO\bullet + O_2 \quad (3)$$

$$RH_2C\text{-}O_4\text{-}CH_2R \rightarrow 2RCHO + H_2O_2 \quad (4)$$

The source for the main primary intermediates of 1,4-dioxane is 1,4-dioxan-α-oxyl radical generated, as described by several authors [10,34,50], through the formation of tetroxide ***I*** (Scheme 1), which is the one obtained in the reactions similar to Eqs. 1-3. In agreement with Stefan and Bolton [34], the α-oxyl radical was degraded either through ΔC-C splitting at the α-C position (route A, Scheme 1) or through an intramolecular reaction (H abstraction from the α′-C position) followed by fragmentation (route B, Scheme 1).

In route A (Scheme 1), another carbon-centered radical generated through an oxidative ring opening mechanism initiated by •OH is once again precursor for the formation of corresponding tetroxide (***II)*** in reactions similar to Eqs. 1-2. ***II*** decomposes either to EGDF (Eq.4-type reaction) or alkoxyl radicals (Eq. 3-type reaction) that lead to EGMF and formaldehyde [10,34,51]. Such decomposition of 1,4-dioxane through a linear tetroxide appears to be an important pathway for both heterogeneous AOPs, as EGDF and EGMF were detected in all the experiments, although the formation of EGDF seems to be predominant, as only trace concentrations of EGMF were detected.

The further decomposition of EGDF in UV/TiO_2 process is started with H-abstraction by •OH or HO_2• attack [34,50]. This O_2-demanding transformation process over another tetroxide intermediate may eventuate in either producing alkoxyl radicals

(Eq.3-type) to give formic acid, glyoxal and glycolic acid as final products or generating ester intermediate (Eq.4-type) that hydrolyses to glycolic and formic acids [50,51].

The decay of EGDF in heterogeneous photo-Fenton oxidation, however, is different from photocatalytic degradation. Namely, in the pH conditions tested in the Fe^0-based photo-Fenton ($pH_0 \approx 8.5$; Figs. 4 and 5), EGDF is hydrolysed rapidly into ethylene glycol (Scheme 2) [8]. Ethylene glycol was also reported as the primary intermediate in the classic Fenton process; however, in the latter, ethylene glycol was generated through an acidic hydrolysis of EGDF ($pH_0 \approx 2.8$) [10]. Therefore, similar pathway of acid-catalysed hydrolysis is expected to occur in the $Fe^{2+}/H_2O_2/UV$ process (Fig. 6). Regardless of the cause of hydrolysis, ethylene glycol is subsequently degraded to glycolic acid through the formation of glycolaldehyde [10,52], whereas possible generation of some formic acid has been reported as well [52,53].

The major difference between the two heterogeneous AOPs is due to the variation in pH profile because the operating pH of UV/TiO_2 process ($pH_0 \approx 5.7$) was neither acidic nor basic enough for the hydrolysis of EGDF to ethylene glycol to occur. Nevertheless, both AOPs continued through the decomposition of carboxylic acids towards final mineralization. In further oxidation, formic acid is directly mineralized to CO_2 [34,47] at a high reaction rate with •OH (Table 1) [54]. Glycolic acid decomposes to glyoxylic acid which is next rapidly oxidized to oxalic acid [10,47,55]. Oxalic acid appears as one of the most common last detected intermediates before the mineralization of organics [8,34,47]. To a lesser extent, some glyoxylic acid could also decompose to formic acid, which is easily degraded to water and CO_2 [47,55].

According to the general tendency, the rate constants of acids for reactions with OH• are smaller than those of their anions (Table 1) [54-56]. This could probably be the reason for the faster TOC removal and lesser accumulation of carboxylic acids in

Fe^0/H_2O_2/UV process at $pH_0 \approx 8.5$ than in Fe^{2+}/H_2O_2/UV oxidation at $pH_0 \approx 2.8$ because at neutral and slightly basic conditions most of the carboxylic acids under question are in their dissociated form. The accumulation of carboxylic acids could also negatively affect the initial decomposition of 1,4-dioxane, as they compete with the parent compound for the oxidants [34].

Another major difference between the Fe^0-catalysed and Fe^{2+}-based photo-Fenton processes is apparently the greater importance of an alternative degradation route B (Scheme 1) in Fe^0/H_2O_2/UV process. Namely, in the alternative route B, according to Stefan and Bolton [34], 1,4-dioxan-α-oxyl radical is degraded through an intramolecular reaction producing formaldehyde and, thus, formic acid along with the carbon-centered radical (***III***) (Scheme 1). ***III*** is either reduced to methoxyacetaldehyde which is subsequently oxidized to methoxyacetic and acetic acids or undergoes β-scission yielding acetaldehyde and, consequently, acetic acid [10,34,35]. Comparing the profiles of acetic acid during the two photo-Fenton processes (Figs. 5 and 6), it seems to be the presence of Fe^0 that brings about the considerable production of acetic acid (Fig. 5), indicating the more pronounced occurrence of degradation route B (Scheme 1). The subsequent degradation of acetic acid gives formaldehyde, and glycolic and glyoxylic acids as major by-products in free-radical-induced degradation, whereas CO_2 is produced as well, indicating that some mineralization also occurs in that stage of decomposition [47,55,57].

On the other hand, relatively low concentrations of acetic acid were detected only at the very end of the Fe^{2+}-based photo-Fenton experiment (Fig. 6). Therefore, the mixed profile of methoxyacetic and glycolic acids in the Fe^{2+}/H_2O_2/UV oxidation (Fig. 6) at greater extent probably belongs to glycolic acid produced in the degradation of ethylene glycol (route A, Scheme 1). With regard to UV/TiO_2 oxidation, considering the profiles

of both methoxyacetic and acetic acids, the alternative route B was hardly significant in TiO_2–photocatalytic process (Fig. 2).

Conclusions

FTIR was successfully applied as a powerful tool for the mechanistic study and optimization of the heterogeneous AOPs. An extensive chromatography analysis supported by the on-line FTIR monitoring allowed the establishment of the major decomposition pathways of 1,4-dioxane. EGDF was detected as the major primary intermediate in TiO_2-photocatalysis, whereas ethylene glycol was found as the main initial by-product in Fe^0 based photo-Fenton, generated through the basic hydrolysis of EGDF due to the different pH profile. An alternative route of 1,4-dioxane degradation into methoxyacetic and acetic acids was also observed, being more pronounced in photo-Fenton processes and accentuated in the presence of Fe^0. Regardless, both AOPs continued over the decomposition of short chain carboxylic acids, formic acid being the most prevalent intermediate by-product.

Heterogeneous Fe^0/H_2O_2/UV oxidation yielded complete removal of 1,4-dioxane and 85% mineralization of TOC, outperforming the classical photo-Fenton process (75% of TOC), most likely owing to the improved regeneration of Fe^{2+} from Fe^{3+}. Solar light could work as cost-effective alternative for the activation of Fe^0 microspheres, achieving 65% removal of 1,4-dioxane. Although constant addition of H_2O_2 in excess was crucial for the rapid oxidation on Fe^0, the FTIR monitoring showed that significant degradation along with the production of biodegradable by-products is reached by using only half of the stoichiometric amount of H_2O_2 required.

Almost 60% of 1,4-dioxane was degraded in TiO_2-photocatalysis, whereas higher degradation is expected at longer radiation times when considering the almost linear

removal with both UV and solar light (≈7.5 mg kJ^{-1}). Unlike in heterogeneous photo-Fenton where the Fe^0 microspheres did not produce any significant turbidity, the ratio of irradiated surface to reactor volume greatly affected the heterogeneous photocatalysis where activation of TiO_2 particles was expected to occur mainly on the irradiated liquid surface.

Acknowledgements

The research leading to these results has received funding from the European Union's Seventh Framework Programme (FP7/2007-2013) under the grant agreement n° 608490, E4Water project. The collaboration of the Gas Chromatography Service (CIB) of the Spanish National Research Council (CSIC), the Laboratory of Geochemical and Environmental Analyses of the Complutense University of Madrid and the Laboratory of CIFOR-INIA (*Centro de Investigación Forestal, Instituto Nacional de Investigación y Tecnología Agraria y Alimentaria*) is fully appreciated. The Archimedes Foundation (Estonia) is acknowledged for support to Helen Barndõk's Ph.D. studies.

References

[1] T.K.G. Mohr, Environmental Investigation and remediation: 1,4-dioxane and other solvent stabilizers, CRC Press, Boca Raton, 2010.

[2] European Chemicals Bureau (ECB), E.U. risk assessment report: 1,4-dioxane, ISBN 92-894-1252-6, Second Priority List 21 (2002) 1-129, Office for Official Publications of the European Communities, Luxembourg, 2002.

[3] U.S. Environmental Protection Agency (USEPA), Toxicological review of 1,4-dioxane (CAS No. 123-91-1), EPA/635/R-09/005-F, USEPA, Washington, DC, 2010.

[4] National Industrial Chemical Notification and Assessment Scheme (NICNAS), Full public report: 1,4-Dioxane. Priority Existing Chemical No. 7, Australian Government Publishing Service, Canberra, 1998.

[5] U.S. Environmental Protection Agency (USEPA), Treatment Technologies for 1,4-Dioxane: Fundamentals and Field Applications, EPA-542-R-06-009, USEPA, Office of Solid Waste and Emergency Response, Washington, DC, 2006.

[6] J.M. Skadsen, B.L. Rice, D.J. Meyering, A case study in the City of Ann Arbor, Water Utilities, City of Anna Arbor, and Fleis & VendenBrink Engineering, Inc., 2004.

[7] M.J. Zenker, R.C. Borden, M.A. Barlaz, Environ. Eng. Sci. 20 (2003) 423-432.

[8] H. Barndõk, L. Cortijo, D. Hermosilla, C. Negro, A. Blanco, J. Hazard. Mater. 280 (2014) 340-347.

[9] H. Barndõk, D. Hermosilla, L. Cortijo, E. Torres, A. Blanco, Environ. Sci. Pollut. Res. 21 (2014) 5701-5712.

[10] N. Merayo, D. Hermosilla, L. Cortijo, Á. Blanco, J. Hazard. Mater. (2014).

[11] M.H. So, J.S. Han, T.H. Han, J.W. Seo, C.G. Kim, Water Sci. Technol. 59 (2009) 1003-1009.

[12] J.H. Suh, M. Mohseni, Water Res. 38 (2004) 2596-2604.

[13] A. Fujishima, T.N. Rao, D.A. Tryk, J. Photochem. Photobiol., C 1 (2000) 1–21.

[14] A.L. Linsebigler, G.Q. Lu, J.T. Yates, Chem. Rev. 95 (1995) 735-758.

[15] D. Hermosilla, N. Merayo, R. Ordonez, A. Blanco, Waste Manage. 32 (2012) 1236-1243.

[16] C.P. Huang, C. Dong, Z. Tang, Waste Manage. 13 (1993) 361-377.

[17] E. De Torres-Socias, I. Fernandez-Calderero, I. Oller, M.J. Trinidad-Lozano, F.J. Yuste, S. Malato, Chem. Eng. J. 234 (2013) 232-239.

[18] C. Mendoza-Marin, P. Osorio, N. Benitez, J. Hazard. Mater. 177 (2010) 851-855.

[19] I. Oller, S. Malato, J.A. Sanchez-Perez, M.I. Maldonado, W. Gernjak, L.A. Perez-Estrada, J.A. Munoz, C. Ramos, C. Pulgarin, Ind. Eng. Chem. Res. 46 (2007) 7467-7475.

[20] T.F.C.V. Silva, A. Fonseca, I. Saraiva, V.J.P. Vilar, R.A.R. Boaventura, Water Res. 47 (2013) 3543-3557.

[21] P.A. Soares, T.F.C.V. Silva, D.R. Manenti, S.M.A.G.U. Souza, R.A.R. Boaventura, V.J.P. Vilar, Environ. Sci. Pollut. Res. 21 (2014) 932-945.

[22] B.S. Souza, F.C. Moreira, M.W.C. Dezotti, V.J.P. Vilar, R.A.R. Boaventura, Catal. Today 209 (2013) 201-208.

[23] D. Hermosilla, M. Cortijo, C.P. Huang, Chem. Eng. J. 155 (2009) 637-646.

[24] H.M. Coleman, V. Vimonses, G. Leslie, R. Amal, Water Sic. Technol. 55 (2007) 301-306.

[25] T. Vescovi, H.M. Coleman, R. Amal, J. Hazard. Mater. 182 (2010) 75-79.

[26] C.N. Chang, Y.S. Ma, G.C. Fang, A.C. Chao, M.C. Tsai, H.F. Sung, Chemosphere 56 (2004) 1011-1017.

[27] N. Merayo, D. Hermosilla, L. Blanco, L. Cortijo, A. Blanco, J. Hazard. Mater. 262 (2013) 420-427.

[28] D. Hermosilla, M. Cortijo, C.P. Huang, Sci. Total Environ. 407 (2009) 3473-3481.

[29] R.F.F. Pontes, J.E.F. Moraes, A. Machulek, Jr., J.M. Pinto, J. Hazard. Mater. 176 (2010) 402-413.

[30] J.J. Pignatello, E. Oliveros, A. MacKay, Crit. Rev. Environ. Sci. Technol. 36 (2006) 1-84.

[31] V. Maurino, P. Calza, C. Minero, E. Pelizzetti, M. Vincenti, Chemosphere 35 (1997) 2675-2688.

[32] E. Khan, W. Wirojanagud, N. Sermsai, J. Hazard. Mater. 161 (2009) 1024-1034.

[33] H.-S. Son, J.-K. Im, K.-D. Zoh, Water Res. 43 (2009) 1457-1463.

[34] M.I. Stefan, J.R. Bolton, Environ. Sci. Technol. 32 (1998) 1588-1595.

[35] H.-S. Kim, B.-H. Kwon, S.-J. Yoa, I.-K. Kim, J. Chem. Eng. Jpn. 41 (2008) 829-835.

[36] APHA, AWWA, WPCF (Eds.), Standard Methods for the Examination of Water and Wastewater, Washington, DC, 2005.

[37] H. Pobiner, Anal. Chem. 33 (1961) 1423-1428.

[38] N. Merayo, D. Hermosilla, C. Negro, A. Blanco, Chem. Eng. J. 232 (2013) 519-526.

[39] X. Liang, X. Zhu, E.C. Butler, J. Hazard. Mater. 190 (2011) 168-176.

[40] D.H. Bremner, A.E. Burgess, D. Houllemare, K.C. Namkung, Appl. Catal. B-Environ. 63 (2006) 15-19.

[41] M. Kallel, C. Belaid, R. Boussahel, M. Ksibi, A. Montiel, B. Elleuch, J. Hazard. Mater. 163 (2009) 550-554.

[42] M. Kallel, C. Belaid, T. Mechichi, M. Ksibi, B. Elleuch, Chem. Eng. J. 150 (2009) 391-395.

[43] J. Prousek, E. Palackova, S.A. Priesolova, L. Markova, A. Alevova, Sep. Sci. Technol. 42 (2007) 1505-1520.

[44] J.A. Bergendahl, T.P. Thies, Water Res. 38 (2004) 327-334.

[45] V. Kavitha, K. Palanivelu, Chemosphere 55 (2004) 1235-1243.

[46] W.K. Shieh, J.A. Lepore, I. Zandi, Water Sci. Technol. 38 (1998) 145-153.

[47] W.J. Cooper, C.J. Cramer, N.H. Martin, S.P. Mezyk, K.E. O'Shea, C. von Sonntag, Chem. Rev. 109 (2009) 1302-1345.

[48] C. vonSonntag, H.-P. Schuchmann, Peroxyl radicals in aqueous solutions, in: Z. Alfassi (Ed.), Peroxyl radicals, John Wiley, New York, 1997, pp. 173-234.

[49] J.E. Bennett, R. Summers, Can. J. Chem.-Rev. Can. Chim. 52 (1974) 1377-1379.

[50] M.A. Beckett, I. Hua, Environ. Sci. Technol. 34 (2000) 3944-3953.

[51] H. Barndõk, D. Hermosilla, C. Han, D.D. Dionysiou, C. Negro, Á. Blanco, Appl. Catal. B-Environ. 180 (2016) 44-52.

[52] The Dow Chemical Company, http://dowac.custhelp.com/app/answers/detail/a_id/11979 (2014), (accessed March 13, 2015).

[53] W.J. Rossiter, P.W. Brown, M. Godette, Sol. Energy Mater. 9 (1983) 267-279.

[54] G.V. Buxton, C.L. Greenstock, W.P. Helman, A.B. Ross, J. Phys. Chem. Ref. Data 17 (1988) 513-886.

[55] N. Karpel Vel Leitner, M. Dore, Water Res. 31 (1997) 1383-1397.

[56] B. Ervens, S. Gligorovski, H. Herrmann, Phys. Chem. Chem. Phys. 5 (2003) 1811-1824.

[57] Y. Tan, Y.B. Lim, K.E. Altieri, S.P. Seitzinger, B.J. Turpin, Atmos. Chem. Phys. 12 (2012) 801-813.

Tables

Table 1. Physicochemical constants of the studied carboxylic acids

acid / anion	*pKa*	*Aqueous phase reaction rate constant with OH• ($M^{-1}s^{-1}$)*
acetic acid		1.6×10^7 [54]
acetate ion	4.75	8.5×10^7 [54]
formic acid		1.4×10^8 [54]
formate ion	3.75	3.2×10^9 [54]
glycolic acid		6.0×10^8 [54]
glycolate ion	3.83	8.6×10^8 [54]
glyoxylic acid		3.6×10^8 [56]
glyoxylate ion	3.20	2.6×10^9 [56]
methoxyacetic acid		NF
methoxyacetate ion	3.57	NF
oxalic acid		1.4×10^6 [54]
hydrogen oxalate ion	1.27 / 4.27	4.7×10^7 [54] / 1.9×10^8 [56]
oxalate ion		7.7×10^6 [54] / 1.6×10^8 [56]

NF = not found

Figures

Fig.1. Comparison of UV-assisted and solar photocatalysis: degradation of TOC and the decrease of 1,4-dioxane peak in relative absorbance units (A.U.) monitored by FTIR spectrometry. $C_{0;dioxane}$=7050 mg L^{-1}; pH_0≈5.7.

Fig.2. Metabolites of 1,4-dioxane during UV/TiO_2 treatment: (A) chromatographic analysis; (B) FTIR monitoring of the major peaks in relative absorbance units (A.U.). $C_{0;dioxane}$=7050 mg L^{-1}; pH_0≈5.7.

Fig.3. Comparison of Fe^0-based heterogeneous photo-Fenton processes for 1,4-dioxane removal: (A) COD removal; (B) decrease of 1,4-dioxane peak in relative absorbance units (A.U.) monitored by FTIR spectrometry. $C_{0;dioxane}$=7050 mg L^{-1}; pH_0≈8.5.

Fig.4. FTIR monitoring of the peak of ethylene glycol (EG) during the oxidation of 1,4-dioxane by heterogeneous Fe^0–based photo-Fenton, employing either UV or solar radiation (peak height in relative absorbance units (A.U.)). $C_{0;dioxane}$=7050 mg L^{-1}; pH_0≈8.5.

Fig.5. Metabolites of 1,4-dioxane during heterogeneous Fe^0–based UV photo-Fenton process: (A) chromatographic analysis of the major reaction intermediates; (B) FTIR monitoring of the peaks of selected carboxylic acids in relative absorbance units (A.U.). $C_{0;dioxane}$=7050 mg L^{-1}; pH_0≈8.5.

Fig.6. Metabolites of 1,4-dioxane during homogeneous Fe^{2+}–based UV photo-Fenton process. $C_{0;dioxane}$=7050 mg L^{-1}; pH_0≈2.8.

Fig.7. FTIR monitoring of the peaks of 1,4-dioxane and ethylene glycol during heterogeneous Fe^0–based UV photo-Fenton processes (A) with continuous H_2O_2 additions up to the stoichiometric ratio of H_2O_2/COD_0=2.125; (B) with continuous H_2O_2 additions up to the ratio of H_2O_2/COD_0=1.0625 (50% of the stoichiometric ratio). $C_{0;dioxane}$=7050 mg L^{-1}; pH_0≈8.5.

Scheme 1. Simplified schematic of 1,4-dioxane decomposition routes.

Scheme 2. Decomposition route for the basic hydrolysis of EGDF into ethylene glycol.

1 FIGURE 1

2

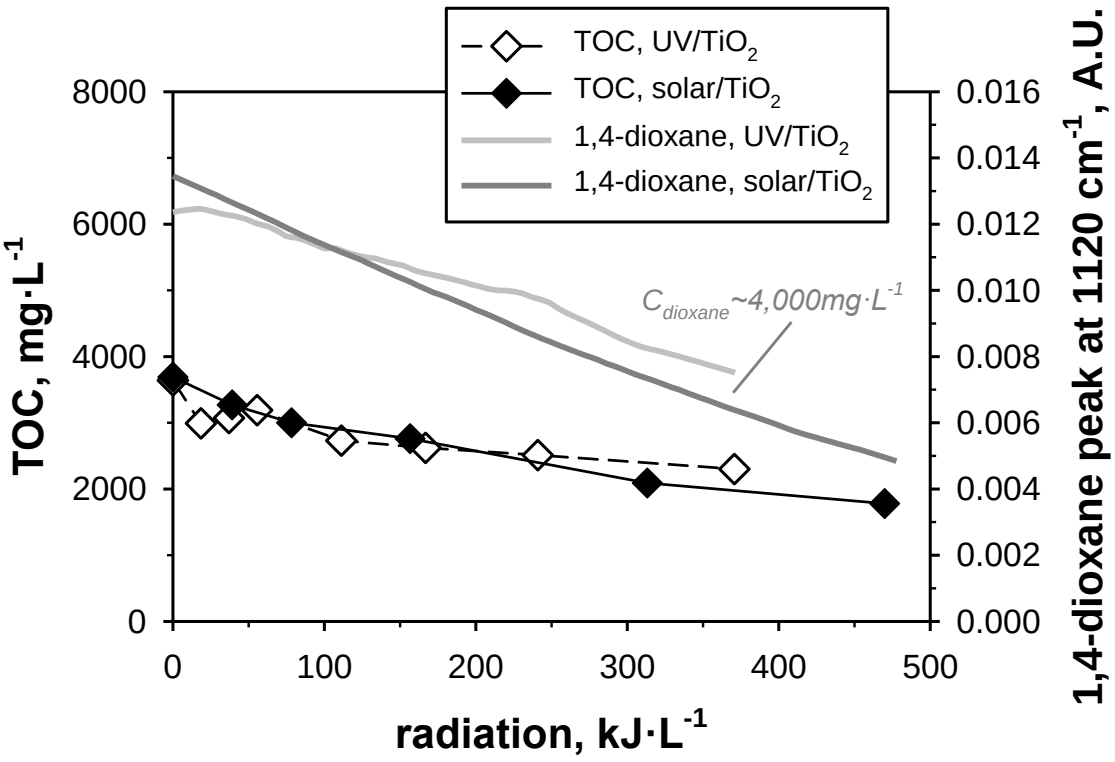
TOC, UV/TiO2
TOC, solar/TiO2
1,4-dioxane, UV/TiO2
1,4-dioxane, solar/TiO2
Cdioxane~4,000mg·L-1
TOC, mg·L-1
1,4-dioxane peak at 1120 cm-1, A.U.
radiation, kJ·L-1
0
2000
4000
6000
8000
0.000
0.002
0.004
0.006
0.008
0.010
0.012
0.014
0.016
0
100
200
300
400
500

1 FIGURE 2

2

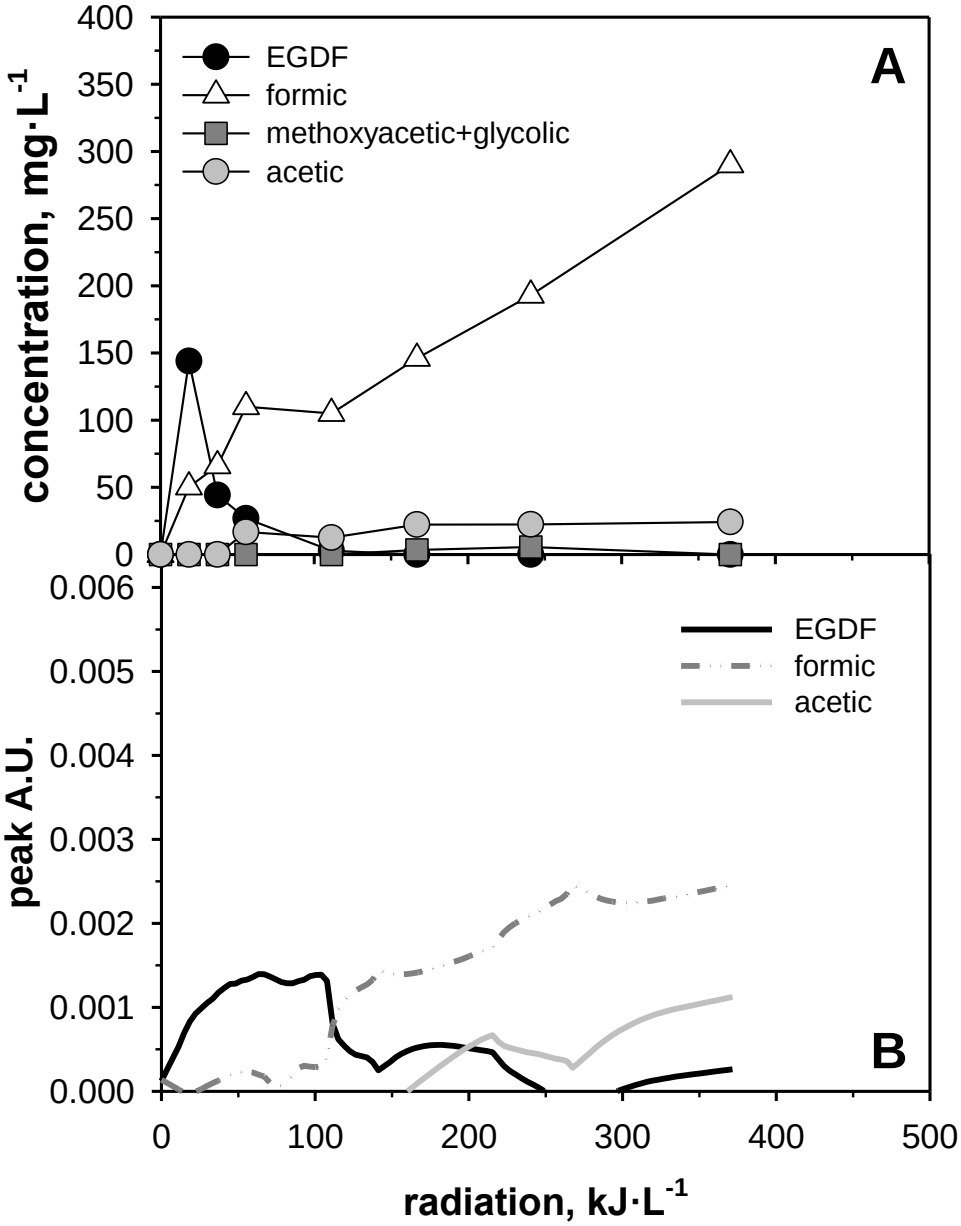
A
EGDF
formic
methoxyacetic+glycolic
acetic
concentration, mg·L-1
400
350
300
250
200
150
100
50
0
B
EGDF
formic
acetic
peak A.U.
0.006
0.005
0.004
0.003
0.002
0.001
0.000
0
100
200
300
400
500
radiation, kJ·L-1

1 FIGURE 4

2

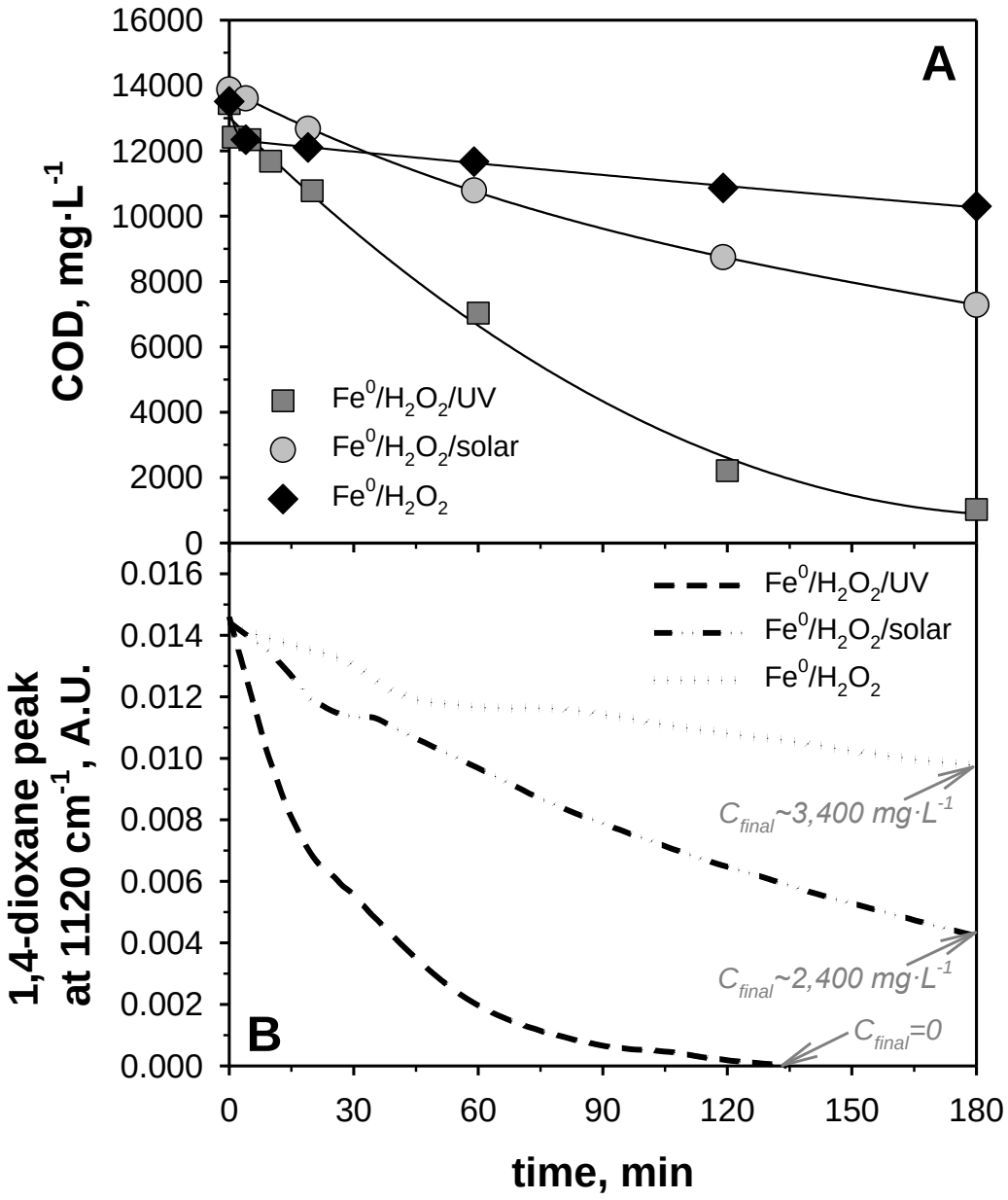
A
COD, mg·L-1
16000
14000
12000
10000
8000
6000
4000
2000
0
Fe0/H2O2/UV
Fe0/H2O2/solar
Fe0/H2O2
B
1,4-dioxane peak at 1120 cm-1, A.U.
0.016
0.014
0.012
0.010
0.008
0.006
0.004
0.002
0.000
Fe0/H2O2/UV
Fe0/H2O2/solar
Fe0/H2O2
Cfinal~3,400 mg·L-1
Cfinal~2,400 mg·L-1
Cfinal=0
0
30
60
90
120
150
180
time, min

1 FIGURE 5

2

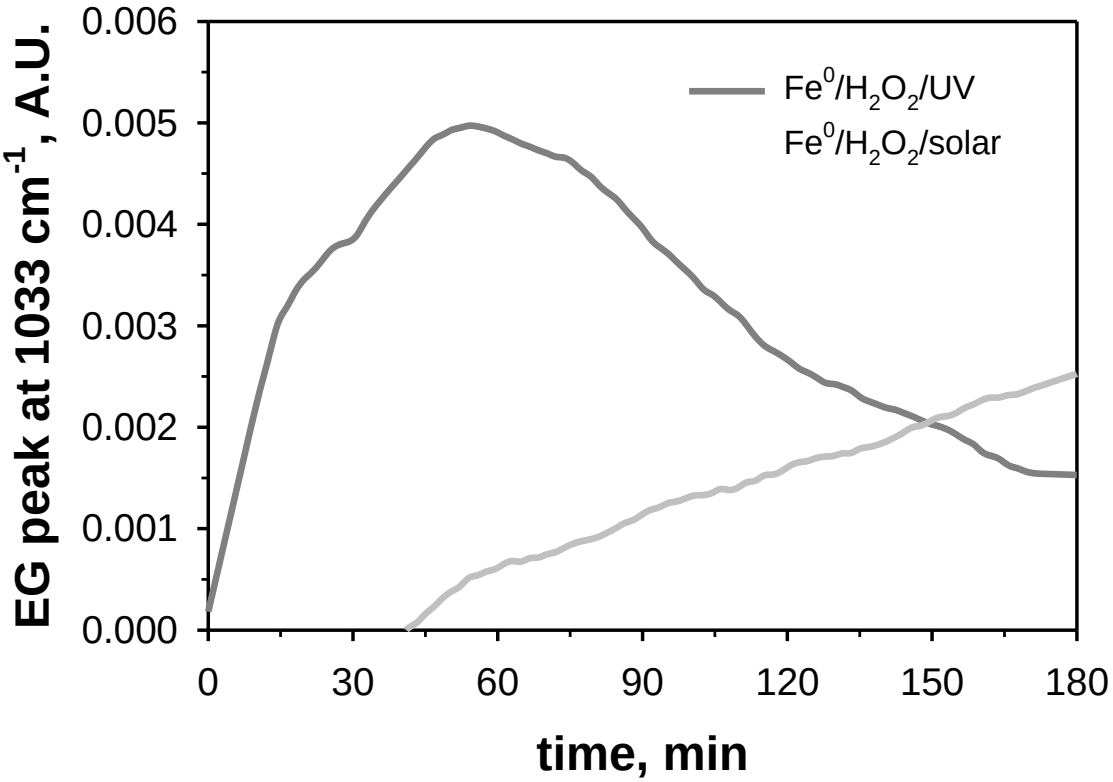
EG peak at 1033 cm-1, A.U.
0.006
0.005
0.004
0.003
0.002
0.001
0.000
0
30
60
90
120
150
180
time, min
Fe0/H2O2/UV
Fe0/H2O2/solar

1 FIGURE 6

2

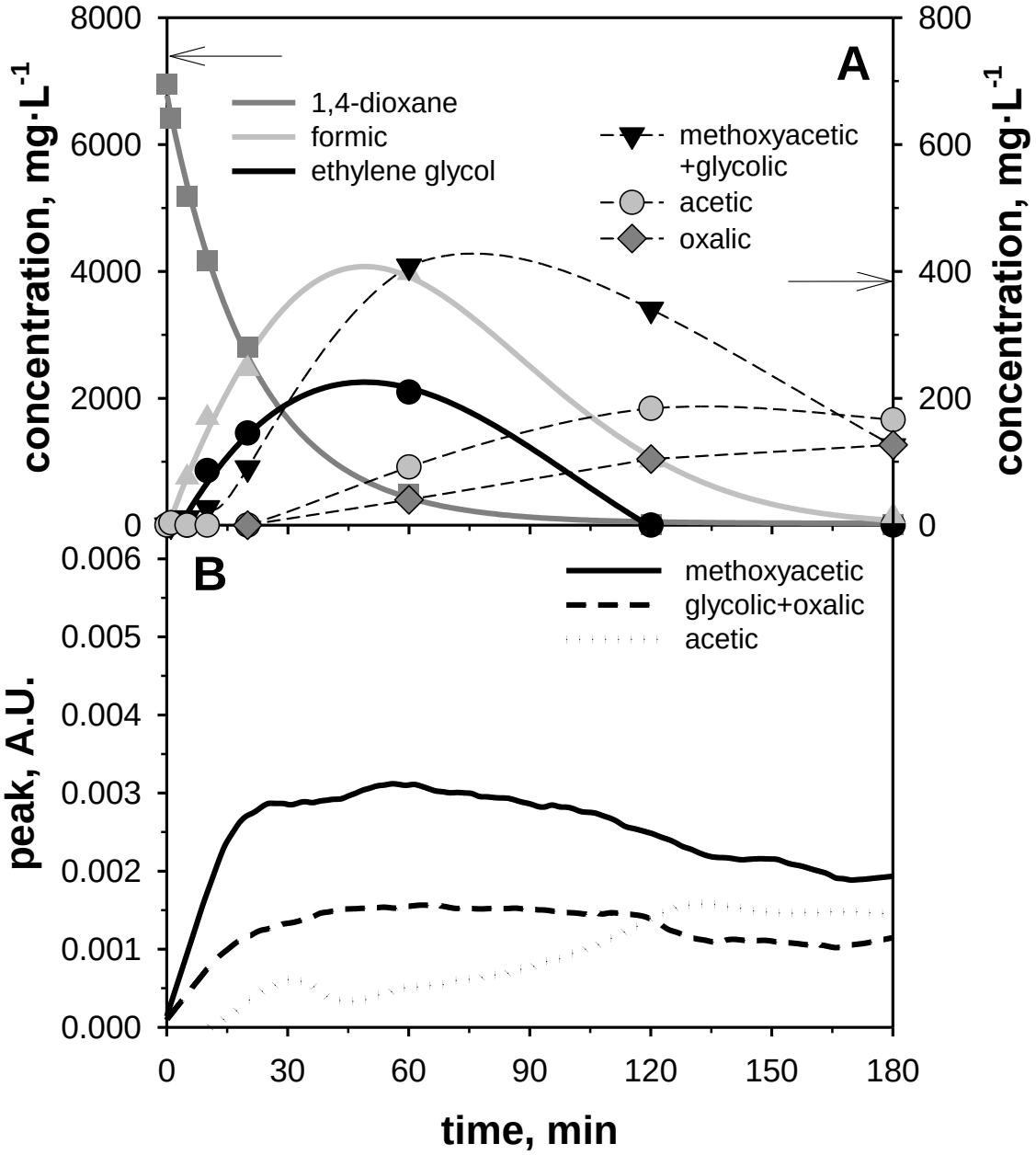
A
B
1,4-dioxane
formic
ethylene glycol
methoxyacetic
+glycolic
acetic
oxalic
methoxyacetic
glycolic+oxalic
acetic
concentration, mg·L-1
peak, A.U.
time, min
8000
6000
4000
2000
0
800
600
400
200
0
0.006
0.005
0.004
0.003
0.002
0.001
0.000
0
30
60
90
120
150
180

1 FIGURE 7

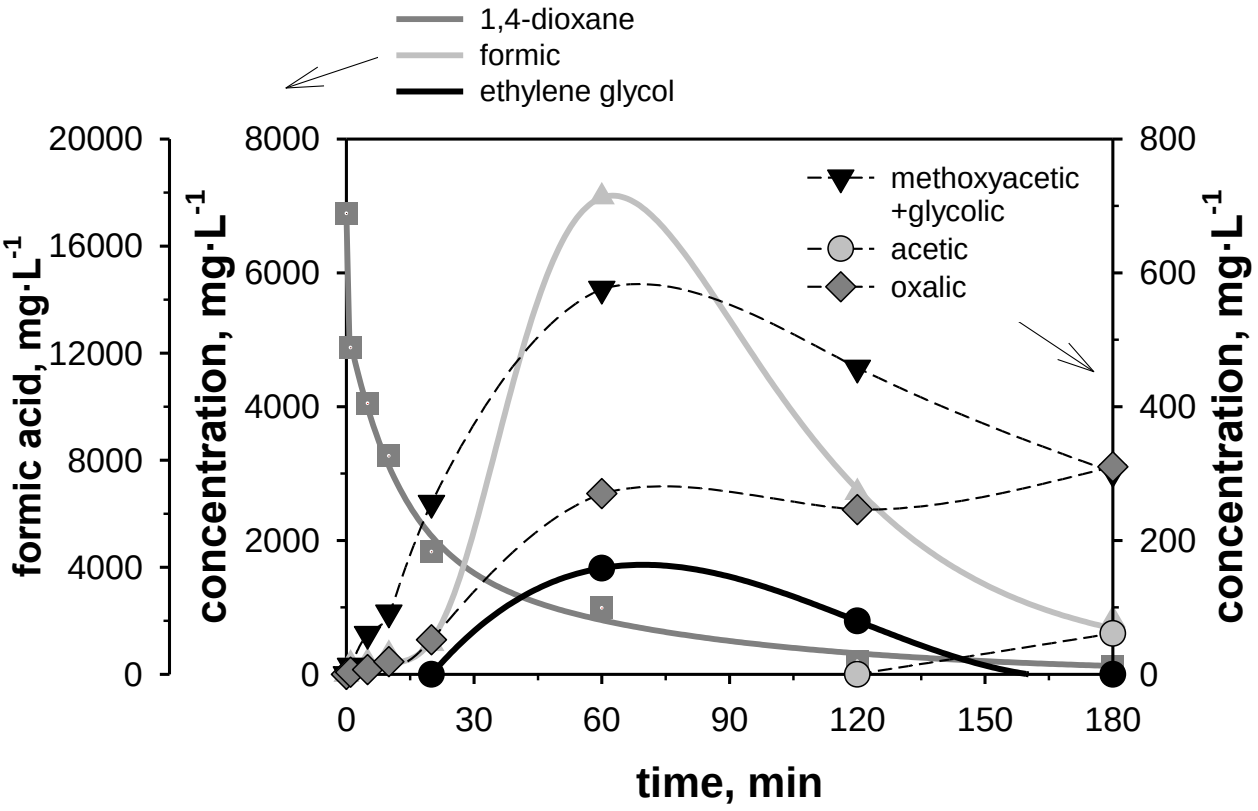
1,4-dioxane
formic
ethylene glycol
methoxyacetic
+glycolic
acetic
oxalic
formic acid, mg·L-1
concentration, mg·L-1
concentration, mg·L-1
time, min
0
4000
8000
12000
16000
20000
2000
6000
8000
200
400
600
800
30
60
90
120
150
180

1 FIGURE 8

2

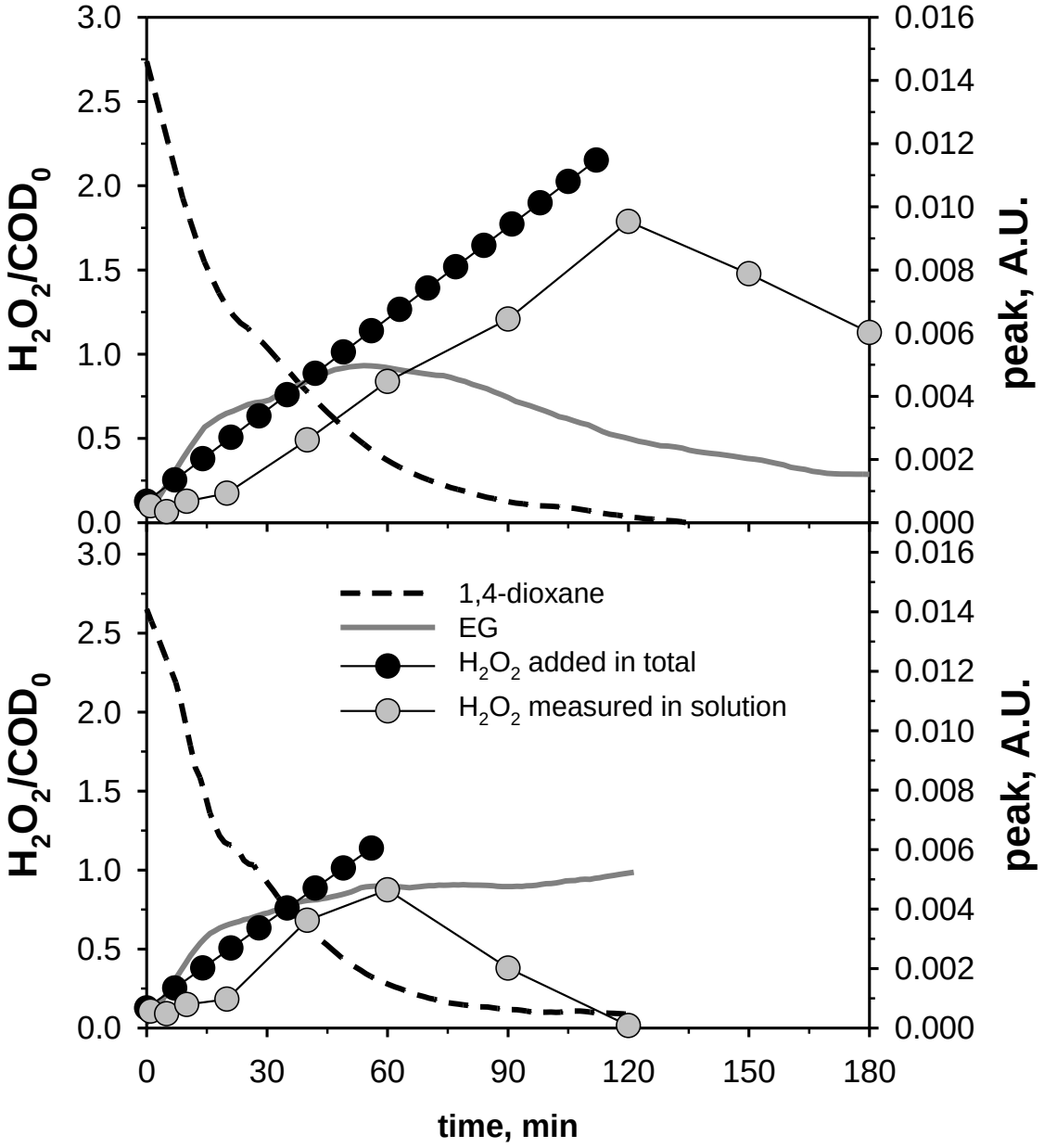
3.0
2.5
2.0
1.5
1.0
0.5
0.0
0.016
0.014
0.012
0.010
0.008
0.006
0.004
0.002
0.000
H2O2/COD0
peak, A.U.
1,4-dioxane
EG
H2O2 added in total
H2O2 measured in solution
0
30
60
90
120
150
180
time, min

1 SCHEME 1

2

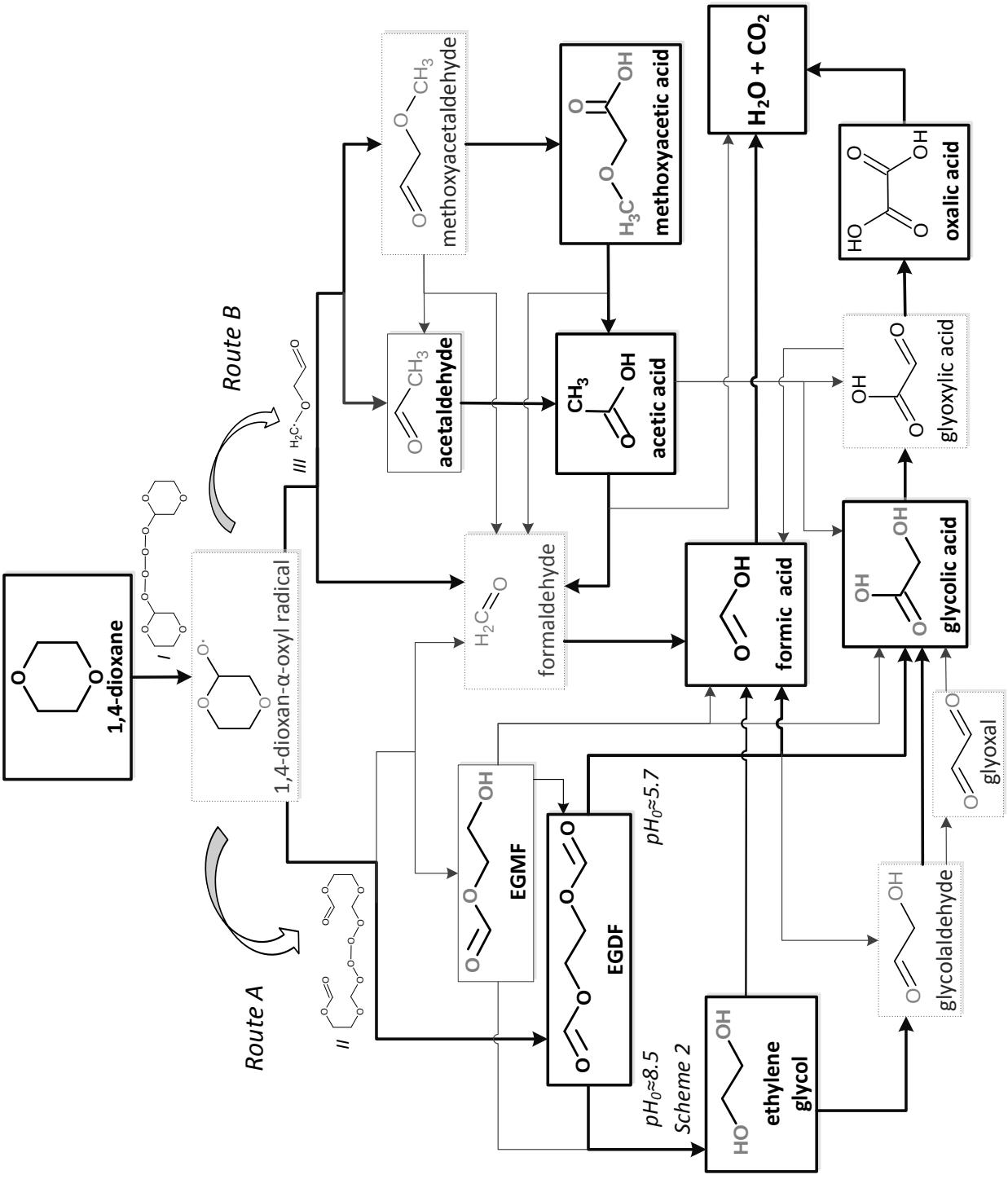
1,4-dioxane
I
1,4-dioxan-α-oxyl radical
Route B
III
Route A
II
methoxyacetaldehyde
methoxyacetic acid
acetaldehyde
acetic acid
formaldehyde
formic acid
glyoxylic acid
oxalic acid
H2O + CO2
glycolic acid
glycolaldehyde
glyoxal
EGMF
EGDF
pH0≈5.7
pH0≈8.5
ethylene glycol
Scheme 2

SCHEME 2

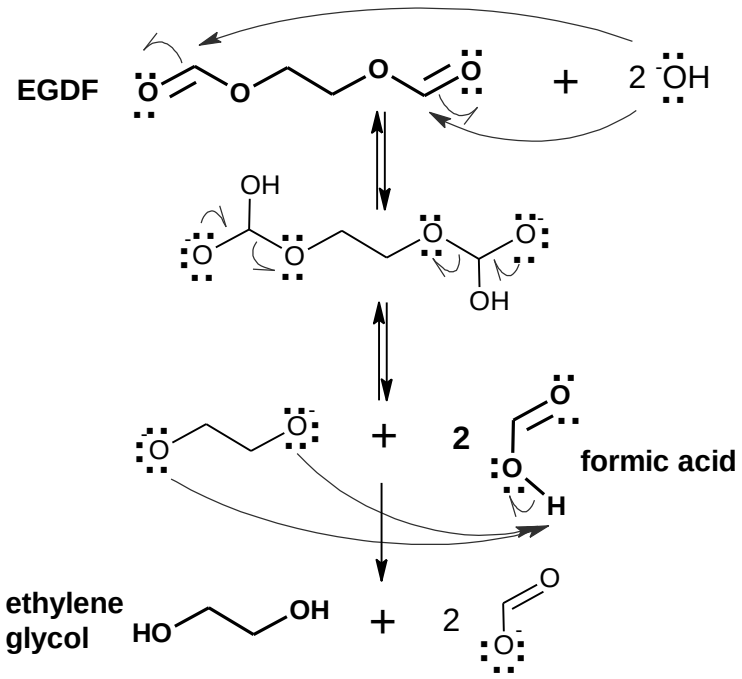

*Graphical Abstract

HIGHLIGHTS

- FTIR spectroscopy serves as a powerful tool for on-line reaction monitoring.
- Heterogeneous Fe^0-based photo-Fenton and TiO_2-photocatalysis were investigated.
- Catalytic oxidation of an emerging water pollutant, 1,4-dioxane, was accomplished.
- Major decomposition pathways of 1,4-dioxane were established and compared.
- Effects of light source, iron precursors, and H_2O_2 addition profile were assessed.

PUBLICATION VII

H. Barndõk, D. Hermosilla, A. Blanco

Comparison and predesign cost assessment of ozonation, electro-oxidation and heterogeneous photo-Fenton processes for the treatment of wastewaters from chemical industry

In progress

Comparison and predesign cost assessment of ozonation, electro-oxidation and heterogeneous photo-Fenton processes for the treatment of wastewaters from the chemical industry

Helen Barndõk, Daphne Hermosilla* and Ángeles Blanco

Department of Chemical Engineering, Universidad Complutense de Madrid, Avda. Complutense, s/n, 28040 Madrid. E-mail addresses (in order of appearance): hbarndok@quim.ucm.es, dhermosilla@quim.ucm.es, ablanco@quim.ucm.es

* Corresponding author:

Tel.: +34 91 394 4645; fax: +34 91 394 4243.

E-mail address: dhermosilla@quim.ucm.es (Daphne Hermosilla)

ABSTRACT

The preliminary cost analysis of the industrial implementation of different advanced oxidation processes (AOPs) was carried out for the pre-treatment of industrial wastewater from a chemical manufacturing industry contaminated with 1,4-dioxane. With the aim on reaching decontamination with minimal production of residues, basic ozone (O_3) oxidation, conductive diamond electrochemical oxidation (CDEO) and heterogeneous zero valent iron (Fe^0)-based photo-Fenton processes were chosen for the bio-augmentation study. According to the respirometric assays, all studied AOPs were fit to increase the biodegradability of the wastewater. Sufficient biodegradability (≈60%) was reached when the pre-treatment was conducted until 40% of COD removal, at which point most of the 1,4-dioxane was degraded to ethylene glycol and short chain carboxylic acids. Thus, 40% of COD removal was chosen as the design point for the subsequent financial pre-design of an AOP unit with a capacity of treating 43800 $m^3 \cdot y^{-1}$. According to the preliminary analysis of capital investment and annual operational expenses, UV photo-Fenton is the cheapest option at the chosen design point (4.1 $€ \cdot m^{-3}$), followed very closely by ozonation treatment (4.3 $€ \cdot m^{-3}$), whereas CDEO and solar/Fe^0/H_2O_2 treatments resulted more costly (5.2 and 6.2 $€ \cdot m^{-3}$, respectively). At the current design point, the sunlight-driven photo-Fenton is unfeasible due to the cost and size of the required plant space, but it could become an important alternative for lower COD reductions (<20%). On the other hand, to reach COD removals above 50%, O_3 appears to be more economic process, whereas the price of the BDD unit still limits its industrial application, despite its high oxidant-efficiency.

Keywords: 1,4-dioxane, biodegradability, AOPs, ozone, electrochemical oxidation, photo-Fenton, cost analysis.

1. Introduction

Along with the growing global water demand for processing and manufacture, the quality of water is becoming one of the biggest problems of the industrial world. One of the common emerging contaminants released with industrial wastewaters is 1,4-dioxane, a widely used industrial solvent, generated also as a by-product in chemical manufacturing (Mohr, 2010). This cyclic ether is easily found in the effluents of conventional wastewater treatment plants (WWTPs), indicating the inefficiency of traditional secondary treatments for complete removal of this compound (Mohr, 2010, Skadsen *et al.*, 2004, USEPA, 2006, Zenker *et al.*, 2003). 1,4-Dioxane may pose a multitude of harmful effects, such as kidney failure and liver damage, while animal studies reported its tumour promoter properties (ECB, 2002, NICNAS, 1998, USEPA, 2010). Thus, the treatment of industrial wastewaters containing 1,4-dioxane is crucial to prevent the pile-up of this persistent and bio-accumulative chemical in the environment.

Through an extensive research during the last two decades, advanced oxidation processes (AOPs) have shown great capacity to decontaminate effluent streams containing biorefractory substances (Andreozzi *et al.*, 1999, Comninellis *et al.*, 2008). 1,4-Dioxane removal from synthetic solutions with ultrapure water has been achieved with various common AOPs (Maurino *et al.*, 1997, Merayo *et al.*, 2014), whereas the fastest reductions have been reported with photo-Fenton processes (Chitra *et al.*, 2012). Although highly efficient, the classical Fenton processes have various disadvantages, like the need for acidification and subsequent neutralization, the production of iron sludge, and, additionally, the cost of UV radiation (Hermosilla *et al.*, 2009, Pignatello *et al.*, 2006). Thus, it is of great interest to search for more cost-effective and less residues-producing techniques, e.g. by employing solar light, using solid iron sources and milder pH conditions to avoid iron leaching.

As an alternative, the conductive diamond electrochemical oxidation (CDEO) also offers very high removals of refractory organics and, in addition, no generation of secondary pollution (Rodrigo *et al.*, 2010). However, its efficiency seems to be limited by the mass transport to the available electrode surface comprised of an expensive material with little know-how in industrial applications (Cañizares *et al.*, 2009). Ozonation treatment, on the contrary, is a widely implemented method in full scale operations, producing no residues either (Bertanza *et al.*, 2013), but the cost of ozone (O_3) production in prolonged treatment times could limit its viability for the treatment of highly loaded industrial wastewaters (Muñoz *et al.*, 2008)

In this framework, with the focus on reaching contaminant removal with minimal consumption of chemicals and minimal production of residues, a comparative study of 1,4-dioxane degradation in real industrial wastewaters was carried out, using heterogeneous photo-Fenton oxidation with zero valent iron (Fe^0) microspheres in neutral pH conditions (Barndõk *et al.*, 2016a), CDEO on boron doped diamond (BDD) electrodes (Barndõk *et al.*, 2014b) and basic ozonation (O_3/OH^-; Barndõk *et al.*, 2014a). Significant removals of 1,4-dioxane (>90%) were achieved by all of the studied AOPs. However, to adequately compare the performances and the industrial feasibility of the aforementioned AOPs, an economic analysis is required.

The total cost of an AOP, including capital investment and running process costs (Chatzisymeon *et al.*, 2010), depends directly on the process scale which is determined by the plant capacity and the chosen design point. Although high chemical oxygen demand (COD) and total organic carbon (TOC) removals were reported with all three processes, the total mineralization of organics in highly loaded industrial wastewaters by using AOPs is usually considered unfeasible. Therefore, the combination of AOPs with conventional methods, like biological process with activated sludge, for instance,

is the preferred option (Oller *et al.*, 2011). Thus, if the combination with biological treatment is the aim, the point of sufficient biodegradability enhancement by advanced oxidation pre-treatment determines the size and the oxidant requirements of the AOP, and, thus, its total cost.

Therefore, the objective of this study was to compare the previously optimized AOPs, basic ozonation, CDEO and heterogeneous Fe^0-based photo-Fenton, as possible pre-treatments to increase the biodegradability of an industrial wastewater containing 1,4-dioxane in order to recycle the effluent to the conventional biological process of the WWTP in the industry. For the financial pre-design, a preliminary analysis of capital investment and annual operational expenses was carried out, according to the chosen design point.

2. Materials and methods

Industrial wastewater contaminated with 1,4-dioxane was provided by a chemical manufacturing industry (COD=475±25 $mg \cdot L^{-1}$; pH_0=8.8±0.1; alkalinity=950±50 $mgCaCO_3 \cdot L^{-1}$; conductivity=2.0±0.1 $mS \cdot cm^{-1}$). Analytical grade chemicals were supplied by Merck KGaA (Darmstad, Germany) and Panreac S.A. (Barcelona, Spain). Synthetic 1,4-dioxane solution (C_0=7050 $mg \cdot L^{-1}$) for reaction intermediates study was prepared with deionized water and 1000 $mg \cdot L^{-1}$ of $CaCO_3$ to simulate the conditions with industrial wastewater. Sodium hydroxide (NaOH, 98.0%) was used for additional pH control in ozonation trials when needed. Sodium sulphate (Na_2SO_4, 99.0%) was added as supporting electrolyte in CDEO trials. Hydrogen peroxide (H_2O_2, 30% v/v) and Fe^0 (>98.3% Fe; <1% C; <1% N; <0.7% O) were used in the Fenton-based processes. The Fe^0 microspheres with 1 μm of particle size and 800 $m^2 \cdot kg^{-1}$ of surface area were obtained from BASF (ZVI Microspheres 800, Ludwigshafen, Germany).

The procedures of ozonation in bubble column, CDEO in a batch recirculation unit and photo-Fenton experiments with different light sources were described previously (Barndõk *et al.*, 2016a, Barndõk *et al.*, 2014a, Barndõk *et al.*, 2014b). All wastewater analyses were made according to the Standard Methods for the Examination of Water and Wastewaters (American Public Health Association, 2005). The analysis of pH, conductivity, COD, TOC were carried out as reported in previous publications (Barndõk *et al.*, 2014a, Barndõk *et al.*, 2014b). The additional measures taken for adequate sample manipulation in Fenton-based processes (filtration, quenching, H_2O_2 analysis) were described in detail by Merayo *et al.* (2014). The chromatographic methods for the analysis of 1,4-dioxane and its reaction intermediates are described in detail in a parallel study (Barndõk *et al.*, 2016b).

Biodegradability of pre-treated wastewater samples was assessed by respirometry trials in an ECHO R6 (Echo Instruments, Slovenske Konjice, Slovenia) respirometer equipped with an incubation cabin (at 20°C) with 6 parallel measuring channels and gas analyser. The trials were conducted in the presence of constant supply of air, using a controlled quantity of biosludge from the WWTP of a local paper mill (1.5 $g \cdot L^{-1}$ in final solution; OECD, 2010) mixed either with the industrial wastewater sample, with a blank sample of deionized water or with a reference sample of a biodegradable substrate containing the same COD as the wastewater sample. A stock solution of concentrated biodegradable substrate with 100,000 $mg \cdot L^{-1}$ of COD was prepared and diluted to the COD required for every separate experiment. The COD of the biodegradable organic matter was provided by: 25% yeast, 25% peptone, 20% Na-acetate, 20% glucose and 10% urea. Nutrients were added to all tests (including blank samples with water) in a form of NH_4Cl, KH_2PO_4, $MgSO_4$, $FeCl_3$ and $CaCl_2$. The pH of all the waters was adjusted to about 7.0-7.5 before the addition of sludge. All the samples were aerated for

30 min before adding the sludge. The respirometric measurement was based on analysing the carbon dioxide (CO_2) content in the incoming and outgoing air and the output data was the accumulated production of CO_2 during 60min of the vital activity of the bacteria. The results were corrected by subtracting the results of endogenous activity with the blank sample. Finally, the biodegradability was calculated by Equation 1:

$$Biodegradability, \% = \frac{Respiration_{wastewater, mgCO_2}}{Respiration_{reference\ sample, mgCO_2}} \times 100 \quad (1)$$

3. Results and discussion

3.1. Design point

The respirometric trials of biodegradability assessment showed that all three AOPs increased the initial biodegradability of the industrial wastewater (≈6%), whereas the bio-augmentation seemed to correlate with the previous COD removal by AOP, indifferent to the pre-treatment (Figure 1). Therefore, as a simplification, COD removal was taken as the basis of design point selection, according to which, sufficient biodegradability (≈60%) was reached when advanced oxidation pre-treatment was conducted up to 40% removal of COD.

This simplification was also supported by the analysis of reaction intermediates, since the decomposition of 1,4-dioxane took a rather similar course in all AOP experiments. Namely, as shown for electrochemical oxidation in Figure 2, the oxidation of 1,4-dioxane by hydroxyl radical (•OH) occurred through the generation of ethylene glycol diformate (EGDF) and ethylene glycol monoformate (EGMF) as its primary intermediates. EGDF and EGMF were hydrolysed to ethylene glycol (EG) in basic conditions maintained by the presence of carbonaceous alkalinity (pH_0≈8.5). It can be visualised that at the point of 40% COD removal, most of the 1,4-dioxane is degraded to EG and short chain carboxylic acids that are not expected to produce any inhibitory

effect on the subsequent biological treatment (Shieh *et al.*, 1998), in agreement with the biodegradability assays.

3.2. Capital cost

To evaluate the industrial implementation of the studied AOPs, a pre-design economic assessment was made, considering an AOP treatment capacity of 43800 $m^3 \cdot y^{-1}$ which is the flow rate of the industry producing the wastewater under concern. The size and cost of AOP units were found taking into account both the experimentally found oxidant requirements and the existing literature on such treatments. When necessary, the prices were rescaled for different treatment capacities, using the logarithmic relationship known as the six-tenths-factor rule (Equation 2) (Chatzisymeon *et al.*, 2010, Peters *et al.*, 2003), whereas all the prices were updated, considering the change in chemical engineering plant cost index (CEPCI, 2015).

$$Price_{new} = Price_{reference} \times \left(\frac{Capacity_{new}}{Capacity_{reference}}\right)^{0.6} \times \frac{CEPCI_{actual}}{CEPCI_{past}} \quad (2)$$

The ultimate dimension parameters to determine the cost of the different AOP units, in accordance with the chosen design point, are presented in Table 1. Considering the necessary total O_3 production, the cost of the ozonation unit (including generator, dosification system and refrigeration) was facilitated by two commercial manufacturers of industrial ozonation systems (Xylem and Primozone). The price of the CDEO unit was found based on the literature (Cañizares *et al.*, 2009, Chatzisymeon *et al.*, 2010) and the average unit price of BDD provided by NeoCoat SA (14,000 $€ \cdot m^{-2}$). The price of the UV photo-Fenton unit was found by the study of Muñoz *et al.* (2008), whereas the cost of solar photo-Fenton was calculated by the necessary compound parabolic collector (CPC) area (Muñoz, 2006), considering the unit price of CPC to be 349 $€ \cdot m^{-2}$ (De Torres-Socias *et al.*, 2015).

Based on the price of AOP unit, the fixed capital investment was found incorporating the estimated cost of piping, valves, and electrical work (30%), site work (10%), engineering (15%), contractor (15%) and contingency (20%) (Kommineni *et al.*, Mahamuni & Adewuyi, 2010). The working capital investment required for the plant start-up was considered 15% of the fixed capital investment (Chatzisymeon *et al.*, 2010).

3.3. Operation cost

The operating parameters used for the assessment were the cost of energy, chemicals, maintenance, analytic monitoring and labour-hours. The energy consumption for CDEO and UV photo-Fenton was obtained from experimental data, taking into account the price of the industrial electricity in Spain (0.1 €·kWh^{-1}; Eurostat, 2015). Additional consumption in pumping, cooling and reagent injection operations was added according to the literature (10-40% depending on the process; Chang *et al.*, 2008, Karat, 2013, Kommineni *et al.*, Mahamuni & Adewuyi, 2010). The total energy consumed by an industrial O_3 generator was considered to be 18 kWh·kgO_3^{-1}, already including both O_3 generation and the additional consumption for refrigeration, in accordance with the commercial providers (Xylem, Inc.) and the literature (Karat, 2013). In solar applications, pumping was considered the main source of electricity withdrawal, in correlation with the area of the compound parabolic collector, as described in detail by Muñoz (2006).

The chemicals cost was calculated, considering the latest industrial prices, wherefore all the prices were updated by the annual cost indexes for chemical products (INE, 2015). The price of the off–fence O_2 gas for O_3 production was 85 €·t^{-1} (Karat, 2013) and the optimized industrial consumption rate was considered 10 kgO_2·kgO_3^{-1} (Muñoz, 2006). The costs of the rest of the reagents were 0.45 €·kg^{-1} for H_2O_2 (50%),

0.3 €·kg^{-1} for NaOH, 0.09 €·kg^{1} for Na_2SO_4 and 5 €·kg^{-1} for Fe^0 powder (Alibaba, 2015). The calculations were done assuming 90% of catalyst recovery on daily basis, whereas the waste catalyst landfilling was considered to cost 0.07 €·kg^{-1} (Muñoz, 2006).

The annual cost of maintenance and parts replacement was considered to be 3% of the fixed capital investment for CDEO and solar-enhanced systems and 1.5% for ozonation. The maintenance (mainly lamps replacement) of UV photo-Fenton was calculated as 45% of annual electricity consumption (Mahamuni & Adewuyi, 2010).

The cost of the required labour and the laboratory work for analytic monitoring was found by consulting with a local firm that offer wastewater treatment solutions, considering the required work as an additional task for the existing personnel.

3.4. Total cost

The total annual cost of the treatments consisting of annual capital investment and annual operation cost was found by Equation 4, defining the useful life of AOP plant at 15 years (Muñoz *et al.*, 2008) and using an interest rate of 5%, leading to a capital recovery factor (CRF) of 9.6% (Equation 5; Chatzisymeon *et al.*, 2010).

$$Total\ cost, \frac{€}{y} = Capital\ investment, € \times CRF, \frac{\%}{y} + Operation\ cost, \frac{€}{y} \quad (4)$$

$$CRF, \% = \frac{interest,\% \times (1+interest,\%)^{years}}{(1+interest,\%)^{years}-1} \quad (5)$$

The main components of the total investment required for the industrial implementation of the AOPs under study are presented in Table 2. According to this preliminary economic assessment, UV photo-Fenton is the cheapest option at the chosen design point (4.1 €·m^{-3} for 40% COD removal at a plant capacity of 43800 m^3·y^{-1}), followed very closely by ozonation treatment (4.3 €·m^{-3}). Meanwhile, CDEO and solar/Fe^0/H_2O_2 treatments were found to be more costly (5.2 and 6.2 €·m^{-3}, respectively). Although much less energy is consumed in solar photo-Fenton process

(≈4,000 €·y^{-1}) than in UV photo-Fenton treatment (≈59,000 €·y^{-1}), the sunlight-driven process is unfeasible in this scale due to the cost of CPC installation (≈1,495,000 €) and the required plant space (2254 m^2).

Due to the different reaction kinetics of the studied processes, their economic comparison is quite different when changing the objective of organics degradation. According to the graph of annual costs as a function of COD removal (Figure 3), UV enhanced photo-Fenton is the most economical solution at COD removals in the range of 20-45%, whereas ozonation appears to be more suitable application when the AOP is designed for COD removals higher than 50% at which UV photo-Fenton becomes unviable due to the excessive electricity expenses. Although faster and, thus, more energy-efficient reduction is achieved with CDEO than with O_3, the cost of the electro-oxidation unit with BDD electrodes still limits its industrial application. While ozonation technology exhibits much great know-how of full scale implementation, CDEO is still a process not yet fully explored in the field of industrial wastewater treatment. However, the advances in the field of conductive diamond technology could change that situation, converting CDEO an important competitor to both O_3 and Fenton-based processes in the future.

In addition, it is important to note that solar photo-Fenton appears to become profitable at COD removals below 20%, as shown in Figure 3, provided that the enterprise has the space required for the CPC unit. As the cost and viability of the solar/Fe^0/H_2O_2 application is directly related to the CPC area, the required area was plotted as a function of both COD removal and plant capacity (Figure 4A). According to this 3D-plot, if 20% of COD removal was sufficient, the CPC area required to treat 43800 $m^3 \cdot y^{-1}$ would decrease to approximately 500 m^2, whereas the area to treat 10000 $m^3 \cdot y^{-1}$ would be around 130 m^2. These are space requirements that still become an

obstacle for many industrial plants, but could already be considered by many others (according to the proposal of Muñoz (2006), one of the solution would be installing the CPC unit on the rooftops of the existing facilities). On the other hand, when considering the treatment for even smaller wastewater flows, it is important to note that the predicted annual costs of all the studied AOPs (in terms of €·m^{-3}) shoot up for capacities lower than 10000 $m^3 \cdot y^{-1}$, as shown for solar photo-Fenton in Figure 4B.

The predictions presented in Table 1 principally allow the comparison of the installation and the operation costs of the different technologies. Nonetheless, care must be taken when interpreting the exact figures based on laboratory scale experimentation, since much more efficient use of the oxidant is expected in fully optimized industrial units. There are several factors affecting different AOPs, such as the position and the number of UV lamps in the photo-Fenton reactor, the bubble size and the O_3 injection method used in ozonation process (bubble diffusers, venturi eductors, membrane contactors, etc.), the flow pattern and the configuration of electrodes in the electrolytic cell, and the thickness of the illuminated wastewater layer and the configuration of the solar collector in solar photo-Fenton. Moreover, an AOP unit can be comprised of one reactor or multiple consecutive units, depending on the optimal combination, whereas the size of the reactor(s) can greatly affect the process efficiency as well. For instance, the mass transfer and, thus, the oxidation rate in an electrolytic flowcell is greater when the layer of water between the electrodes is thinner, and the industrial BDD units normally consist of small modules of electrodes in multiple stacks. On the other hand, the contact time and, thus, the oxidation rate with O_3 is greater in large full scale reactors, especially when pressure driven O_3 injection is used that allows greater dissolution of O_3 than the bubble diffusers. Furthermore, for any of these AOPs, before an actual industrial implementation, a preliminary pilot scale study coupled with the real

biological treatment unit of the fabric would be obligatory in order to correctly determine the optimal design point of biodegradability enhancement. Nevertheless, since similar hypothesis were used to calculate the cost of each treatment, this preliminary cost assessment permits comparing these four processes, offering a good insight of the components constituting the final price of the treatments.

Moreover, for any of these AOPs, before an actual industrial implementation, a preliminary pilot scale study coupled with the real biological treatment unit of the fabric would be obligatory in order to correctly determine the optimal design point of biodegradability enhancement.

Conclusions

Basic ozonation, CDEO and heterogeneous Fe^0-based photo-Fenton were all proven fit for increasing the biodegradability of an industrial wastewater containing 1,4-dioxane. According to the respirometric assays, sufficient biodegradability (≈60%) was reached when advanced oxidation pre-treatment was conducted up to 40% removal of COD. At that point, most of the 1,4-dioxane was degraded to EG and short chain carboxylic.

To evaluate the possible industrial implementation of the studied AOPs, a pre-design economic assessment based on lab scale experimentation was made for an AOP unit planned to reach 40% of COD removal with a capacity to treat 43800 $m^3 \cdot y^{-1}$ of wastewater. According to this preliminary cost assessment, UV photo-Fenton is the cheapest option at the chosen design point (4.1 $€ \cdot m^{-3}$), followed very closely by ozonation treatment (4.3 $€ \cdot m^{-3}$), whereas CDEO and solar/Fe^0/H_2O_2 treatments resulted more costly (5.2 and 6.2 $€ \cdot m^{-3}$, respectively). At 40% COD removal, the sunlight-driven process is unfeasible due to the cost of CPC installation and the required plant space, but it could become an important alternative for lower COD reductions (<20%). In

general, the photo-Fenton applications seem to be more suitable as pre-treatments with low COD removals. However, at COD removals above 50%, ozonation appears to be a more economic process. Although more energy-efficient reduction is achieved with CDEO than with O_3, the cost of the BDD unit still limits its industrial application.

Since similar hypothesis were used to calculate the cost of each treatment, this preliminary economic assessment permits comparing these four processes, offering a good insight of the components constituting the final price of the treatments. Nonetheless, care must be taken when interpreting the exact figures based on laboratory scale experimentation, since much more efficient use of the oxidant is expected in fully optimized industrial units.

Acknowledgements

The research leading to these results has received funding from the European Union's Seventh Framework Programme (FP7/2007-2013) under the grant agreement n° 608490, E4Water project. The collaboration of the Gas Chromatography Service (CIB) of the Spanish National Research Council (CSIC), the Laboratory of Geochemical and Environmental Analyses of the Complutense University of Madrid and the Laboratory of CIFOR-INIA (*Centro de Investigación Forestal, Instituto Nacional de Investigación y Tecnología Agraria y Alimentaria*) is fully appreciated. The Archimedes Foundation (Estonia) is acknowledged for support to Helen Barndõk's Ph.D. studies.

References

Alibaba (2015). Chemicals Market, www.alibaba.com, Accessed: June 5, 2015.

American Public Health Association (2005). *Standard methods for the examination of water and wastewater*. Washington, D.C.

Andreozzi, R., Caprio, V., Insola, A. & Marotta, R. (1999). Advanced oxidation processes (AOP) for water purification and recovery. *Catalysis Today* 53, 51-59.

Barndõk, H., Blanco, L., Hermosilla, D. & Blanco, Á. (2016a). Heterogeneous photo-Fenton processes using zero valent iron microspheres for the treatment of wastewaters contaminated with 1,4-dioxane. *Chemical Engineering Journal 284 (2016) 112-121*.

Barndõk, H., Cortijo, L., Hermosilla, D., Negro, C. & Blanco, A. (2014a). Removal of 1,4-dioxane from industrial wastewaters: Routes of decomposition under different operational conditions to determine the ozone oxidation capacity. *Journal of Hazardous Materials* 280, 340-347.

Barndõk, H., Hermosilla, D., Cortijo, L., Torres, E. & Blanco, A. (2014b). Electrooxidation of industrial wastewater containing 1,4-dioxane in the presence of different salts. *Environmental Science and Pollution Research* 21, 5701-5712.

Barndõk, H., Hermosilla, D., Han, C., Dionysiou, D. D., Negro, C. & Blanco, Á. (2016b). Degradation of 1,4-dioxane from industrial wastewater by solar photocatalysis using immobilized NF-TiO2 composite with monodisperse TiO2 nanoparticles. *Applied Catalysis B: Environmental* 180, 44-52.

Bertanza, G., Papa, M., Pedrazzani, R., Repice, C. & Dal Grande, M. (2013). Tertiary ozonation of industrial wastewater for the removal of estrogenic compounds (NP and BPA): a full-scale case study. *Water Science and Technology* 68, 567-574.

Cañizares, P., Paz, R., Saez, C. & Rodrigo, M. A. (2009). Costs of the electrochemical oxidation of wastewaters: A comparison with ozonation and Fenton oxidation processes. *Journal of Environmental Management* 90, 410-420.

CEPCI (2015). Economic indicators: Chemical Engineering Plant Cost Index. *Chemical Engineering, http://www.chemengonline.com/pci-home, Accessed June 12, 2015*.

Comninellis, C., Kapalka, A., Malato, S., Parsons, S. A., Poulios, L. & Mantzavinos, D. (2008). Advanced oxidation processes for water treatment: advances and trends for R&D. *Journal of Chemical Technology and Biotechnology* 83, 769-776.

Chang, Y., Reardon, D. J., Kwan, P., Boyd, G., Brant, J., Rakness, K. L. & Furukawa, D. (2008). Evaluation of Dynamic Energy Consumption of Advanced Water and Wastewater Treatment Technologies. Denver: Awwa Research Foundation.

Chatzisymeon, E., Diamadopoulos, E. & Mantzavinos, D. (2010). Comparison and predesign cost estimation of advanced oxidation processes for olive mill wastewater treatment. *Proceedings of the 2nd International Conference on Hazardous and Industrial Waste Management*. 5-8 October (2010), Chania.

Chitra, S., Paramasivan, K., Cheralathan, M. & Sinha, P. K. (2012). Degradation of 1,4-dioxane using advanced oxidation processes. *Environmental Science and Pollution Research* 19, 871-878.

De Torres-Socias, E., Prieto-Rodriguez, L., Zapata, A., Fernandez-Calderero, I., Oller, I. & Malato, S. (2015). Detailed treatment line for a specific landfill leachate remediation. Brief economic assessment. *Chemical Engineering Journal* 261, 60-66.

ECB (2002). European Union Risk Assessment Report. 1,4-dioxane (CAS No: 123-91-1). *2nd Priority List* 21, 1-129.

Eurostat (2015). http://appsso.eurostat.ec.europa.eu/nui/show.do?dataset=nrg_pc_205_c&lang=en, Accessed: June 4, 2015.

Hermosilla, D., Cortijo, M. & Huang, C. P. (2009). Optimizing the treatment of landfill leachate by conventional Fenton and photo-Fenton processes. *Science of the Total Environment* 407, 3473-3481.

INE (2015). Instituto Nacional de Estadística, www.ine.es, Accessed: June 5, 2015.

Karat, I. (2013). Advanced Oxidation Processes for Removal of COD from Pulp and Paper Mill Effluents. A Technical, Economical and Environmental Evaluation. *Industrial Ecology*. Stockholm: Royal Institute of Technology.

Kommineni, S., Zoeckler, J., Stocking, A., Liang, S., Flores, A., Kavanaugh, M., Rodriguez, R., Browne, T., Roberts, R., Brown, A. & Stocking, A. Advanced Oxidation Processes. *National Water Research Institute, http://www.nwri-usa.org/pdfs/TTChapter3AOPs.pdf,* Accessed: June 12, 2015.

Mahamuni, N. N. & Adewuyi, Y. G. (2010). Advanced oxidation processes (AOPs) involving ultrasound for waste water treatment: A review with emphasis on cost estimation. *Ultrasonics Sonochemistry* 17, 990-1003.

Maurino, V., Calza, P., Minero, C., Pelizzetti, E. & Vincenti, M. (1997). Light-assisted 1,4-dioxane degradation. *Chemosphere* 35, 2675-2688.

Merayo, N., Hermosilla, D., Cortijo, L. & Blanco, Á. (2014). Optimization of the Fenton treatment of 1,4-dioxane and on-line FTIR monitoring of the reaction. *Journal of Hazardous Materials*.

Mohr, T. K. G. (2010). *Environmental Investigation and remediation: 1,4-dioxane and other solvent stabilizers*. Boca Raton: CRC Press.

Muñoz, I. (2006). Life Cycle Assessment as a Tool for Green Chemistry: Application to Different Advanced Oxidation Processes for Wastewater Treatment. *Chemistry Department*. Bellaterra: Autonomous University of Barcelona.

Muñoz, I., Malato, S., Rodriguez, A. & Domenech, X. (2008). Integration of environmental and economic performance of processes. Case study on advanced oxidation processes for wastewater treatment. *Journal of Advanced Oxidation Technologies* 11, 270-275.

NICNAS (1998). 1,4-Dioxane: Priority Existing Chemical No. 7: Full Public Report. Australian Government Publishing Service, Canberra: National Industrial Chemical Notification and Assessment Scheme.

OECD (2010). Activated Sludge, Respiration Inhibition Test (Carbon and Ammonium Oxidation). *OECD guidelines for the testing of chemicals* 209.

Oller, I., Malato, S. & Sanchez-Perez, J. A. (2011). Combination of Advanced Oxidation Processes and biological treatments for wastewater decontamination-A review. *Science of the Total Environment* 409, 4141-4166.

Peters, M. S., Timmerhaus, K. D. & West, R. E. (2003). *Plant Design and Economics for Chemical Engineers, 5th Ed.* New York: McGraw-Hill.

Pignatello, J. J., Oliveros, E. & MacKay, A. (2006). Advanced oxidation processes for organic contaminant destruction based on the Fenton reaction and related chemistry. *Critical Reviews in Environmental Science and Technology* 36, 1-84.

Rodrigo, M. A., Canizares, P., Sanchez-Carretero, A. & Saez, C. (2010). Use of conductive-diamond electrochemical oxidation for wastewater treatment. *Catalysis Today* 151, 173-177.

Shieh, W. K., Lepore, J. A. & Zandi, I. (1998). Biological fluidized bed treatment of ethylene and propylene glycols. *Water Science and Technology* 38, 145-153.

Skadsen, J. M., Rice, B. L. & Meyering, D. J. (2004). The occurence and fate of pharmaceuticals, personal care products, and endocrine disrupting compounds in a municipal water use cycle: A case study in the City of Ann Arbor. *Water Utilities, City of Anna Arbor, and Fleis & VendenBrink Engineering, Inc.*

USEPA (2006). Treatment Technologies for 1,4-Dioxane: Fundamentals and Field Applications, EPA-542-R-06-009. Washington D.C.: U.S. Environmental Protection Agency, Office of Solid Waste and Emergency Response.

USEPA (2010). Toxicological review of 1,4-dioxane (CAS No. 123-91-1), EPA/635/R-09/005-F. Washington, DC: U.S. Environmental Protection Agency.

Zenker, M. J., Borden, R. C. & Barlaz, M. A. (2003). Occurrence and treatment of 1,4-dioxane in aqueous environments. *Environmental Engineering Science* 20, 423-432.

Tables

Table 1. Ultimate dimension parameters determining the size and cost of the AOP unit for the treatment of 43800 $m^3 \cdot y^{-1}$ of industrial wastewater until 40% of COD removal (rescaling based on lab scale experimentation)

AOP	Dimension parameter	Value
O_3	ozone production	4.2 $kgO_3 \cdot h^{-1}$
CDEO (BDD)	electrode area	37 m^2
UV/Fe^0/H_2O_2	UV intensity	40 $mJ \cdot h^{-1}$
Solar/Fe^0/H_2O_2	CPC area	2254 m^2

Table 2. Estimation of the total costs of different AOPs for the treatment of 43800 $m^3 \cdot y^{-1}$ of industrial wastewater until 40% of COD removal

	O_3	CDEO (BDD)	UV/Fe^0/H_2O_2	Solar/Fe^0/H_2O_2
CAPITAL INVESTMENT				
Fixed capital investment, €	366,823	881,361	237,904	1,494,574
Working capital investment, €	55,023	132,204	35,686	224,186
Total capital investment, €	**421,847**	**1,013,566**	**273,590**	**1,718,760**
Annual capital cost, €·y^{-1}	**40,642**	**97,649**	**26,358**	**165,589**
Capital cost per m^3, €·m^{-3}	*0.9*	*2.2*	*0.6*	*3.8*
OPERATION AND MAINTENANCE (O&M) COST				
Energy	65,752	59,218	58,632	3,620
Chemicals	37,830	5,830	29,912	18,677
Repairs and maintenance	5,502	26,441	26,392	44,845
Labour	25,000	25,000	25,000	25,000
Analysis	12,000	12,000	12,000	12,000
Annual O&M cost, €·y^{-1}	**146,085**	**128,489**	**151,936**	**104,142**
O&M cost per m^3, €·m^{-3}	*3.3*	*2.9*	*3.5*	*2.4*
TOTAL COST				
Total annual cost, €·y^{-1}	**186,726**	**226,138**	**178,294**	**269,731**
Annual cost per m^3, €·m^{-3}	*4.3*	*5.2*	*4.1*	*6.2*

Figures

Figure 1. Evolution of the biodegradability of industrial wastewater as a function of the COD removal in its pre-treatment by different AOPs.

Figure 2. Concentration profiles of 1,4-dioxane (C_0=7050 mg/L) and its intermediate decomposition products along with the COD removal during the CDEO treatment.

Figure 3. Previsied annual cost of different AOPs for varying COD removals at the plant capacity of 43800 $m^3 \cdot y^{-1}$.

Figure 4. CPC area required for the solar photo-Fenton treatment as a 3D-function of COD removal (5-40%) and plant capacity (1000-45000 $m^3 \cdot y^{-1}$).

FIGURE 1

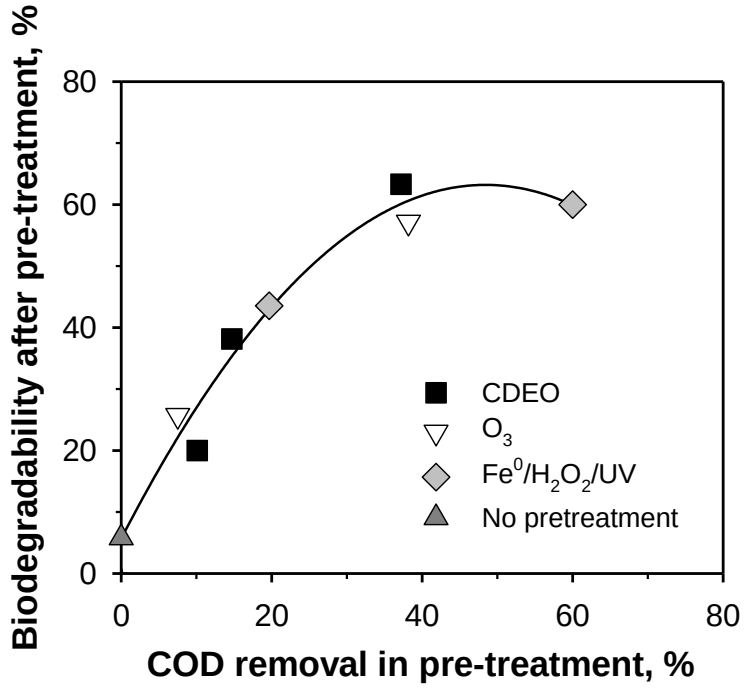

Figure 1. Evolution of the biodegradability of industrial wastewater as a function of the COD removal in its pre-treatment by different AOPs.

FIGURE 2

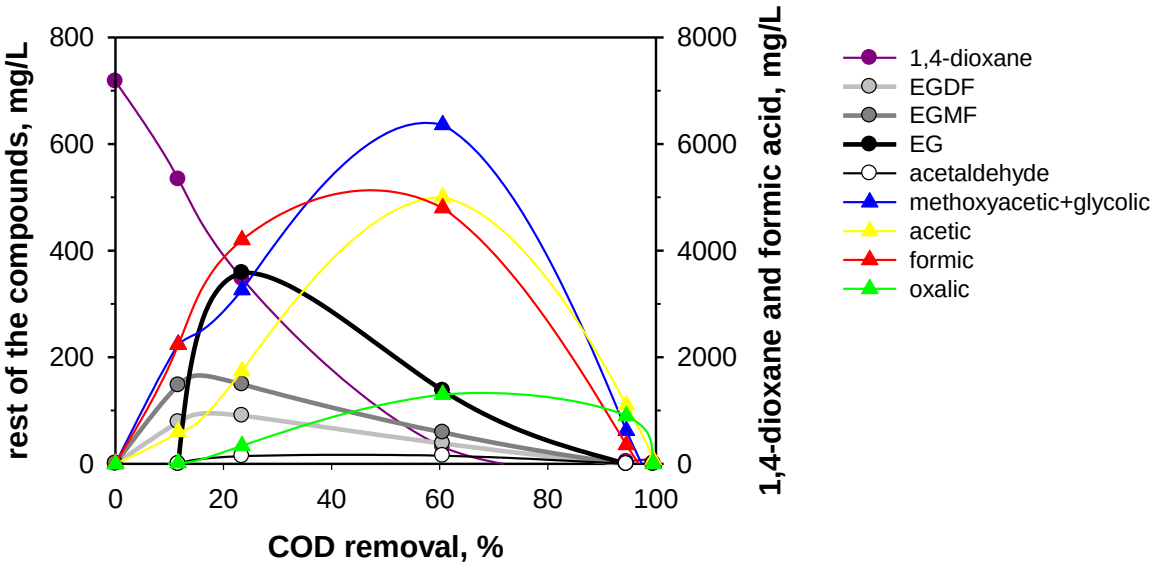

Figure 2. Concentration profiles of 1,4-dioxane (C_0=7050 mg/L) and its intermediate decomposition products along with the COD removal during the CDEO treatment.

FIGURE 3

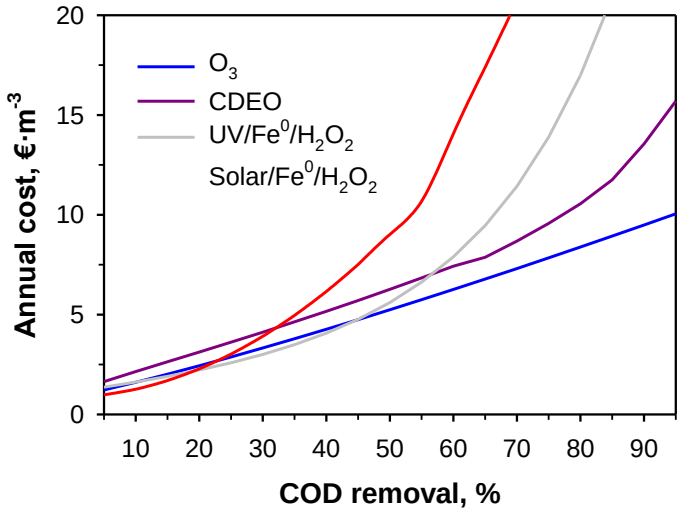

Figure 3. Prevised annual cost of different AOPs for varying COD removals at the plant capacity of 43800 $m^3 \cdot y^{-1}$.

FIGURE 4

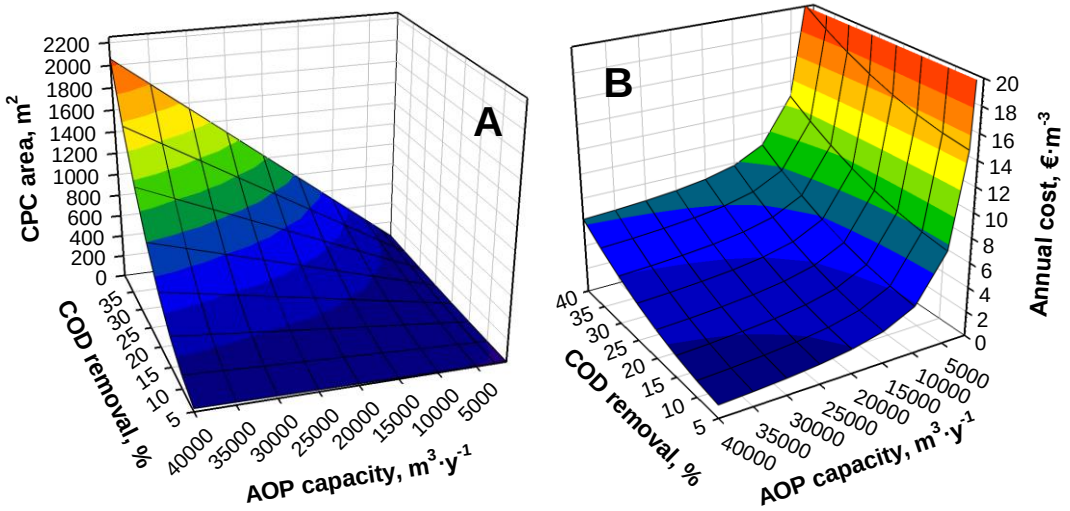

Figure 4. 3D plots of (A) CPC area and (B) annual cost required for the solar photo-Fenton treatment as functions of COD removal (5-40%) and plant capacity (1000-40000 $m^3 \cdot y^{-1}$).

AUXILIAR PUBLICATION

H. Barndõk, D. Hermosilla, L. Cortijo, C. Negro, A. Blanco

Assessing the Effect of Inorganic Anions on TiO_2-Photocatalysis and Ozone Oxidation Treatment Efficiencies

Journal of Advanced Oxidation Technologies 15 (2012) 125-132

Assessing the Effect of Inorganic Anions on TiO_2-Photocatalysis and Ozone Oxidation Treatment Efficiencies

Helen Barndõk, Daphne Hermosilla*, Luis Cortijo, Carlos Negro, and Ángeles Blanco

Department of Chemical Engineering, Complutense University of Madrid, Avda. Complutense s/n, 28040 Madrid, Spain

Abstract:
Considering the application of AOPs might be limited for the treatment of industrial wastewater with high inorganic load, and that partial results reported to date regarding this particular are inconclusive, even opposite in some cases, the effect of inorganic anions on the oxidation efficiency of photocatalysis and ozonation has been further assessed with statistical significance. While the presence of sulphate and chloride did not appreciably affect the photocatalytic oxidation of phenol, nitrate significantly enhanced the removal of COD (≈ 8-15%). The addition of carbonate simply increased the pH, which strongly inhibited the photocatalytic process; whereas if pH=5 was kept constant, the reduction of the COD was not affected by the presence of carbonate. On the other hand, sulphate, chloride and nitrate did not significantly affect the degradation of phenol by ozonation; whereas the presence of carbonate apparently enhanced the reduction of COD. It is actually proved that this improvement in the efficiency of the treatment was produced by the pH buffering effect of these ions, rather than to its presence itself, which actually significantly reduced the removal of COD (5-10%) by radical scavenging action in comparison to when the treatment was performed in the absence of anions in the solution adjusting the pH to similar basic values (≈9.5-13.5). When ozonation was performed at a pH close to neutral (6.5 ± 0.2) or basic (12 ± 0.2), at which the indirect oxidation of hydroxyl radical is surely widely active, the results were significantly enhanced in any case (COD removal ≈ 70-75%), whether in the absence or the presence of these anions; despite the significant slight radical scavenging effect (COD removal ≈ 65-70%) that was attributed to the addition of carbonate.

Keywords: photocatalysis; ozonation; radical scavengers; carbonate; sulphate; nitrate; chloride

Introduction

Advanced oxidation processes (AOPs) involving *in situ* generation of highly reactive transitory species like H_2O_2, $OH\cdot$, O_3, $O_2^{-}\cdot$ are applied when conventional wastewater treatment techniques become insufficient to treat persistent contaminants (1-3). Particularly, ozonation and photocatalytic oxidation with semiconductor catalysts, typically TiO_2, have been widely assessed and applied at industrial scale for this purpose (4-7).

Inorganic anions have been identified to reduce the efficiency of different AOPs (8-10), but actual comparison of their effect at different ion concentration values has been poorly assessed. In general, the produced loss of treatment efficiency attributed to the presence of inorganic anions has been explained by the scavenging effect of reactive radical ionic species and the generation of other by-radicals with weaker oxidation potentials (11-14). For example, chloride (Cl^-) has been addressed to scavenge hydroxyl radicals producing hydroxide and chlorine radical (15-17). Moreover, Cl^- may generate additional "hole"-scavenging in photocatalytic processes.

Similar inhibition mechanisms have been also attributed to other anionic species with a significant presence in wastewater, like sulphate (SO_4^{2-}) and nitrate (NO_3^-) (16-18); although other authors have addressed an insignificant effect of Cl^-, SO_4^{2-}, and NO_3^- on the efficiency of TiO_2-photocatalysis (19, 20). In addition, several authors have reported an improved oxidation efficiency of several AOPs caused by the strong oxidation potential of $SO_4\cdot^-$ radical itself (10, 21-24).

Besides radical scavenging, some anions (e.g. NO_3^-, SO_4^{2-}) may raise the turbidity of the solution, which causes the screening of UV radiation when applying photocatalytic treatments (10, 22); and the competitive adsorption of inorganic anions has been also proposed as an additional potential mechanism of inhibition, "stealing" surface active sites from organic molecules (10, 16, 25). Nevertheless, Wang *et al.* (26) observed no significant relationship between adsorption

*Corresponding author; E-mail: dhermosilla@quim.ucm.es

inhibition and photodegradation rate, attributing all the observed oxidation loss to the radical scavenging action exerted by NO_3^-, Cl^- and SO_4^{2-}. In addition, the competitive adsorption of anions is unlikely to occur under basic conditions because the amphoteric nature of TiO_2 will lead to the repulsion of negative electrostatic forces (22, 27, 28). Particularly, Epling and Lin (29) observed that photo-bleaching of anionic dyes was partially inhibited in the presence of HNO_3 and $NaHCO_3$, while it was accelerated for cationic ones.

Finally, most research assessing the effect of the presence of inorganic anions on the performance of ozone oxidation has been devoted to bicarbonate (HCO_3^-) and carbonate (CO_3^{3-}) action scavenging OH· radical (30-33):

$$CO_3^{2-} + OH\cdot \rightarrow CO_3^{3-} + OH^- \quad (1)$$

$$HCO_3^- + OH\cdot \rightarrow HCO_3\cdot + OH^- \quad (2)$$

$$HCO_3^- + OH\cdot \rightarrow CO_3\cdot^- + H_2O \quad (3)$$

In fact, Chiang *et al*. (33) used HCO_3^- and CO_3^{2-} to scavenge OH· radical in order to study direct oxidation by molecular ozone; and Song *et al*. (35) justified the reduced mineralization of CI Reactive Yellow 145 by ozone oxidation at pH>11.0 by the radical scavenging effect of HCO_3^-/CO_3^{2-} ions. On the other hand, Lair *et al.* (36) found that the presence of HCO_3^-/CO_3^{2-} inhibited the degradation of naphthalene by photocatalysis; but HCO_3^- has been reported to produce a negligible effect on the photocatalytic oxidation of Acid Orange 7 (26) and TNT (37).

In short, several authors have previously assessed in part the effect of inorganic anions on the degradation efficiency of several AOPs, although the reported results are inconsistent and have not been analyzed in terms of statistical significance. Therefore, the main objective of this essay aims to further assess the significance of the effect the most common anions present in industrial wastewater (SO_4^{2-}, Cl^-, NO_3^- and CO_3^{2-}) have on the treatment efficiency of phenol by ozonation and TiO_2-photocatalysis. These treatments were selected because they are AOPs widely applied with success in several industrial applications (4-7); while phenol was chosen because it is a commonly used model compound for the assessment of AOPs, and its nature and behaviour have been widely described when it is treated by ozonation or TiO_2-photocatalysis (1, 22, 38-43).

Experimental and Methods

Materials

All used chemicals were analytical grade, provided by PANREAC S.A. (Barcelona, Spain). Phenol was available in its purest form (99.99%) and diluted with ultra-pure deionized water to the concentration of 200 $mg\cdot L^{-1}$ prior to experiment performance (initial COD= 480 $mg\cdot L^{-1}$). One of the inorganic anions selected to perform this essay (SO_4^{2-}, Cl^-, NO_3^- or CO_3^{2-}) was then added to the solution as the corresponding sodium salt at one of the following concentrations: 250, 500, 1000, and 2000 $mg\cdot L^{-1}$. Every experiment was repeated 3-6 times to minimize the standard deviation of the results.

UV/TiO_2 Oxidation

Aeroxide® TiO_2 P25 (Evonik, Essen, Germany) photocatalyst, with a specific surface area of 50 ± 15 $m^2\cdot g^{-1}$ and an average primary particle size of 21 nm, was first added to the solution at the concentration of 5 $g\cdot L^{-1}$. This optimum TiO_2 dosage resulted from preliminary trials performed using catalyst concentration values ranging from 1 $g\cdot L^{-1}$ to 10 $g\cdot L^{-1}$; and has been previously reported to produce optimal results in the treatment of industrial wastewater (44-46).

The oxidation treatment was carried out in a magnetically-stirred and specially shaped glass reactor (3 L) provided with the necessary ports in the upper part to insert pH and redox potential probes, which furthermore made possible the withdrawal of 5-ml aliquots from the reacting suspension for monitoring the evolution of the COD. The source of UV irradiation was a vertically located medium-pressure mercury vapour lamp (450 W; model 7825-34, ACE Glass Inc., Vineland, NJ, USA), inserted in a quartz cooling jacket, which radiates a total light power of 175.8 W covering from the infrared to the far ultraviolet wavelength regions. The whole assembly was placed in a photochemical safety cabin assisted with a cooling system. The treated solution was 2 L, and every experimental run was conducted for 2 hours. The photocatalyst was immediately separated from every collected sample by means of a 0.45 μm-pore filter at 15, 30, 45, 60, 90, and 120 min from the beginning of the treatment.

In the absence of inorganic anions, and when SO_4^{2-}, Cl^- and NO_3^- ions were added to the solution, the initial pH after the addition of the catalyst was approximately 5.0, and decreased thereafter to approximately 4.0 along the initial 30 min of reaction; keeping this value constant until the end of the experiment. The addition of Na_2CO_3 caused the initial pH to rise to about 10.0 to 12.0, depending on the added salt concentration, and was kept buffered by the presence of HCO_3^-/CO_3^{2-} ions. Therefore, additional experiments were carried out for testing the effect of pH alone: a) continuously adjusting pH to 5.0 (± 0.2) and 4.0 (± 0.2) after the addition of Na_2CO_3; and b) keeping pH=12.0 (± 0.2) when treating phenol in the absence

of anions. pH was adjusted to acid values adding 1M H_2SO_4, as the effect of SO_4^{2-} was first checked to be non significative on the performance of the treatment; whereas 1N NaOH was added to perform the experiments keeping basic pH values.

Ozonation

Ozonation experiments were conducted in a glass jacketed cylindrical bubble reactor (height=1 m, diameter=5 cm) with a continuous feed of ozone gas (4.0 $L \cdot min^{-1}$) produced from ordinary grade air passed through polycarbonate filters, and subsequently enriched with oxygen. The system consisted of an ozone generator (Model 6020, Rilize, Gijón, Spain), a flow controller Bronkhorst® (Model F-201AV, Ruurlo, The Netherlands), and an ozone on-line analyzer (Model 964C, BMT Messtechnik GMBH, Berlin, Germany). Ozone consumption was pH dependent, but did not resulted significantly different among the tested ions presence, resulting 0.39 ± 0.05 g/L when the initial pH value of the solution was not adjusted (pH=5.7); 0.48 ± 0.06 g/L when the pH was maintained at 6.5; and 0.67 ± 0.07 g/L for a constant pH = 12.0. Unconsumed ozone was sent to a catalytic ozone destructor.

A peristaltic pump (Masterflex® Console Drive, Cole-Parmer Instrument Company, Illinois, USA) was used to recirculate the solution under treatment (1 L) through the reactor, and probes for pH and redox potential and dissolved oxygen (ProODO, YSI Inc., Ohio, USA) measurement. Temperature was kept at 25 ºC using a thermostatic bath (Model FL300, JULABO Labortechnik GmbH, Seelbach, Germany), which was aided by the reactor glass jacket itself.

Every experiment was performed for 30 min. The initial pH value of the prepared phenol solution (200 $mg \cdot L^{-1}$) averaged 5.7 (±0.2), and was not modified by the addition of SO_4^{2-}, Cl^- or NO_3^-. During the first 5 min of ozone treatment, pH decreased to approximately 3.2, and was kept more or less constant thereafter. On the other hand, the addition of Na_2CO_3 caused pH to rise to about 12 to 13 (depending on the added concentration), and was kept buffered by the presence of HCO_3^-/CO_3^{2-} ions, as it was previously described when performing photocatalytic trials. When the initial pH was adjusted to 5.7 after the addition of Na_2CO_3, it resulted to rise to a 6.5 constant value after 5 min. In order to set proper comparisons, additional experiments were therefore carried out for every considered ion keeping the pH value constant at 6.5 and 12.0. 1M H_2SO_4 was added to acidify the solution in the experiments performed in the presence of HCO_3^-/CO_3^{2-}; whereas 1N NaOH was used for increasing and keeping constant the pH in the experiments developed at pH= 6.5 and 12 when no ions or SO_4^{2-}, Cl^- and NO_3^- were added.

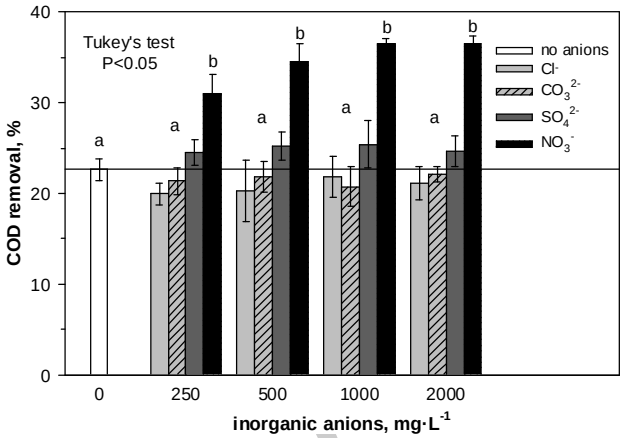

Figure 1. Reduction of the COD after a 2h photocatalytic oxidation treatment of phenol (200 $mg \cdot L^{-1}$) in the absence and after the addition of chloride, sulphate, or nitrate without pH adjustment (initial pH=5.0±0.2); or in the presence of carbonate at pH=5.0 (Mean ± standard deviation, n=3-6. Letters label homogeneous groups of values).

Analytical Methods

On-line pH, redox potential, and dissolved oxygen measurements were carried out every minute. The degradation of phenol was assessed as the achieved reduction in chemical oxygen demand (COD), which was measured according to the Standard Methods for the Examination of Water and Wastewater (APHA, 2005) by the colorimetric method at 600 nm using an Aquamate-spectrophotometer (Thermos Scientific AQA 091801, Waltham, USA).

Statistical Analysis

One-way ANOVA was run (Statplus, 2009) to determine the significance of the observed differences among experiments. *Post hoc* all pairwise comparisons were performed using Tukey's test ($P < 0.05$). Linear regression was used to explain the strong relationship between some treatment variables.

Results and Discussion

UV/TiO_2 Oxidation

The UV/TiO_2 oxidation treatment of phenol achieved a 23% reduction of the COD in the absence of inorganic anions, and the process was not significantly affected by the presence of Cl^-, SO_4^{2-} or HCO_3^-/CO_3^{2-} (Figure 1). In absolute terms, while the removal of COD decreased ≤ 3% when Cl^- or HCO_3^-/CO_3^{2-} were added at any of the tested concentrations, the presence of SO_4^{2-} increased the efficiency of the treatment an additional 2-3%. These non-significant effects were shown along the whole performance of the treatment

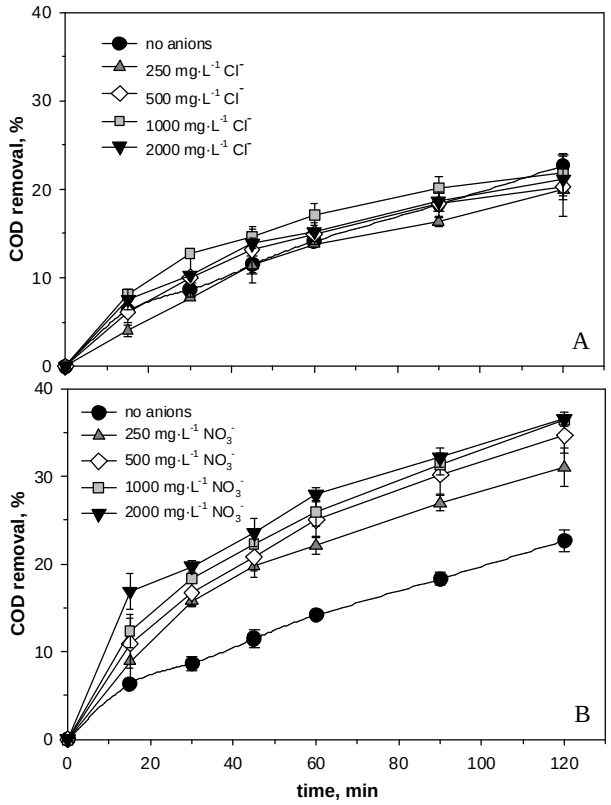

Figure 2. COD removal evolution along the UV/TiO_2 oxidation treatment of phenol (200 mg·L^{-1}) without pH adjustment (initial pH=5.0±0.2) in the presence of (A) chloride, or (B) nitrate (Mean ± standard deviation, n=3-6).

(e.g. Cl^-, Figure 2A), indicating that SO_4^{2-}, Cl^-, and HCO_3^-/CO_3^{2-} were non-effective radical scavengers, nor competitors for active sites on TiO_2, in the performed photocatalytic degradation of phenol; whereas the oxidative contribution of $SO_4^{\cdot -}$ radical was confirmed (10, 21-24).

On the other hand, a significant increase in the reduction of the COD was observed when NO_3^- was added to the solution (Figure 1). While the addition of 250 mg·L^{-1} of NO_3^- enhanced the removal of COD up to a 31%, the presence of the highest tested dosage of 2000 mg·L^{-1} achieved an almost 37%. Differences among results produced at different NO_3^- concentration were not statistically significant; so the presence of 250 mg·L^{-1} of NO_3^- was enough to almost saturate the potential effect. In addition, almost all the improvement of the oxidation efficiency was produced during the first 15-30 minutes of treatment, as denoted by the observed changes in the slopes of the curves illustrating the evolution of the removal of COD along reaction time (Figure 2B). All the curves, whether in the presence or the absence of NO_3^-, keep more or less parallel thereafter; thus showing no further treatment enhancement.

A brown colour that progressively darkened the solution was observed along photocatalytic treatment in the presence of NO_3^-, suggesting the formation of some chromatic phenol derivatives (e.g. benzoquinone (39, 47, 48)); whereas no remarkable colour change was noticed in the presence of other anions. The presence of NO_3^- (or $NO_3^{\cdot}$ radical) may therefore be able to drift phenol's route of degradation towards the production of certain intermediates that accumulate near TiO_2 particles and accelerate further intermediate coupling reactions on its surface (18, 49). In addition, some authors have proved the ability of NO_3^- to absorb UV-light yielding OH·, which may represent a strong homogenous "accelerating" effect for the on-going photo-degradative process (25, 50, 51).

When the solution was not acidified after the addition of Na_2CO_3 , the produced buffered alkaline pH values (10-12) strongly reduced the removal of COD in comparison to the experiments performed at an initial pH=5.0 (COD removal ≈ 22.5%, Figure 3A), which results were identical to those achieved adjusting pH=4.0. As a higher concentration of CO_3^{2-} was added, a higher pH value was reached, and a lower removal of COD was achieved. In the presence of 250 mg·L^{-1} of CO_3^{2-} (pH≈10.5), the reduction of the COD dropped to ≈12%; whereas at the highest concentration of 2000 mg·L^{-1} (pH≈11.5), a poor 5% removal was just achieved after a 2-hours oxidation treatment.

This effect of the presence of CO_3^{2-} has been previously attributed to the production of $CO_3^{\cdot -}$ radical, which scavenges OH·, and therefore causes poorer COD removal efficiencies (15, 26, 35-37). In order to check this out, further trials were performed in the absence of anions adjusting pH to 12.0 (± 0.2). Very poor results (COD removal < 5%), equal to those produced in the presence of a high amount of CO_3^{2-}, were achieved. A radical scavenging effect may therefore be neglected; whereas a strong effect of pH itself was supported (Figure 3B). As TiO_2 surface is negatively charged at pH>6.8, and the presence of phenol as negatively-charged phenolate species is significant at higher pH values, its adsorption on the surface of the catalyst is therefore hindered by the action of repulsive electrostatic forces (22, 27, 28). In addition, a lower degradation rate at higher pH values has been attributed to the fact that a higher concentration of OH^- prevents UV-light from penetrating the solution to effectively reach the surface of the catalyst (52).

Ozonation

In the absence of inorganic anions, the ozone oxidation of phenol produced a 55% removal of COD

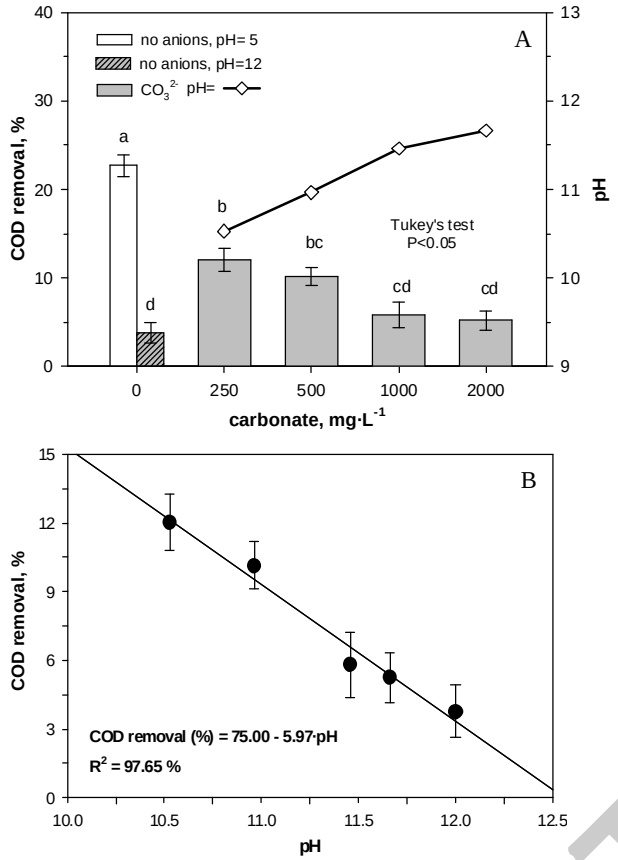

Figure 3. (A) Reduction of the COD after a 2h photocatalytic oxidation treatment of phenol (200 mg·L^{-1}) in the presence of carbonate without adjusting the pH (Mean ± standard deviation, n=3-6. Letters label homogeneous groups of values). (B) A strong correlation was found between pH and COD removal when UV/TiO_2 treatment was performed under alkaline conditions in the presence or the absence of carbonate.

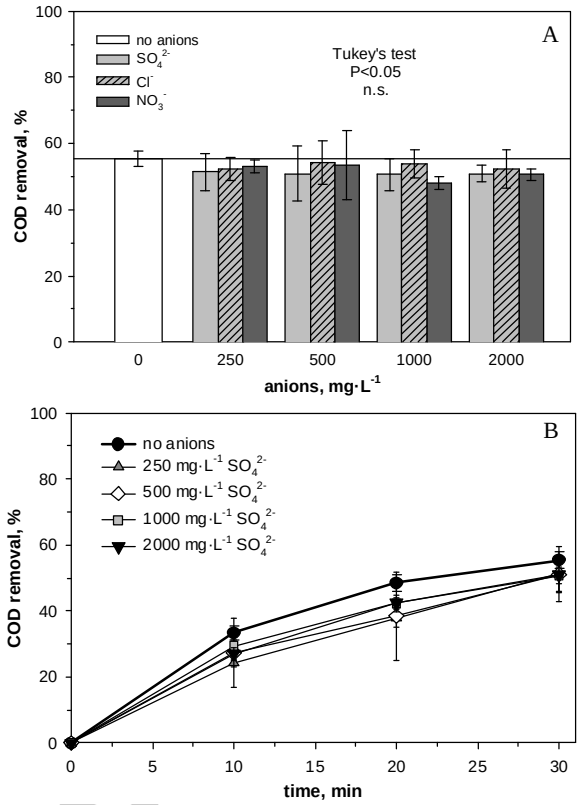

Figure 4. (A) Removal of COD after a 30-min ozone oxidation treatment of phenol (200 mg·L^{-1}) in the absence of inorganic anions and in the presence of chloride, sulphate and nitrate without adjusting the pH (initial pH=5.7±0.2). (Mean ± standard deviation, n=3-6. n.s.=non-significant differences were found). (B) The evolution in time of the reduction of the COD in the presence of sulphate is shown as an example.

after a 30-minute-treatment without adjusting the pH (Figure 4A); whereas the addition of SO_4^{2-}, Cl^-, or NO_3^- resulted in a non-significant detrimental effect on the treatment efficiency (COD removal ≥50% in any case). A similar pH evolution along the treatment was observed in the absence of anions and when SO_4^{2-}, Cl^-, or NO_3^- were added to the solution; that is, initial pH averaged 5.7 ± 0.2, and then decreased to 3.2 ± 0.2 along the first 5 min of treatment, keeping more or less constant thereafter (the formation of carboxylic acids in the degradation process of phenol may acidify the solution, e.g. (53-56)). In addition, whether in the absence of anions or in the presence of SO_4^{2-}, Cl^-, or NO_3^- in the solution, no significant differences were shown in the reduction of COD along the whole treatment time, as shown for all tested SO_4^{2-} concentration values in Figure 4B. SO_4^{2-}, Cl^-, and NO_3^- were therefore ineffective radical scavengers when phenol was treated by ozone oxidation under acid conditions.

Provided there is a pH threshold below which the leading degradation mechanism of the ozonation treatment of every organic substance in the solution is direct oxidation by molecular ozone, and above which indirect oxidation after O_3 decomposition to OH· is predominant (11), and considering the above reported results under pretty strong acid conditions, it is reasonable to suppose that direct ozonation is widely dominating the oxidation process; thus potential radical scavengers could not produce much effect on the results.

On the other hand, the addition of CO_3^{2-} to the solution increased pH to basic values and the removal of COD was improved in comparison to when no anions were added and pH was not adjusted (Figure 5A). While the addition of 250 mg·L^{-1} of CO_3^{2-} (pH≈12.5-9.5) increased the efficiency of the 30-minute ozonation treatment close to a 60% COD removal, the addition of 500 mg·L^{-1} (pH≈13.0-10.5) significantly increased the efficiency of the treatment to about the 65%. No significant greater enhancement was achieved adding up to 2000 mg·L^{-1} of CO_3^{2-}.

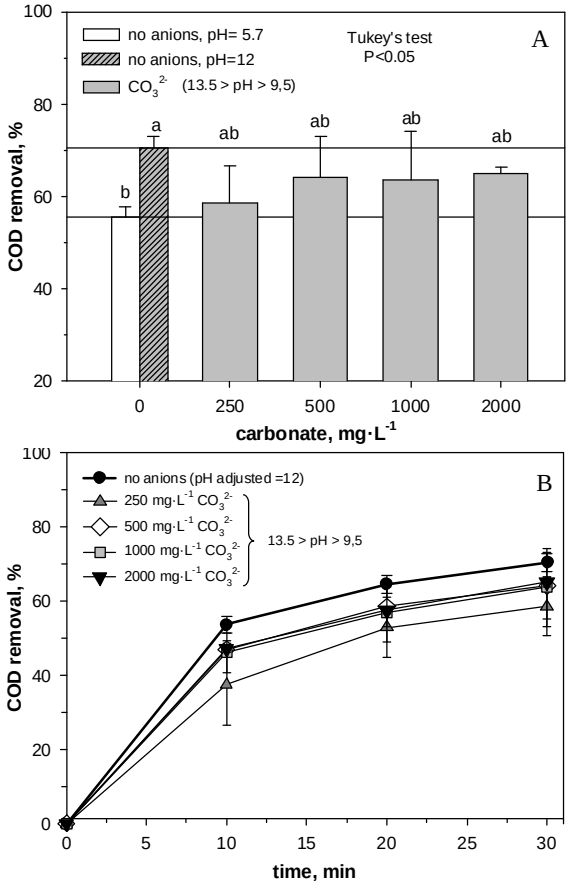

Figure 5. (A) Reduction of the COD after a 30-min ozone oxidation treatment of phenol (200 mg·L^{-1}) in the absence of anions at pH=5.7 or 12; and after the addition of carbonate without adjusting the pH (Mean ± standard deviation, n=3-6. Letters label homogeneous groups of values). (B) Evolution in time of the removal of COD in the absence of anions at pH=12, and in the presence of carbonate without pH adjustment.

When ozonation treatment was carried out in the absence of CO_3^{2-}, but pH was adjusted to similar basic values (pH≈12-11), the reduction of the COD resulted even higher (≈70%; Figure 5A); which supports the hypothesis that this apparent removal enhancement attributed to the presence of CO_3^{2-} was really caused by the increase of the pH value itself, which promotes the production of OH· radical when OH^- anion concentration is higher (33, 34). In fact, the ozonation process seems actually partially hampered after the addition of CO_3^{2-} when the results achieved at similar pH values are compared, which has been previously explained by an OH· scavenging effect (32, 34, 35). Finally, the effect of CO_3^{2-} on the ozonation efficiency of phenol was mainly produced during the first 10 minutes of treatment; after 20 minutes, no further effect was accounted for, as denoted by the changes in the slopes of the curves representing the evolution of COD removal along the time this treatment was performed (Figure 5B).

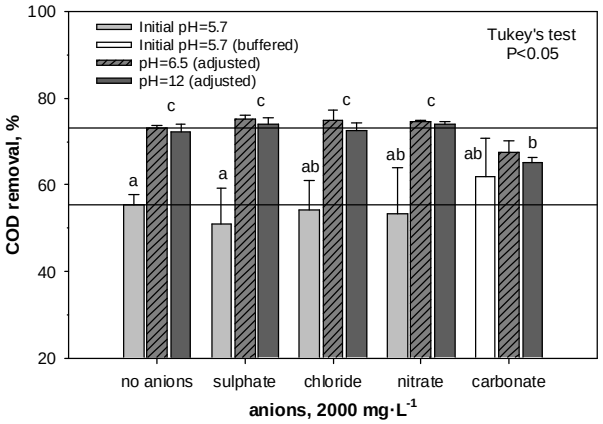

Figure 6. COD removal after a 30-min ozonation treatment of phenol (200 mg·L^{-1}) in the absence or the presence (2000 mg·L^{-1}) of sulphate, chloride, nitrate, or carbonate with or without adjusting the pH.

In order to compare further results under acid conditions, pH adjustment to 5.7 was set after the addition of Na_2CO_3. After several attempts, it was checked out that the actual pH value was buffered to 6.5 (±0.2) by the air present in the bubble column and the action of HCO_3^-/CO_3^{2-} equilibrium. The addition of 500 mg·L^{-1} of CO_3^{2-} under these conditions enhanced significantly the degradation of phenol by ozone, producing up to a 68% COD removal; whereas in the absence of ions, or when the addition of an equivalent concentration of the other tested anions, it resulted in about a 55% reduction of the COD if pH was not adjusted (pH=5.7 ± 0.2; Figure 6). On the other hand, when all the experiments were repeated adjusting the pH to 6.5 or 12, it resulted that about the 75% of the initial COD was removed, whether no inorganic anion was added to the solution, whether SO_4^{2-}, Cl^-, or NO_3^- were added.

These results show that, regardless whether direct or indirect oxidation is the leading mechanism in the ozonation treatment of phenol, the presence of SO_4^{2-}, Cl^-, and NO_3^- is not significantly scavenging radicals and does not significantly affect the degradation process. It is additionally shown that ozonation treatment is significantly enhanced at a pH value close to neutral (6.5), or under basic conditions (12.0), which was surely caused by the promotion of OH· indirect oxidation (11). On the other hand, it has been also addressed that the ozonation rate of phenolic compounds increases at higher basic pH values, as it also does the degree of deprotonation and dissociation into phenolate species (57). The oxidation treatment efficiency is therefore also improved under these conditions because the ozone-phenolate reaction is faster than the ozone-phenol one (40). Finally, the significant lower COD removal rate addressed to the

addition of CO_3^{2-} supports a radical scavenging effect that has been previously attributed to the presence of HCO_3^-/CO_3^{2-} (31, 32).

Conclusions

Although other authors have reported inconclusive to even contradictory conclusions regarding the effect of inorganic anions on the performance of several AOPs, it has been really demonstrated with statistical significance that the addition of SO_4^{2-} and Cl^- did not reduce the efficiency of the photocatalytic treatment of phenol when the pH of the solution was not adjusted (pH≤5); and an identical negligible effect was found when CO_3^{2-} was added and pH was adjusted to similar acid values.

On the other hand, the presence of NO_3^- significantly enhanced the photocatalytic reduction of the COD (≈15%). This effect may be explained by the ability of NO_3^- to absorb UV light, leading to an additional production of OH· radicals; the enhancement of the adsorption of phenol on the surface of TiO_2; and the acceleration of intermediate reactions on the catalyst surface.

The addition of CO_3^{2-} without pH adjustment resulted in an apparent loss of efficiency of the photocatalytic treatment of phenol, which was really caused by the generated higher pH value itself (pH≈10.0-12.0), as phenol adsorption on the catalyst surface was hampered under alkaline conditions due to the repulsive electrostatic forces that are manifested (both TiO_2 surface and phenolate species are negatively charged at such alkaline pH values).

Likewise, the presence of SO_4^{2-}, Cl^-, or NO_3^- did not reduce the efficiency of the treatment to a significant extent when phenol was oxidized by ozone; whether results without adjusting the initial pH value of the solution (pH=5.7) were always 15-20% worse in terms of the achieved reduction of the COD than those performed under adjusted close to neutral (pH= 6.5) or basic (pH=12.0) conditions.

Finally, the addition of CO_3^{2-} negatively affected the efficiency of ozonating phenol by a 5-10% COD removal due to the manifested radical scavenging effect under both close to neutral (pH=6.5) and basic (pH=9.5-13.5) conditions; whereas there was no such an effect when the pH was adjusted to keep its initial acid value (pH=5.7).

Acknowledgements

This research was developed in the framework of the following projects: "PROLIPAPEL" (S-0505/ AMB-0100), funded by the Regional Government of Madrid (Comunidad Autónoma de Madrid), Spain; "AGUA Y ENERGÍA" (CTM2008-06886-C02-01), funded by the Ministry of Science and Innovation of Spain (Ministerio de Ciencia e Innovación); and "AQUAFIT4USE" (211534), funded by the European Comission. Archimedes Foundation (Estonia) sponsors H. Barndõk's PhD at Complutense University of Madrid.

References

(1) Esplugas, S.; Giménez, J.; Contreras, S.; Pascual, E.; Rodríguez, M. *Water Res*. **2002**, *36*, 1034-1042.

(2) Comninellis, C.; Kapalka, A.; Malato, S.; Parsons, S.A.; Poulios, I.; Mantzavinos, D. *J. Chem. Technol. Biotechnol*. **2008**, *83*, 769-776.

(3) Hermosilla, D.; Cortijo, M.; Huang, C.P. *Sci. Total Environ*. **2009**, *407*, 3473-3481.

(4) Diebold, U. *Surf. Sci. Rep*. **2003**, *48*, 53-229.

(5) Chong, M.N.; Jin, B.; Chow, C.W.K.; Saint, C. *Water Res*. **2010**, *44*, 2997-3027.

(6) Lucas, M.S.; Peres, J.A.; Lan, B.Y.; Puma, G.L. *Water Res*. **2009**, *43*, 1523-1532.

(7) Lovato, M.E.; Martín, C.A.; Cassano, A.E. *Chem. Eng. J*. **2009**, *146*, 486-497.

(8) Pignatello, J. *J. Environ. Sci. Technol*. **1992**, *26*, 944-951.

(9) Lu, M.C. *Chemosphere* **1997**, *35*(10), 2285-2293.

(10) Burns, R.A.; Crittenden, J.C.; Hand, D.W.; Selzer, V.H.; Sutter, L.L.; Salman, S.R. *J. Environ. Eng*. **1999**, *125*(1), 77-85.

(11) Hoigné, J.; Bader, H. *Water Res*. **1976**, *10*, 377-386.

(12) Matthews, R.W. *J. Chem. Soc. Faraday Trans. 1* **1984**, *80*(2), 457-71.

(13) Bahnemann, D.; Cunningham, J.; Fox, M.A.; Pelizzetti, E.; Serpone, N.; Pichat, P. In *Aquatic and Surface Photochemistry*; Helz, G. R.; Zepp, R. G.; Crosby D. G., Eds.; Lewis: Boca Raton, 1994; pp 261-316.

(14) Guillard, C.; Lachheb, H.; Houas, A.; Ksibi, M.; Elaloui, E.; Herrmann, J.M. *J. Photochem. Photobiol. A* **2003**, *158*, 27-36.

(15) Abdullah, M.; Low, G.K.C.; Matthews, R.W. *J. Phys. Chem*. **1990**, **94**(17), 6820-6825.

(16) Yalap, K.S.; Balcioglu, I.A. *J. Adv. Oxid. Technol*. **2009**, *12*(1), 134-143.

(17) Papadam, T.; Xekoukoulotakis, N.P.; Poulios, I.; Mantzavinos, D. *J. Photochem. Photobiol. A* **2007**, *186*, 308-315.

(18) Wong, C.C.; Chu, W. *Chemosphere* **2003**, *50*, 981-987.

(19) Wenhua, L.; Hong, L.; Sao'an, C.; Jianquing, Z.; Chunan, C. *J. Photochem. Photobiol. A* **2000**, *131*, 125-132.

(20) Rincón, A.G.; Pulgarin, C. *Appl. Catal. B* **2004**, *51*, 283-302.

(21) Serrano, K.; Michaud, P.A.; Comninellis, C.; Savall, A. *Electrochim. Acta* **2002**, *48*, 431-436.

(22) Kashif, N.; Ouyang, F. *J. Environ. Sci*. **2009**, *21*, 527-533.

(23) Méndez-Díaz, J.; Sánches-Polo, M.; Rivera-Utrilla, J.; Canonica, S.; von Gunten, U. *Chem. Eng. J*. **2010**, *165*, 300-306.

(24) Rastogi, A.; Al-Abed, S.R.; Dionysiou, D.D. *Appl. Catal. B* **2009**, *85*, 171-179.

(25) Chen, H.Y.; Zahraa, O.; Bouchy, M. *J. Photochem. Photobiol. A* **1997**, *108*, 37-44.

(26) Wang, K.; Zhang, J.; Lou, L.; Yang, S.; Chen, Y. *J. Photochem. Photobiol. A*. **2004**, *165*, 201-207.

(27) Hu, C.; Yu, J.C.; Hao, Z.; Wong, P.K. *Appl. Catal., B*. **2003**, *46*, 35-47.

(28) Habibi, M.H.; Hassanzadeh, A.; Mahdavi, S. *J. Photochem. Photobiol. A*. **2005**, *172*, 89-96.

(29) Epling, G.A.; Lin, *Chemosphere* **2002**, *46*, 937-944.

(30) Hoigné, J.; Bader, H. *Water Res.* **1985**, *19*(8), 993-1004.

(31) Glaze, W.H.; Kang, J.W. *Ind. Eng. Chem. Res*. **1989**, *28*(11), 1573-1580.

(32) Ma, J.; Graham, N.J.D. *Water Res*. **2000**, *34*(15), 3822-3828.

(33) Alaton, I.A.; Kornmüller, A.; Jekel, M.R. *J. Environ. Eng*. **2002**, *128*(8), 689-696.

(34) Chiang, Y.P.; Liang, Y.Y.; Chang, C.N.; Chao, A. C. *Chemosphere* **2006**, *65*, 2395-2400.

(35) Song, S.; Xu, X.; Xu, L.; He, Z.; Ying, H.; Chen, J. *Ind. Eng. Chem. Res*. **2008**, *47*, 1386-1391.

(36) Lair, A.; Ferronato, C.; Chovelon, J.M.; Herrmann, J.M. *J. Photochem. Photobiol. A* **2008**, *193*, 193-203.

(37) Schmelling, D.C.; Gray, K.A.; Kamat, P.V. *Water Res.* **1997**, *31*(6), 1439-1447.

(38) Ahmed, S.; Rasul, M.G.; Martens, W.N.; Brown, R.; Hashib, M.A. *Desalination* **2010**, *261*, 3-18.

(39) Li, K.Y.; Kuo, C.H.; Weeks, J.L. *AIChE J*. **1979**, *25*, 583-591.

(40) Matheswaran, M.; Moon. I.S. *J. Ind. Eng. Chem*. **2009**, *15*, 287-292.

(41) Chiou, C.H.; Wu, C.Y.; Juang, R. S. *Chem. Eng. J*. **2008**, *139*, 322-329.

(42) Siedlecka, E.M.; Więckowska, A.; Stepnowski, P. *J. Hazard. Mater*. **2007**, *147*, 497-502.

(43) Kusic, H.; Koprivanac, N.; Bozic, A. L. *Chem. Eng. J*. **2006**, *123*, 127-137.

(44) Chang, C. N.; Ma, Y. S.; Fang, G. C.; Chao, A.C.; Tsai, M.C.; Sung, H.F. *Chemosphere* **2004**, *56*, 1011-1017.

(45) Muneer, M.; Qamar, M.; Saquib, M.; Bahnemann, D.W. *Chemosphere* **2005**, *61*, 457-468.

(46) Shifu, C.; Yunzhang, L. *Chemosphere* **2007**, *67*, 1010-1017.

(47) Abbas, O.; Rebufa, C.; Dupuy, N.; Kister, J. *Talanta* **2008**, *77*, 200-209.

(48) Sobczynski, A.; Duczmal, L.; Zmudzinski, W. *J. Mol. Catal*. **2004**, *213*, 225-230.

(49) Makarova, O.V.; Rajh, T.; Thurnauer, M.C. *Sci. Technol*. **2000**, *34*, 4797-4803.

(50) Fox, M. In *Concepts of Inorganic Photochemistry*; Adamson, A. W.; Fleishauer, P. D., Eds.; Wiley-Interscience: New York, 1975; pp 333-380.

(51) Stumm, W.; Morgan, J. *J. Aquatic Chemistry*; Wiley-Interscience: New York, 1996, pp 1040.

(52) Qamar, M.; Muneer, M.; Bahnemann, D. *J. Environ. Manage*. **2006**, *80*(2), 99-106.

(53) Huang, C.R.; Shu, H.Y. *J. Hazard. Mater*. **1995**, *41*, 47-64.

(54) Lan, B.Y.; Nigmatullin, R.; Puma, G.L. *Water Res.* **2008**, *42*, 2473-2482.

(55) Zhang, F.F.; Yediler, A.; Liang, X.M.; Kettrup, A. *J. Environ. Sci. Health, Part A: Toxic/Hazard. Subst. Environ. Eng*. **2002**, *37*, 707-713.

(56) Hermosilla, D.; Cortijo, M.; Huang, C.P. *Chem. Eng. J*. **2009**, *155*, 637-646.

(57) Hoigné, J.; Bader, H. *Water Res*. **1983**, *17*(2), 185-194.

Received for review November 19, 2011. Revised manuscript received November 21, 2011. Accepted November 22, 2011.